The University of Aston in Birmingham

THE GEOCHEMISTRY OF RADIOACTIVE WASTE DISPOSAL

by

Nigel Davison

A thesis submitted for the degree of Doctor of

Philosophy, 1987.

Summary

The present study attempted to identify the significant parameters which affect radionuclide migration from a low level radioactive waste disposal site located in a clay deposit. From initial sorption studies on smectite minerals, increased K_d with decreasing initial cation concentration was observed, and three sorption mechanisms were identified. The observation of anion dependent sorption was related to the existance of a mechanism in which an anion-cation pair are bound to the clay surface through the anion. The influence of competing cations, typical of inorganic groundwater constituents, depended on:
(1) Ni/Co:M^{n+} (M^{n+} = competing cation) ratio, (2) nature of M^{n+},
(3) total solution ionic strength.

The presence of organic material in groundwater is well documented, but its effect on cation sorption has not been established. An initial qualitative investigation involving addition of simple organic ligands to Ni(Co)-hectorite samples demonstrated the formation of metal complexes in the clay interlayers, although some modified behaviour was observed. Further quantitative examination involving likely groundwater organic constituents and more comprehensive physical investigation confirmed this behaviour and enabled separation of the organic compounds used into two classes, according to their effect on cation sorption;
(i) acids, (ii) amine compounds.

X-ray photoelectron spectroscopy, scanning electron microscopy and Mössbauer spectroscopy were used to investigate the nature of transition metal ions sorbed onto montmorillonite and hectorite. Evidence strongly favoured the sorption of the hexaaquo cation, although a series of sorption sites of slightly different chemical characteristics were responsible for broadened peak widths observed in XPS and Mössbauer investigations. The surface sensitivity of XPS enabled recognition of the two surface sorption sites proposed in earlier sorption studies. Although thermal treatment of Fe^{3+}/Fe^{2+}-hectorite samples left iron atoms bonded to the silicate sheet structure, Mössbauer evidence indicated the presence of both ferric and ferrous iron in all samples.

Key words: Montmorillonite, Hectorite, Sorption, Radioactive waste

To Mum, Martin, Claire

and

in memory of my Father.

ACKNOWLEDGEMENTS

I should like to record my sincere gratitude to my academic supervisor, Prof. W. R. McWhinnie, for his invaluable advice and assistance and unfailing support during my period as a research student.

I am most grateful to Dr. Alan Hooper of the CEGB for giving up his valuable time and expertise on my visits to Berkeley (and whilst at Aston) and also to Dr. Roger Newman for initiating the project. I must also thank Dr. Paul Woollam for the use of a γ-spectrometer and the research staff at Berkeley generally for their support and friendship.

The interest of Dr. J. W. Gaskarth is also acknowledged.

I should also like to thank Eric Hartland and Richard Wightman, members of the geology department and Narsim Murthy for his invaluable help with atomic absorption analysis and for obtaining Mossbauer spectra of a number of samples.

Thanks are also due to the technical staff of the Department of Chemistry for their assistance in a variety of matters.

I am indebted to my sister Claire for time and patience in producing the typescript.

I wish to acknowledge the University of Aston for the provision of a studentship and the sponsorship offered by the CEGB.

Finally, I should like to thank Janet, Mum, Dad, Claire and Martin for moral support throughout the last four years.

LIST OF CONTENTS

		PAGE NO.
Title Page		1
Thesis Summary		2
Dedication		3
Acknowledgements		4
List of Contents		5
List of Illustrations		8
List of Tables		13
Chapter One - Introduction		21
1.1	Background	22
1.2	Origins and classification of nuclear waste	23
1.3	Radioactive waste disposal	25
1.4	Role of clay minerals in radioactive waste disposal	28
1.5	Characteristic features of clay minerals	30
1.6	Factors affecting cation sorption on clay minerals	39
1.7	Role of cement in radioactive waste disposal	60
1.8	Aims	61
1.9	Selection of clay minerals	63
Chapter Two - Physical Techniques		64
2.1	Atomic absorption spectrophotometry	65
2.2	Ion chromatography	65
2.3	γ-spectrometry	66
2.4	X-ray diffraction	66
2.5	Infrared spectroscopy	67
2.6	Ultraviolet and visible spectrophotometry	67
2.7	Diffuse reflectance spectrophotometry	67
2.8	X-ray photoelectron spectroscopy	68
2.9	Mössbauer spectroscopy	68
2.10	Electron spin resonance spectroscopy	69
2.11	X-ray fluorescence	70
2.12	Differential thermal analysis	70
2.13	Scanning electron microscopy	70
2.14	Gas-liquid chromatography	71
2.15	Titrimetric determination of cobalt	71
2.16	Titrimetric determination of nickel	72
2.17	pH measurement	72
2.18	Ignition of samples	73
2.19	Chemicals	73

		PAGE NO.
Chapter Three -	Cobalt and nickel sorption on hectorite and montmorillonite and the influence of competing inorganic cations	74
3.1	Introduction	75
3.2	Clay mineral analysis	75
3.3	Determination of cation exchange capacity	77
3.4	Preparation of sodium saturated montmorillonite	79
3.5	Interaction of clay minerals with nickel and cobalt solutions	80
3.5.1	Problems associated with the analysis of supernatent liquids from clay mineral suspensions	80
3.5.2	Macroscopic effects	97
3.5.3	Microscopic effects	123
3.6	Influence of competing cations on nickel and cobalt sorption	128
3.6.1	Macroscopic effects	128
3.6.2	Microscopic effects	143
3.7	Discussion	146
Chapter Four -	The influence of organic species on sorption	195
4.1	Introduction	196
4.2	Macroscopic effects	197
4.2.1	Influence of organic compounds on atomic absorption analysis of nickel and cobalt	197
4.2.2	Qualitative effect of model organic ligands on cobalt and nickel saturated hectorite	204
4.2.3	The influence of typical organic groundwater constituents on sorption properties of nickel and cobalt hectorite	207
4.2.4	The desorption of tris(ethylenediamine)nickel(II) from exchange sites on hectorite by inorganic cations	222
4.3	Microscopic effects	224
4.3.1	Preparation of ^{60}Co doped hectorite	224
4.3.2	Influence of solutions of organic compounds on the stability of ^{60}Co-hectorite.	225
4.4	Redox properties of tris(2,2'-bipyridyl)cobalt(III) exchanged hectorite	225
4.4.1	Preparation of $[Co(bipy)_3]^{3+}$-hectorite	227
4.4.2	Generation of $[Co(bipy)_3]^{+}$-hectorite	227
4.4.3	Reduction of nitrobenzene	228
4.5	Discussion	231
Chapter Five -	Physical investigation into the nature of sorbed metal ions on montmorillonite and hectorite	271
5.1	Introduction	272
5.2	X-ray photoelectron spectroscopy	272

PAGE NO.

5.3 Scanning electron microscopy 278
5.4 Mossbauer spectroscopic investigation of iron ions exchanged onto hectorite 282
5.4.1 Preparation of Fe^{3+}-hectorite 282
5.4.2 Preparation of Fe^{2+}-hectorite 290
5.4.3 Preparation of $^{57}Fe^{3+}$-hectorite 293
5.4.4 Thermal treatment of iron doctored clay samples 293
5.5 Discussion 301
Compendium 347
Appendix One - Instrumental settings for atomic absorption analysis 351

Appendix Two - Sorption on centrifuge tube walls 352

References 353

LIST OF ILLUSTRATIONS

FIGURE		PAGE NO.
1	Schematic illustration of the disposal vault concept of nuclear waste isolation.	27
2	Hypothetical sequence of events occurring during leaching of radionuclides from a vault disposal site.	29
3	Diagrammatic sketch showing sheet structure of silica tetrahedrons arranged in a hexagonal network.	31
4	Diagrammatic sketch showing sheet structure of the octahedral units.	31
5	Atom arrangement in the unit cell of the two layer clay mineral kaolinite (schematic).	33
6	Atom arrangement in the unit cell of the three layer mineral pyrophyllite.	35
7	Metal ions released by montmorillonite after various periods of settling and ultracentrifugation.	84
8	Metal ions released from a Ni-montmorillonite upon successive redispersion.	88
9	Metal ions released from a Ni-hectorite upon successive redispersion.	92
10	Anion effect on variation of nickel sorbed on Na-montmorillonite with time.	100
11	Anion effect on variation of nickel retained on Na-montmorillonite with time.	101
12	Anion effect on variation of nickel released by Na-montmorillonite with time.	102
13	Anion effect on variation of cobalt sorbed on Na-montmorillonite with time.	106
14	Anion effect on variation of cobalt retained on Na-montmorillonite with time.	107

FIGURE		PAGE NO.
15	Anion effect on variation of cobalt released by Na-montmorillonite with time.	108
16	Variation of nickel and cobalt sorbed on natural hectorite with time.	113
17	Variation of nickel and cobalt on natural hectorite with time.	114
18	Variation of nickel and cobalt released from natural hectorite with time.	115
19	Variation of nickel sorbed on Na-montmorillonite with initial nickel solution volume.	120
20	Variation of nickel released from a Ni-montmorillonite with initial solution volume.	121
21	Ni sorption isotherm on Na-montmorillonite.	122
22	Log K_d(Ni) versus log equilibrium Ni concentration for nickel sorption on Na-montmorillonite.	125
23	Cobalt sorption isotherm, on Na-montmorillonite.	126
24	Log K_d(Co) versus log equilibrium Co concentration for cobalt sorption on Na-montmorillonite.	127
25	Variation of % Ni/Co sorbed with initial solution concentration when in competition with Magnesium at constant 0.04M molarity.	131
26	Variation of % Ni/Co sorbed with initial solution concentration when in competition with Calcium at constant 0.04M molarity.	132
27	Variation of % Ni/Co sorbed with initial solution concentration when in competition with Sodium at constant 0.04M molarity.	133
28	Variation of % Ni/Co sorbed with initial solution concentration when in competition with Potassium at constant 0.04M molarity.	134

FIGURE		PAGE NO.
29	Variation of log K_d(Ni/Co) with final solution concentration in competition experiments at constant (0.04M) molarity.	135
30	Variation of log K_d(Ni) with log initial metal ion concentration in experiments at variable molar strength.	141
31	Variation of log $K_d(M^{n+})$ with log initial metal ion concentration in experiments at variable molar strength.	142
32	Illustration of how SO_4^{2-} (or HSO_4^-) may bind to positive edge sites of clay crystals.	155
33	Langmuir plot of data from cobalt sorption on Na-montmorillonite.	164
34	Langmuir plot for nickel sorption on Na-montmorillonite.	165
35	In K_s'(Co) versus $\overline{X}_{Co}$ for cobalt sorption on Na-montmorillonite.	168
36	In K_s'(Ni) versus $\overline{X}_{Ni}$ for nickel sorption on Na-montmorillonite.	169
37	Langmuir sorption isotherm for nickel uptake on Na-montmorillonite, extended to include data at low cation concentrations.	174
38	Langmuir sorption isotherm for cobalt sorption on Na-montmorillonite, extended to include data at low cation concentrations.	175
39	Competitive Langmuir plots for cobalt/nickel sorption on Na-montmorillonite in the presence of competing cations at constant total molarity (0.04M).	185
40	Competitive Langmuir plots for magnesium/calcium/potassium sorption on Na-montmorillonite in the presence of competing cations, at constant total molarity (0.04M).	186

FIGURE		PAGE NO.
41	Variation of apparent H^+ released into solution from a Na-montmorillonite with total metal ion sorbed using solutions of differing ionic strength.	192
42	Variation of apparent H^+ released into solution from a Na-montmorillonite with metal ion (Ni, Mg or Ca) sorbed using solutions of differing ionic strength.	193
43	Atomic absorption analysis of nickel in the presence of organic compounds.	199
44	Atomic absorption analysis of cobalt in the presence of organic compounds.	203
45	Infrared spectra of (A) Co-hectorite/pentanoic acid (B) Co-hectorite only.	239
46	Infrared spectra of (A) Ni-hectorite/ethylenediamine (B) Ni-hectorite only.	244
47	% Ni(Co) desorbed from Ni(Co)-hectorite by various organic 'ligands' at a number of initial solution concentrations.	251
48	% Ni desorbed from Ni/en-hectorite by inorganic cations.	260
49	Infrared spectrum of $[Ni(en)_3]^{2+}$-hectorite + Cu^{2+}.	263
50	UV/visible spectrum of equilibrium solution remaining from treatment of $[Ni(en)_3]^{2+}$-hectorite with Cu^{2+}.	264
51	Desorption of Cobalt from a Co-60/hectorite by organic 'ligand' solutions.	266
52	Room temperature Mössbauer spectrum of Fe^{3+}-hectorite.	291
53	Mössbauer spectrum of Fe^{2+}-hectorite taken at 80K.	292
54	Room temperature Mössbauer spectrum of $^{57}Fe^{3+}$-hectorite.	294
55	Room temperature Mössbauer spectrum of Fe^{3+}-hectorite after heating to 400°C.	295

FIGURE		PAGE NO.
56	Mössbauer spectrum (80K) of Fe^{3+}-hectorite thermally treated at 400°C.	296
57	Mössbauer spectrum of Fe^{2+}-hectorite after heating to 400°C, taken at 80K.	297
58	Room temperature Mössbauer spectrum of Fe^{2+}-hectorite heated to 400°C.	298
59	Room temperature Mössbauer spectrum of $^{57}Fe^{3+}$-hectorite heated to 400°C.	299
60	Co2p binding energy region from XPS spectrum of Co^{2+}-hectorite: (A) with no ion etching (B) after 10 mins ion etching.	302
61	Co2p region from XPS spectrum of Co^{2+}-hectorite/2 wash: (A) prior to ion etching (B) after 10 mins etching	303
62	Co2p region from XPS spectrum of Co^{2+}-hectorite/5 wash: (A) unetched (B) after 10 mins etching	304
63	Co2p photopeak from Co^{2+}-hectorite computer fitted to: (A) 2 peaks (B) 4 peaks	309
64	Ni2p region from XPS spectrum of Ni^{2+}-hectorite: (A) with no ion etching (B) after 5 mins etching.	312
65	Ni2p binding energy region from Ni^{2+}-hectorite/2 wash: (A) unetched (B) after 5 mins ion etching	313
66	Ni2p region of XPS spectrum from Ni^{2+}-hectorite/5 wash: (A) unetched (B) after 5 mins etching	314
67	Ni2p region from XPS spectrum of $NiSO_4$-montmorillonite: (A) unetched (B) after 2 mins etching (C) after 10 mins etching	321

LIST OF TABLES

TABLE		PAGE NO.
1	The principle types of ILW and LLW generated in the U.K.	24
2	Estimated total radioactive waste volumes in the U.K.	25
3	Cation affinity series for montmorillonite (from ability of cation to displace another from an exchange site.	43
4	Maximum uptake data from single cation solutions.	44
5	Order of % reduction in adsorption from a 4 element solution compared with the single element solution.	44
6	Affinity series for Ni, Co, Cr sorption on montmorillonite.	45
7	Order of sorption affinities of transition metals for Na-montmorillonite and treated red clay.	45
8	Comparative metal ion uptake affinity sequences.	46
9	K_d values for nickel sorption on Hanford Soils.	52
10	XRF analysis of montmorillonite and hectorite.	76
11	XRD data from natural and glycolated montmorillonite and hectorite.	76
12	Characteristic DTA peaks from montmorillonite and hectorite.	78
13	I.R. absorption peaks from montmorillonite and hectorite samples.	78
14	Cation exchange capacities of montmorillonite and hectorite.	81
15	Concentration of metal ions apparently released into distilled water by montmorillonite samples.	81
16	Apparent concentrations of metal ion released by natural montmorillonite after various periods of settling and ultracentrifugation.	83

TABLE		PAGE NO.
17	Apparent concentration of metal ion released from a Ni-montmorillonite on successive redispersion by distilled water.	87
18	Cations apparently released by natural hectorite into a distilled water solution.	90
19	Apparent concentration of metal ions released from a Ni-hectorite on successive washing with distilled water.	90
20	Relative metal ion concentrations (peak heights) in supernatent from a Na-montmorillonite sample treated with a 2ppm Ni^{2+} solution.	94
21	Distribution coefficients from initial measurements on cobalt sorption on Na-montmorillonite at low level.	96
22	Anion effect on variation of nickel sorbed on Na-montmorillonite with time.	98
23	Anion effect on variation of nickel retained on Na-montmorillonite with time.	98
24	Anion effect on variation of nickel released from Na-montmorillonite with time.	99
25	Anion effect on variation of cobalt sorbed on Na-montmorillonite with time.	104
26	Anion effect on variation of cobalt retained on Na-montmorillonite with time.	104
27	Anion effect on variation of cobalt released by Na-montmorillonite with time.	105
28	Variation of nickel and cobalt sorbed on natural hectorite with time.	110
29	Variation of nickel and cobalt retained on natural hectorite with time.	110

TABLE		PAGE NO.
30	Variation of nickel and cobalt released from natural hectorite with time.	111
31	Nickel sorbed on Na-montmorillonite upon successive treatment with nickel chloride solution.	112
32	Nickel released from a nickel chloride saturated montmorillonite.	112
33	Influence of volume of added nickel solution on sorption by Na-montmorillonite.	117
34	Variation of nickel released from a nickel-montmorillonite, with initial solution volume.	117
35	Variation of nickel sorption on hectorite with particle size and nickel released with subsequent redispersion in distilled water.	118
36	Nickel sorption isotherm data on Na-montmorillonite.	119
37	Cobalt sorption isotherm data on Na-montmorillonite.	119
38	Cobalt sorption on Na-montmorillonite, at low concentration.	124
39	Cobalt released from a cobalt treated montmorillonite.	124
40	Nickel sorption on Na-montmorillonite, at low concentration.	129
41, 42, 43, 44	Nickel sorption on Na-montmorillonite at constant molar strength in the presence of competing cations (M^{n+}).	130
45, 46, 47, 48	Desorption of nickel from montmorillonite previously contacted with constant (0.04M) molar strength solutions containing competing cations.	137
49, 50, 51, 52	Cobalt sorption on Na-montmorillonite at constant molar strength in the presence of competing cations (M^{n+}).	138

TABLE		PAGE NO.
53, 54, 55, 56	Desorption of cobalt from montmorillonite previously contacted with constant (0.04) molar strength solutions containing competing cations.	139
57, 58, 59, 60	Nickel sorption on Na-montmorillonite at variable molar strength in the presence of competing cations.	140
61	Nickel sorption on Na-montmorillonite at low concentration in the presence of competing cations (M^{n+}).	144
62	Cobalt sorption on Na-montmorillonite at low concentration in the presence of competing cations (M^{n+}).	145
63	Summary of sorption data from Ni(II)/Co(II) interactions with Na-montmorillonite and hectorite.	151
64	Langmuir isotherm data and selectivity coefficients derived for cobalt sorption on Na-montmorillonite.	162
65	Langmuir isotherm data and selectivity coefficients derived for nickel sorption on Na-montmorillonite.	163
66	Langmuir isotherm data derived from nickel sorption on Na-montmorillonite at low concentration.	173
67	Langmuir isotherm data derived from cobalt sorption on Na-montmorillonite at low concentration.	173
68	Cation composition in final solutions from selected low level nickel sorption experiments.	177
69, 70, 71	Competitive Langmuir isotherm data derived for cobalt sorption in the presence of competing cations at constant molar strength.	183
72, 73 74	Competitive Langmuir isotherm data derived for nickel sorption in the presence of competing cations at constant molar strength.	184

TABLE		PAGE NO.
75	Comparison of nickel distribution coefficient (K_d(Ni)) variation with total solution molarity (at constant 1:1 M^{n+}:Ni).	191
76	Influence of organic material on nickel detection by atomic absorption.	198
77	Influence of organic material on cobalt detection by atomic absorption.	201
78	Proportion of amine complexes formed in the Ni/NH_3 systems at a number of different NH_3:Ni ratios.	202
79	d(001) values obtained from Ni-hectorite treated with model organic ligands.	206
80	Peaks derived from diffuse reflectance spectra of Ni-hectorite treated with model organic ligands.	206
81	d(001) values obtained from Co-hectorite treated with model organic ligands.	208
82	Peaks derived from diffuse reflectance spectra of Co-hectorite treated with model organic ligands.	208
83	Diffuse reflectance data from Ni- and Co-hectorite, rinse and wash.	210
84	d(001) values for Ni- and Co-hectorite, rinse and wash.	210
85	Physical characteristics of Ni-hectorite clay samples after treatment with solutions of organic 'ligands'.	212
86	Physical characteristics of equilibrium solutions remaining from treatment of Ni-hectorite clays with organic 'ligands'.	213
87	Physical characteristics of Co-hectorite clay samples after treatment with solutions of organic ligands.	215

TABLE		PAGE NO.
88	Physical data from equilibrium solutions remaining after treatment of Co-hectorite clays with organic ligands.	216
89	Physical data from equilibrium solutions remaining after treatment of Ni-hectorite clays with organic 'ligand' solutions at various concentrations.	218
90	Physical characteristics of Ni-hectorite clay samples after treatment with ammonia solutions at various concentrations.	218
91	Physical data from equilibrium solutions remaining after treatment of Co-hectorite clays with organic ligand solutions at various concentrations.	219
92	Physical characteristics of Co-hectorite clay samples after treatment with organic 'ligand' solutions at various concentrations.	219
93	Physical characteristics of Ni/Co-hectorite clay samples after treatment with organic 'ligand' solutions at various concentrations.	221
94	Physical data from equilibrium solutions remaining after treatment of Ni/Co-hectorite samples with organic 'ligand' solutions.	221
95	Nickel (copper) content and pH values of equilibrium solutions remaining after contacting $[Ni(en)_3]^{2+}$-hectorite with a number of inorganic salt solutions.	223
96	Cobalt released from a ^{60}Co-hectorite by solutions of organic compounds.	226
97	Reaction parameters using clay catalysed nitrobenzene reduction.	230
98	Corrected silicon 2p binding energy from montmorillonite and hectorite.	274

TABLE		PAGE NO.
99	Cobalt $2p_{\frac{3}{2}}$ binding energies for cobalt treated hectorite samples.	274
100	XPS parameters from hectorite after nickel sorption.	276
101	$Ni2p_{\frac{3}{2}}$ binding energies for nickel chloride sorbed on montmorillonite.	277
102	$Ni2p_{\frac{3}{2}}$ binding energies for nickel sulphate treated montmorillonite samples.	279
103	SEM/EDAX analysis of nickel sulphate treated 'Berkbond' montmorillonite, before washing.	280
104	SEM/EDAX analysis of nickel sulphate treated 'Berkbond' montmorillonite, after washing.	281
105	Analytical data from SEM/EDAX analysis of nickel chloride treated 'Berkbond' montmorillonite.	283
106	SEM/EDAX analysis of natural 'Berkbond' montmorillonite.	284
107	SEM/EDAX analysis of nickel sulphate treated 'Steetly' montmorillonite, before washing.	285
108	SEM/EDAX analytical data from nickel sulphate treated 'Steetly' montmorillonite, after washing.	286
109	SEM/EDAX analysis of 'Steetly' montmorillonite after treatment with nickel chloride, before washing.	287
110	SEM/EDAX analytical data from 'Steetly' montmorillonite after nickel chloride treatment and subsequent washing.	288
111	SEM/EDAX analysis of natural 'Steetly' montmorillonite.	289
112	Mössbauer parameters recorded from iron-exchanged hectorite.	330

TABLE		PAGE NO.
113	Mössbauer parameters of Fe^{3+} sorbed onto montmorillonite and hectorite.	329
114	Mössbauer parameters of Fe^{2+} exchanged onto various sorbents.	337

CHAPTER ONE

INTRODUCTION

1.1 BACKGROUND

At the present time there is serious debate on an international scale about the continued development and expansion of nuclear power. Most studies conclude, however, that production of nuclear energy will expand greatly in the next few decades,[1] and it appears ultimately that the progressively increasing requirement for power all over the world makes nuclear power the sole solution. The International Atomic Energy Authority reports that the world's nuclear capacity increased by 11% in 1980 and that the world's nuclear reactors supplied some 8% of the world's total electricity. Predictions were that nuclear electricity generation would provide 13% of the world supply by 1990[2].

The development of the nuclear power industry leads to a continuous and increasing production of the radioactive wastes which accompany the whole fuel cycle, beginning with uranium ore extraction and ending in spent-fuel reprocessing. The wastes can be stored safely in the relatively short term. However, the increasing generation and bulk of active material makes ultimate long term disposal unavoidable, this being necessarily secured in such a way that the segregation of the radionuclides generated, from man and the biosphere, is effected for the time needed to allow their decay to safe radioactivity levels.

The stringent requirements of a radioactive waste disposal site inevitably involve utilization of the inherent properties of clay minerals as a barrier to radionuclide migration.

ORIGINS AND CLASSIFICATION OF NUCLEAR WASTE

Radioactive by-products are produced at every stage of nuclear energy generation.

The winning of uranium from ores frees radium and other radioactive elements, which contaminate water supplies if released to the environment. The preparation of reactor fuel gives rise to wastes that require special handling, while the generation of energy from fissionable atoms in nuclear reactors also results in the production of hazardous material. Radioactivity stems both from the neutron activation of structural materials in the reactor and from the fission products formed in the fission process. Solvent recovery of unspent uranium and plutonium from used reactor fuel by reprocessing produces the largest proportion of active waste associated with the fuel cycle.

Most radioactive waste is a complex mixture composed mainly of inorganic species (transuranics, rare earths, transition metals, OH^-, Cl^-, PO_4^{3-} as well as plutonium and uranium) and, less commonly, organic constituents (ethylenediaminetetraacetic acid (EDTA), nitrilotriacetic acid (NTA), tributyl phosphate (TBP), oxalic acid).

A simple classification of the solid waste arising is as follows;[3]

Very low level wastes (VLLW) - wastes whose very low levels of activity mean that they can be safely disposed of without specific authorisation under the Radioactive Substances Act, 1960. Thus, disposal with household refuse (dustbin disposal) is acceptable for up to $0.1m^3$ of

material containing less than 400kBq* beta/gamma activity or single items containing less than 40kBq beta/gamma activity.

Low level wastes (LLW) - wastes containing radioactive materials other than those acceptable for dustbin disposal, but not exceeding 4GBq/tonne alpha (about 100mCi/tonne) or 12GBq/tonne beta/gamma (about 300mCi/tonne) activity.

Intermediate level wastes (ILW) - wastes with radioactivity levels exceeding the upper boundaries for LLW, but which do not require heat generation to be taken into account in the design of storage or disposal facilities.

High level wastes or heat generating wastes (HLW or HGW) - wastes in which the temperature may rise significantly as a result of their radioactivity, so that this factor has to be taken into account in designing storage or disposal facilities.

Table 1 lists the principle types of ILW and LLW in the U.K.[4]

The disposal methods employed in waste management consequently depend on the category of material under consideration.

Table 1 - The principle types of ILW and LLW generated in the U.K.[4]

ILW	LLW
Fuel cladding Sludges, resins and concentrates Pu contaminated material Graphite Filters Miscellaneous equipment	Resins from secondary circuits Filters from secondary circuits Miscellaneous equipment Protective clothing

* $1Ci = 3.7 \times 10^{10} Bq = 3.7 \times 10^{10}$ disintegrationss^{-1}

Table 2 - Estimated total radioactive waste volumes in the U.K.[3,4]

Date	Volume of waste arisings/m^3		
	HLW	ILW	LLW
1981	-	30 000	a
2000	4 300	85 000	650 000

a - LLW is largely disposed of as it is produced, so no accumulated volume is recorded.

1.3 RADIOACTIVE WASTE DISPOSAL

Predicted volumes of radioactive waste arising up to the year 2000 (table 2) indicate that this steady accumulation necessitates the formation of a disposal strategy.

Radioactive waste is far from a uniform substance. It is a mixture of elements with greatly different half-lives, specific energies, and chemistry. These variations in characteristics bring about the need for diversified strategies in waste management. Options presently being considered (mainly for HLW) involve seabed disposal[5], disposal in subduction zones, transmutation, ejection into space and even burial on the moon, but the most commonly accepted method is underground burial within some extensive geologic formation.

Two systems of underground vault disposal are necessary; (1) HL and long lived IL (LLIL) wastes require disposal site integrity to remain intact for many thousands of years due to the presence of long lived radionuclides (2) Short lived IL (SLIL) and low level wastes require a less sophisticated vault design to give roughly 500 years containment.

Both strategies encompass a multibarrier vault design, an outline of which is given in Fig. 1.

Each individual barrier is capable of very high radionuclide retention. Assessment of vault effectiveness involves evaluation of the suitability of the waste form, its containment, the backfilling materials placed around the waste, and the host rock.

The waste form, especially of the highly active material, should be such that it guarantees lowest leachability of radionuclides, and relevant properties include chemical, mechanical, thermal and radiation stability.

It is very probable that the liquid HL and LLIL waste will be solidified - a matrix of glass appears most acceptable[6,7], but more recently ceramic[8] and metal matrix[9] forms (coated particles in a metal matrix) have been considered. LL and SLIL waste will most probably be immobilised in cement, bitumen or organic polymers.[10]

The container within which the waste is encased must act as a further barrier to radionuclide migration and, hence, must show a desirable stability under the specific geologic conditions, such as Eh and pH. Materials under consideration are titanium, copper, nickel-based alloys and stainless steel (for HL and LLIL waste[4]) and ordinary steel for LL and SLIL waste.[11]

The overpack material must act as a significant barrier to migration of any radionuclides leached by groundwater intrusion, from the waste form. For both vault systems the overpack will consist of an expanding clay with additives such as pH buffers.

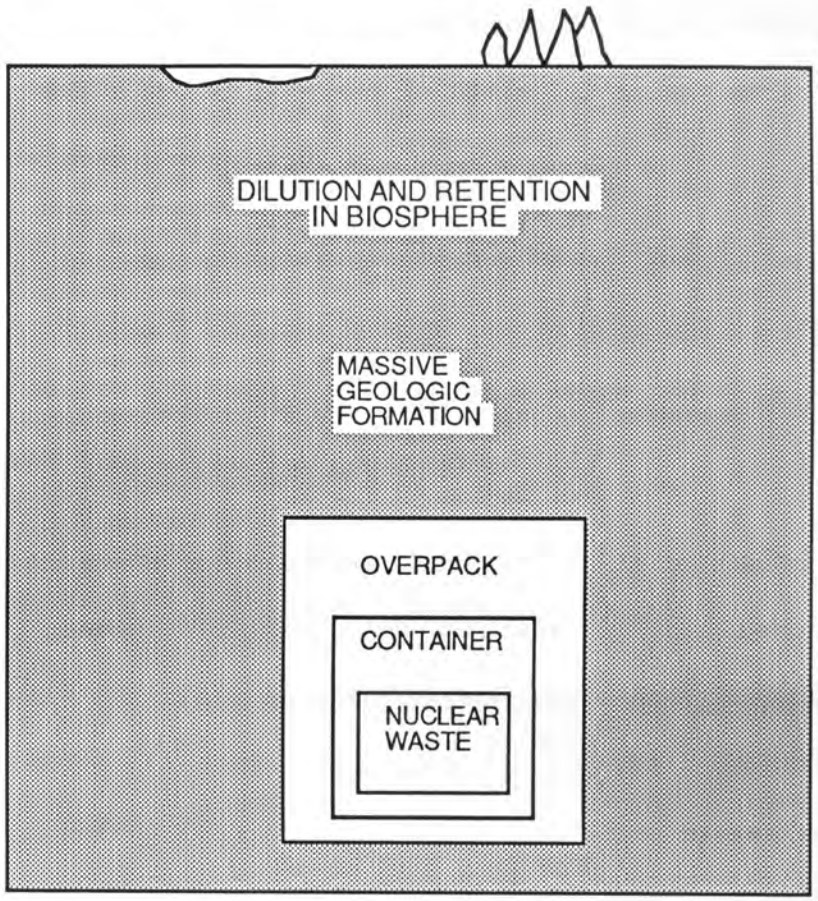

FIG 1-SCHEMATIC ILLUSTRATION OF THE DISPOSAL VAULT CONCEPT OF NUCLEAR WASTE ISOLATION

The final barrier to radionuclide migration is the host rock formation, which should have the desirable thermal, mechanical, sorption and general physical properties. Typical materials under investigation for HL and LLIL waste burial are volcanic tuffs, anhydrite, granite, basalt, shale and clay minerals while for LL and SLIL wastes, clay minerals dominate proposals.

Although the multibarrier approach appears to rely on a number of distinct barriers for its integrity, it must not be forgotten that the system has to show compatibility as a whole, so interactions between different components is undesirable.

In all of the waste disposal concepts, it is implicitly assumed (more probably only for HL and LLIL wastes) that groundwater will eventually penetrate to the disposal vault and initiate leaching of radionuclides from the waste form.[2,12,13] The hypothetical sequence of events occuring within such a waste isolation system would be as shown in Fig. 2. Hence, to evaluate the usefulness of a burial disposal technique, the ability of individual barriers to sorb and retain radionuclides must be assessed.

1.4 ROLE OF CLAY MINERALS IN RADIOACTIVE WASTE DISPOSAL

Clay minerals exhibit a wide variety of roles in radioactive waste disposal. As well as being the only real candidate to be considered as overpack material in the HL and LLIL waste vault system, clay deposits also exhibit potential to act as the host geologic formation e.g. Boom clay in Belgium.[14] Other suggested host rocks will rely to a certain extent on secondary clay minerals deposited in fissures,

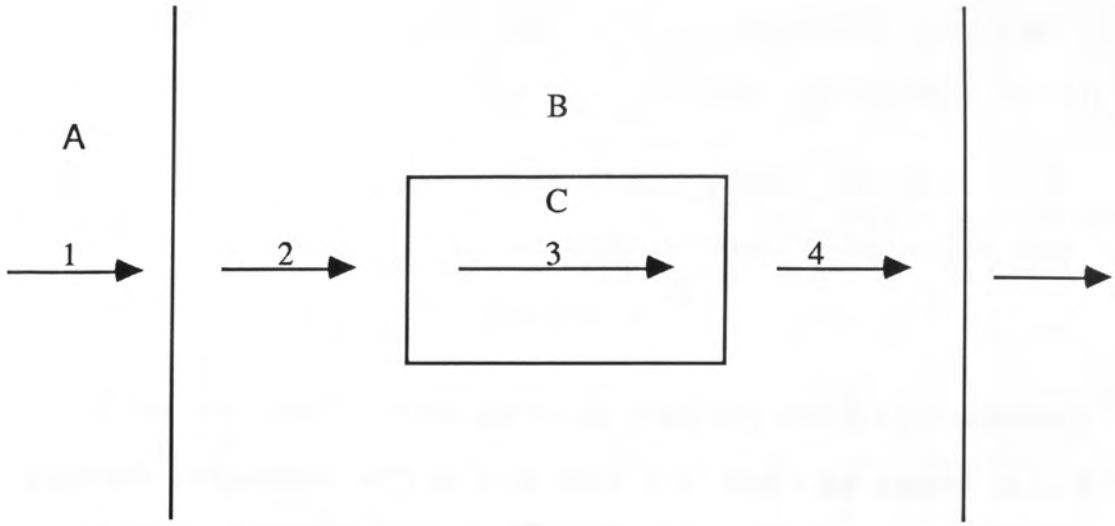

A - GEOLOGIC BARRIER, B - BACKFILL BARRIER,
C - CANISTER + WASTEFORM.

1 - GROUNDWATER MOVEMENT,
2 - RETARDED GROUNDWATER MOVEMENT,
3 - RADIONUCLIDE LEACHING,
4 - RETARDED MIGRATION.

FIG 2. HYPOTHETICAL SEQUENCE OF EVENTS OCCURING DURING LEACHING OF RADIONUCLIDES FROM A VAULT DISPOSAL SITE.

pores, vesicles and fractures for sorption properties e.g. basalt, halite.[15]

The feasibility of emplacing radioactive wastes in sub-seafloor geologic formations is dependent on the radionuclide sorption properties of widely dispersed clay minerals e.g. Abyssal red clay.[16]

Clay minerals will constitute the host geologic formation in LL and SLIL waste disposal, as recently proposed by NIREX (Nuclear industry radioactive waste executive).[17]

Clays can also be found as particle coatings which will dominate sorption properties of the bulk rock e.g. smectite coated silica particles in basalt deposits.[18]

1.5 CHARACTERISTIC FEATURES OF CLAY MINERALS

In order to understand the properties exhibited by clay minerals, a knowledge of their structural characteristics is required.[19] Two structural units are involved in the atomic lattices of clay minerals. One is the $(SiO_4)^{4-}$ unit which may be called the silica tetrahedron. When three oxygen atoms of each silica tetrahedron are linked to similar units, a continuous sheet structure, the phyllosilicate structure, is formed (Figure 3).

The sheet of silicon-oxygen atoms is capable of indefinite extension in two dimensions.

In most structures the silica tetrahedral units are arranged in the form of "hexagonal" rings, which repeat indefinitely throughout the sheet structure. The electrically unsatisfied (valence) oxygen atom of each tetrahedron points vertically upward in the sketched arrangement. This silicon-oxygen structure is called the tetrahedral or silica sheet.

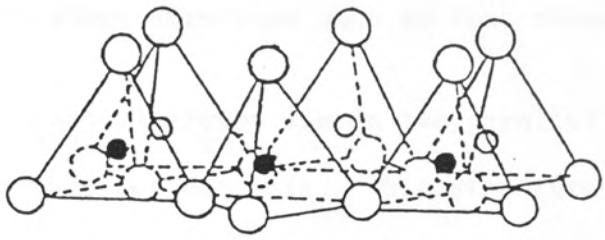

○ and ◌ = oxygen, ● and ○ = silicon

Fig.3 - Diagrammatic sketch showing sheet structure of silica tetrahedrons arranged in a hexagonal network.

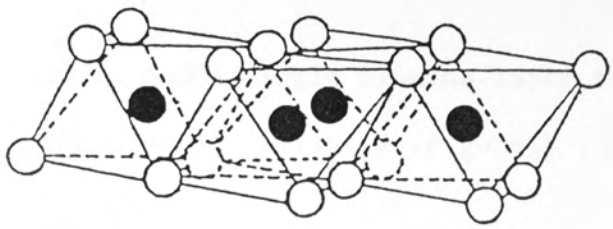

○ and ◌ = hydroxyls, ● = aluminium

Fig.4 - Diagrammatic sketch showing sheet structure of the octahedral units.

The second structural unit involves the coordination of an aluminium atom to six oxygen atoms, or hydroxyl groups, which are arranged in a regular octahedron environment, within which the aluminium atom is centrally located. The sharing of oxygen atoms by neighbouring octahedra results in a sheet structure such as that shown in Figure 4.

The oxygen atoms and hydroxyl groups lie in two parallel planes, with aluminium atoms sandwiched between them. This structure is called the gibbsite ($Al(OH)_3$), octahedral or alumina sheet.

The tetrahedral and octahedral structures have closely similar a and b dimensions, so the two sheets may effectively be condensed onto one another to form a single composite layer. The fourth oxygen atom protruding from the tetrahedral sheet is now shared with the octahedral sheet.

The linking of one silica and a single alumina layer forms the basis of the structure of the mineral kaolinite (Figure 5).

As the valency contribution of each aluminium ion to each coordinating anion is one-half, the "valency" oxygens of the silica sheet, which all point vertically upwards, have to be linked to two aluminium atoms. Each oxygen atom thus receives one valency-share from a silicon ion and half from each of two aluminium ions and is electrically satisfied. Each aluminium ion is coordinated with three oxygen atoms linked to silicon atoms and to three hydroxyl units. Since the basic kaolinite structure consists of one tetrahedral and one octahedral sheet, it is called a two-layer clay mineral. This combination of the two sheets is called a unit layer. Kaolinite forms crystals which contain many of these unit layers stacked above each other, thereby giving extension

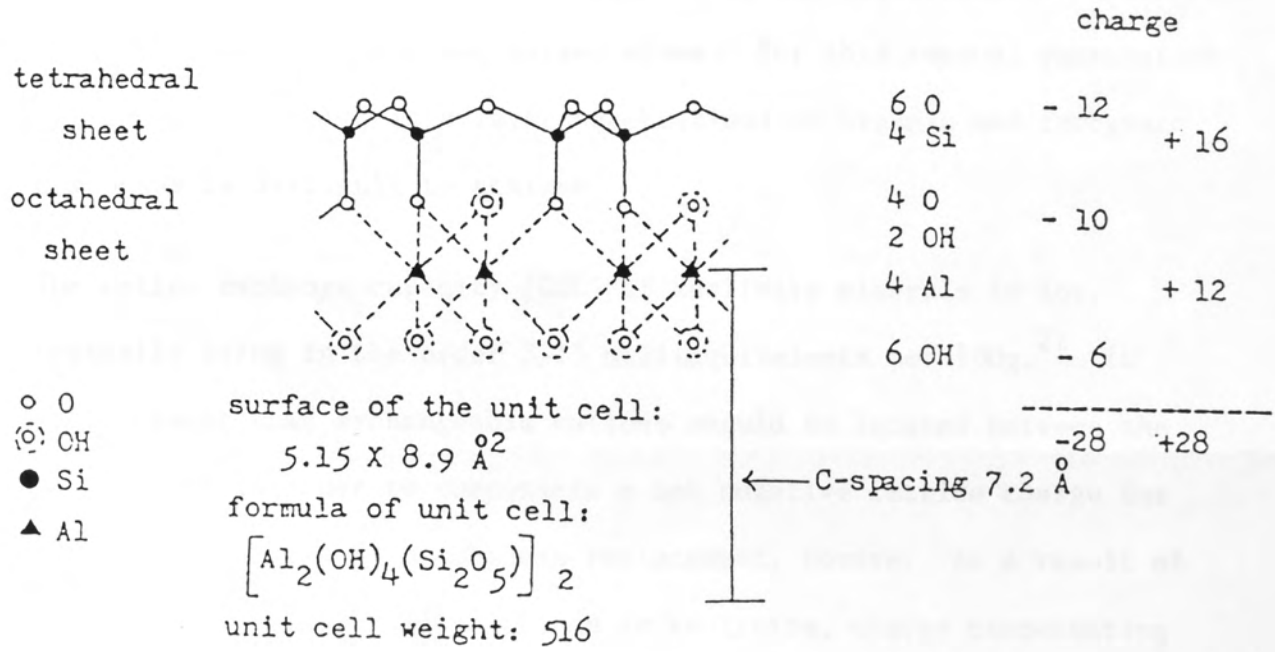

Fig.5 - Atom arrangement in the unit cell of the two layer clay mineral kaolinite (schematic).

along the c-axis.

The distance between a certain plane in the unit layer and the corresponding plane in the next unit layer is called the d(001), basal or c-spacing. The basal spacing is characteristic for a particular group of clay minerals, being typically 7.15Å[20] for kaolinite.

The unit layers are firmly held together by the electrostatic interaction between hydroxyl groups and oxygen atoms. For this reason, penetration between unit layers (interlayer penetration) of organic and inorganic compounds is difficult to achieve.

The cation exchange capacity (CEC) of kaolinite minerals is low, typically being in the order 3-15 milliequivalents per 100g.[21] It would appear that exchangeable cations should be located between the unit layers in order to compensate a net negative lattice charge due to a small degree of isomorphous replacement. However, as a result of the strong interlayer interactions in kaolinite, charge compensating (i.e. exchange) cations are only found at the surface of a stack of unit layers constituting a particle.

The gibbsite layer considered above in the two-layer mineral kaolinite, consists of two sheets of hydroxyl units with linking cations: the top sheet is similar to the bottom one and so condensation of a further silica network, completes a sandwich structure of two silica sheets with a gibbsite sheet between. This structure is capable of indefinite extension in two dimensions. The 2-dimensional structure formed is called the pyrophyllite layer (Figure 6) and the mineral pyrophyllite is built up of successive layers stacked above one another.

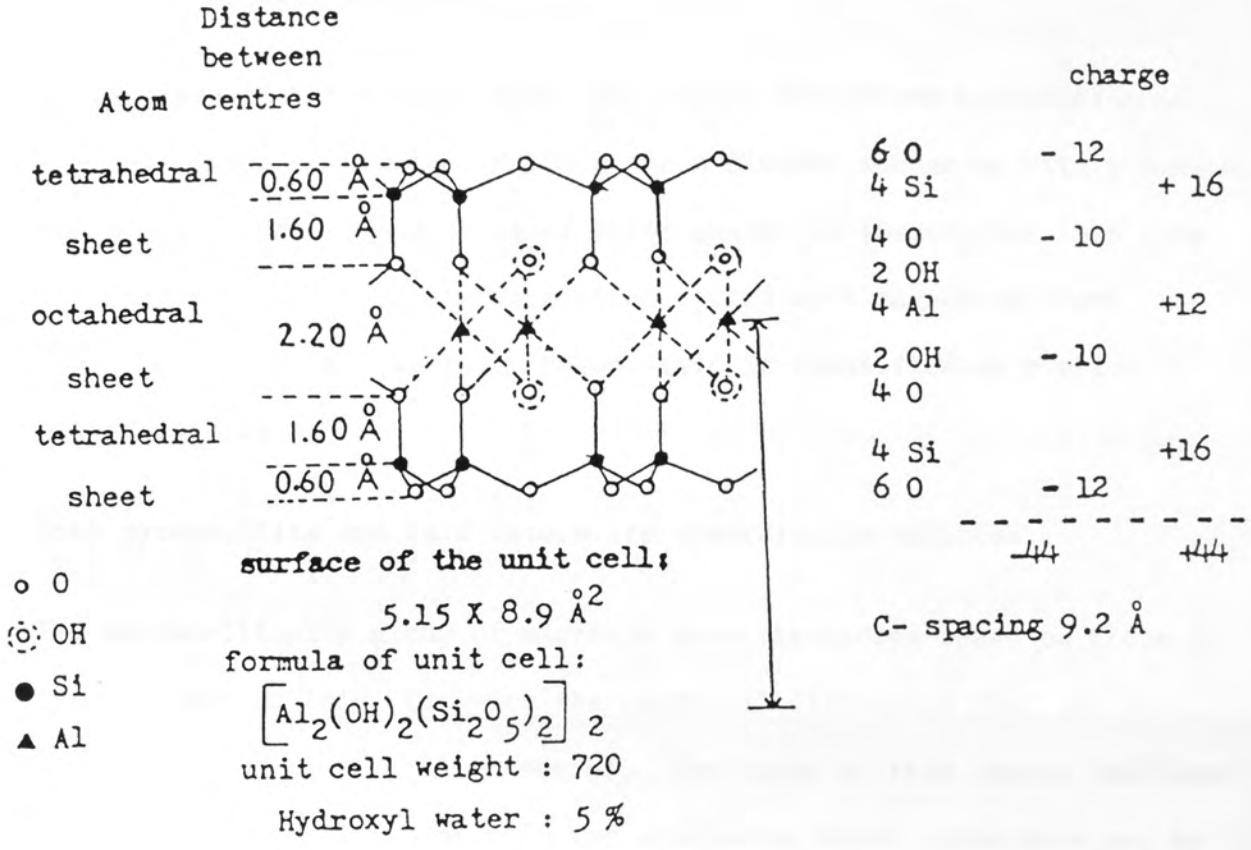

Fig.6 - Atom arrangement in the unit cell of the three layer mineral pyrophyllite.

The aluminium atoms in this structure occupy only two out of every three octahedral lattice sites, and so pyrophyllite is classified as a dioctahedral mineral.

In the case of the mineral talc, two silica sheets are condensed onto a single sheet of brucite, $Mg(OH)_2$, in a similar manner as with gibbsite. Again a unit layer consisting of three sheets is formed, but this time with all the octahedral lattice sites filled with magnesium atoms (c.f. $Mg^{2+}x3=+6$, $Al^{3+}x2=+6$). Hence, talc is classified as a trioctahedral mineral.

Both pyrophyllite and talc layers are electrically balanced.

The montmorillonite group of minerals have structures based on those of pyrophyllite or talc, but with the essential difference that the unit layers are not electrically neutral. The cause of this charge imbalance is isomorphous replacement. In the octahedral sheet, aluminium may be replaced by magnesium,[22, 23] iron,[22, 24] nickel,[25] lithium[22] and other atoms, and to a lesser extent, silicon in the tetrahedral sheet can be replaced by aluminium. In clay minerals, the replacement of a lattice cation by another of lower charge is very often the case, resulting in an excess of negative charge. This excess negative lattice charge may be compensated for by the adsorption on the layer surfaces, of cations which are too large to be accommodated into the interior of the lattice.

In an aqueous environment, these charge compensating cations can be exchanged with other cations in solution. The amount of exchangeable cations can be determined analytically and this characteristic of clay minerals is called the cation or base exchange capacity and is expressed

in milliequivalents per 100g of dry clay (meq/100g).

Unlike the kaolinite minerals, the montmorillonite group have only weak Van der Waals attractions between unit layers due to tetrahedral sheet being positioned adjacent to tetrahedral sheet. Hence, interlayer expansion becomes easier, and polar organic molecules as well as inorganic cations can be sorbed onto the internal surfaces. Thus apparently two types of exchange site exist: (1) those within the interlayer region of the clay responsible for $\simeq$80% of the exchange capacity in montmorillonite, (2) those on the external surface due to compensation of excess negative charge resulting from broken bonds.

The presence of the interlayer cations causes an increase in basal spacing of montmorillonites as compared with pyrophyllite although the difference is smaller than the size of the compensating cation due to its partial withdrawl into the holes of the tetrahedral sheet.

A basal-spacing of 9.8Å[22] is typical of a sodium saturated montmorillonite, although unlike kaolinite, this cannot be taken as the value consistently found for montmorillonite samples in general: hydrated sodium-montmorillonite has a basal-spacing of 12.5Å[26] and calcium-montmorillonite has a value of 15.4Å.[26] Hence, the c-spacing is characteristic of the species sorbed in the interlayer region. Organic molecules may also be absorbed by montmorillonite[27] showing consequent shifts in the c-dimension e.g. absorbed glycerol exhibits a c-spacing of 17.7Å.[28]

The three-sheet clay minerals are called smectities and are classed into dioctahedral and trioctahedral types. Of the dioctahedral type,

montmorillonite, beidellite and nontronite form the end-members and a complete set of solid solutions exists between them. Montmorillonite has 0.33 of the octahedral aluminium atoms replaced by magnesium per unit formula so requiring 0.33 sodium ions to compensate for the excess negative lattice charge.

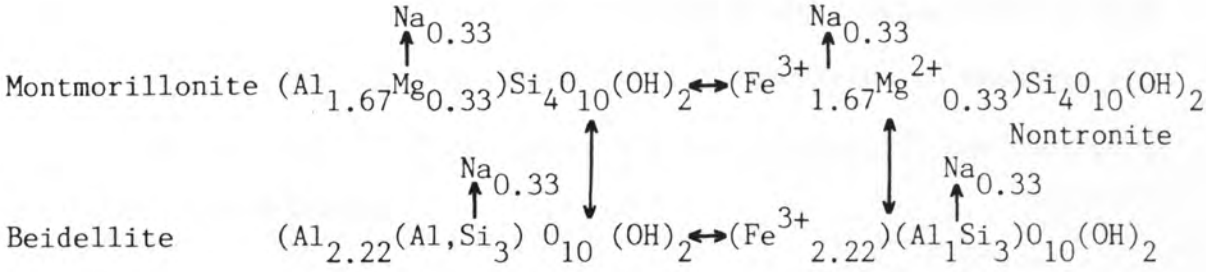

There is also a series of minerals of the trioctahedral type with two end members represented by the formulae:

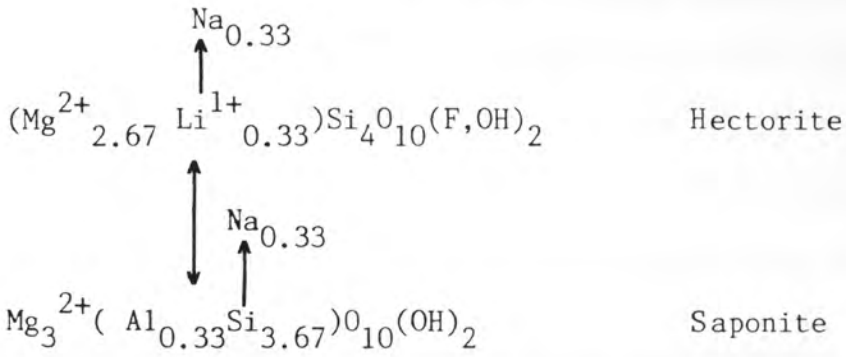

Apparently there is a complete range of solid solutions between the two extremes. Hectorite has 0.33 of its octahedral magnesium atoms replaced by lithium, per unit formula, which then necessitates the admission of 0.33 sodium ions to compensate for the negative lattice charge.

A value for the basal-spacing of 15.8Å was quoted by Nagelschmidt[22] for hectorite.

In the above theoretical formulae, the exchangeable cation has been indicated as sodium. This is not necessarily the natural form of the mineral, for other cations such as Ca^{2+} and K^{+} may be absorbed. The structural formula is not influenced in any way by the inclusion of other cations, but the properties of the mineral may be considerably affected.

These exchangeable cations can be replaced by many other cations from an aqueous solution. Hence, the ability of smectites to exchange out active radionuclides from solution, and their potential usefulness as a barrier to migration.

The ion exchange phenomenon of clay minerals can be envisaged from structural characteristics, but clay formations exhibit other useful properties which are relevant to radioactive waste disposal. These include a very low permeability (typical values being of the order 4 to 10 x 10^{-3} cm^2 s^{-1} cm^{-1} through a 1cm thick slab),[19] a crushing strength of 3.5kgm^{-2} for a ball clay and 6.1kgm^{-2} for a plastic clay,[6] a thermal conductivity of 0.9 Jm^{-1} s^{-1} K^{-1} (for Boom clay)[29] and also the ability to swell and flow plastically to seal and fill voids.

1.6 FACTORS AFFECTING CATION SORPTION ON CLAY MINERALS

Cation exchange mechanisms in clays

Already an appreciable quantity of data has been accumulated regarding the exchange of different cations with a wide range of clay minerals under a variety of conditions. The results of those studies indicate that extrapolation of cation behaviour from one mineral to another, and the effects of system variables on cation exchange can be somewhat unreliable.

A useful outline, however, can be drawn from these studies of the relevant variables which influence the sorption process. Factors which are pertinent are sorbate ion, exchangeable sorbent ion on the clay, clay mineral type itself, cation exchange capacity of the clay, concentration of competing cations in solution, pH, presence of anions, presence of ligands.

Initially it was simply assumed that an ion with greater electrostatic charge, would be more strongly sorbed and for ions of the same charge the smaller ion would be most strongly held by its closer approach to the clay surface. However, considerations of the hydrated ion radius indicated that the smaller ion will be more strongly solvated and, therefore, have a greater hydrated ion radius. In general, a high charge:size ratio will give maximum sorption and the series of ionic replacement will be $M^{3+} > M^{2+} > M^{+}$. Simple ion exchange theory was initially followed[19] and is governed by the laws of mass-action from which the selectivity coefficient (K_s) is straight-forwardly calculated as:[30]

$$K_A^B = \frac{(M_B)_r \ (M_A)_s}{(M_A)_r \ (M_B)_s}$$

for two monovalent ions, A and B, of the same sign, where $(M_A)_r$, $(M_B)_r$ and $(M_A)_s$, $(M_B)_s$ are activities in solid and solution phases respectively.*

* In the nuclear industry the distribution coefficient (K_d) is often used in preference to K_s, where:

$$K_d = \frac{V}{M} \frac{(C_1 - C_2)}{C_2}$$

V = volume of contacting solution
M = mass of sorbent
C_1 = initial solution metal ion concentration
C_2 = final solution metal ion concentration

An inconsistent selectivity coefficient with varying ratios of ions on the clay surface indicated by Van Olphen[31] suggests deviation from ideal behaviour. Cations, in these cases have differing selectivities for the exchange sites.

Egozy[32] observed variable distribution coefficients with salt concentration, pH and increased loading on the clay, for cadmium and cobalt sorption on montmorillonite. He proposed two classes of adsorption sites, one being a 'classic' cation-exchange site, and the other being due to 'broken bonds' at edges of the montmorillonite particles. The presence of these two sites was also proposed by Peigneur et al[33] to explain the behaviour of a number of montmorillonite clays towards cobalt sorption. Clays with a larger particle size showed a lower selectivity coefficient due to the decreased contribution of 'broken bond' sites.

Initial studies by Hodgson[34] on the reactions of cobalt with montmorillonite in the presence of excess $CaCl_2$ showed the bound cobalt to consist of at least two main forms, one of which could be specifically exchanged with cations of Cu^{2+},Zn^{2+},Ni^{2+},Fe^{2+},Mn^{2+} or more Co^{2+}. Further investigation[35] of this specific sorption (i.e. not purely electrostatic) indicated no involvement of edge surfaces, but suggested combination with external basal surfaces and to a limited extent, with internal basal surfaces.

Maes et al[36] showed that the extent of irreversible adsorption of Co^{2+} and Zn^{2+} ions in sodium-montmorillonite depended on the composition of the solid phase. Below 70% of the cation exchange capacity, the exchange was completely reversible, but beyond this cations became

irreversibly fixed and it was recognised that there was no thermodynamic justification for expressing a selectivity coefficient. This adsorption process was discussed in terms of involving either structural hydroxyl groups of the clay or residual structural hydroxyaluminium compounds resulting from acid pretreatment.
De Mumbrum[37] also inferred involvement of structural hydroxyl groups in sorption of Cu^{2+} and Zn^{2+} on montmorillonite, vermiculite and chlorite. Swartzen-Allen et al[38] described the formation of $Al\text{-}OH_2^+$ groups by breaking of Al-O-Al linkages at crystal edges, giving rise to charged groups such as $Al\text{-}O^-$ and Al^+. Upon proton adsorption these give rise to $Al\text{-}OH_2^+$. These sites appear to be most important on illite and kaolinite (as opposed to montmorillonite).

Inconsistency in selectivity coefficient along a given isotherm was observed for $Na^+\text{-}Ca^{2+}$, $K^+\text{-}Ca^{2+}$ exchange on montmorillonite by Banin.[39] He attributed this variation to structural properties of the mineral, namely tactoid formation in the calcium state. A minimum is found in the monovalent-divalent selectivity coefficients, at approximately the 10% exchange level, which is attributed to initial sorption of monovalent ions on external surfaces of the tactoids, which results in a steadily decreasing K_s until invasion of internal surfaces occurs forcing apart the constituent platelets of the tactoid.

The importance of tactoid structure on selectivity was reported by McBride[40] who observed considerable deviation from ideal mass-action behaviour for exchange between ions of unequal charge.

Some uptake of metals by clay minerals may be by a non-exchange

reaction. Tiller[41] observed two forms of specifically sorbed Co^{2+} and Zn^{2+} ions on montmorillonite, one of which was exchangeable with other cations and another which proved unexchangeable. The latter form was considered to result from lattice penetration. Traynor et al[42] observed sorption of $[M(bipyridyl)_3]^{2+}$ (M = Fe, Cu, Ru) complexes beyond the cation exchange capacity of hectorite. They proposed reaction to occur by two mechanisms: (1) replacement of Na^+ ions in the native mineral by cation exchange up to the cation exchange capacity, and (2) intersalation of excess salt beyond the exchange capacity.

The influence of cation hydration, ionic size, charge and polarizability has been studied in regard to the strength of bonding forces with clays. Various approaches have yeilded the same or similar orders with respect to the relative strength of interactions of inorganic cations with clay surfaces.

Hodgson[34] evolved a relative affinity series for a number of cations with montmorillonite from measurement of the effeciency of each ion to release ^{58}Co from a previously prepared ^{58}Co-montmorillonite (table 3).

Table 3 - Cation affinity series for montmorillonite (from ability of cation to displace another from an exchange site)[34,43]

Hodgson	$Cu^{2+} > Co^{2+} > Zn^{2+} > Fe^{3+} = Fe^{2+} = Ni^{2+} = Mn^{2+} > Mg^{2+} = NH_4^+$
Basu et al	$Zn^{2+} > Mn^{2+} > Ni^{2+} = Co^{2+} > Cu^{2+}$

Basu et al[43] also used displacement reactions on transition metal saturated montmorillonite, but exchanged H^+ ions for the respective metal (table 3).

Carter[44] found maximum uptake of metal ion on montmorillonite and kaolinite from single element solutions to depend on the nature of the cation (table 4). In competition experiments using four metals, a different affinity series is observed, but this is difficult to interpret as solutions were made to represent an industrial effluent and metal concentrations varied widely (table 5).

Table 4 - Maximum uptake data from single cation solutions[44]

Montmorillonite	$Cr^{3+} = Fe^{3+} > Zn^{2+} > Cu^{2+} = Ni^{2+} > Cd^{2+} > Pb^{2+}$
Kaolinite	$Cr^{3+} = Fe^{3+} > Zn^{2+} > Cu^{2+} > Ni^{2+} = Pb^{2+} > Cd^{2+}$

Table 5 - Order of % reduction in adsorption from a four element solution compared with the single element solution[44]

Montmorillonite	$Zn^{2+} > Cu^{2+} > Ni^{2+} > Cr^{3+}$
Kaolinite	$Cu^{2+} > Zn^{2+} > Cr^{3+} > Ni^{2+}$
decreasing % reduction $\longrightarrow$	

Basu et al[45] obtained a selectivity sequence from exchange isotherms of Ni-, Co- and Cr- saturated clays obtained against Na^+, K^+, NH_4^+, H^+, Mg^{2+} and Al^{3+} ions (table 6). A consistent order of release was observed

except for the anomalous behaviour of H^+.

Table 6 - Affinity series for Ni, Co, Cr sorption on montmorillonite[45]

Cr > Ni = Co

Experimental studies on manganese, cobalt, nickel, copper and zinc sorption from a seawater solution, on Na-montmorillonite and treated red clay were carried out by Takematsu[46] in connection with the mechanism by which transition metals are removed from marine environments.

Measurement of selectivity coefficients indicated the varying degree to which sorption of individual cations occurred (table 7).

Table 7 - Order of sorption affinities of transition metals for Na-montmorillonite and treated red clay[46].

Cu > Zn > Ni > Co > Mn

The variable cation affinity sequences indicated above may be due either to the solution composition or nature of the clay mineral surface.

Carter's[44] results for sorption from multi-element solutions demonstrate different affinity sequences for heavy metal sorption onto montmorillonite and kaolinite (table 5). This indicates selectivity differences between the clays, although the complex nature of Carter's solutions do not enable simple conclusions to be drawn.

Farrah et al[47] observed different comparative uptake affinity sequences on kaolinite, illite and montmorillonite when studying competitive adsorption from solutions having initial metal ion concentrations equal

(8.3×10^{-5}M) (table 8). These sequences differ from those previously proposed[48] in a study in which an excess of one cation (1.7×10^{-4}M) was allowed to contact the clay prior to the addition of varying amounts of a second divalent cation. With illite and kaolinite, the species added first tended to attain a near saturation value, with the second species taking up additional sites. Some displacement occurred when the concentration of added cation approached or exceeded the equilibrium concentration of the initial cation. On montmorillonite, displacement occurred more readily and calculation of selectivity coefficients indicated the order of preference was Ca>Pb>Cu>Mg>Cd>Zn. Farrah et al concluded that relative ranking orders had little meaning unless the specific basis for the comparison was clearly enunciated.

Table 8 - Comparative metal ion uptake affinity sequences[47]

Kaolinite	Zn>Cu>Ca>Pb>Cd>Mg
Illite	Ca>Zn>Pb>Cu>Cd>Mg
Montmorillonite	Pb>Ca>Cu>Zn>Cd>Mg

In their study on copper sorption, Menzel et al[49] observed a higher proportion of copper sorbed as $Cu(OH)^+$ on kaolinite than on montmorillonite. This was apparently caused by kaolinite facilitating deprotonation of water in the hydration sphere of sorbed copper(II).

Jensen[50] also found cation sorption behaviour to be dependent on the type of clay mineral used. Kaolinite demonstrated a lower K_d value than both montmorillonite and illite for all metal ions studied but

the latter two could not be ranked in any consistent order.

The nature of the sorbent clay mineral was observed to influence the sorption of $Ni(NO_3)_2$ at pH6 and $Cu(NO_3)_2$ at pH5, which did not follow the same trend as the cation exchange capacity of the minerals concerned[51] i.e. order for sorption: chlorite>illite>kaolinite

cation exchange capacities: illite>chlorite>kaolinite

However, Farrah et al[47] did observe increasing metal ion sorption with increasing cation exchange capacity of the clay, i.e. montmorillonite> illite>kaolinite. This behaviour was observed by Carter[44] but she used initial metal ion concentrations higher than the cation exchange capacities of montmorillonite or kaolinite so her results were rather predictable. Monsef-Mirzai's[52] study involving copper and chromium sorption on montmorillonite and kaolinite indicated a much more significant uptake by the former mineral, as expected.

The influence of clay mineral type on sorption was clearly exhibited in exchange isotherms of $[Co(pn)_3]^{3+}$ (pn = 1,2-propylenediamine) on Na-laponite and Na-vermiculite. The complex was more strongly sorbed on the latter clay due, according to Sarkar et al,[53] to its higher charge density.

The exchange properties of clay minerals also depend on the nature of the exchangeable cation initially associated with the surface. Most experimental observations indicate the predictable response of increasing metal ion sorption with decreasing charge and increasing hydrated size of the exchangeable ion. For example, Garcia-Miragoya et al[54] equilibrated low concentrations (15-200ppb) of cadmium with

samples of homoionic clays. The amount of cadmium sorbed on the montmorillonite depended on the exchangeable cation, decreasing in the order, Na->K->Ca->Al-montmorillonite. A very high affinity of cadmium for the montmorillonite surface at these concentrations was found, although the Al-clay was somewhat anomalous in behaviour, allowing only weaker sorption.

Nickel sorption onto H-, Na- and Ca- saturated montmorillonites was studied by Bansal et al[55] at a number of pH's and temperatures. They stated that adsorption followed the order, Na->H->Ca-montmorillonite, although nickel showed a high affinity for all clays. A further study[56] of nickel adsorption onto monoionic montmorillonites indicated a high affinity of nickel for the clay surface and adsorption increased as follows:

Mg-<Ca-<Na-montmorillonite.

An increased cation uptake with increasing pH is widely reported. Most authors agree that the main cause for this increase is a decrease in competition from H^+ ion as the pH rises. However, Tiller[57] apparently observed significant dissolution of hectorite at low pH values, which brought appreciable quantities of magnesium and silicon into solution.

Carter[44] found an increase in uptake for most metals between pH0 and 4 on montmorillonite and kaolinite but little difference between pH4 and 9. A decrease in Fe(III) adsorption with decreasing pH was observed by Whittig et al[58] on montmorillonite. This effect was attributed to increased competition from H^+ ions and modification of the iron speciation - negligable dissolution of the clay was observed.

Farrah et al[48,59] also attributed increased sorption of lead, copper,

zinc and cadmium, on three clays, with increased pH, to decreasing competition from H^+ ions. Their data indicate that this competitive effect should virtually disappear at pH6, at which point sorbed metal ion concentration will be at a maximum. An initial investigation of the sorption of cobalt and zinc on Na-montmorillonite by Maes et al[36] indicated increased metal ion uptake with increasing pH, in the pH range 4.6-6. Peigneur et al[33] consequently compared the ion exchange behaviour, towards the cobalt ion, of five Na-montmorillonite clays at a number of solution pH's. Differences in ion exchange behaviour of the clays were interpreted as arising from the presence of two sorption sites - one in the interlayer region (i.e. due to isomorphous substitution) and the other at the particle edges. A decreased selectivity coefficient with decreased pH was apparent for all clays and was attributed to decreasing participation of the very much pH dependent 'broken bond' site in the exchange reaction. Similar conclusions were drawn from further work by the same group[60] on transition metal (Co, Ni, Cu, Zn, Cd) ion exchange in montmorillonites. An increase in exchange capacity observed with increasing pH was again attributed to participation of the 'broken bond' site.

In Bansal et al's[55] investigation into the sorption of nickel(II) at relatively low concentrations on H-, Na- and Ca-montmorillonites, an increased nickel uptake was observed with increasing pH up to a maximum at pH6. Bansal et al, however, like many authors, fail to attach any significance to changes in metal ion speciation with pH. For example, a study by Sylva et al[61] on the hydrolysis of lead(II) at low solution concentrations (2×10^{-3} and 1×10^{-4}M) indicated the presence of a large proportion of the lead as $[Pb(OH)]^+$, $[Pb_3(OH)_4]^{2+}$, $[Pb_4(OH)_4]^{4+}$

and $[Pb_6(OH)_8]^{4+}$ species at pH7. The decreasing metal ion sorption from pH6 to 10 following a maximum at pH6 observed by Bansal et al,[55] may be due to a decreased affinity of the clay surface for the new solution species at higher pH because of their increasing size (i.e. greater difficulty in penetrating clay interlayers) and lower charge density.

Whittig et al's[58] observation of increased iron(III) uptake with increasing pH, mentioned earlier, was attributed to some extent to speciation effects. However, from consideration of electrostatic interactions the dominant species apparently present in solution at pH2.5, $[Fe_2(OH)_2]^{4+}$, should be sorbed less strongly than the Fe^{3+} present at lower pH's. This effect is not observed and so it would appear that pH variations can play two roles in influencing sorption. At low pH's (probably less than 6) competition of H^+ ions with the metal ions dominates sorption. At high pH values, speciation of the metal ion is most influential.

Additional evidence in support of this concept was gained from Farrah et al's[62] observation of copper(II) sorption on montmorillonite and illite. They observed a steady uptake of metal ion with increasing pH until a pH of 6 when precipitation took place. However, complexation of the copper in solution by tartaric acid and oxalate prevented precipitation of $Cu(OH)_2$, and further uptake of copper on the clays was observed up to a pH of ≃9. A continued sorption of metal ion beyond pH6 due to decreased H^+ ion competition would, therefore, apparently occur if speciation did not become important at this point, as predicted above. The precipitation of uncomplexed copper(II) appears to

contradict results of Bansal et al[55] who found no nickel precipitation up to pH values of 10, but concentrations used in their studies were much lower than that used by Farrah et al[62] and hence did not facilitate precipitation.

Anion exchange is exhibited by clay minerals to a much lesser extent than cation exchange, although it may influence the latter.

The sorption of Cl^-, SO_4^{2-}, PO_4^{3-}, triphosphate[37] and NO_3^-[52] on montmorillonite have all been reported. Bingham et al[63] observed a maximum of about 0.5meq of acetate sorbed/g of montmorillonite at pH<6. At between pH6 and 8 the amount of acetate adsorbed dropped to about one-tenth this value. Contacting the acetate-clay complex with solutions of a number of anions rendered the following order of effectiveness of acetate removal: $NO_3^- \simeq Cl^- < SO_4^{2-} < H_2PO_4^- < OH^- \simeq F^-$.

Monsef-Mirzai et al[64] reported that the extent of sorption of copper(II) onto montmorillonite was dependent on the nature of the counter-ion present in the initial solution. Contact of the clay with 0.1M solutions of copper(II) chloride, sulphate, nitrate or perchlorate was followed by washing with distilled water. The copper released by washing was thought to be associated with edge sites on the clay lattice ('labile') and the remaining Cu with the interlayer region ('exchanged'). The amount of copper 'exchanged' increased as follows: $SO_4^{2-} < Cl^- < ClO_4^- \simeq NO_3^-$, whereas the 'labile' portion followed the order: $ClO_4^- < NO_3^- < Cl^- < SO_4^{2-}$.

Traynor et al[42] concluded that an intersalation reaction was responsible for sorption of metal-bipyridyl complexes of Cu^{2+}, Fe^{2+} and Ru^{2+}

beyond the cation exchange capacity of hectorite and that this uptake depended on the nature of the counter-ion in the order:

SO_4^{2-} , $Br^- > ClO_4^-$, Cl^-.

Organic or inorganic ligands may similarly influence the sorption process by effectively altering speciation. Gee et al's[65] study of sorption onto soil from the Hanford low level waste disposal site revealed much lower K_d values for ^{60}Co-EDTA sorption ($K_d \simeq 1.0$) than for the uncomplexed ion ($K_d \simeq 5000$). Further studies on the effect of organic ligands on sorption behaviour of Hanford soil were undertaken by Swanson.[66] Uptake of strontium and cesium was unaffected but europium, nickel and cobalt all showed significantly decreased sorption in the presence of EDTA and DTPA (diethylenetriaminepentaacetic acid). A comparison of K_d values obtained for nickel sorption is shown in Table 9.

Table 9 - K_d values for nickel sorption on the Hanford Soils[66]

Initial nickel concentration /M	Initial EDTA concentration /M	$K_d/ml g^{-1}$
1.1×10^{-7}	-	9.5×10^3
1.1×10^{-7}	3.0×10^{-5}	6.4×10^1

Peigneur et al's[67] observations on ion exchange of poly-amine complexes of some transition metal ions in montmorillonite led them to conclude that the overall stability constants of these complexes exceed the corresponding values in solution by some three orders of magnitude.

The exchange of bis(ethylenediamine)copper(II) ions for Ca^{2+} was shown to be much more favourable than for the uncomplexed metal ion.

The exchange of Ca^{2+} and Mg^{2+} for Na^{+} on bentonite from perchlorate solutions was found to be independent of exchanger composition, whereas in a chloride medium the total adsorbed metal increased with the amount of Ca^{2+} or Mg^{2+} adsorbed. Sposito et al[68] inferred bivalent cation sorption on internal clay surfaces and monovalent metal-chloride (i.e. $CaCl^{+}$, $MgCl^{+}$) sorption on external surfaces. Further evidence for the complexing effect of Cl^{-} was gained from Egozy's[32] study of cadmium sorption on montmorillonite. He concluded that decreased adsorbability of cadmium in concentrated chloride solutions was due to complex formation.

One can conclude from the above evidence that a large number of experimental variables affect ion-exchange in a clay/solution system. No clear pattern emerges from these studies which enables a simple prediction of sorption behaviour, although some trends do occur, and therefore observations are unique to the relevant system composition. A prediction of cation sorption behaviour on clay minerals in a groundwater environment must therefore involve assessment of all influential variables, both in solution and solid phases.

Nature of the sorbed ion

Investigations, over the past few years, using a wide variety of physical techniques, have led to increased understanding of the nature of metal species sorbed on clay minerals. As well as bulk properties, X-ray photoelectron spectroscopy (XPS) and electron spin resonance

(ESR) spectroscopy techniques have revealed information on species sorbed at clay particle surfaces.

The chemical nature of mineral adsorbed iron species was first probed by XPS in the work of Koppelman et al.[69] The reaction of kaolinite with $Fe(NO_3)_3$ solutions revealed a distinct Fe2p photopeak at a binding energy 1.1eV lower than lattice Fe^{3+} in nontronite and 1.1eV higher than lattice Fe^{2+} in chlorite. Similar Fe2p photopeaks were observed for both chlorite and illite which had been subjected to similar Fe^{3+} treatment. The lowering of binding energy for adsorbed Fe^{3+} relative to lattice Fe^{3+} was interpreted to indicate that electron density in the Stern layer, where ions are adsorbed, is donated to the metal ion.

Adsorption of $[Co(H_2O)_6]^{2+}$ on chlorite was investigated by Koppelman et al[70] at pH values of 3 and 7 using XPS. It was observed that the Co2p binding energy of the adsorbed Co^{2+} species was independent of pH, but was 0.5eV lower than Co^{2+} substituted in an octahedral site in lusakite. It was suggested that the degree of reduction in the adsorbed metal ion 2p binding energy was dependent upon the oxidation state of the adsorbed species. Furthermore, it was noted that the binding energy for adsorbed Co^{2+} was significantly different from that of $Co(OH)_2$ indicating absence of precipitation.

Tewari et al[71] studied the adsorption of Co(II) on Al_2O_3 and ZrO_2 using XPS and electrophoretic mobility measurements. A comparison of binding energies for adsorbed Co^{2+} with those for cobalt oxides and hydroxides revealed that cobalt adsorbed on alumina and zirconia

exists as $Co(OH)_2$.

The chemical nature of cobalt adsorbed on MnO_2 has been studied by Murray et al.[72] From the cobalt binding energies and the separation energies for the $Co2p_{\frac{1}{2}}$ and $Co2p_{\frac{3}{2}}$ energy levels, it was concluded that cobalt was adsorbed on MnO_2 as a Co(III) species. Examination of the binding energies for manganese and oxygen indicated that the surface region of the substrate was characteristic of predominantly Mn(IV).

Examination of the mode of bonding of the metal ions Cu(II) and Ni(II) to clay minerals has been investigated by Koppelman et al.[51] Comparison of the adsorbed Ni^{2+} binding energy with that of Ni^{2+} substituted in an octahedral site in lizardite revealed a lowering (0.4eV) of Ni2p binding energy for the adsorbed species. This result was consistent with that observed for Co(II) adsorption. The adsorbed copper species did not show the same reduction in Cu2p binding energy relative to dioptase. It was concluded that the adsorbed Cu(II) was present as $Cu(OH)^+$.

ESR is a powerful probe in determining the nature of metal ions sorbed onto clay minerals, due to its high sensitivity. McBride[73] studied the sorption of Cu^{2+} onto hectorite using ESR. Wet Cu^{2+} exchanged hectorite samples demonstrated an ESR signal typical of $[Cu(H_2O)_6]^{2+}$, but which decreased on lowering the pH, due to surface hydrolysis. The presence of both $[Cu(H_2O)_4]^{2+}$ and $[Cu(H_2O)_6]^{2+}$ was observed in air dry samples, but at 110°C all the copper had transformed to $[Cu(H_2O)_4]^{2+}$. Drying the exchanged samples at 170°C removed some of

the ligand water of $[Cu(H_2O)_4]^{2+}$ thereby forcing Cu^{2+} to coordinate with silicate oxygens of the interlamellar region.

Monsef-Mirzai et al[64] obtained the ESR spectrum of Cu(II) sorbed on montmorillonite from a high background concentration of NaCl(5M) and postulated a $[CuCl_5]^{3+}$ species was responsible for the low g factor observed. In the same study, ESR parameters for montmorillonite exchanged with VO^{2+} and Mn^{2+} indicated slow hydrolysis of the exchanged ion from a simple hexaaquo species to a hydroxo species.

In a further ESR study, Monsef-Mirzai et al[74] probed the nature of vanadium(III) and chromium(III) sorbed onto kaolinite. They concluded that the two resonances observed for the vanadium(IV) treated clay were due to sorption on the kaolinite surface and association with an iron oxide impurity. Cr(III) is apparently initially sorbed as hexaaquochromium(III) which may undergo slow hydrolysis, resulting in deprotonation and possible formation of dimers and oligomers.

^{57}Fe Mössbauer spectroscopy has found wide application in the study of minerals themselves[75] as well as to species sorbed upon them.[76]

From the basic structure of a 2:1 layer silicate, it can be seen that two different types of coordination exist at the octahedral sites, one site having two OH groups in cis coordination and being twice as abundant as the other site where OH groups are in a trans arrangement. Mössbauer spectra of clay minerals, e.g. montmorillonite and nontronite[75] often show two ferric components with isomer shifts characteristic of octahedral coordination. The component with the larger quadrupole splitting has been assigned to the trans site and the second component

to cis coordination.

Banin et al[76] used Mössbauer spectroscopy to characterise iron ions adsorbed on the interlayer surface of montmorillonite. An ion-exchange method was used to prepare a mixed Fe^{2+}/Fe^{3+}-clay. At room temperature the spectrum showed an Fe(III) site with $\delta = 0.34 mms^{-1}$ and $\Delta = 0.64 mms^{-1}$ only, but at 80K an additional Fe(II) site with $\delta = 1.04 mms^{-1}$ and $\Delta = 3.12 mms^{-1}$ was also revealed. Banin proposed this Fe(II) to be situated within a frozen water matrix below 210K, thus providing an appreciable recoil free fraction, but at higher temperatures the water melted, effectively releasing the Fe(II) from its fixed environment and dramatically lowering the recoil free fraction.

Ultraviolet/visible spectroscopy has proved particularly useful in the study of metal ions sorbed on clay mineral surfaces upon treatment with ligands[77] or after thermal dehydration.[78]

Most water saturated, transition metal exchanged clays contain the octahedral hexaaquo-complex in the interlamellar space.[77] However, heating of these clays to different temperatures results in the formation of new interlamellar species. Tarasevich et al[78] studied the dehydration products of Co-montmorillonite by diffuse reflectance spectroscopy. The air dry sample demonstrated the presence of $[Co(H_2O)_6]^{2+}$, but after heating to 70°C a five coordinated complex resulted due to interaction with three water molecules and two surface oxygen atoms of the upper and lower interlayer surfaces. At 150 and 200°C, the clay apparently showed tetrahedral coordination to three oxygens of one interlayer surface and one remaining H_2O molecule.

Sorption of the bis(ethylenediamine(en)) complex of copper on montmorillonite results in the removal of bound axial water molecules.[77]

i.e. $[Cu(en)_2(H_2O)_2]^{2+} + 2Na^+ - clay \longrightarrow [Cu(en)_2]^{2+} - clay + 2Na^+ + 2H_2O$

The d-d absortion band system shows a hypsochromic shift compared to the species found in solution, apparently due to an increased tetragonal distortion resulting from the replacement of axial water molecules by the silicate surface oxygens.

This conclusion contradicts the observation[79] that a number of glasses containing transition metal ions show a bathochromic shift compared with the metal ion in solution. In a glass matrix, the transition metal ion is surrounded by an environment of oxygen atoms, which are in turn bonded to silicon atoms. This decrease in the absorption maximum indicates that the silicate oxygen should be placed lower in the spectrochemical series than water and thus the replacement of axial water molecules by silicate oxygen atoms on sorption of $[Cu(en)_2(H_2O)_2]^{2+}$ by the clay should lead to a bathochromic shift.

A further study of the mono-complex of copper, $[Cu(en)(H_2O)_4]^{2+}$, indicates a disproportionation on the clay surface to the bis-complex and hexaaquo complex, respectively.[77]

Associated sorption mechanisms

The presence of iron(III) and manganese(II) and (IV) oxides and hydroxides as coatings, and inherent organic matter have also been proposed as factors which can influence the overall sorption properties of clay minerals.

In his comprehensive review on the role of hydrous manganese and iron oxides on sorption properties of soils and sediments, Jenne[80] suggests four possible controls on heavy metal concentration: (1) organic matter, (2) clays, (3) carbonates, (4) hydrous iron and manganese oxides. He indicates that hydrous oxides of manganese and iron are nearly ubiquitous in clays, soils and sediments, and their common occurrence as coatings allows the oxides to exert chemical activity far out of proportion to their bulk concentrations. It is proposed that hydrous Mn and Fe oxide surface sorption sites are largely specific for the heavy metals and furnish the principle control in the fixation of cobalt, nickel, copper and zinc on soils and sediments.

The influence of iron and manganese oxides on metal ion uptake has also been studied by Means et al[81] who investigated the adsorption of ^{60}Co and various actinides associated with soils and sediments from the radioactive waste burial site at Oak Ridge National Laboratory. Selective dissolution of manganese oxides, iron oxides and organic matter from a number of soil samples and subsequent analysis indicated a strong correlation between total ^{60}Co, ^{244}Cm, ^{241}Am and ^{238}Pu versus manganese oxide concentration, with a much smaller influence exhibited by the iron oxide component.

Takematsu[46] has also studied the sorption of manganese, cobalt, nickel, copper and zinc on laboratory prepared manganese oxides and hydrated ferric oxide, as well as Na-montmorillonite and a treated red clay. He observed a sorption affinity sequence of $Mn < Co < Ni < Zn < Cu$ for Na-montmorillonite, treated red clay and hydrated ferric oxide, although distribution coefficients for hydrated ferric oxide were two orders of

magnitude larger. However, the affinity sequence observed for manganese oxides was Ni<Zn<Co<Mn≤Cu.

The role of hydrous manganese and iron oxides may not be as effective as would seem, from the above studies, due to dissolution processes.[80] In Leenheer et al's[82] study of chemical interactions at an industrial waste disposal site, he observed dissolved iron content to be very closely related to the organic waste concentration. This effect was attributed to dissolution and probable complexation by organic acids of iron derived from sesquioxide coatings on granular materials.

Farrah et al[47] noted that natural clays which contain organic material are liable to show much larger variations in sorption behaviour than pure clays since the role of the organic component is unpredictable. Studies of metal ion uptake on humic acid indicated a marked increase with pH and an affinity sequence of Pb, Cu>Zn, Cd>Ca, Mg.

1.7 ROLE OF CEMENT IN RADIOACTIVE WASTE DISPOSAL

Cement plays an essential part in the LL and SLIL waste disposal system described earlier. Although the geologic siting of the repository in a clay formation should provide an effective barrier to radionuclide migration, the containment must enhance the integrity of the waste by providing a further obstacle. The influence of cement on the chemical form of any leached radionuclides must be considered, especially since this may influence sorption properties on the clay minerals once the container is breached.

NIREX[11] propose that cement should fulfill a dual role in LL and SLIL waste disposal; (1) It will act as a physical barrier to water movement

and (2) It will maintain groundwater in its vicinity at a highly alkaline pH, thus rendering most radionuclides almost completely insoluble.

Soroka[83] reports that cement paste consists of about 65% lime, part of which is present as free $Ca(OH)_2$. This is readily leached out by pure water and will give a solution pH of approximately 12.4. A study of diffusion of strontium, cesium and cobalt in cement by Muurinen et al[84] indicates precipitation of cobalt in the cement due to high pH.

From their diffusion experiments on Cl^-, I^- and Cs^+ in cement pastes, Atkinson et al[85] proposed a model in which relatively large pores are interconnected by much finer ones. Most of their observations could be explained in terms of bulk liquid diffusion constrained by a porous medium, although Cs^+ shows an even lower diffusivity than predicted.

1.8 AIMS

The initial objectives of the work were to assess the sorption properties of cobalt and nickel on clay minerals surrounding a LL radioactive waste disposal site.

The CEGB have disposal vaults on nuclear reactor sites into which are deposited certain non-reusable components from the reactor operations which have become irradiated. The waste is composed dominantly of steel structures which after neutron activation will contain a number of radioactive isotopes, but predominantly ^{60}Co and ^{63}Ni. The disposal vault is a concrete lined underground trench in the local host rock formation. Groundwater intrusion may leach out small quantities of

^{60}Co and ^{63}Ni into the surrounding geology. A safety assessment involves a study of the effectiveness of this geologic barrier in preventing radionuclide migration.

The present work aims to investigate the uptake of cobalt and nickel from aqueous solution by two clay minerals, montmorillonite and hectorite. Ideally, it aims to identify the processes by which that uptake is caused and to generate sensible distribution coefficients for use in mathematical models of radionuclide migration. The effects of other groundwater constituents on the uptake of the metals are investigated so that their relative importance on radionuclide sorption may be assessed. The results may thus be applied not only to a specific geological setting, but also to different chemical conditions such as those governed by the nature of the waste form from which the leachate is derived.

Although the original investigation was based on a specific set of sites, the work has much wider application. All four sites being investigated by NIREX[11] for their potential in LL and SLIL waste disposal lie on clay mineral deposits;

Bradwell - London clay
Killingholm - boulder clay
Fulbeck - clay of the Lower Lias
Elstow - Oxford clay

A safety assessment must be undertaken for each site and this will essentially concentrate on the chemical, geological and hydrogeological properties of the clay formations.

A considerable presence of ^{60}Co, ^{63}Ni and ^{59}Ni in LL and SLIL waste is inevitable. Large quantities are present in AGR cladding waste,[4] PWR primary resins[4] and will occur from steel wastes in reactor decommissioning.[86,87]

The presence of ^{60}Co in leachate and on sediments surrounding the waste burial sites at Maxy Flats and Oak Ridge has been observed by a number of workers.[81,88] The migration of ^{60}Co through the surrounding bedrock of apparently high sorption capacity indicates that selection of the correct site and groundwater conditions is critical to the integrity of a radioactive repository. These factors can only be assessed by laboratory experiments.

1.9 SELECTION OF CLAY MINERALS

The most common clays considered in the literature for their potential as a backfill barrier and host geologic formation are the smectites.

The following two smectites were used in experimental work:

(1) Montmorillonite - this is one of the most ubiquitous clay minerals.

(2) Hectorite - although less common, it has a very low iron content which facilitates the use of techniques such as Mössbauer spectroscopy and diffuse reflectance, to identify species sorbed on the clay itself.

CHAPTER TWO

PHYSICAL TECHNIQUES

2.1 ATOMIC ABSORPTION SPECTROPHOTOMETRY

Determination of nickel, cobalt, copper, iron, magnesium, calcium, sodium, potassium, silicon and aluminium in solution was accomplished using a Perkin Elmer Model 460 Atomic Absorption Spectrophotometer. The flame conditions and instrumental settings are summarised in Appendix 1.[89] Absorbance of the solutions was automatically recorded and converted to parts per million of metal ion in solution.

Standard solutions were made up using 'AnalaR' reagents (to avoid the influence of acid in BDH standards) and 0.1% CsCl was added to all standards and samples to suppress ionization effects. Titrimetric analysis of $NiCl_2.6H_2O$ and $CoCl_2.6H_2O$ solids, for the purpose of making up accurate standards, yeilded the following results:

$NiCl_2.6H_2O$: 97.6 % Purity

$CoCl_2.6H_2O$: 99.1 % Purity

Analytical errors were estimated by determining the relevant metal ion concentration in a number of samples on at least four occasions.

2.2 ION CHROMATOGRAPHY

Analyses were performed on a Dionex 2010i instrument with an eluent flow rate of 1 ml/min through a HPIC-CS5 column. The eluent consisted of 0.05M oxalic acid and 0.095M lithium hydroxide (both sparged with helium for 45 minutes before use to remove dissolved air), and addition of the complexant 4-(2-pyridylazo)resorcinol monosodium salt, monohydrate in a post column reactor enabled colourimetric determination of cobalt, nickel, copper, zinc and manganese.

2.3 Υ-SPECTROMETRY

The Υ-spectrometer used for ^{60}Co analysis had a sample changer in which samples were transferred into a lead shield, mounted on perspex carriers and, were accurately positioned above the detector by a linear actuator. Positional jigs were available to reproducibly locate a variety of calibrated geometries both close to the detector and at a distance if countrate reduction was required. The detector was a high purity germanium crystal (EG and G Ortec) of co-axial p-type with a diameter of 55.5mm and volume of 161cm^3. The detector was connected to a Model 673 gated integrator (EG and G Ortec) as its main amplifier. The multichannel analyser was a model ND66 (Nuclear Data Inc.) and the associated analysis and system control computer was a PDP Micro-11 (Digital Equipment Corporation).

Each of the sample solutions were presented to the spectrometer sample changer in the following form; 5cm^3 of solution was extracted into a 5cm^3 pipette tip, which was then sealed at both ends with 'nescofilm' and emplaced in a polyethylene container (radius = 4.5cm, height = 16cm). After covering with clingfilm the sample could then be positioned in the sample changer.

A 200ppb ^{60}Co standard was used to calibrate the spectrometer.

2.4 X-RAY DIFFRACTION

Diffraction traces were obtained from a Phillips X-ray diffractometer system using Co$K\alpha$ radiation with an iron filter. Traces were recorded at $1^o 2\theta$ per minute in the range $1\text{-}4 \times 10^3$ counts per second, and could

be observed from $3^{o}2\theta$ upwards.

2.5 INFRARED SPECTROSCOPY

Infrared spectra in the range 4000-250cm^{-1} were recorded using a Perkin Elmer 599B spectrometer, controlled by a model 3600 data station, running Perkin Elmer software. Solid state specimens were prepared as KBr discs by pressing a mixture of sample and powdered KBr ('Spectrosol' grade). A ratio of 0.5mg sample:170mg KBr was used in the study of clay specimens and expansion of spectra in the ranges 3600-1800cm^{-1}, 1800-1150cm^{-1} and 1150-300cm^{-1} aided peak identification.

2.6 ULTRAVIOLET AND VISIBLE SPECTROPHOTOMETRY

Ultraviolet/visible solution spectra were performed on a Pye Unicam SP800B spectrophotometer, using glass cells, over the range 300-800nm.

Initial attempts at obtaining solid ultraviolet/visible spectra involved preparation of a methanol/clay mull which was then painted onto the side of a glass cell prior to analysis. This procedure proved unsuccessful due to the production of spurious peaks which were probably a result of scattering due to particle size effects. Diffuse reflectance spectrophotometry was deemed more suitable (see section 2.7).

2.7 DIFFUSE REFLECTANCE SPECTROPHOTOMETRY

Solid state spectra in the range 250-700nm were recorded on a Pye Unicam SP800B instrument with an SP890 diffuse reflectance attachment. The sample was sandwiched between two quartz plates then placed in the analysing beam and reflectance was compared with that from a standard MgO sample.

2.8 X-RAY PHOTOELECTRON SPECTROSCOPY (XPS)

XPS spectra were determined using a Kratos XSAM 800 ESCA-Auger spectrometer employing either MgKα (1253.6eV) or AlKα (1486.6eV) as incident radiation, at a sample chamber pressure of 10^{-9} Torr.

Samples were presented as pressed powders.

Initially, raw binding energies were corrected using the $Au4f_{\frac{7}{2}}$ (binding energy = 84.0eV*)[90] peak obtained from each sample used as an admixture with gold powder. Apparently this technique was not effective in preventing sample charging, so it was decided that the $Si2p_{\frac{1}{2},\frac{3}{2}}$ binding energy obtained from the clay itself should be used as an internal standard. This holds three advantages: (i) high silicon content of clay minerals, (ii) a single $Si2p_{\frac{1}{2},\frac{3}{2}}$ peak is expected due to silicon appearing only in tetrahedral lattice positions, (iii) solution treatment of the clays does not alter the nature of the silicon lattice site. The absolute $Si2p_{\frac{1}{2},\frac{3}{2}}$ binding energy was determined using the $Au4f_{\frac{7}{2}}$ photopeak, obtained from a very thin film of gold vapour deposited on the sample surface, and the C1s photopeak (binding energy = 284.6eV)[91] from background contamination. Ion etching was accomplished using an Argon ion gun at 5KV, 25mA producing a specimen current of approximately 20μA.

2.9 MÖSSBAUER SPECTROSCOPY

A constant acceleration type spectrometer was employed in which a range of velocities was scanned linearly and repeatedly. The γ-rays were detected using a gas filled proportional counter, counts being recorded

*1eV = 96.49 $kJmol^{-1}$

on 512 channels of an Ino-Tech 5200 multichannel analyser such that the velocity interval per channel was constant. A 25mCi source of ^{57}Co diffused into a palladium foil was used, the spectrometer being calibrated relative to iron metal (all isomer shifts quoted are relative to iron metal).

The position, width, intensity of each line and standard deviation of these three parameters were obtained by computer fitting the experimental data on a Harris H800 computer system using a program written by A. J. Stone which follows the procedure described by Bancroft et al.[92] This program has a facility for constraining any set of parameters or combination of parameters in order to obtain convergence.

Discs of powdered samples were enclosed in cellotape and rigidly held by thin card. For Mössbauer analysis in an oxygen free environment, samples were enclosed in an 'araldite' matrix, under nitrogen.

Spectra at 77K were obtained using an Oxford Instruments cryostat.

2.10 ELECTRON SPIN RESONANCE (ESR) SPECTROSCOPY

ESR spectra were recorded on a Japan Electron Optics Limited (JEOL) PE-1X type spectrometer, operating in the X-band microwave region, at 100 kHz. Samples were contained in quartz tubes in order to remove the possibility of additional signals from components of glass tubes. A manganese(II) salt diluted with magnesium oxide was utilized as standard.

2.11 X-RAY FLUORESCENCE

Analyses were performed on a Phillips PW1400 sequential X-ray spectrometer using a Rhodium anode. Five analysing crystals cover the wavelength range of the spectrometer, with the secondary radiation being detected using either a scintillation or gas flow detector. Amplified pulses are fed into a DEC computer system where comparison with a set of internationally accepted silicate standards gives the parts per million (ppm) of element present.

'Major element' analysis involved the fusion of a dry powdered specimen (15%) with a borax flux (85%) at 1100^{o}C to form a glass, which was then pressed into a circular disc for analysis. This technique enabled high elemental concentrations to be determined.

2.12 DIFFERENTIAL THERMAL ANALYSIS

A Stanton Redcroft DTA 673-4 instrument was used for thermal analysis. This consists of two small Rh-Pt crucibles situated over separate thermocouples, inside a furnace. One crucible contained a standard calcined alumina, the other the sample material, and the temperature was raised up to a value of 950^{o}C at a rate of 20^{o}C/min.

2.13 SCANNING ELECTRON MICROSCOPY

Electron microscopy was performed using a Cambridge 5150 Mk.2 system operated at 20kV and 1A, with a KIVEX X-ray analytical detector.

Aluminium sample stubs were covered with a thin layer of colloidal graphite, before clay sample was deposited, in order to prevent analysis

of the underlying aluminium holder. The clay sample was then coated with a layer of carbon in order to prevent charging effects.

2.14 GAS-LIQUID CHROMATOGRAPHY (GLC)

The identification of certain reaction products was performed using GLC. Analyses were carried out using a Pye Unicam Ltd. GCD gas chromatograph with the following specifications:

Column - stainless steel

Length of column - 2m

Diameter of column - 0.6cm

Packing of the column - 25% silicon grease on phase prep. A.

Carrier gas - Nitrogen

Carrier gas flow rate - 30 ml min^{-1}

Temperature of column - 160^{o}C

Detector - Flame ionisation

2.15 TITRIMETRIC DETERMINATION OF COBALT[93]

Reagents:

(a) 0.01M EDTA solution - 3.7225g of disodium dihydrogen ethylenediaminetetra-acetate dihydrate was dissolved in distilled water and diluted to one litre in a volumetric flask.

(b) 50% ammonium thiocyanate solution - 50g of ammonium thiocyanate was dissolved in 70cm^3 of water. If any precipitate appeared, it was filtered off and the remaining solution made up to 100cm^3 using distilled water.

(c) 50% ammonium acetate solution

Procedure

To an appropriate aliquot of the sample solution (containing 2-12mg of Co) was added $5cm^3$ of ammonium thiocyanate solution and $50cm^3$ of acetone. It was then titrated with the standard EDTA solution until the blue colour disappeared.

$1cm^3$ 0.01M EDTA = 0.589mg cobalt

2.16 TITRIMETRIC DETERMINATION OF NICKEL[94]

Reagents:
(a) 0.01M EDTA solution
(b) Murexide indicator (homogeneously ground mixture of 1% murexide in KNO_3)
(c) 1M NH_4Cl

Procedure

An appropriate aliquot of the sample solution (containing from 2-12mg nickel) was diluted to $100cm^3$ with distilled water, and 0.05g of the murexide indicator added, followed by $10cm^3$ of 1M ammonium chloride solution. Concentrated ammonia solution was added dropwise until the pH was about 7, as shown by the yellow colour of the solution. This solution was titrated with 0.01M EDTA solution until the end point was approached, when the solution was rendered strongly alkaline with about $10cm^3$ of concentrated ammonia, and the titration continued until the colour changed from yellow to blue-violet.

$1cm^3$ 0.01M EDTA = 0.587mg nickel

2.17 pH MEASUREMENT

A Corning Model 12 pH meter was used to record pH values.

2.18 IGNITION OF SAMPLES

The ignition of clay samples up to a temperature of 1100^{o}C was carried out using a Carbolite MFHT Furnace with a three phase mains supply, utilising a Pt-Rh thermocouple for temperature measurement.

2.19 CHEMICALS

Materials of mainly 'AnalaR' grade were obtained from commercial sources and generally used without further purification. Montmorillonite was obtained from the Steetly Co. Ltd. and hectorite from NL Industries Ltd. (Calfornia).

CHAPTER 3

COBALT AND NICKEL SORPTION ON HECTORITE AND MONTMORILLONITE AND THE INFLUENCE OF COMPETING INORGANIC CATIONS

3.1 INTRODUCTION

Clay minerals have a large capacity for transition metal ion sorption,[95,44] but the extent of uptake has been shown by a number of studies[44,33,62] to be a function of several factors including solution pH, concentration of the metal ion and nature of any ligands present.

Some inconsistency in sorption results from a number of workers has been observed which necessitated an investigation of basic sorption properties and the formulation of typical sorption isotherms. Having established the exchange behaviour from simple mono-ionic nickel and cobalt solutions, extensions of the study to more complex solution compositions was undertaken. This enabled some conclusions to be drawn about the relative influence of typical groundwater constituents on sorption processes.

However, typical clay mineral impurities have very different cation exchange properties and so a thorough physical investigation of the montmorillonite and hectorite used was undertaken to assess purity.

3.2 CLAY MINERAL ANALYSIS

3.2.1 X-ray flourescence

'Major element' analysis of montmorillonite and hectorite furnished the results in Table 10.

3.2.2 X-ray diffraction

Standard XRD spectra were gained from natural hectorite and mont-

Table 10 - XRF analysis of montmorillonite and hectorite.

Sample / % oxide	montmorillonite	hectorite
Fe_2O_3	10.53	0.10
MnO	0.01	<0.01
TiO_2	0.29	0.02
CaO	1.81	0.52
K_2O	0.37	0.07
S	0.05	0.01
P_2O_5	0.10	0.03
SiO_2	51.69	58.52
Al_2O_3	12.07	0.21
MgO	2.15	27.05
Na_2O	0.11	1.78
H_2O 110°C	14.89	6.90
1100°C	5.99	2.90

Table 11 - XRD data from natural and glycolated montmorillonite and hectorite.

Sample	d(001)/Å
flocculated montmorillonite	15.2 ± 0.03
flocculated hectorite	12.7 ± 0.02
glycolated montmorillonite	17.1 ± 0.03
glycolated hectorite	17.8 ± 0.03

morillonite. Characteristic d(001) spacings were obtained from flocculated clay samples and are shown in Table 11.

Glycolation was performed by exposing the clay to an enclosed atomsphere of ethylene glycol, at 60°C, for 5 days (Table 11).

3.2.3 Differential thermal analysis

Table 12 summarises the characteristic peaks from thermal analysis of the two minerals.

3.2.4 Infrared spectroscopy

I.R. absorption peaks from KBr pressed powder samples are detailed in Table 13.

3.3 DETERMINATION OF CATION EXCHANGE CAPACITY

Cation exchange capacities of the clay minerals were determined using the method of Peech.[96]

A sample of clay was weighed, sufficient to give about 4 milli-equivalents of total exchangeable cations, into a small Büchner funnel fitted with a moist 5.5cm filter paper. The clay was leached with small portions of 1N ammonium acetate, using gentle suction, and the filtrate caught in a 250cm^3 Büchner flask. The clay was leached until about 225cm^3 of filtrate had been collected. The clay was then washed on the Büchner funnel with small portions of 95% ethanol, being drained well between additions to remove excess ammonium acetate. After 150cm^3 of ethanol had been leached through the clay, the excess alcohol was drained by applying gentle

Table 12 - Characteristic DTA peaks from montmorillonite and hectorite.

Sample	endothermic peaks/^{o}C	exothermic peaks/^{o}C
montmorillonite	189(m), 585(m-s), 876(w)	925(w)
hectorite	129(m), 831(m-s)	
Relative peak intensity: w - weak, m - medium, s - strong		

Table 13 - I.R. Absorption peaks from montmorillonite and hectorite samples

Sample	Absorption peaks /cm^{-1}								
Montmorillonite	3591(m,br) 3220(vw) 3398(m)	2912(vw) 2840(vw)	1623(m)	1031(s) 918(w) 791(w) 688(vw) 515(m-s) 421(m) 347(vw) 1107(sh) 870(m-w) 768(w) 593(vw) 468(m-s) 396(vw)					
Hectorite	3677(w) 3424(m,br) 3623(w)	2921(vw) 2848(vw)	1632(m)	1060(sh) 1006(s)	694(w)	664(w) 645(w)	528(sh) 465(s)	377(m)	
relative intensity: w - weak, m - medium, s - strong, sh - shoulder, br - broad									

suction for a few minutes, although the clay was not allowed to dry and crack. The ethanol washings were discarded. The clay was then transferred, with filter paper to a Kjeldahl flask, 400cm^3 of water added along with 10g of sodium chloride and 15cm^3 of 1N sodium hydroxide. The flask was connected to a condenser and 200cm^3 of solution distilled into 30cm^3 of 0.2N sulphuric acid. The excess acid was titrated with 0.1N sodium hydroxide using methyl red indicator.

For a 25g sample of clay:

cm^3 of 0.2N sulphuric acid consumed x 0.8 = c.e.c., in meq/100g clay.

Determinations were carried out in duplicate (Table 14).

3.4 PREPARATION OF SODIUM SATURATED MONTMORILLONITE

Conversion of the montmorillonite sample into a mono-ionic sodium form (Na-montmorillonite) was accomplished in accordance with the method used by Posner and Quirk.[97]

The original powdered clay was washed with 1M NaCl solution and separated by decantation, this treatment being repeated six times. The montmorillonite was then suspended in 1M NaCl solution at pH3, adjusted with hydrochloric acid, for approximately one hour followed by separation from the solution by centrifugation. After this procedure was repeated four times, the montmorillonite was resuspended in 1M NaCl solution at pH3, stirred for around 36 hours, separated again by centrifugation and washed twice with distilled water. It was then dialysed against deionised water for 20 days

and oven dried at 110°C.

3.5 INTERACTION OF CLAY MINERALS WITH NICKEL AND COBALT SOLUTIONS

3.5.1 Problems associated with the analysis of supernatent liquids from clay mineral suspensions

It is well known[31] that some clay mineral size fractions lie in the colloidal range. Some clay suspensions contain colloidal clay particles even after centrifugation. In initial sorption experiments this phenomenon was observed and was found to appreciabely influence the cation analysis techniques used.

3.5.1.1 Atomic absorption analysis

To investigate the possibility of cation release from natural montmorillonite, which would consequently affect sorption experiments, a portion of natural montmorillonite (10g) was added to distilled water ($100cm^3$). The supernatent remaining after centrifugation (3000rpm for 15 mins) was analysed by atomic absorption (table 15).

Similar experiments were carried out using Na-montmorillonite which had been partially dialysed and completely dialysed. In both cases, the clay (0.8g) was dispersed in distilled water ($20cm^3$), shaken for 1 hour, then centrifuged and the supernatent analysed (table 15).

Results for the natural montmorillonite sample indicated release of significant proportions of sodium, calcium, magnesium and iron into solution from the clay. The sodium-clay again exhibited the

Table 14 - Cation exchange capacities of montmorillonite and hectorite.

Sample	cec(meq/100g)
montmorillonite	81
hectorite	58

Table 15 - Concentration of metal ions apparently released into distilled water by montmorillonite samples.

Sample	metal ion released to supernatent from clay (meq/100g)						
	Na	K	Mg	Ca	Fe*	Co	Ni
Natural montmorillonite	0.78	<0.0003	0.24	0.14	0.024	<0.0003	<0.0003
Na-montmorillonite:- at intermediate stage of dialysis	1.21	<0.0003	0.020	<0.004	2.9	<0.0003	<0.0003
Na-montmorillonite:- fully dialysed	3.9	0.06	0.82	<0.004	5.9	<0.0003	<0.0003

* Fe is assumed present as Fe^{3+}.

presence of a number of cations in solution, however, the relative quantities of cations released exhibited a very different distribution.

It is proposed that a number of inorganic salts were associated in small amounts with the natural montmorillonite and accounted for the sodium, magnesium and calcium released. Calcium was removed upon continued dialysis (i.e. becomes undetectable - Table 15) as expected, but sodium, magnesium and iron increased in concentration.

This was due to the analysis of clay particles suspended in the supernatent solutions. Support for this proposal is gained from the fact that XRF analysis reveals a high proportion of iron in the clay lattice and a low proportion of calcium, which was probably in exchange sites and has been replaced by sodium in the Na-montmorillonite - this was reflected in the supernatent analyses.

3.5.1.1.2 To investigate this hypothesis further, a number of montmorillonite suspensions were treated so as to leave increasing quantities of clay in suspension, prior to analysis.

Three suspensions, comprising natural montmorillonite (10g) and distilled water ($100cm^3$) were shaken for 3 days, then ultracentrifuged for 10 mins, 30 mins and 90 mins respectively and the supernatent analysed for metal ions (Table 16, Fig.7). An additional 7 samples comprising natural montmorillonite (1g) and distilled water ($200cm^3$) were shaken by hand for 1 minute and allowed to settle for periods of 10 mins, 30 mins, 100 mins, 160 mins, 280 mins, 18 hr and 48 hr respectively, before withdrawal of an aliquot of supernatent for analysis. Results are presented in Table 16 and Fig.7.

Table 16 - Apparent concentrations of metal ion released by natural montmorillonite after various periods of settling and ultracentrifugation.

Sample	ultracent-rifugation time/mins	settling time/mins	metal ions released by clay (meq/100g)				
			Na	K	Ca	Mg	Fe
1	90	-	0.91	0.13	0.50	0.18	0.0021
2	20	-	0.87	0.11	0.52	0.19	0.0054
3	8	-	0.91	0.12	0.50	0.20	0.025
4	-	2880	1.05	0.012	0.31	0.17	1.2
5	-	1080	1.20	0.013	0.28	0.16	1.3
6	-	280	2.3	0.25	0.26	0.17	1.3
7	-	160	2.4	0.29	0.27	0.17	2.0
8	-	100	2.4	0.33	0.31	0.19	2.4
9	-	30	2.6	0.43	0.25	0.35	5.0
10	-	10	2.9	0.52	0.24	0.40	7.5

Fig.7 - Metal ions released by montmorillonite after various periods of settling and ultracentrifugation.

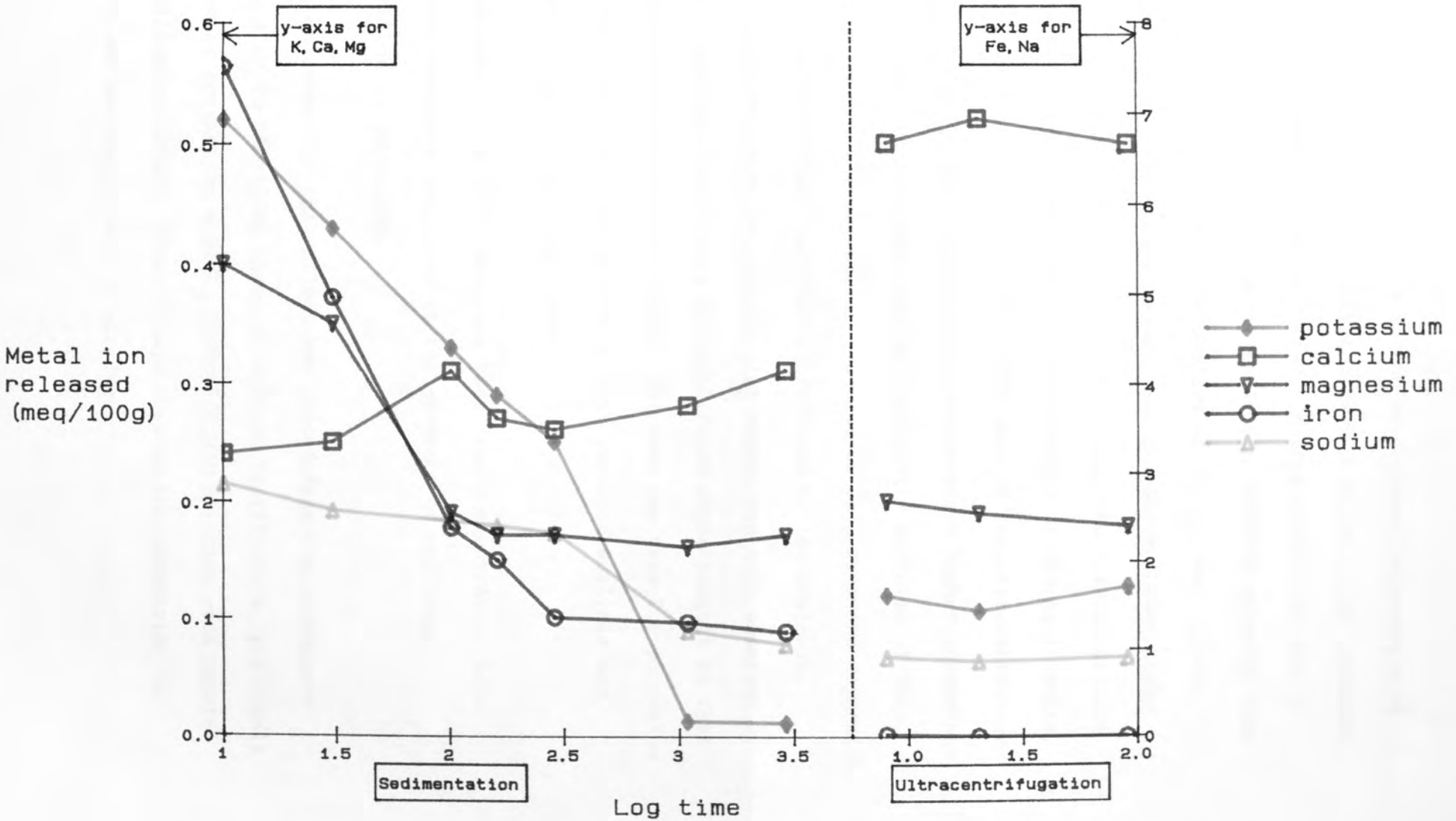

Iron and sodium concentrations in the supernatent increased with decreasing settling and centrifuging time pointing to an increased quantity of suspended clay particles. Magnesium did not show a consistent increase in concentration, which would be expected from previous conclusions, until the smaller settling times, as did potassium. Also, calcium, magnesium and potassium showed higher concentrations after ultracentrifugation than the initial settled solutions. This was again due to the presence of inorganic salts, which, due to the longer shaking times used in the ultracentrifuged samples, showed greater dissolution and therefore higher concentrations. All calcium analyses may be interpreted in terms of this one source of metal ions, but in the case of potassium and magnesium, cations from colloidal clay also contributed to the analysis. Hence, magnesium from the colloid clay source was only observed at small settling times where it contributed significantly to that released by entrained metal salts. The same was true for potassium except that the contribution due to clay particle analysis was observed at longer settling times.

It is apparent from these analyses that iron concentration acts as a very sensitive indicator to the presence of colloidal montmorillonite particles.

3.5.1.1.3 Further evidence for this effect was gained from the successive redispersion in distilled water of a Ni-montmorillonite, previously prepared by contacting a $NiCl_2$ ($200cm^3$/0.10M) solution with natural montmorillonite (20g). After 3 days shaking the suspension was filtered and the solid left to air dry.

This Ni-montmorillonite (5.0g) was initially redispersed in distilled water ($50cm^3$), shaken for 3 days and the supernatent from centrifugation (3000rpm for 20 mins) of a small aliquot of suspension analysed for various metal ions, before filtration of the whole sample. The air dry clay was again redispersed in distilled water ($50cm^3$) and the above procedure repeated. The air dry clay from this second redispersion was treated similarly twice more except that ultracentrifugation (40,000rpm for 45 mins) was used to separate the supernatent for analysis. Metal ion concentrations in solution are shown in Table 17 and Fig.8.

The increase observed in iron concentration between redispersions 1 and 2, and 3 and 4 was due to a decrease in total solution cation concentration which stabilised the clay and permited more clay to appear in the colloidal state. The apparently anomalous drop between the second and third treatments was due to utilization of a higher centrifugation speed which deposited a larger proportion of clay particles from solution.

Sodium and potassium concentrations did not increase in parallel with the iron concentrations, as expected from previous proposals, but they did reach a steady value which indicated the increased contribution of colloidal clay particles to the analysis compared with solution. Although nickel and magnesium concentrations successively decreased with increased number of redispersions, they did decrease less rapidly relative to calcium concentrations. Since calcium analysis was due solely to imbibed salts (see earlier), the extra contribution to magnesium and nickel concentrations must

Table 17 - Apparent concentration of metal ions released from a Ni-montmorillonite on successive redispersion by distilled water.

Redispersion	Metal ion released into solution (meq/100g)					
	Na	K	Ca	Mg	Fe	Ni
1	0.33	0.15	2.4	0.81	0.0012	9.2
2	0.15	0.082	0.09	0.20	0.50	1.4
3	0.13	0.067	0.036	0.042	0.010	0.46
4	0.13	0.061	0.008	0.026	0.17	0.24

Fig.8 - Metal ions released into solution from a Ni-montmorillonite upon successive redispersion.

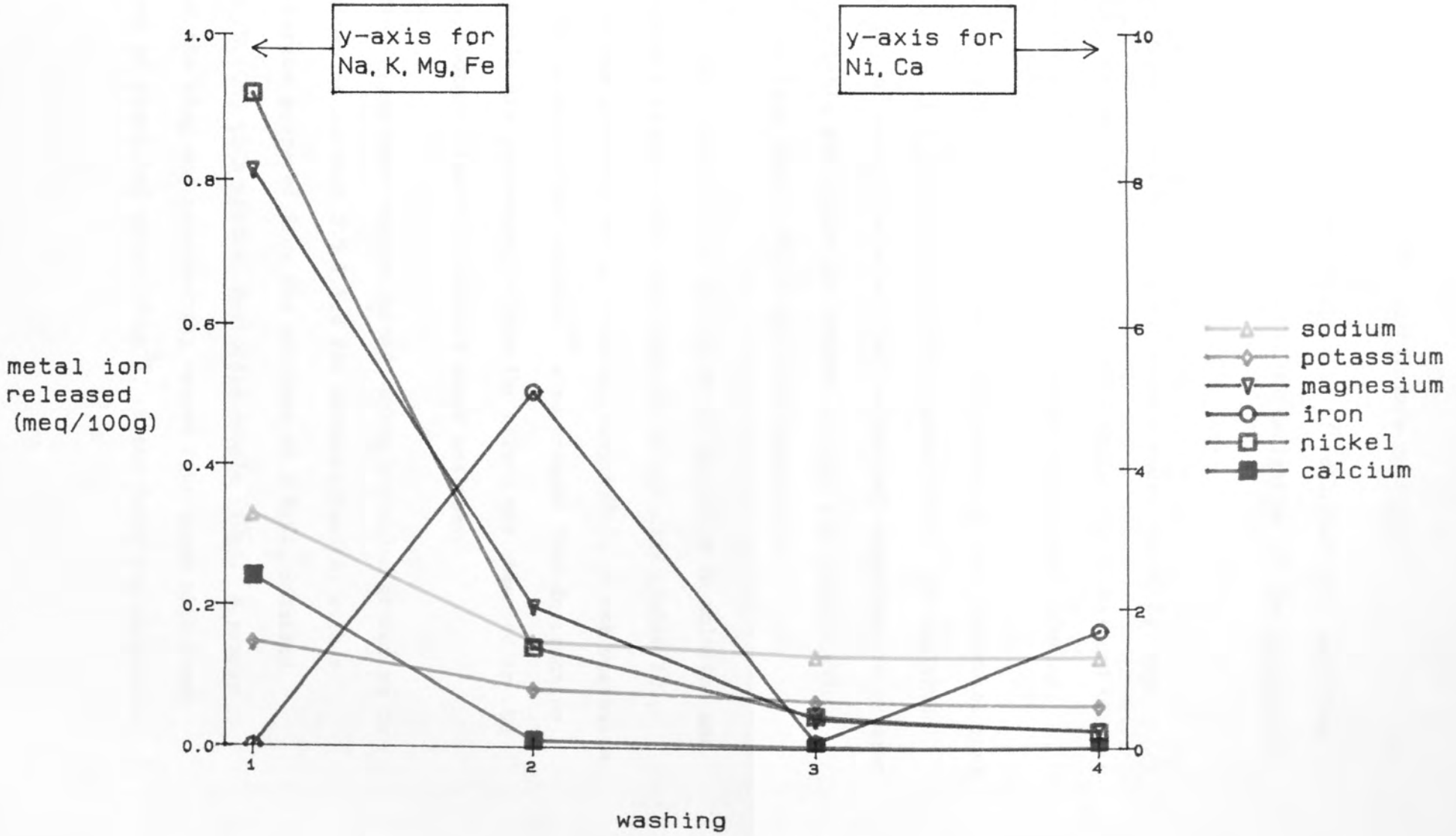

have been due again to clay particulate analysis.

3.5.1.1.4 Observation of the apparent analysis of colloidal clay particles from supernatent solutions led to investigation of the possibility of similar anomalies with hectorite.

In a simple initial experiment, natural hectorite (0.5g) was dispersed in distilled water ($40cm^3$), shaken for 3 days and then ultracentrifuged before analysis of the supernatent solution.

Results from Table 18 indicated the presence of only two metal ions in solution, but both in significant quantities. XRF analysis (Table 10) of hectorite shows that sodium and magnesium are present in appreciable quantities as opposed to iron and calcium which contribute less than 1.5% of the clay composition.

The relative concentration of sodium to magnesium in solution was appreciabely higher than that observed in the clay (Table 10), but this was probably due to chemical suppression of the magnesium signal by aluminium and silicon[98] also present from destruction of the silicate framework. A similar effect was observed in the earlier montmorillonite/distilled water analyses.

3.5.1.1.5 A further experiment was performed, using a similar procedure to that shown in section 3.5.1.1.3 for montmorillonite, with a Ni-hectorite prepared from the addition of a $NiCl_2$ solution ($100cm^3$/0.10M) to a natural hectorite sample (10g). A sample (5g) of the clay was successively washed four times with fresh portions of distilled water ($50cm^3$), on the first two occasions

Table 18 - Cations apparently released by natural hectorite into a distilled water solution.

Sample	metal ion in supernatent (meq/100g)					
	Na	Ca	Mg	Fe	Co	Ni
natural hectorite	6.9	<0.004	5.5	<0.001	<0.0003	<0.0003

Table 19 - Apparent concentration of metal ions released from a Ni-hectorite on successive washing with distilled water.

Wash	Metal ion released into solution (meq/100g)			
	Na	Ca	Mg	Ni
1	7.4	0.14	1.35	4.0
2	1.4	0.021	0.074	0.124
3	0.66	0.014	0.037	0.074
4	0.38	0.010	0.070	0.104

the supernatent being separated by centrifugation and the latter two by ultracentrifugation, before analysis. Concentration of solution species determined are shown in Table 19 and Fig.9.

The initial ion-exchange of nickel onto hectorite released a number of interlayer cations, a fraction of which were retained on the clay as imbibed salts, after the filtration process. This accounts for the high release of all cations observed in the first clay washing. The calcium and sodium solution concentrations continued to fall with successive washing as opposed to the leveling off in magnesium and nickel concentrations. This suggested that calcium and sodium were released by continual desorption of imbibed metal salt, but an additional contribution due to suspended clay particles became dominant after the first clay washing in the case of nickel and magnesium.

Although magnesium concentration acts as an indicator to the presence of colloidal hectorite particles, it did not exhibit the sensitivity of iron from colloidal montmorillonite particles.

The possible effects that colloidal clay particles may have had on analysis led to the use of ultracentrifugation (40,000rpm for 45 mins) for separation purposes as a standard procedure.

3.5.1.2 Ion chromatographic analysis

The main feature of ion chromatographic analysis is the ion-exchange column through which an eluent (+ injected sample) is passed. Metal ions have different affinities for the exchange resin and

Fig.9 - Metal ions released into solution from a Ni-hectorite upon successive redispersion.

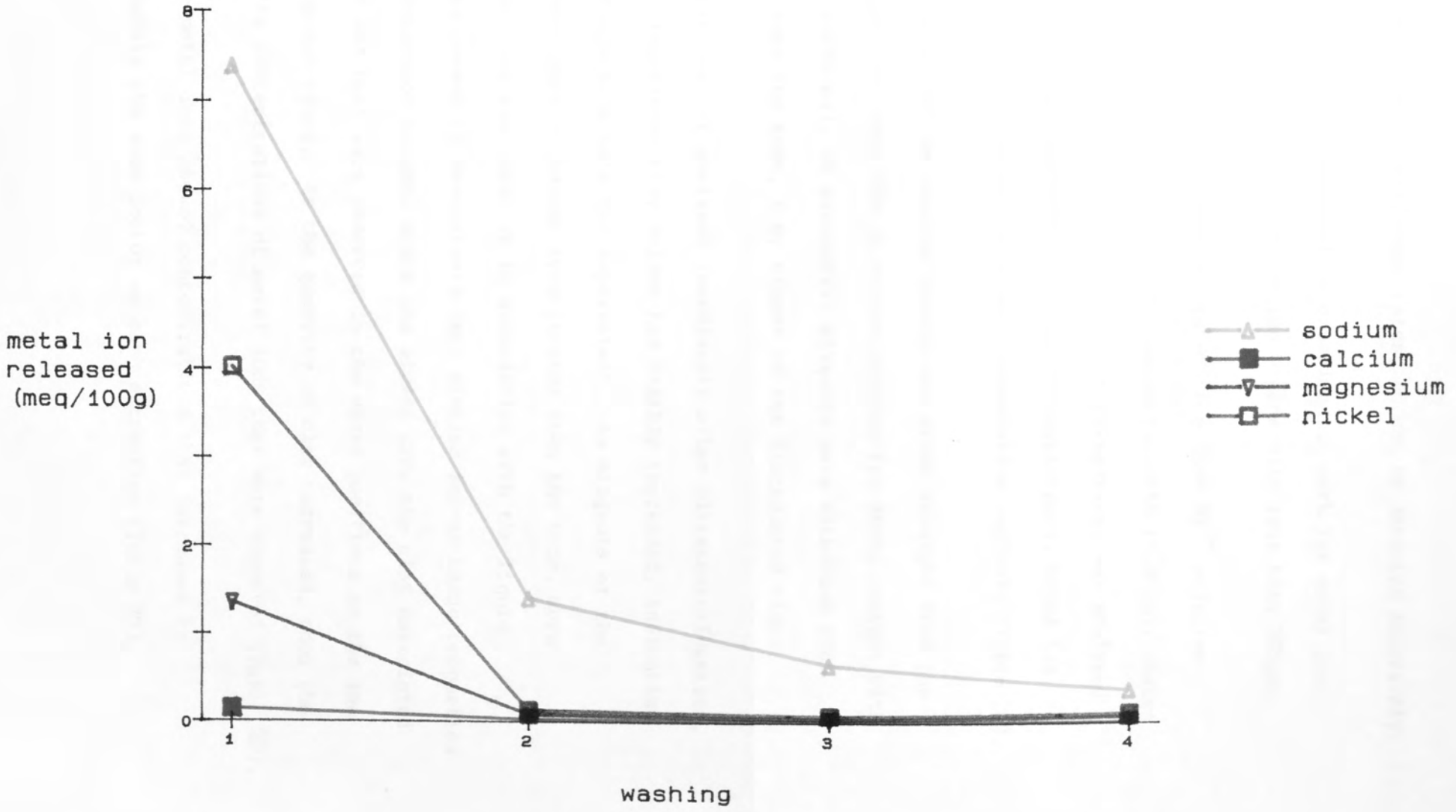

hence are eluted at different rates, so can be detected separately.

Ion chromatography was used in experimental work for metal ion determination at low concentration - generally less than 500ppb.

The supernatent from a sample, in which a 2ppm Ni^{2+} solution ($12.6cm^3$) had been added to a Na-montmorillonite (0.252g), shaken for 3 days, then separated by ultracentrifugation, was analysed a number of times and exhibited little consistency, metal ion concentration increasing with each consecutive analysis (Table 20).

On each occasion the analyte sample was drawn straight from the centrifuge tube into the injection syringe (to avoid contact with further surfaces), so successive aliquots were withdrawn from further down the tube, i.e. closer to the flocculated clay.

The sample was not analysed immediately after ultracentrifugation, and the flocculated clay volume had visibly increased, indicating some redispersion into the supernatent. As aliquots of the supernatent were withdrawn from further down the tube, more colloidal clay was taken up in association with the liquid. This clay seemed to demonstrate very similar ion-exchange properties to the separator column, since the eluent drew the clay associated ions off and they were observed in the usual positions on the ion chromatograph trace. As the quantity of clay increased, then the larger the concentrations of metal ions that were observed (Table 20).

All five metal ions showed concentrations that increased by approximately the same factor on each extraction (Table 20),

Table 20 - Relative metal ion concentrations *(peak heights) in supernatent from a Na-montmorillonite sample treated with a 2ppm Ni^{2+} solution.

Sample	Ni peak ht. /cm	Zn peak ht. /cm	Cu peak ht. /cm	Mn peak ht. /cm	Co peak ht. /cm
analysis 1	4.6	3.2	-	0.7	-
analysis 2	7.1	4.7	0.3	1.0	0.3
analysis 3	79.0	36.8	2.8	6.5	3.2
after re-centrifugation	0.76	1.7	-	-	-

*peak heights taken as directly proportional to concentration[99]

indicating that the ions originated from the same source, to an increasing extent.

Upon re-centrifugation, immediate nickel analysis generated a value which was more compatible with the nickel isotherm determined at higher concentrations (see section 3.5.2.10), and it appeared that a clay particle contribution was no longer significant.

3.5.1.3 γ-spectrometric analysis

Experiments at low level with ^{60}Co as a radio-label utilized γ-spectrometric analysis which essentially compared the sample γ-ray emission with that from a 200ppb ^{60}Co standard. The whole of the supernatent solution ($\simeq 12.6cm^3$) was poured into a poly-ethylene container (radius = 3.5cm, height = 2cm), sealed and analysed as such.

Initial analysis on supernatents from cobalt solutions ($12.6cm^3$) of 1ppm and 100ppb which had been contacted with Na-montmorillonite (0.252g) for 3 days before ultracentrifugation, revealed distribution coefficients which were much lower than expected from extrapolation of the cobalt sorption isotherm (section 3.5.2.11) determined at higher concentrations (Table 21).

When pouring off the supernatents for analysis, a slight brown colouration was observed in both the above cases. A small portion of the clay thus appeared to have been transferred to the analyte container and contributed to the count observed. If, as expected, the clay had a much higher activity than the final 'equilibrium'

Table 21 - Distribution coefficients from initial measurements on cobalt sorption on Na-montmorillonite at low level.

Initial sample cobalt concentration	$K_d(cm^3/g)$
1ppm	1.1×10^3
100ppb	1.3×10^3
*100ppm	4.2×10^3

*for comparison (see section 3.5.2.10)

solution, it would appear that the majority of the activity in these initial two experiments was from the clay inherent in the analyte solutions.

A repeat of the above experiments using an alternative analyte preparation (see section 2.3) gave much more sensible K_d values.

3.5.2 Macroscopic effects

A batch technique was used to study the reaction of cobalt and nickel solutions with montmorillonite and hectorite.

3.5.2.1 Portions (10g) of Na-montmorillonite were placed in seven 250cm^3 flasks, separately covered with a standard solution of nickel chloride (100cm^3/0.1M) and shaken for periods of 1 to 7 days. The solid was filtered off and the amount of nickel remaining in solution was determined. The solids remaining from the above treatment were dried at room temperature in air, then covered with distilled water (100cm^3) and shaken for a further 3 days. The suspension was filtered and the amount of nickel released into solution determined.

Results are shown in tables 22, 23 and 24 and plotted in figs.10, 11 and 12.

3.5.2.2 Portions (10g) of Na-montmorillonite were placed in seven 250cm^3 flasks, separately covered with a standard solution of nickel sulphate (100cm^3/0.1M) and shaken for periods of 1 to 7 days. The solid was filtered off and the amount of Ni remaining in solution determined volumetrically. The solid was air dried at

Table 22 - Anion effect on variation of nickel sorbed on Na-montmorillonite with time.

Time/Days	Ni sorbed (meq/100g)		
	$NiSO_4$	$NiCl_2$	$Ni(ClO_4)_2$
1	58	49	47
2	57	54	52
3	59	58	56
4	59	56	56
5	59	53	56
6	59	54	56
7	59	56	56

Table 23 - Anion effect on variation of nickel retained on Na-montmorillonite with time.

Time/Days	Ni retained (meq/100g)		
	$NiSO_4$	$NiCl_2$	$Ni(ClO_4)_2$
1	46	42	38
2	44	42	41
3	45	45	45
4	44	47	45
5	47	45	45
6	44	45	44
7	45	47	45

Fig.10 - Anion effect on variation of nickel sorbed on Na-montmorillonite with time.

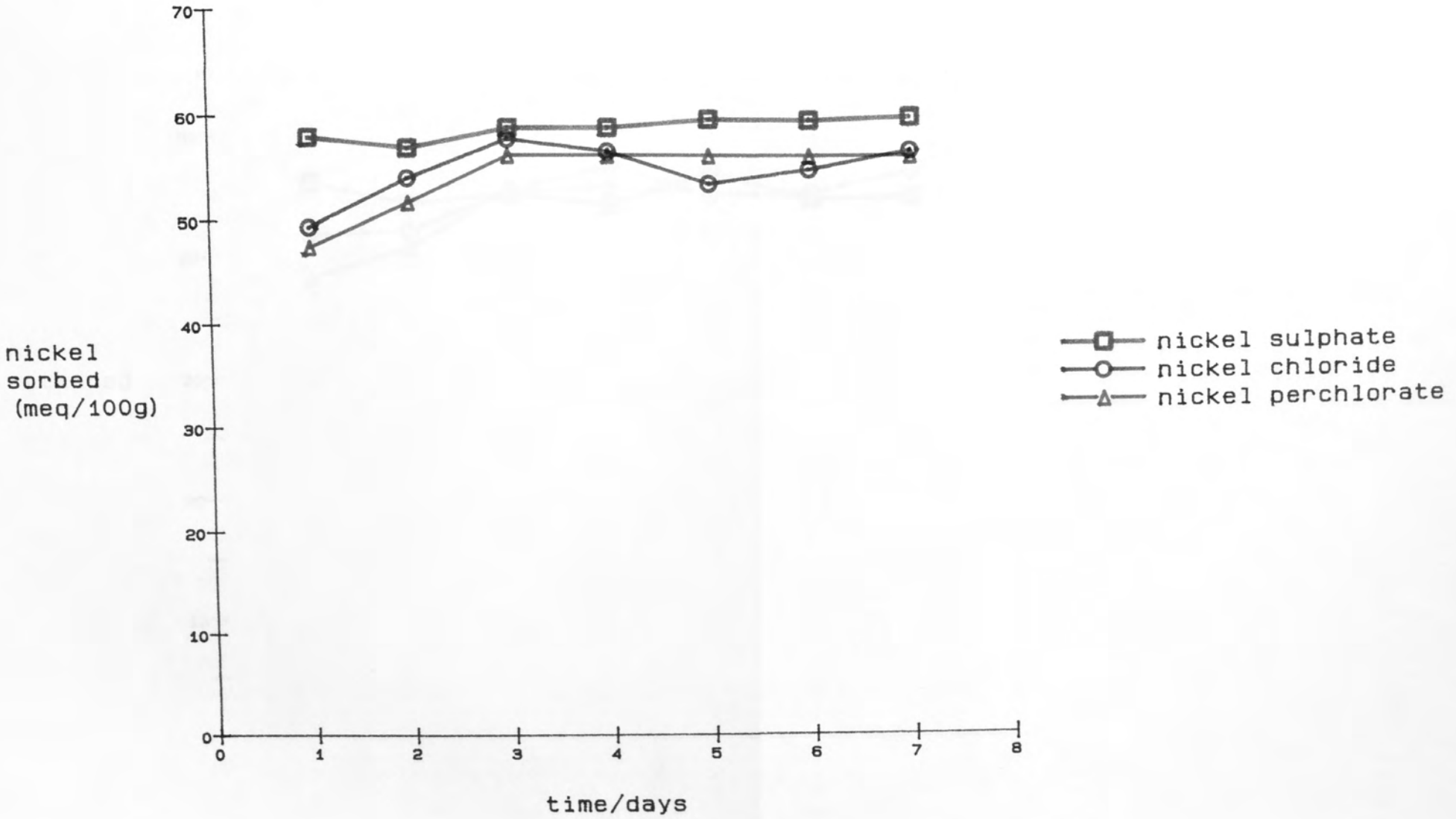

Fig.11 - Anion effect on variation of nickel retained on Na-montmorillonite with time.

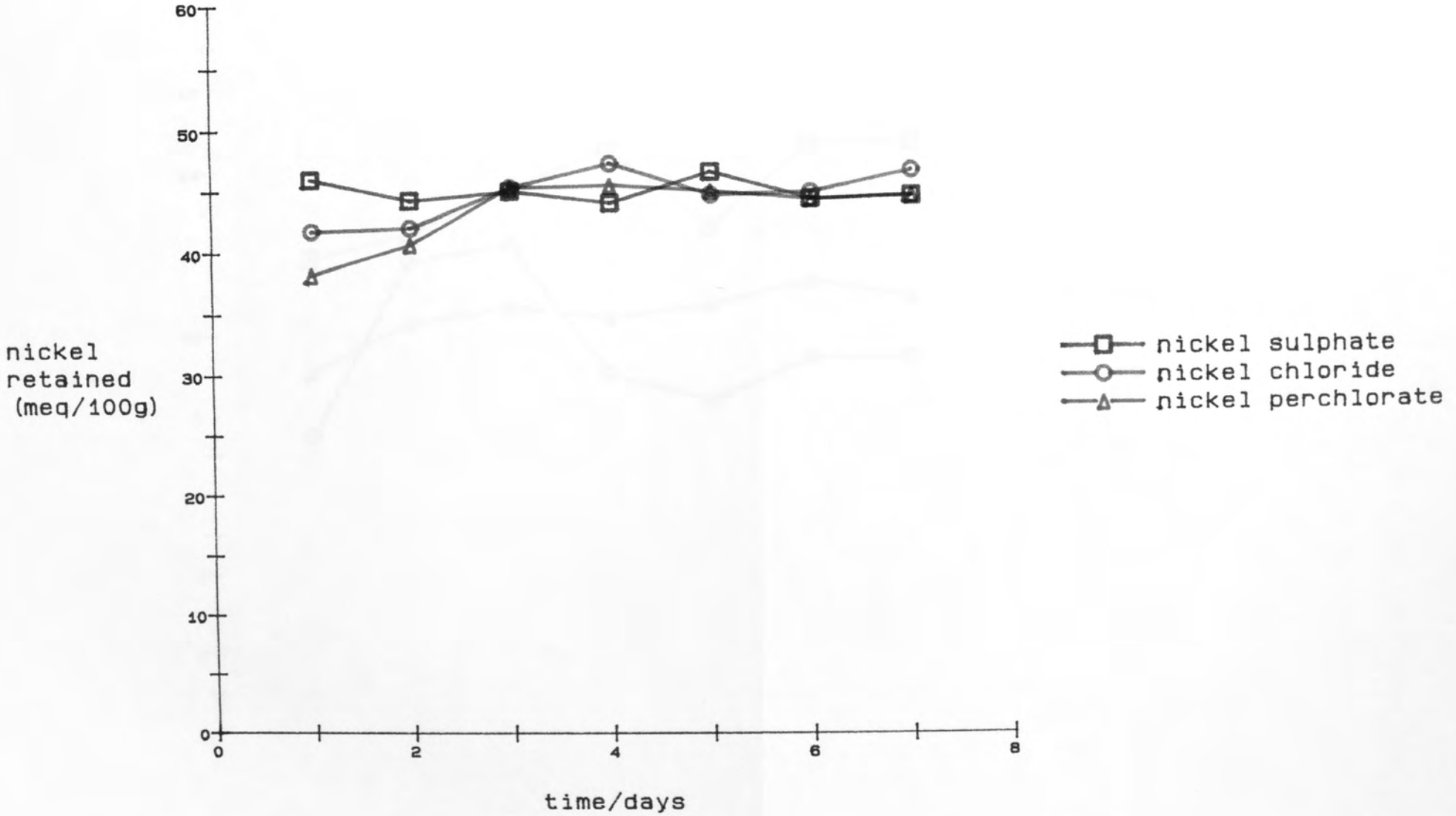

Fig.12 - Anion effect on variation of nickel released by Na-montmorillonite with time.

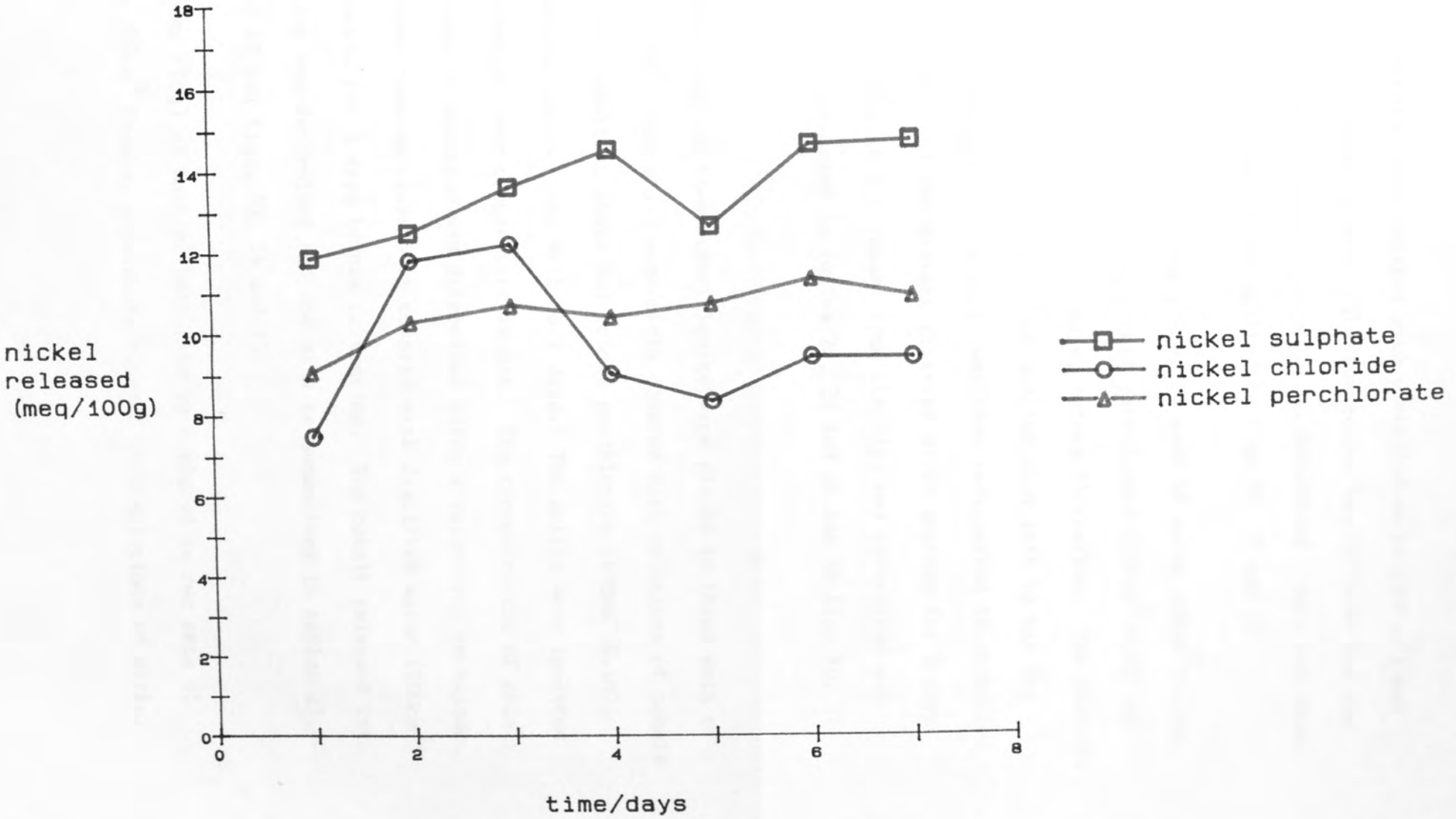

room temperature, then covered with distilled water ($100cm^3$) and shaken for a further 3 days. The suspension was filtered and the amount of nickel released into solution determined. Data are shown in tables 22, 23 and 24 and plotted in figs.10, 11 and 12.

3.5.2.3 Na-montmorillonite (10g) was placed in each of seven $250cm^3$ flasks, contacted with a solution of nickel perchlorate ($100cm^3$/0.1M) and shaken for a period of 1 to 7 days, before filtration. The filtrate was analysed for remaining nickel and the clay left to air dry at room temperature. This solid was then redispersed in distilled water ($100cm^3$) and the mixture filtered after shaking for 3 days. The amount of nickel released from the clay was determined and results are presented in tables 22, 23 and 24 and in figs.10, 11 and 12.

3.5.2.4 Portions (10g) of Na-montmorillonite were placed in three sets of seven $250cm^3$ flasks and separately covered with solutions of cobalt chloride, cobalt sulphate and cobalt perchlorate ($100cm^3$/0.1M), then shaken for periods of 1 to 7 days. The solids were isolated and dried at room temperature in air. The concentration of cobalt remaining in solution was determined using a volumetric technique. The above treated clays were covered with distilled water ($100cm^3$) and shaken for 3 days before filtration. The cobalt released into solution was determined and the data is summarised in tables 25, 26 and 27 and figs. 13, 14 and 15.

3.5.2.5 Portions (10g) of natural hectorite were placed in two sets of seven $250cm^3$ flasks, separately covered with solutions of nickel

Table 25 - Anion effect on variation of cobalt sorbed on Na-montmorillonite with time.

Time/Days	Co sorbed (meq/100g)		
	$CoSO_4$	$CoCl_2$	$Co(ClO_4)_2$
1	56	55	58
2	60	60	58
3	61	58	59
4	60	60	59
5	58	60	58
6	60	60	60
7	61	59	59

Table 26 - Anion effect on variation of cobalt retained on Na-montmorillonite with time.

Time/Days	Co retained (meq/100g)		
	$CoSO_4$	$CoCl_2$	$Co(ClO_4)_2$
1	46	49	47
2	46	52	48
3	46	48	49
4	45	51	48
5	45	52	48
6	46	50	48
7	47	50	48

Table 27 - Anion effect on variation of cobalt released by Na-montmorillonite with time.

Time/Days	Co released (meq/100g)		
	$CoSO_4$	$CoCl_2$	$Co(ClO_4)_2$
1	10.4	5.9	10.6
2	14	8.0	10.1
3	15	9.8	10.8
4	15	9.5	10.7
5	13	8.4	10.8
6	14	9.6	11.2
7	14	8.4	10.9

Fig.13 - Anion effect on variation of cobalt sorbed on Na-montmorillonite with time.

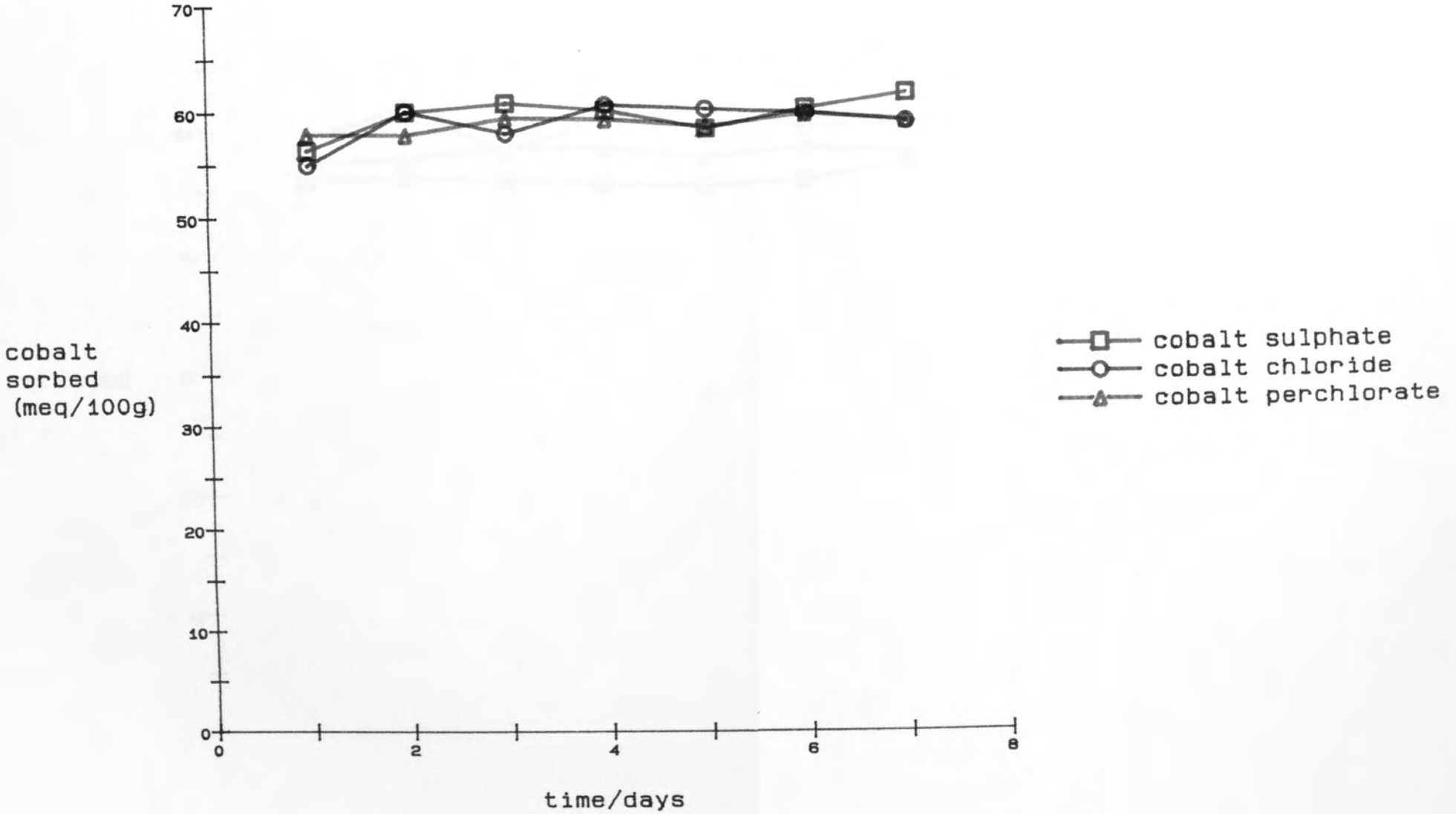

Fig.14 - Anion effect on variation of cobalt retained on Na-montmorillonite with time.

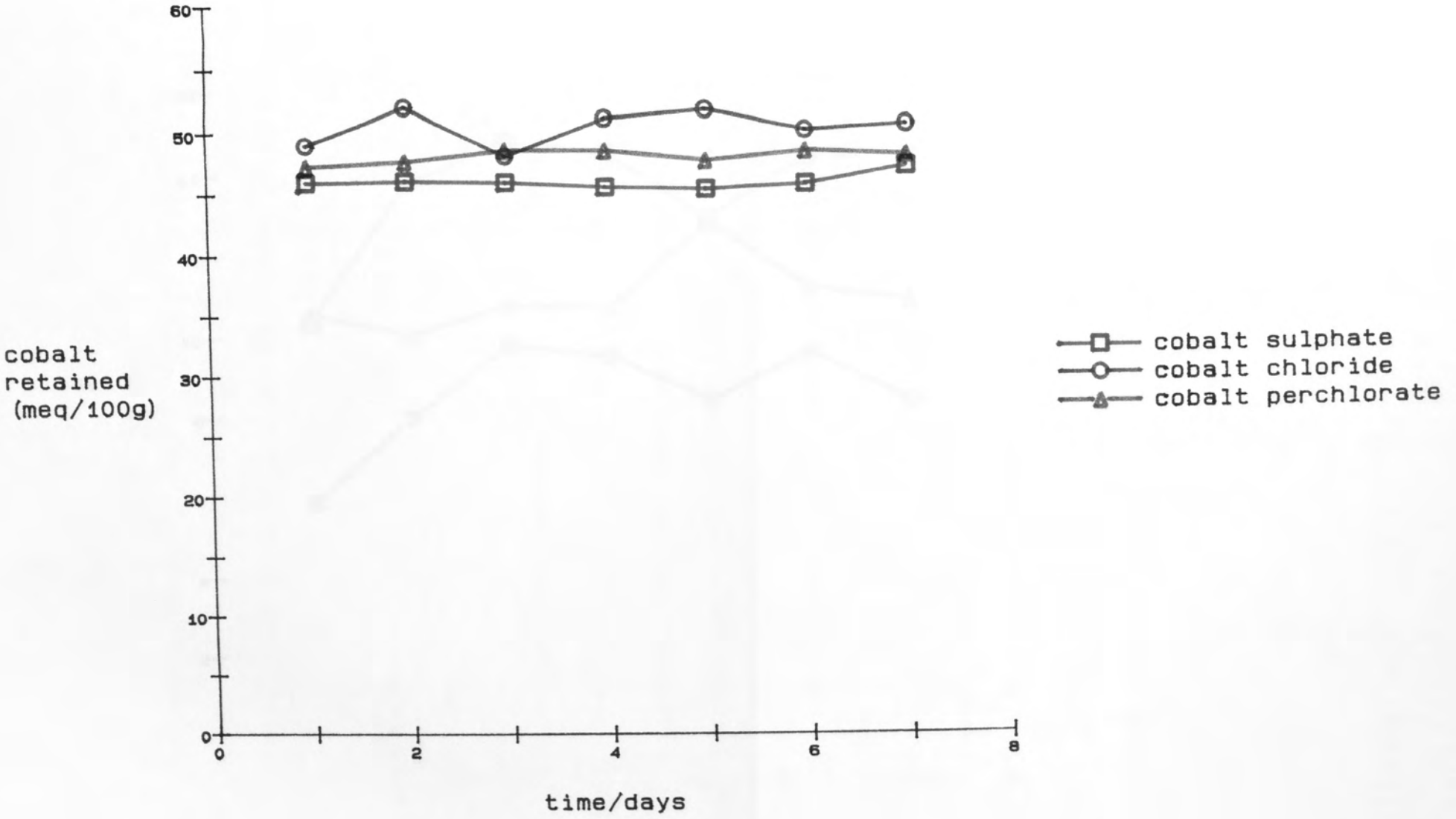

Fig.15 - Anion effect on variation of cobalt released by Na-montmorillonite with time.

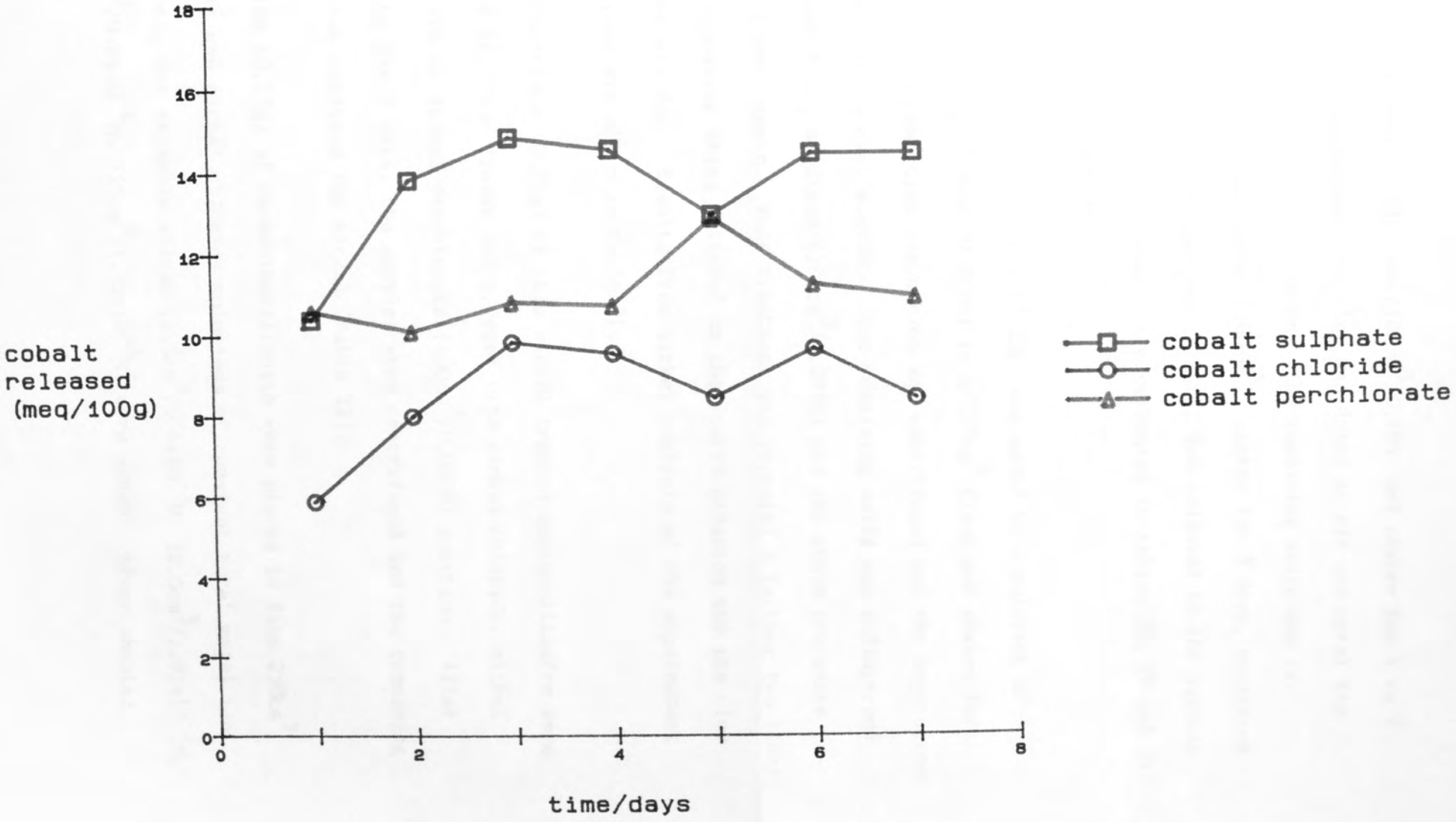

chloride and cobalt chloride ($100cm^3$/0.1M) and shaken for 1 to 7 days. After filtration, the clay was dried in air and metal ion remaining in solution determined. The remaining solid was re-dispersed in distilled water ($100cm^3$), shaken for 3 days, separated by filtration and the quantity of metal ion released to the aqueous phase determined. All results are presented in tables 28, 29 and 30 and figs.16, 17 and 18.

3.5.2.6 A sample of montmorillonite (2.25g) was added to a solution of nickel chloride ($100cm^3$/0.097M) in a $250cm^3$ flask and shaken for 3 days. The resulting suspension was centrifuged and the supernatent analysed for nickel content. The remaining solid was redispersed in fresh $NiCl_2$ solution ($100cm^3$/0.097M) and the above procedure was followed again. This treatment was repeated a further two times, the suspension being filtered on the fourth occasion and the clay left to air dry. Results from nickel analysis of the supernatent solutions are shown in table 31.

Three portions (0.25g) of this nickel treated montmorillonite were placed in $250cm^3$ flasks and covered with nickel chloride, nickel sulphate or nickel perchlorate ($100cm^3$/0.001M) solution. After shaking for 3 days, the samples were centrifuged and the remaining solution analysed for nickel (table 32).

3.5.2.7 Samples (0.25g) of Na-montmorillonite were placed in five $250cm^3$ flasks and nickel chloride solutions of constant total metal ion content, but variable volume ($2.5cm^3$/$9.6x10^{-3}$M, $12.5cm^3$/$1.92x10^{-3}$M, $25cm^3$/$9.6x10^{-4}$M, $125cm^3$/$1.92x10^{-4}$M) were added. After shaking

Table 28 - Variation of nickel and cobalt sorbed on natural hectorite with time.

Time/Days	Metal ion sorbed (meq/100g)	
	$NiCl_2$	$CoCl_2$
1	48	51
2	47	55
3	48	54
4	50	53
5	51	53
6	49	57
7	49	53

Table 29 - Variation of nickel and cobalt retained on natural hectorite with time.

Time/Days	Metal ion retained (meq/100g)	
	$NiCl_2$	$CoCl_2$
1	43	45
2	41	48
3	42	48
4	44	48
5	44	46
6	43	50
7	43	47

Table 30 - Variation of nickel and cobalt released from natural hectorite with time.

Time/Days	metal ion released (meq/100g)	
	$NiCl_2$	$CoCl_2$
1	5.1	6.0
2	5.9	6.5
3	5.8	5.6
4	6.1	5.5
5	6.7	6.2
6	6.0	7.0
7	6.6	6.3

Table 31 - Nickel sorbed on a Na-montmorillonite upon successive treatment with nickel chloride solution.

Nickel chloride treatment	Initial Ni concentration (mmol/L)	Final Ni concentration(C) (mmol/L)	log C	Ni sorbed (meq/100g)	K_d (cm^3/g)	log K_d
1	97.0	90.5	1.96	58	3.2	0.50
2	97.0	95.0	1.98	18	4.0	0.60
3	97.0	96.5	1.98	4	4.1	0.61
4	97.0	97	-	0	-	-
Total nickel sorbed = $80 meq 100^{-1}$						

Table 32 - Nickel released from a nickel chloride saturated montmorillonite.

Sample	Initial Ni concentration (mmol/L)	Final Ni concentration(C) (mmol/L)	log C	Ni released (meq/100g)	K_d (cm^3/g)	log K_d
clay + $NiCl_2$	0.98	1.34	0.13	29	180	2.26
clay + $Ni(ClO_4)_2$	1.01	1.39	0.14	30	178	2.25
clay + $NiSO_4$	1.03	1.44	0.16	33	164	2.21

Fig.16 - Variation of nickel and cobalt sorbed on natural hectorite with time.

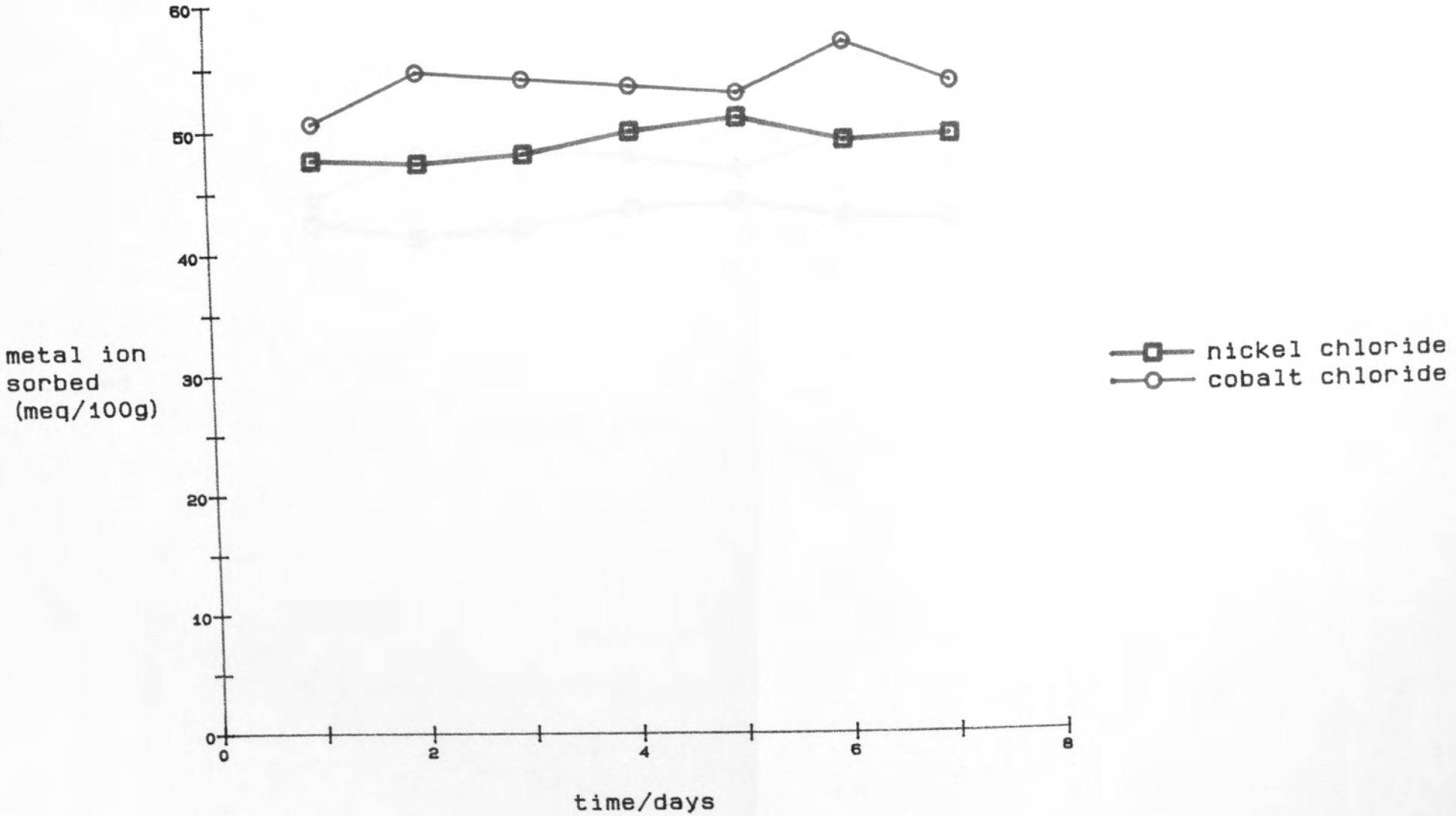

Fig.17 - Variation of nickel and cobalt retained on natural hectorite with time.

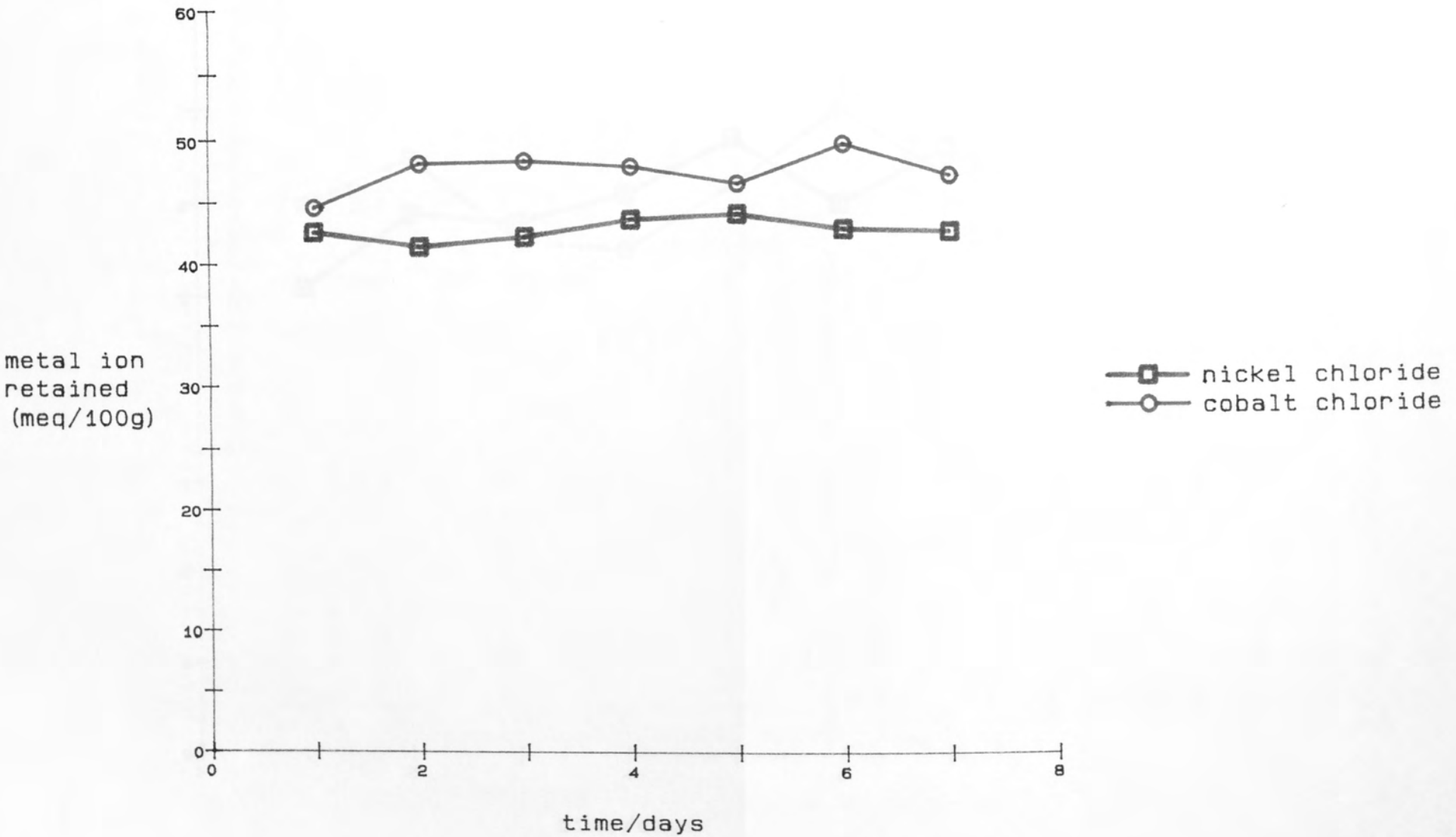

Fig.18 - Variation of nickel and cobalt released from natural hectorite with time.

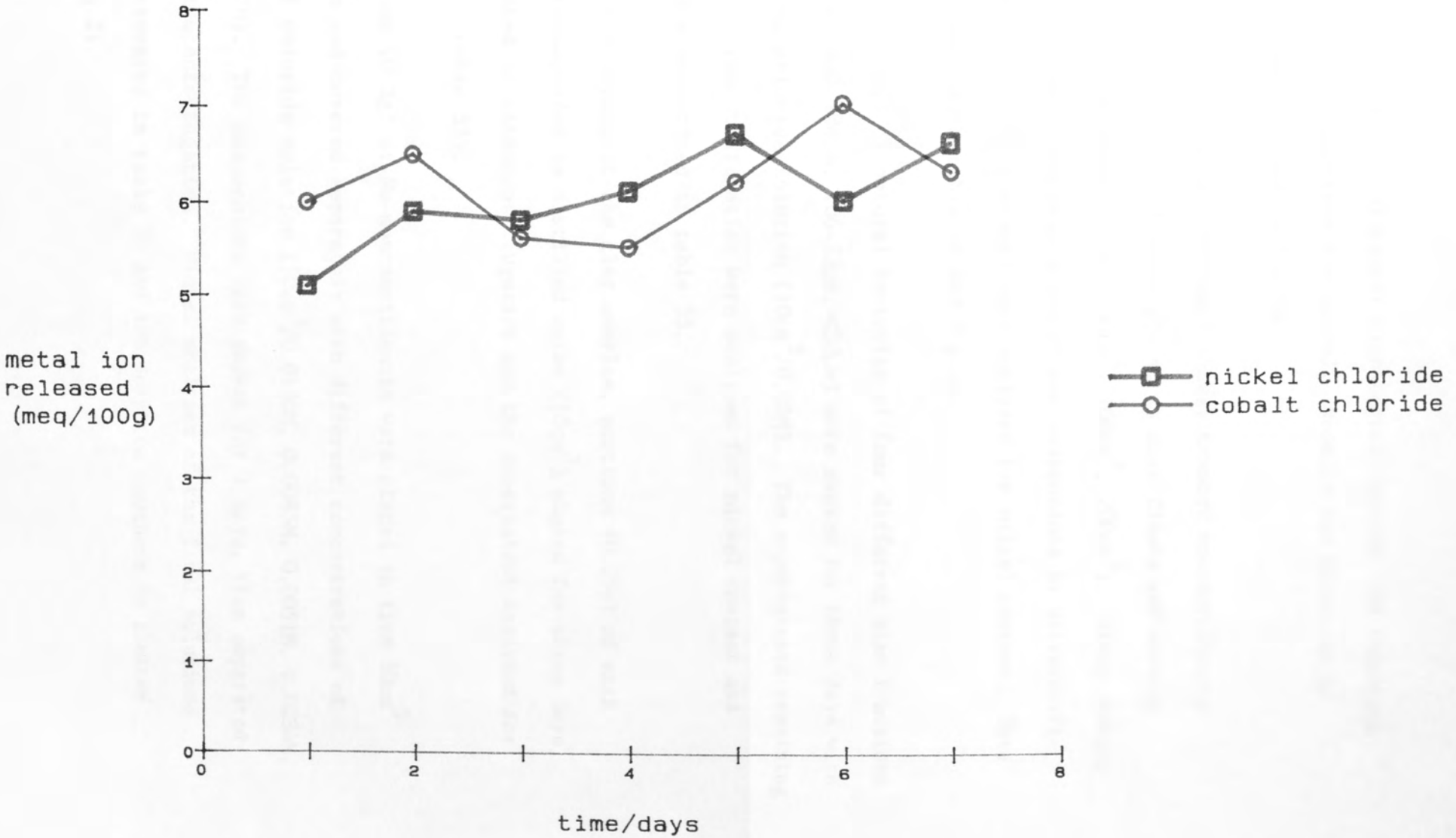

for three days and subsequent ultracentrifugation, the remaining solutions were analysed for nickel. Results are presented in table 33 and plotted in fig.19.

3.5.2.8 Portions (1.0g) of a previously nickel treated montmorillonite (see section 3.5.1.1.3) were placed in four flasks and covered with distilled water ($10cm^3$, $50cm^3$, $100cm^3$, $200cm^3$). After shaking for three days, and separation of the suspensions by ultracentrifugation, the supernatents were analysed for nickel content. Data are presented in table 34 and fig.20.

3.5.2.9 Samples (1.0g) of natural hectorite of four different size fractions (>500μm, 500–106μm, 106–53μm, <53μm) were shaken for three days with a nickel chloride solution ($10cm^3$/0.05M). The supernatents remaining after ultracentrifugation were analysed for nickel content and data are summarised in table 35.

After air drying of the clay samples, portions (0.25g) of each were resuspended in distilled water ($10cm^3$), shaken for three days, separated by ultracentrifugation and the supernatent analysed for nickel (table 35).

3.5.2.10 Portions (0.2g) of Na-montmorillonite were placed in five $50cm^3$ flasks and covered separately with different concentrations of nickel chloride solution ($10cm^3$/0.0170M, 0.0085M, 0.0051M, 0.0034M, 0.0017M). The suspensions were shaken for 3 days, then separated by ultracentrifugation. Nickel analyses of the final solutions are presented in table 36 and the sorption isotherm is plotted in fig.21.

Table 33 - Influence of volume of added nickel solution on sorption by Na-montmorillonite.

Volume of Ni solution used (cm^3)	Initial Ni concentration (mmol/L)	Final Ni concentration (mmol/L)	nickel sorbed (meq/100g)
2.50	9.60	0.35	18.5
12.50	1.92	0.0129	19.1
25.0	0.96	0.023	18.7
125.0	0.192	0.026	16.6

Table 34 - Variation of nickel released from a nickel-montmorillonite, with initial solution volume.

Volume of distilled water used (cm^3)	Final solution Ni concentration (mmol/L)	Ni released (meq/100g)
10.00	4.0	8.0
50.0	0.80	8.0
100.0	0.46	9.2
200.0	0.25	10.0

Table 35 - Variation of nickel sorption on hectorite with particle size and nickel released with subsequent redispersion in distilled water.

Sample particle size (μm)	Initial Ni concentration (mmol/L)	Final Ni concentration (mmol/L)	Ni sorbed (meq/100g)	nickel released on redispersion (mmol/L)	Ni released (meq/100g)
>500	50.1	22	56	0.134	1.07
500-106	50.1	23	55	0.120	0.96
106-53	50.1	21	58	0.138	1.11
<53	50.1	21	58	0.51	4.1

Table 36 - Nickel sorption isotherm data on Na-montmorillonite.

Initial Ni concentration (mmol/L)	Final Ni concentration(C) (mmol/L)	log C	Ni sorbed (meq/100g)	K_d	log K_d	% Ni sorbed
17.0	10.7	1.03	64	30	1.48	38
8.52	2.19	0.34	63	140	2.16	74
5.11	0.34	-0.47	47.7	700	2.85	93.3
3.41	0.068	-1.17	33.4	2500	3.39	98.0
1.70	0.0072	-2.14	16.9	11700	4.07	99.56

Table 37 - Cobalt sorption isotherm data on Na-montmorillonite.

Initial Co concentration (mmol/L)	Final Co concentration(C) (mmol/L)	log C	Co sorbed (meq/100g)	K_d	log K_d	% Co sorbed
17.0	9.8	0.99	71	36	1.56	42
8.48	3.4	0.53	51	76	1.88	60
5.09	0.62	-0.21	44.7	360	2.56	88
3.39	0.104	-0.98	32.9	1600	3.20	96.9
1.70	0.020	-1.70	16.8	4200	3.62	98.8

Fig.19 - Variation of nickel sorbed on Na-montmorillonite with initial solution volume.

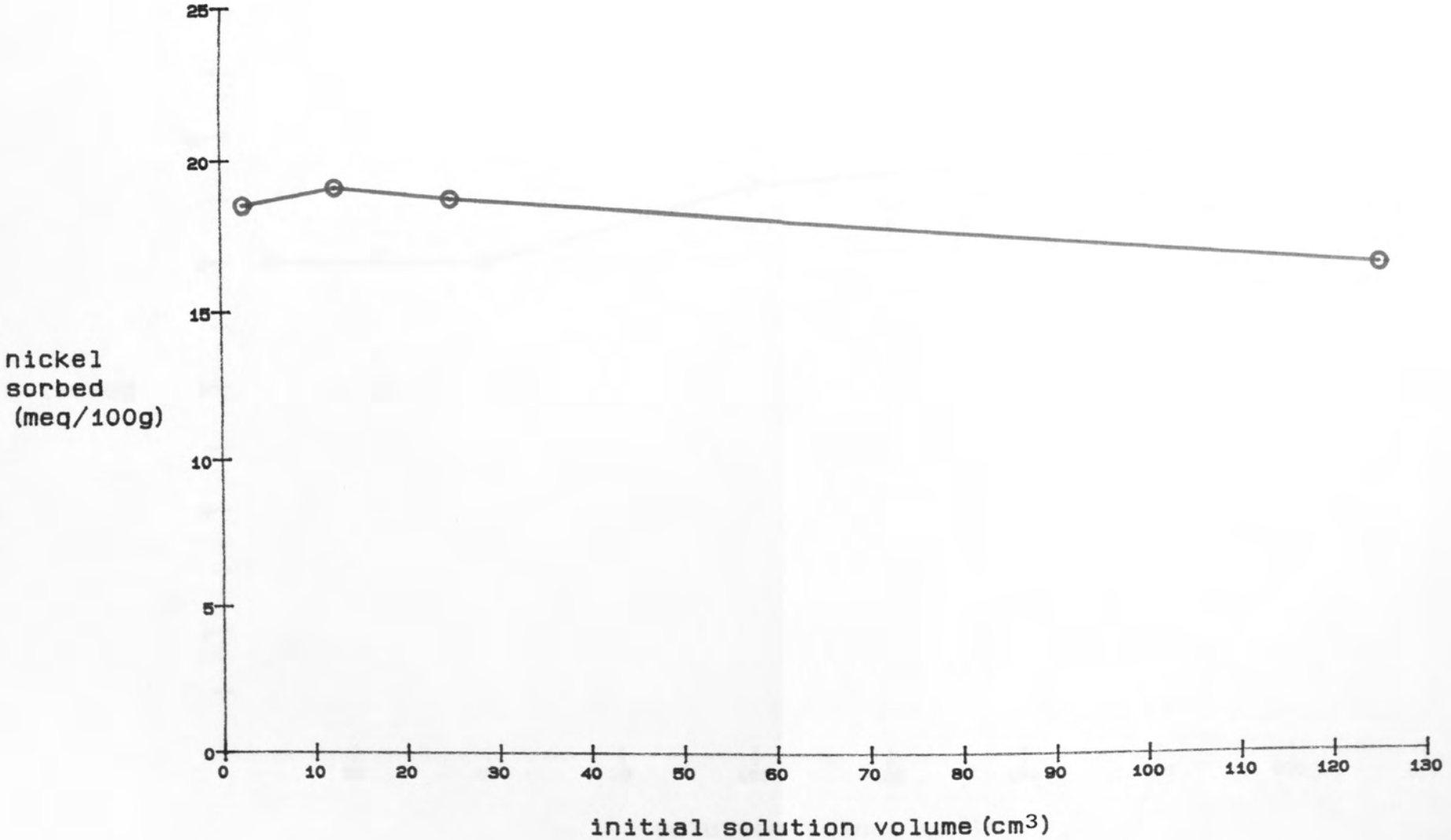

Fig.20 - Variation of nickel released from a nickel-montmorillonite with initial solution volume.

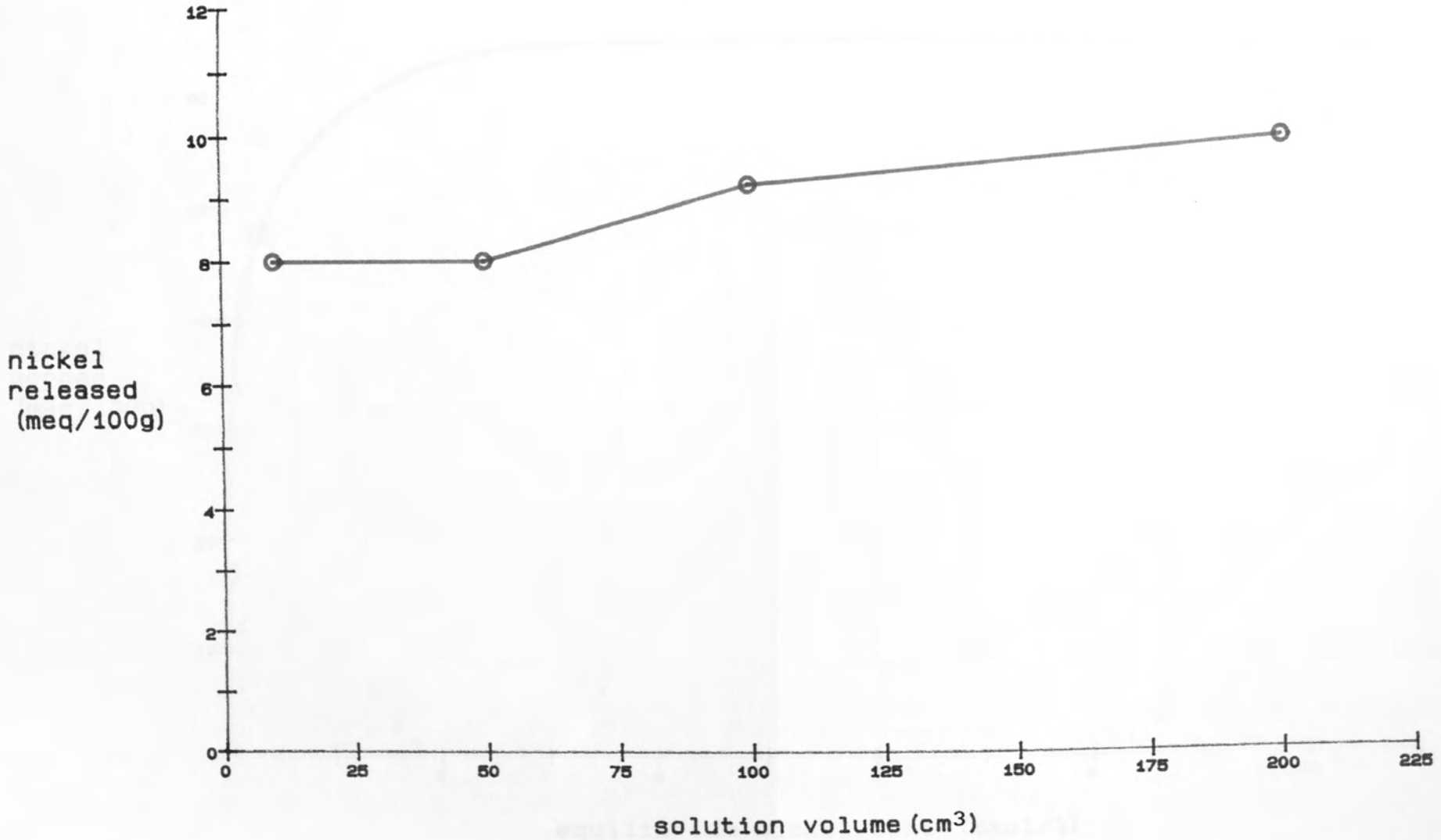

Fig.21 - Nickel sorption isotherm on Na-montmorillonite.

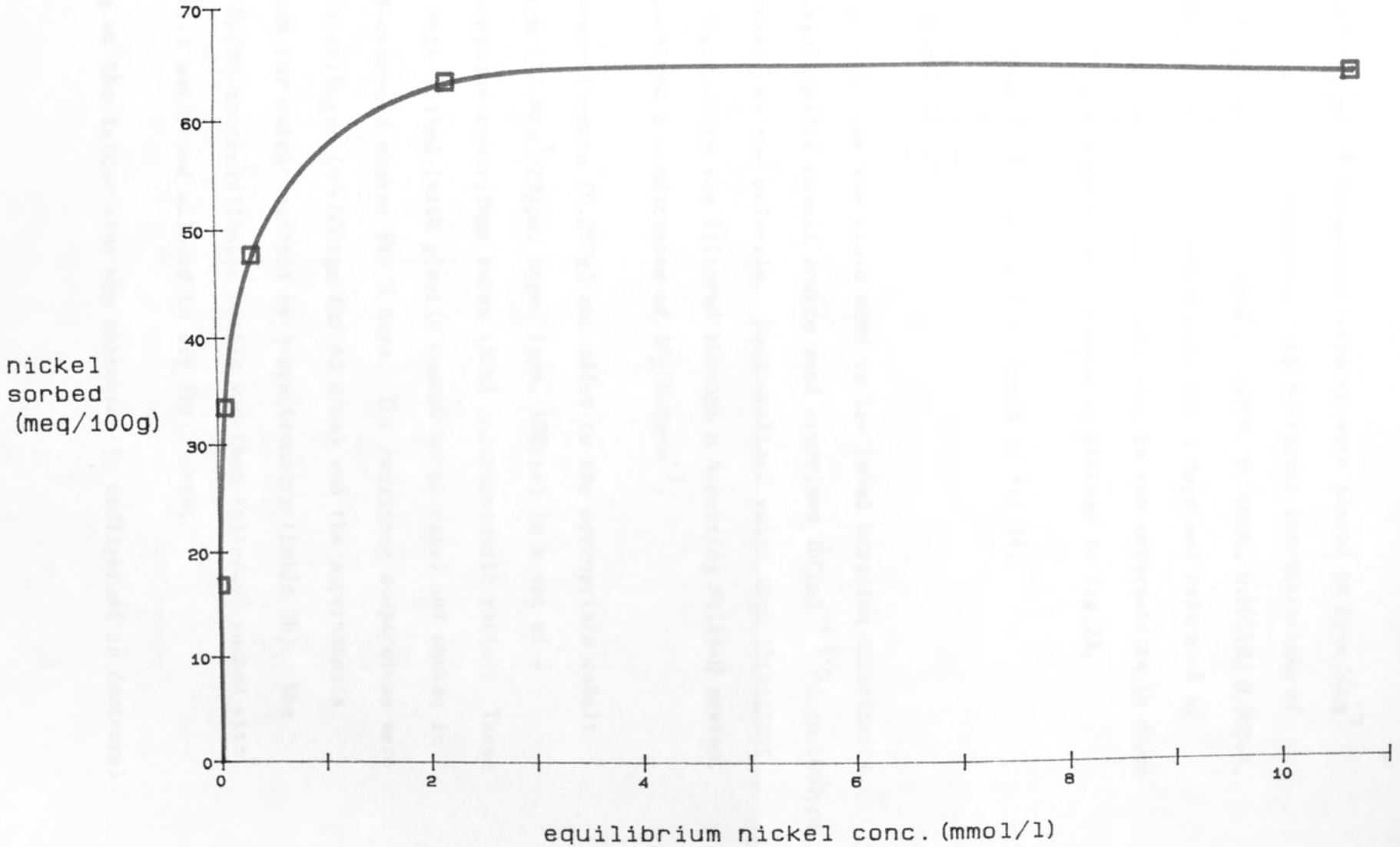

A plot of log K_d versus log C is shown in fig.22.

3.5.2.11 Portions (0.2g) of Na-montmorillonite were placed in five $50cm^3$ flasks and covered separately with different concentrations of cobalt chloride solution ($10cm^3$/0.0170M, 0.0085M, 0.0051M, 0.0034M, 0.0017M). The samples were shaken for 3 days and separated by ultracentrifugation. Cobalt remaining in the supernatents is shown in table 37 and a sorption isotherm is plotted in fig.23.

A plot of log K_d versus log C is shown in fig 24.

3.5.3 Microscopic effects

A batch technique was again used in low level sorption experiments. The radiolabelled cobalt source used comprised $1\mu Ci ml^{-1}$ ^{60}Co in 1000ppm Co carrier, as the chloride. Demineralised water used throughout these experiments was filtered through a 4-housing Milli-Q system, and exhibited a conductance of $18\pm1 Mohm cm^{-1}$.

3.5.3.1 Na-montmorillonite (0.252g) was added to the appropriate cobalt solution ($12.6cm^3$/10ppm, 5ppm, 1ppm, 100ppb) in a set of 4 polypropylene centrifuge tubes (50:1 solution:solid ratio). These tubes were sealed (with plastic coated metal caps) and shaken in an end-over-end shaker for 3 days. The resulting suspensions were ultracentrifuged (40 000rpm for 45 mins) and the supernatents analysed for cobalt content by γ-spectrometry (table 38). The 10ppm Co/Na-montmorillonite sample was then filtered, washed with distilled water and allowed to dry for 3 days.

0.145g of the latter clay was subsequently redispersed in demineral-

Table 38 - Cobalt sorption on Na-montmorillonite, at low concentration.

Initial Co concentration(ppb)	Final Co concentration(ppb)	Co sorbed (meq/100g)	% Co sorbed	K_d
10 000	30	1.70	99.7	1.7×10^4
5 000	<6*	>0.85	>99.8	$>3.9 \times 10^4$
1 000	<3.1*	>0.169	>99.7	$>1.6 \times 10^4$
100	<1.5*	>0.017	>98.5	$>3.2 \times 10^3$

*these are the detection limits derived from the γ-spectrometric analysis - detection limits are dependent on counting time.

Table 39 - Cobalt release from a cobalt treated montmorillonite.

Sample	Equlibrium Co concentration (ppb)	cobalt initially on clay (meq/100g)	% Co released	K_d
Co/Na-montmorillonite	31	1.69	0.45	1.6×10^4

Fig.22 - Log K_d (Ni) versus log (equilibrium Ni conc.) for nickel sorption on Na-montmorillonite.

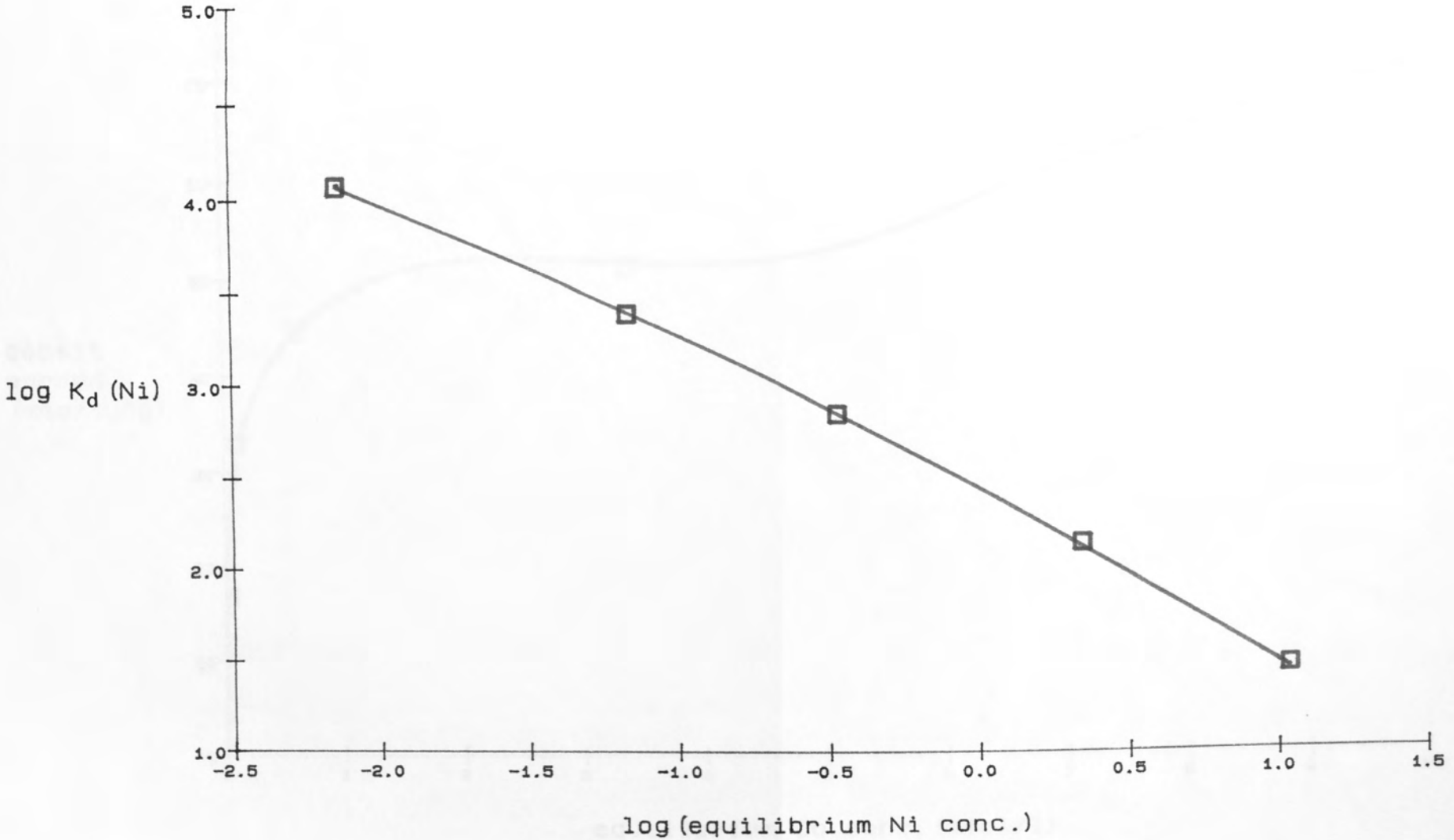

Fig.23 - Cobalt sorption isotherm on Na-montmorillonite.

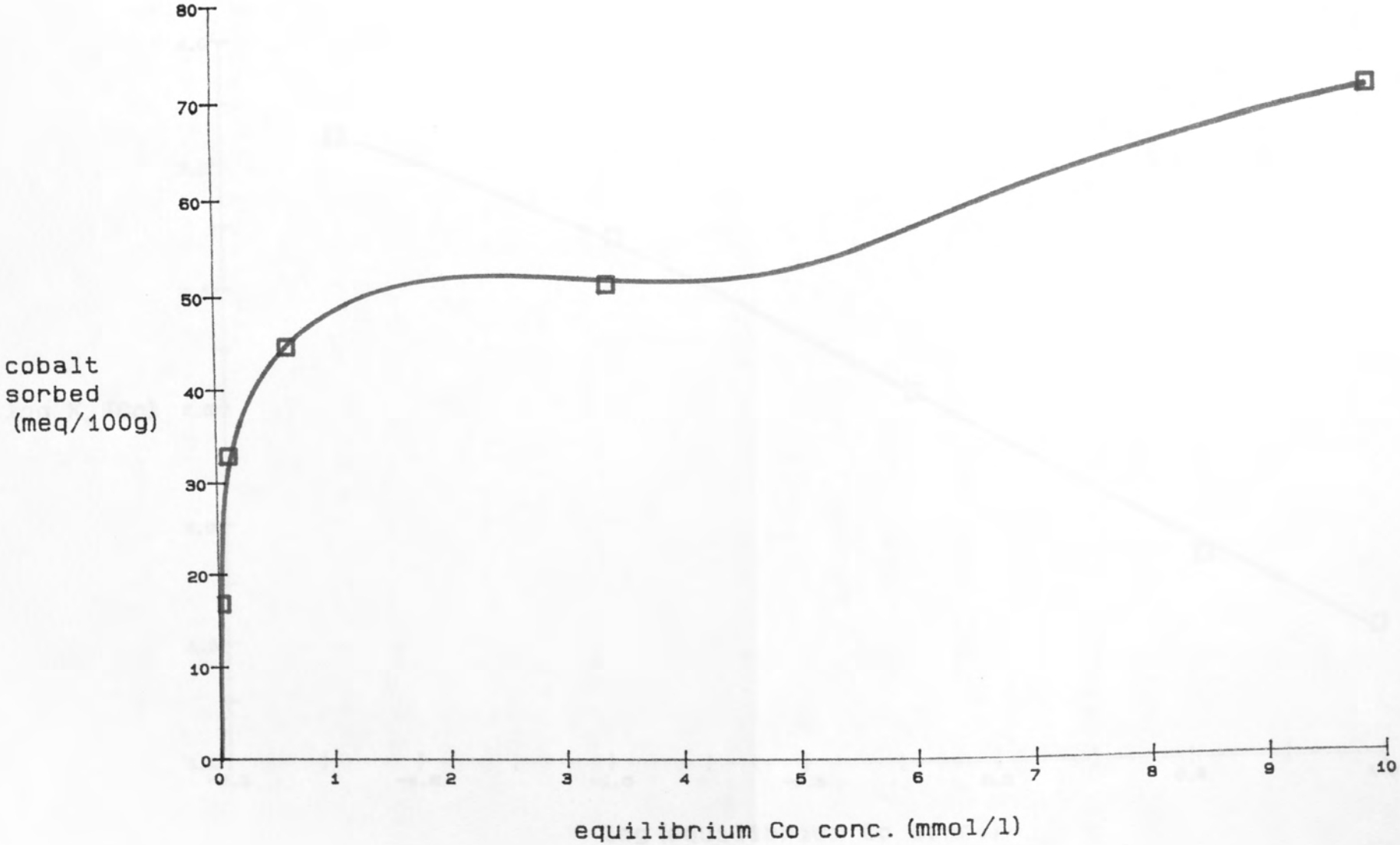

Fig.24 - Log K_d (Co) versus log (equilibrium Co conc.) for cobalt sorption on Na-montmorillonite.

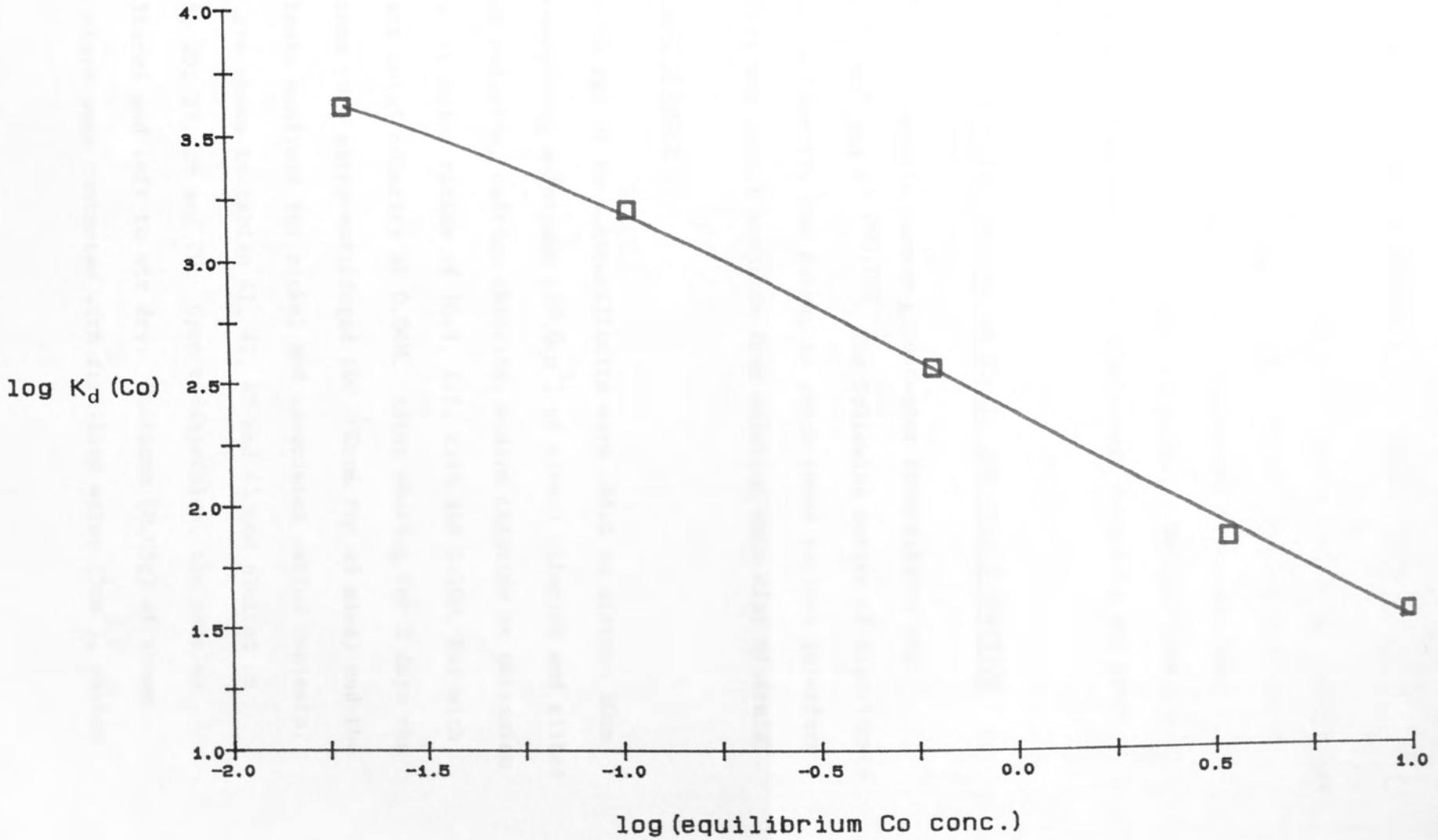

ised water ($10.7cm^3$), shaken for 3 days and the supernatent remaining after ultracentrifugation analysed for cobalt (table 39).

3.5.3.2 Portions of Na-montmorillonite (0.252g) were added to the appropriate nickel solution ($12.6cm^3$/10ppm, 2ppm, 500ppb, 100ppb) in a set of 4 polypropylene centrifuge tubes. The sealed tubes were then shaken for 3 days before ultracentrifugation. Details from ion chromatographic analyses of the supernatent solutions are given in table 40.

3.6 INFLUENCE OF COMPETING CATIONS ON NICKEL AND COBALT SORPTION

Cations which dominate common groundwater compositions are Mg^{2+}, Ca^{2+}, Na^+ and K^+.[100,101] The following series of experiments attempted to identify the extent to which these cations interfere with nickel and cobalt sorption from solution onto clay minerals.

3.6.1 Macroscopic effects

3.6.1.1 Portions (0.2g) of Na-montmorillonite were added to sixteen $50cm^3$ flasks containing solutions ($10.0cm^3$) of nickel chloride and either magnesium chloride, calcium chloride, sodium chloride or potassium chloride, in molar ratios of 10:1, 1:1, 1:10 and 1:100, but with a constant total molarity of 0.04M. After shaking for 3 days the suspensions were ultracentrifuged (40 000rpm for 45 mins) and the supernatents analysed for nickel and associated cation contents. Results are shown in tables 41, 42, 43 and 44 and plotted on figs. 25, 26, 27, 28 and 29. Upon redispersion, the samples were filtered and left to air dry. Portions (0.05g) of these treated clays were contacted with distilled water ($5cm^3$), shaken

Table 40 - Nickel sorption on Na-montmorillonite, at low concentration.

Initial Ni concentration(ppb)	Final Ni concentration(ppb)	Ni sorbed (meq/100g)	% Ni sorbed	K_d
10 000	7	1.70	99.93	6.8×10^4
2 000	6	0.34	99.7	1.6×10^4
500	14	0.083	97.2	1.8×10^3
100	12	0.01	88	3.6×10^2

Tables 41, 42, 43, 44 - Nickel sorption on Na-montmorillonite at constant molar strength in the presence of competing cations (M^{n+}).

Ratio	Initial Ni conc. (mmol/L)	Initial M^{n+} conc. (mmol/L)	Final Ni conc. (mmol/L)	Final M^{n+} conc. (mmol/L)	Ni sorbed (meq/100g)	M^{n+} sorbed (meq/100g)	% Ni sorbed	% M^{n+} sorbed	K_d(Ni)	K_d(M^{n+})
Table 41 Mg:Ni										
100:1	0.408	39.6	0.31	31	1.0	83	24	21	16	13
10:1	3.44	36.4	2.8	29	6.0	73	19	20	11	13
1:1	18.9	20.0	15.5	16.1	34	39	18	19	11	12
1:10	34.4	3.66	28	3.0	70	6.2	20	17	12	10
Table 42 Ca:Ni										
100:1	0.408	39.6	0.35	34	0.57	60	14	15	8	9
10:1	3.44	36.4	3.0	32	4.3	45	13	12	7	7
1:1	18.9	20.0	16.9	16.7	21	33	11	17	6	10
1:10	34.4	3.66	30	2.9	44	8	13	21	7	13
Table 43 Na:Ni										
100:1	0.408	39.4	0.073	38	3.35	7	82		230	
10:1	3.44	36.4	1.06	41	23.8	-25	69		112	
1:1	18.9	20.0	14.3	29	46	-44	24		16	
1:10	34.4	3.66	29	15.2	58	-60	17		10	
Table 44 K:Ni										
100:1	0.408	39.6	0.15	36	2.58	18	63	9	86	5
10:1	3.44	36.4	1.74	34	17.0	10	49	5	49	3
1:1	18.9	20.0	14.8	18.2	41	9	22	9	14	5
1:10	34.4	3.66	29	3.3	54	1.6	16	9	9	5

Fig.25 - Variation of %Ni/Co sorbed with initial solution concentration when in competition with magnesium ions at constant 0.04M molarity.

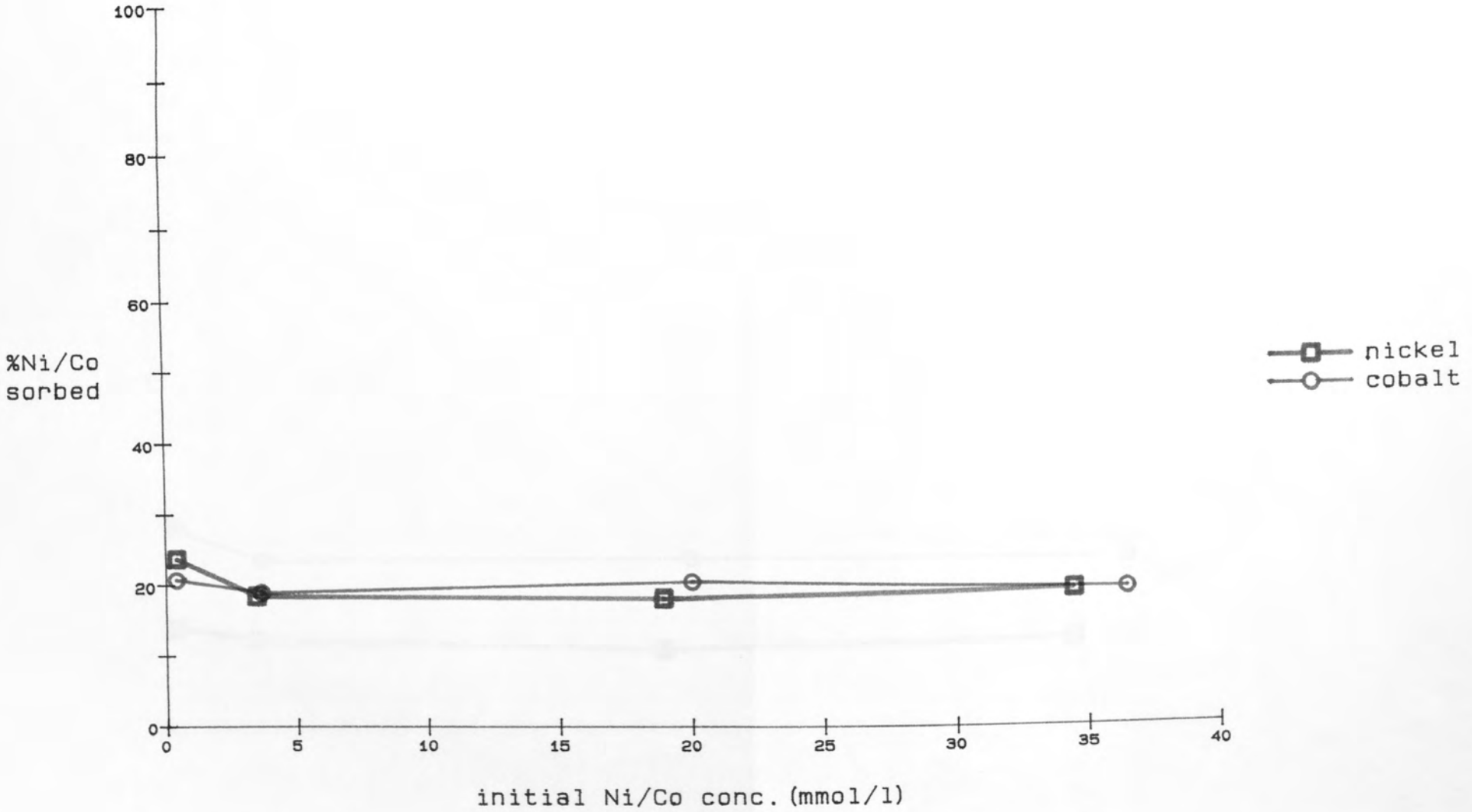

Fig.26 - Variation of %Ni/Co sorbed with initial solution concentration when in competition with calcium ions at constant 0.04M molarity.

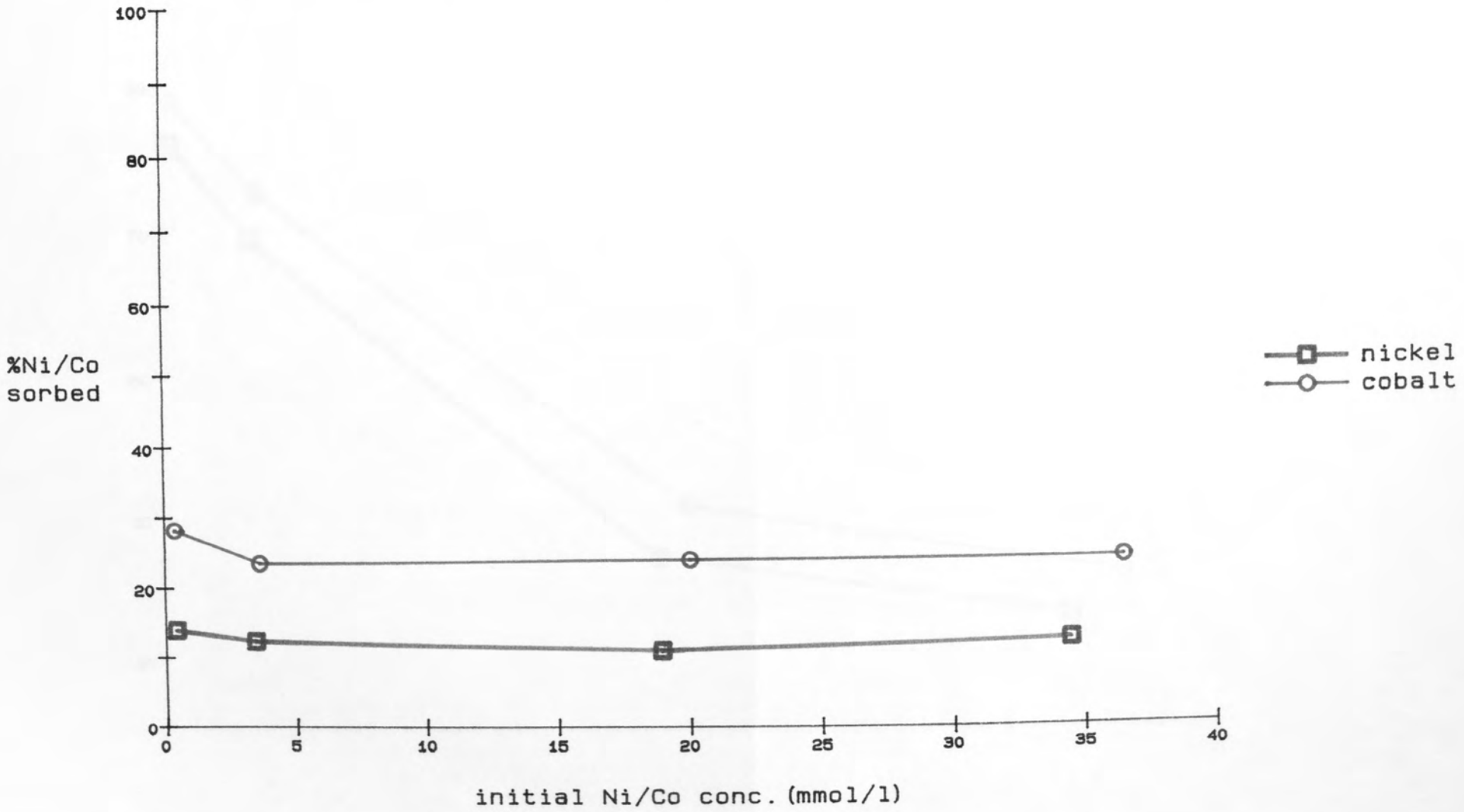

Fig.27 - Variation of %Ni/Co sorbed with initial solution concentration when in competition with sodium ions at constant 0.04M molarity.

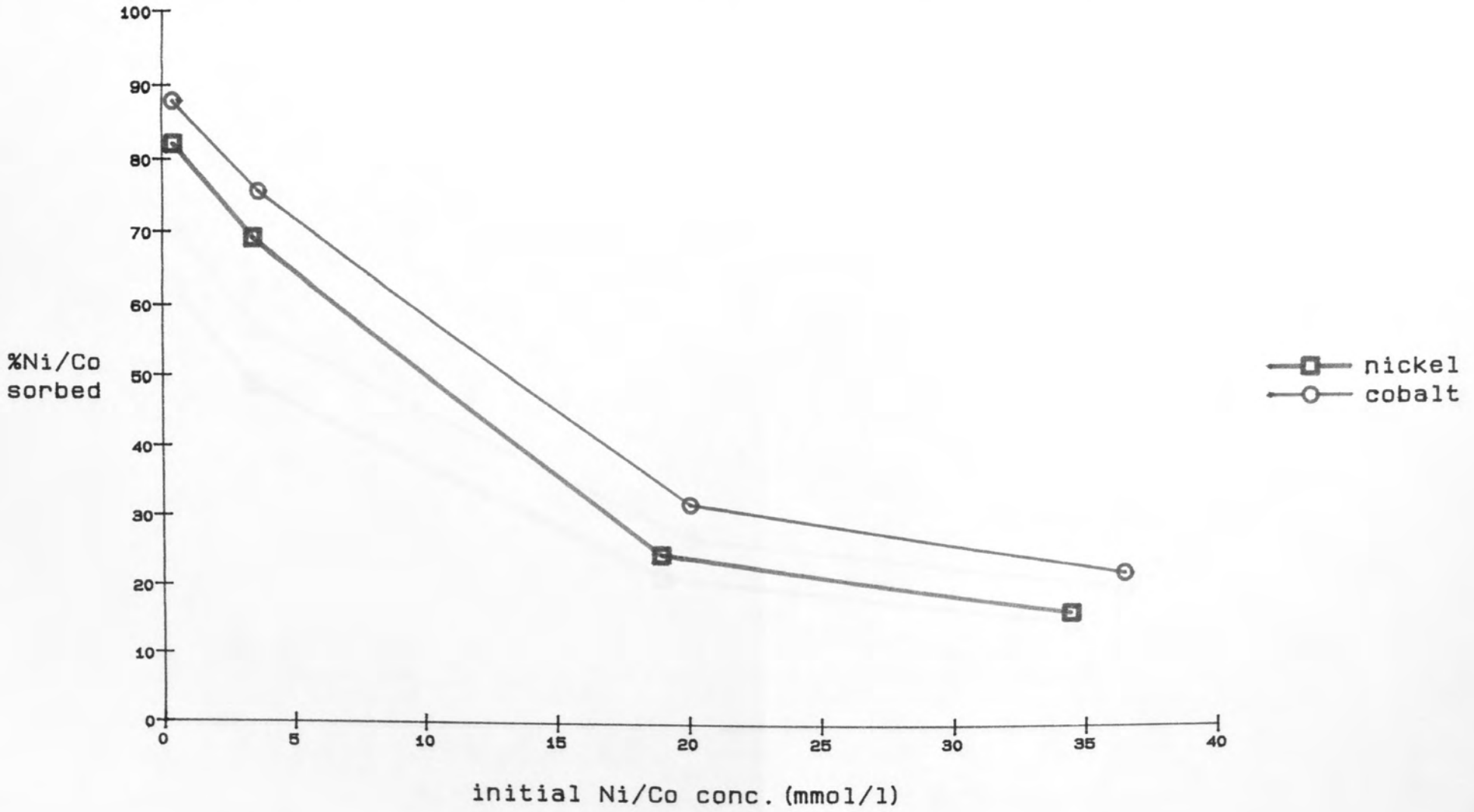

Fig.28 - Variation in %Ni/Co sorbed with initial solution concentration when in competition with potassium ions at constant 0.04M molarity.

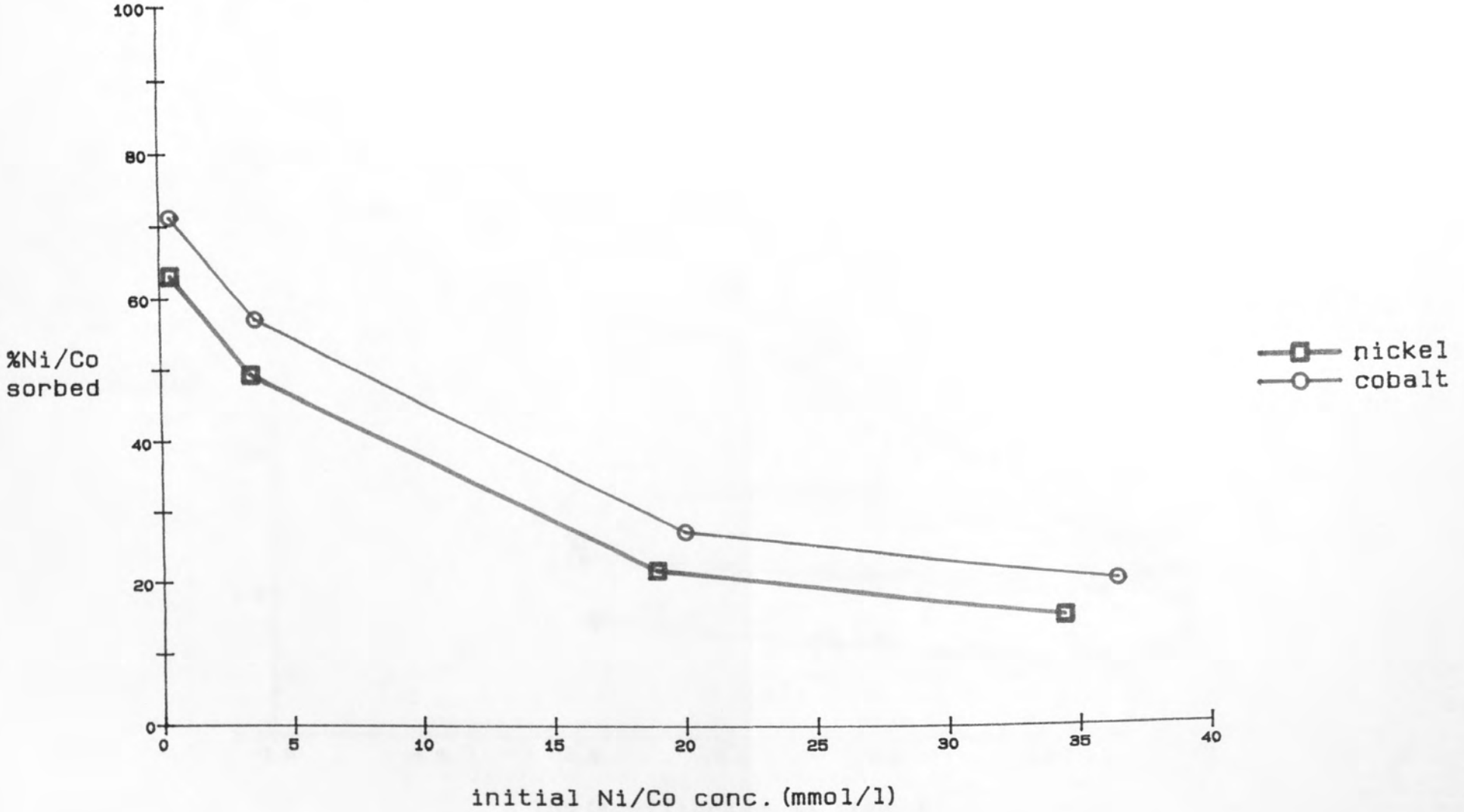

Fig.29 - Variation of log K_d (Ni/Co) with final solution concentration in competition experiments at constant (0.04M) molarity.

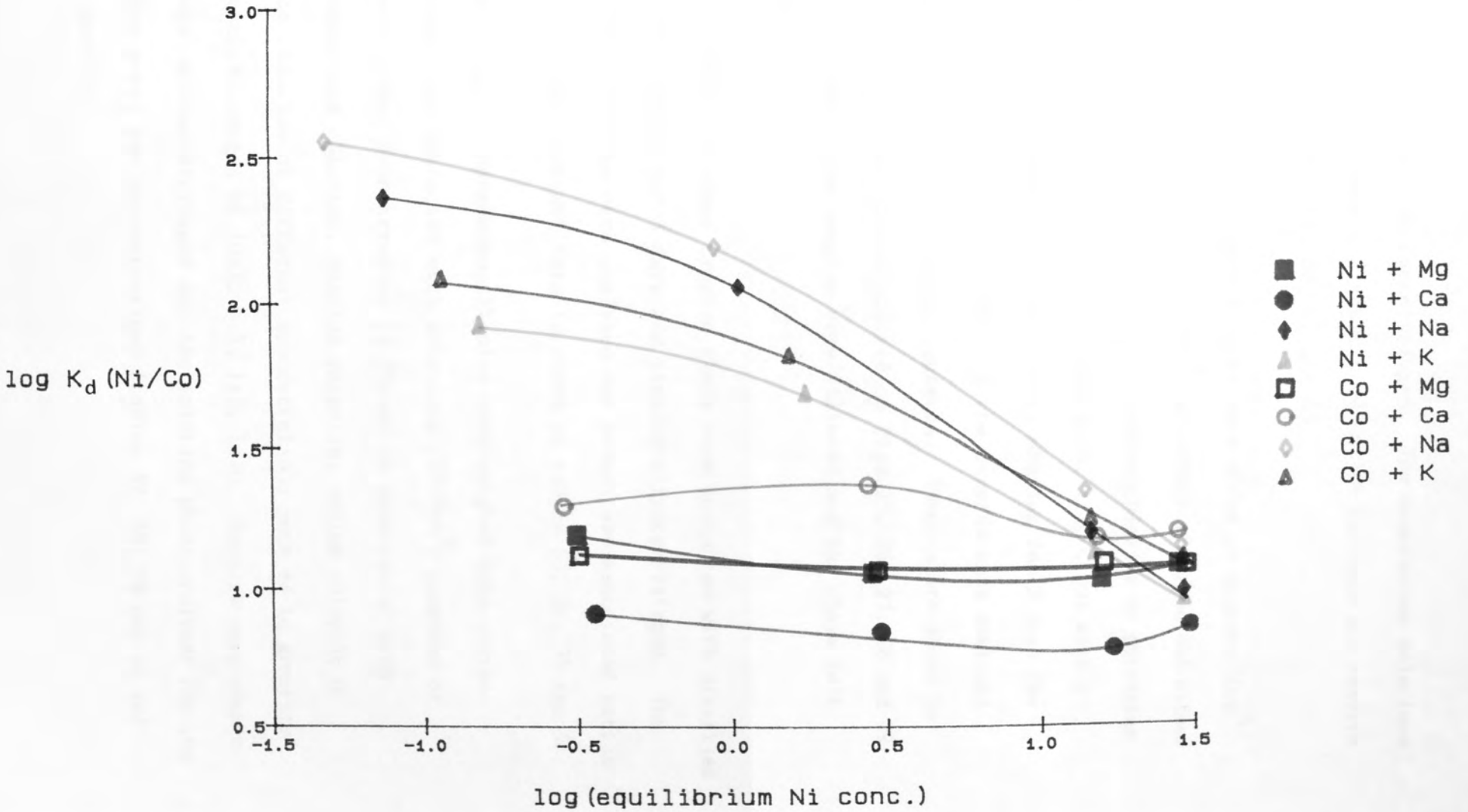

for 3 days and finally ultracentrifuged. The supernatent solutions were analysed for nickel and associated cation contents and results are presented in tables 45, 46, 47 and 48.

3.6.1.2 Portions (0.2g) of Na-montmorillonite were added to sixteen $50cm^3$ flasks containing solutions ($10.0cm^3$) of cobalt chloride and either magnesium chloride, calcium chloride, sodium chloride or potassium chloride in molar ratios of 10:1, 1:1, 1:10, 1:100, but with a constant total molarity of 0.04M. After shaking for 3 days the suspensions were ultracentrifuged and the supernatents analysed for cobalt and associated cation contents. Results are shown in tables 49, 50, 51 and 52 and plotted on figs.25, 26, 27, 28 and 29. Upon redispersion, the samples were filtered and the clays left to air dry.

Portions (0.05g) of these treated clays were contacted with distilled water ($5cm^3$) shaken for 3 days and finally ultracentrifuged. The supernatent solutions were analysed for cobalt and associated cation contents and the relevant data is shown in tables 53, 54, 55 and 56.

3.6.1.3 Portions (0.2g) of Na-montmorillonite were weighed into sixteen $50cm^3$ flasks and contacted with solutions ($10.0cm^3$) composed of a standard nickel concentration (1.70ppm) in combination with either magnesium chloride, calcium chloride, sodium chloride or potassium chloride of different concentrations such as to generate added metal:Ni ratios of 10:1, 5:1, 1:1, 1:10. Samples were shaken for 3 days, ultracentrifuged and the solution phase analysed for the respective metal ion concentrations (tables 57, 58, 59 and 60 and figs.30 and 31).

Tables 45, 46, 47, 48 - Desorption of Ni from montmorillonite previously contacted with constant (0.04M) molar strength solutions containing competing cations.

Initial Ratio	Equilibrium Ni concentration (mmol/L)	Equilibrium M^{n+} concentration (mmol/L)	Ni desorbed (meq/100g)	M^{n+} desorbed (meq/100g)	% Ni desorbed	% M^{n+} desorbed	$K_d(Ni)$	$K_d(M^{n+})$
Table 45 Mg:Ni								
100:1	0.018	1.03	0.35	21	36	25	170	300
10:1	0.015	0.107	0.30	2.15	5	3	2000	3300
1:1	0.035	0.0231	0.71	0.46	2.1	1.2	4800	8000
1:10	0.94	0.0041	1.9	0.082	2.7	1.3	3500	7000
Table 46 Ca:Ni								
100:1	0.0099	0.028	0.20	0.55	35	0.9	190	11000
10:1	0.0131	0.025	0.26	0.50	6	1.1	1500	8000
1:1	0.046	0.0060	0.92	0.12	5	0.4	2100	5000
1:10	0.049	0.029	0.99	0.59	2.2	8	4400	1200
Table 47 Na:Ni								
100:1	0.026	1.37	0.52	14	16		500	
10:1	0.145	0.49	2.9	4.9	12		700	
1:1	0.023	1.05	0.46	10.5	1.0		10000	
1:10	0.051	0.54	1.02	5.4	1.8		6000	
Table 48 K:Ni								
100:1	0.0058	0.80	0.12	8.0	4.7	46	2100	120
10:1	0.0065	0.72	0.13	7.2	0.8	73	13000	40
1:1	0.022	0.75	0.45	7.5	1.1	80	10000	12
1:10	0.037	0.14	0.74	1.4	1.4	90	7000	11

Tables 49, 50, 51, 52 - Cobalt sorption on Na-montmorillonite at constant molar strength in the presence of competing cations (M^{n+}).

Ratio	Initial Co conc. (mmol/L)	Initial M^{n+} conc. (mmol/L)	Equil. Co Conc. C_{Co} (mmol/L)	Equil. M^{n+} Conc. $C_{M^{n+}}$ (mmol/L)	Co sorbed (meq/100g)	M^{n+} sorbed (meq/100g)	% Co sorbed	% M^{n+} sorbed	K_d(Co)	$K_d(M^{n+})$
Table 49 Mg:Co										
100:1	0.396	39.6	0.31	29	0.8	100	21	26	13	23
10:1	3.64	36.4	3.0	27	7	90	19	25	12	17
1:1	20.0	20.0	16.0	15.4	40	40	20	20	13	15
1:10	36.4	3.66	29	3.0	72	7.0	20	19	12	12
Table 50 Ca:Co										
100:1	0.396	39.6	0.28	34	1.1	57	28	14	20	8
10:1	3.64	36.4	2.8	33	9	35	24	10	24	5
1:1	20.0	20.0	15.3	17.0	47	30	24	15	16	9
1:10	36.4	3.66	27	3.1	89	5.2	25	17	16	8
Table 51 Na:Co										
100:1	0.396	39.6	0.048	30	3.48	-50	88		360	
10:1	3.64	36.4	0.89	39	27.5	-10	76		150	
1:1	20.0	20.0	13.7	31	63	-50	32		23	
1:10	36.4	3.66	28	19	82	-80	23		15	
Table 52 K:Co										
100:1	0.396	39.6	0.114	35	2.82	22	71	11	120	6
10:1	3.64	36.4	1.56	28	20.8	44	57	24	67	16
1:1	20.0	20.0	14.6	11.8	54	41	27	41	18	32
1:10	36.4	3.66	29	3.5	76	1	21	5	13	2

Tables 53, 54, 55, 56 - Desorption of cobalt from montmorillonite previously contacted with constant (0.04M) molar strength solutions containing competing cations.

Initial Ratio	Equilibrium Co concentration (mmol/L)	Equilibrium M^{n+} concentration (mmol/L)	Co desorbed (meq/100g)	M^{n+} desorbed (meq/100g)	% Co desorbed	% M^{n+} desorbed	$K_d(Co)$	$K_d(M^{n+})$
Table 53 Mg:Co								
100:1	0.0049	0.45	0.098	9.0	12	9	700	1000
10:1	0.0072	0.024	0.14	0.49	2.1	0.5	5000	18000
1:1	0.060	0.039	1.19	0.78	2.9	1.9	3000	5000
1:10	0.144	0.0085	2.9	0.17	4	2.4	2400	4000
Table 54 Ca:Co								
100:1	0.016	0.027	0.031	0.53	2.8	0.9	400	11000
10:1	0.037	0.031	0.73	0.61	9	1.8	1100	6000
1:1	0.112	0.048	2.2	0.96	5	3	2000	3000
1:10	0.20	0.0165	4.0	0.33	5	6	2100	1500
Table 55 Na:Co								
100:1	0.0049	1.03	0.098	10.3	2.8		3500	
10:1	0.017	0.95	0.33	9.5	1.2		8100	
1:1	0.027	0.85	0.53	8.5	0.8		12000	
1:10	0.049	0.58	0.97	5.8	1.2		8400	
Table 56 K:Co								
100:1	0.0040		0.079		2.8		3500	
10:1	0.0051		0.102		0.5		20000	
1:1	0.034		0.68		1.3		7800	
1:10	0.066		1.32		1.7		5600	

Tables 57, 58, 59, 60 - Nickel sorption on Na-montmorillonite at variable molar strength in the presence of competing cations. (M^{n+})

Ratio	Initial Ni conc. (mmol/L)	Initial M^{n+} conc. (mmol/L)	Equil. Ni conc. (mmol/L)	Equil. M^{n+} conc. (mmol/L)	Ni sorbed (meq/100g)	M^{n+} sorbed (meq/100g)	% Ni sorbed	% M^{n+} sorbed	K_d(Ni)	K_d(M^{n+})	*Initial* pH	*Final* pH
Table 57 Mg:Ni												
10:1	1.70	17.0	1.43	10.0	2.7	71	16	42	9	35	5.77	3.65
5:1	1.70	8.50	1.04	4.8	6.6	37	39	44	32	39	5.88	3.60
1:1	1.70	1.70	0.18	0.19	15.2	15.1	89.4	88.6	420	390	6.43	4.17
1:10	1.70	0.17	0.019	0.0062	16.8	1.1	98.9	96.4	4400	1300	6.36	4.34
Table 58 Ca:Ni												
10:1	1.70	17.0	1.40	12.9	3.0	41	18	24	11	16	6.31	3.49
5:1	1.70	8.50	1.07	4.8	6.3	37	37	43	29	38	6.35	3.72
1:1	1.70	1.70	0.19	0.065	15.1	16.4	88.8	96.2	410	440	6.43	4.16
1:10	1.70	0.17	0.020	0.0015	16.8	1.7	98.8	99.1	4200	5600	6.30	4.46
Table 59 Na:Ni												
10:1	1.70	17.0	0.22	20.7	14.8	-18	86.9		330		5.77	3.88
5:1	1.70	8.50	0.102	8.3	16.0	+1.0	94.0		780		5.71	4.15
1:1	1.70	1.70	0.025	5.1	16.8	-17	98.5		3300		5.93	4.46
1:10	1.70	0.17	0.0141	3.3	16.9	-16	99.2		6000		5.78	4.54
Table 60 K:Ni												
10:1	1.70	17.0	0.54		11.6		68		110		5.56	3.95
5:1	1.70	8.50	0.27		14.3		84.1		260		5.66	4.11
1:1	1.70	1.70	0.099		16.0		94.2		810		5.99	4.43
1:10	1.70	0.17	0.019		16.8		98.9		4400		5.77	4.62
Ni:Blank	1.70	-	0.014	-	16.9	-	99.3	-	6000	-	5.57	4.57

Fig.30 - Variation of log K_d(Ni) with log initial metal ion concentration in experiments at variable molar strength.

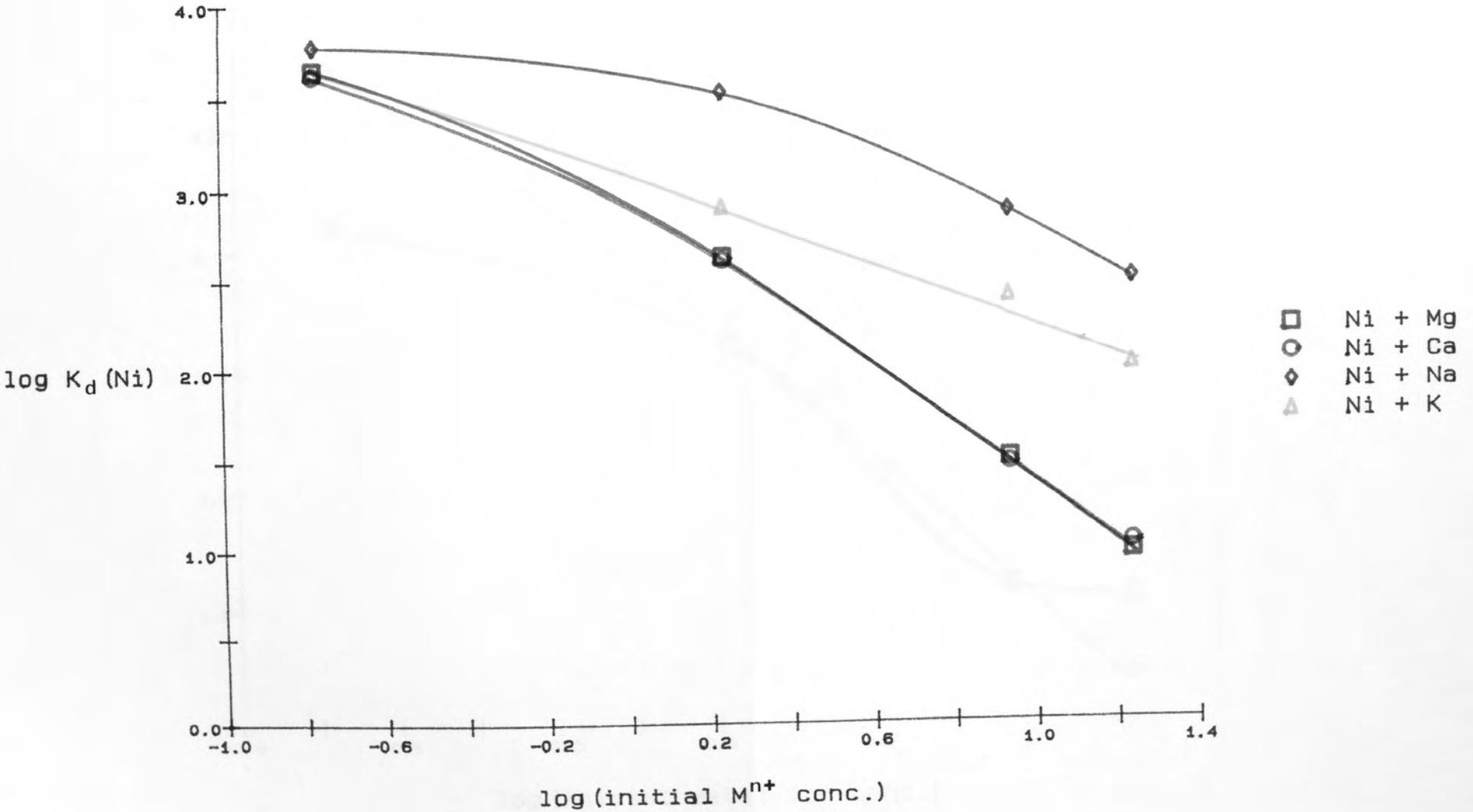

Fig.31 – Variation of log $K_d(M^{n+})$ with log initial metal ion concentration in experiments at variable molar strength.

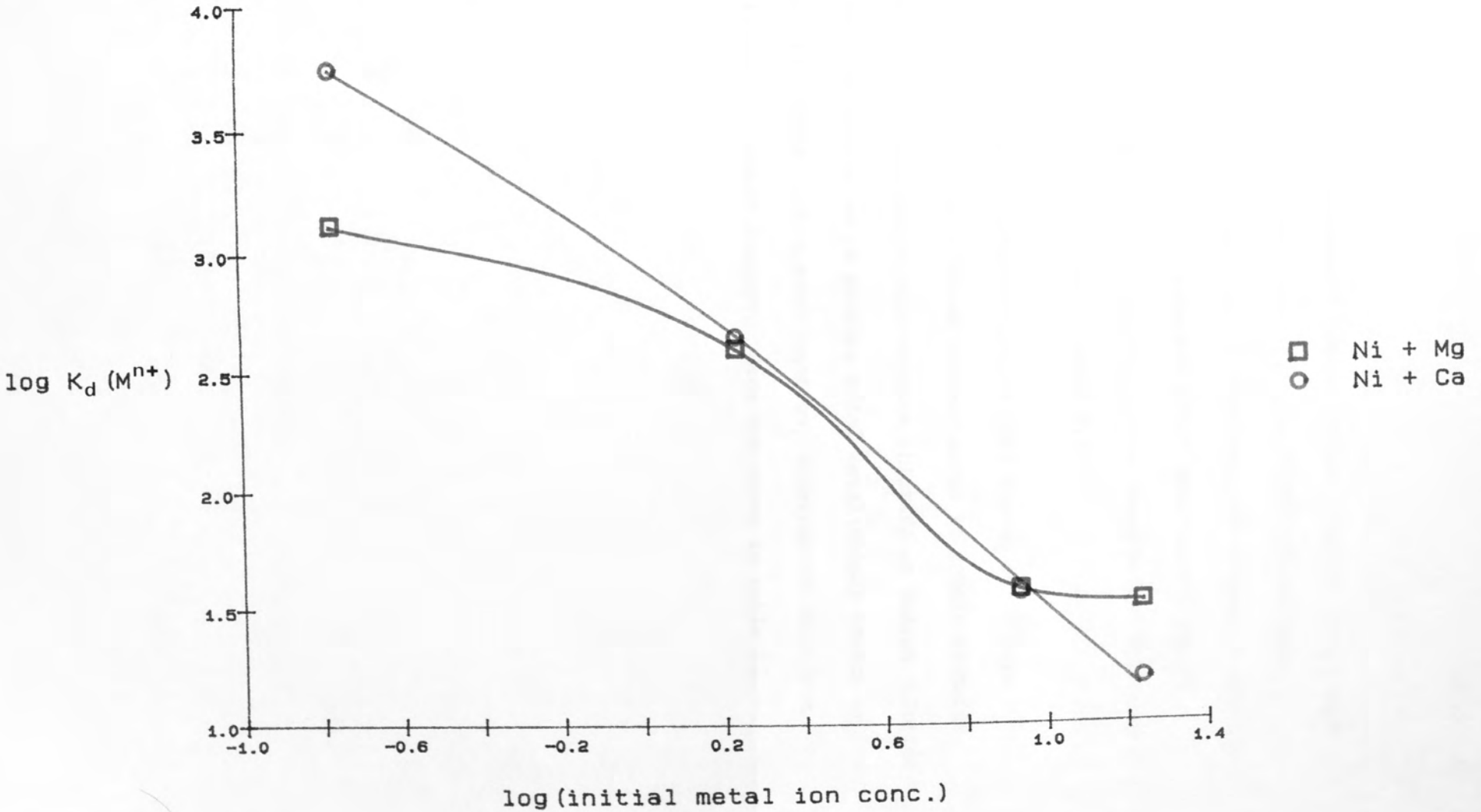

3.6.2 Microscopic effects

3.6.2.1 Portions (0.252g) of Na-montmorillonite were shaken for 3 days with solutions containing a fixed concentration of nickel chloride (2.0ppm Ni^{2+}) in combination with calcium chloride or sodium chloride of such concentrations as to generate added metal:nickel ratios of 100:1 and 1:1. After ultracentrifugation, supernatent solutions were analysed for nickel content (table 61).

3.6.2.2 Portions (0.252g) of Na-montmorillonite were shaken for 3 days with solutions containing a fixed concentration of cobalt chloride (5.0ppm Co^{2+}) in combination with calcium chloride or sodium chloride of such concentrations as to produce added metal:cobalt ratios of 100:1 and 1:1. After ultracentrifugation, supernatent solutions were analysed for cobalt content. Data are shown in table 62.

Table 61 - Nickel sorption on Na-montmorillonite at low concentration in the presence of competing cations (M^{n+}).

Competing Cation	Initial Ni concentration (mmol/L)	Ratio M^{n+}:Ni	Equilibrium Ni concentration (C_{Ni}) (mmol/L)	Log C_{Ni}	Ni sorbed (meq/100g)	% Ni sorbed	K_d(Ni)
-	0.0341	-	1.0×10^{-4}	-3.98	0.341	99.70	1.6×10^{4}
Na	0.0341	1:1	2.9×10^{-4}	-3.53	0.339	99.69	1.6×10^{4}
Na	0.0341	100:1	3.3×10^{-4}	-3.49	0.337	99.0	5.2×10^{3}
Ca	0.0341	1:1	4.7×10^{-4}	-3.33	0.335	98.6	3.6×10^{3}
Ca	0.0341	100:1	8.0×10^{-3}	-2.10	0.26	77	1.6×10^{2}

Table 62 - Cobalt sorption on Na-montmorillonite at low concentration in the presence of competing cations (M^{n+}).

Competing cation	Initial Co concentration (mmol/L)	Ratio M^{n+}:Co	Equilibrium Co concentration (C_{Co}) (mmol/L)	Log C_{Co}	Co sorbed (meq/100g)	% Co sorbed	K_d(Co)
-	0.0848	-	$<1.1 \times 10^{-4}$	-3.97	>0.847	>99.8	$>3.9 \times 10^{4}$
Na	0.0848	1:1	2.0×10^{-4}	-3.70	0.846	99.8	2.1×10^{4}
Na	0.0848	100:1	2.3×10^{-4}	-3.64	0.846	99.7	1.9×10^{4}
Ca	0.0848	1:1	4.4×10^{-4}	-3.36	0.844	99.5	9×10^{3}
Ca	0.0848	100:1	3.8×10^{-2}	-1.42	0.470	55.4	62

3.7 DISCUSSION

The properties of a clay mineral sample are dependent on its composition and therefore its purity. Although a large volume of literature has been generated on many aspects of clay mineral behaviour, the composition of materials used in such studies is very often not fully characterised. An investigation into the purity of reference clay materials carried out under the auspices of the Clay Mineral Society and the OECD[102] revealed the presence of a number of accessory minerals to varying degrees. For example, XRD and infrared analysis of the commonly studied Camp Berteau montmorillonite demonstrated the presence of quartz, mica, feldspar and carbonate impurities.

A comprehensive physical investigation of the montmorillonite and hectorite used in this study did not indicate the presence of appreciable quantities of contaminating minerals.

A standard composition is impossible to derive, due to the very nature of clay mineral structures, but concentrations of elemental oxides usually reside within certain limits. The hectorite analysis (table 10) compared favourably with those of Nagelschmidt[22] and Kerr,[103] which showed SiO_2, Al_2O_3 and MgO contents of 53.1%, 0.6%, 25.3% and 54.0%, 0.14%, 25.9% respectively. It is of interest here to point out that the white appearance of hectorite is due to the very low iron content.

The montmorillonite sample exhibited a higher iron content than a number of other montmorillonites examined in the literature,[103,104]

but lower than that typical of a nontronite sample.[105] This would indicate the clay used here lies somewhere in the range of solid solutions that exists between end members montmorillonite and nontronite.

The DTA results compared favourably with data published in the literature for both clays. Again, due to the non-rigid composition of montmorillonite and hectorite minerals, absolute DTA curves cannot be defined but peaks do appear within characteristic ranges. Endothermic peaks at 129°C and 831°C found for hectorite were consistent with previous literature[21,106] data for hectorite in which endotherms were observed in the ranges 130-170°C and 800-840°C.

The montmorillonite sample exhibited a trace typical of the smectite group of minerals[19,102] but the endotherm at 585°C was at a lower temperature than expected from an end-member montmorillonite sample. However, Odom[95] states that significant replacement of aluminium by iron or magnesium causes a reduction in the temperature at which this peak is found. This evidence supports the conclusions drawn from XRF analysis which revealed a high iron concentration in the montmorillonite.

The first peak in each case (189°C and 129°C for montmorillonite and hectorite respectively) is caused by the expulsion of sorbed water within the interlayer region. Dehydroxylation accounts for the peak at 585°C in montmorillonite and at 831°C in hectorite. The third endotherm at 876°C exhibited by montmorillonite is correlated with breakdown of the mineral lattice to leave an

amorphous material, and this is followed by an exothermic peak at 925°C due to recrystallisation.[106]

XRD data for natural hectorite again demonstrated the absence of contaminating minerals. The d(001) spacing of 12.7Å was indicative of a clay predominantly in the monovalent (i.e. sodium) exchanged form. On glycolation the 12.7Å peak was shifted to 17.8Å, characteristic behaviour for the smectite group of minerals.[27,102]

The montmorillonite clay also showed a characteristic XRD pattern,[102] but both quartz and feldspar appeared as very minor impurities. The d(001) spacing of 15.2Å for natural montmorillonite was typical for a divalent (i.e. calcium) exchanged form. Glycolation of this sample resulted in the characteristic expansion of the d(001) spacing to 17.1Å.[27,102]

Infrared spectroscopic examination of the hectorite revealed only the presence of a trace of quartz indicated by the existence of a very weak absorption band at $694cm^{-1}$,[107] and the characteristic C—H stretch of $-CH_2-$, $-CH_3$ groups of inherent organic material, at $2921cm^{-1}$ and $2848cm^{-1}$.

The montmorillonite exhibited a characteristic infrared spectrum,[102] and also absorption bands at 791, 768, 688 and $396cm^{-1}$ due to a small quartz impurity. The influence of high iron content was characterised by absorption bands at $870cm^{-1}$ and $359lcm^{-1}$ due to bending and stretching vibrations of hydroxyl coordinated to an $AlFe^{3+}$ octahedral pair.[102] Weak absorptions at $2912cm^{-1}$ and $2840cm^{-1}$ were again correlated with the presence of a very small amount of

organic matter.

Cation exchange capacities (table 14) compared favourably with literature values for both hectorite[102,108] and montmorillonite.[39,109]

Having undertaken a comprehensive physical investigation of the two clay materials, they were then utilized in sorption experiments.

Sorption Experiments

An equilibrium time of 3 days was established for cation sorption from observations on sorption of 0.1M nickel and cobalt solutions on the two clays (figs.10, 13 and 16) and was used in all subsequent sorption investigations.

The time required for attainment of equilibrium between a solution of metal ions and clay mineral appears to be very inconsistent throughout the literature. Monsef-Mirzai[52] stated an equilibration time of two days was required for copper sorption on montmorillonite, but her experimental points were somewhat scattered. Carter[44] found that, for a number of metal ions sorbed onto montmorillonite, equilibrium was not attained after 70 days, although this may be due to the relatively crude experimental design used, which may have allowed some vapour loss.

Sorption of cobalt onto Ca-montmorillonite suspended in 0.1M $CaCl_2$ required an equilibration period of greater than 10 days according to Hodgson.[34] Both cadmuim and cobalt required an equilibration time of about 60 hours, when contacted with Na-montmorillonite, by Egozy.[32] Tiller and Hodgson[41] concluded that sorption of cobalt

onto a series of clay minerals, including montmorillonite and hectorite did not readily attain equilibrium (longer than 31 days), but after a period of several days, tended to approach a nearly steady state. Further studies by Bansal et al[55] on the interaction of Ni(II) with H-, Na-, Ca-montmorillonite led to a proposal that equilibrium was achieved after only three hours, but as experiments were only conducted for six hours, this may be an artifact of the experimental conditions used.

All sorption isotherms showed an initial rapid uptake followed by a much slower period of metal ion sorption.

The results summary in table 63 shows that more nickel was sorbed from a solution of nickel chloride on montmorillonite than on hectorite (≃12%). Table 63 also shows that ≃10% more cobalt was sorbed on the montmorillonite than the hectorite. These two observations were consistent with the higher cation exchange capacity of montmorillonite.

A comparison of the sorption behaviour of nickel and cobalt revealed that cobalt was sorbed to a greater extent than nickel on hectorite (≃10%) and montmorillonite (≃8%)(table 63).

A number of sorption studies on clay minerals involving cobalt and nickel indicate different ranking orders for the two ions. This apparent anomaly is more aptly discussed later with details of the low level work, where an explanation is offered.

Further treatment of these clays, after the initial equilibration

Table 63 - Summary of sorption data from Ni(II)/Co(II) interactions with Na-montmorillonite and hectorite.

Clay	Na-Montmorillonite						Hectorite	
Salt	$NiSO_4$	$NiCl_2$	$Ni(ClO_4)_2$	$CoSO_4$	$CoCl_2$	$Co(ClO_4)_2$	$NiCl_2$	$CoCl_2$
Initial Concentration(meq)	20.4	20.0	20.0	19.8	19.6	20.0	19.4	20.2
Average Quantity metal ion sorbed (meq/100g)	59	55	56	60	59	59	49	54
Average Quantity metal ion exchanged (meq/100g)	45	46	45	46	50	48	43	48
Average Quantity metal ion released (meq/100g)	14.0	9.67	10.8	14	9.1	10.9	6.2	6.1
Sorption $K_d(cm^3/g)$	4.1	3.8	3.9	4.3	4.3	4.2	3.4	3.6
Exchange $K_d(cm^3/g)$	2.8	2.9	2.9	3.0	3.4	3.2	2.9	3.1
Release $K_d(cm^3/g)$	32.1	46.5	41.6	32.5	55.1	44.1	69.4	78.4

procedure, with distilled water, released a quantity of the sorbed cation into solution in every case (figs.12, 15 and 18).

This suggested at least two 'types' of metal ion were sorbed upon initial equilibration of the clay, one being more strongly held. A similar behaviour was observed by Monsef-Mirzai,[52] who removed a significant portion of copper ions from montmorillonite, initially equilibrated with various copper solutions, using distilled water.

Maes and Cremers[36] studied the sorption of cobalt on Na-montmorillonite from a 0.01M NaCl solution and attributed the change of sorbability with pH to the change in the relative contribution at two sites on the clay mineral-'broken bonds' and ion-exchange sites. In a study of the sorption of cobalt and cadmium on Na-montmorillonite under various conditions of pH and added salt concentration, Egozy[32] came to the same conclusions. Peigneur et al[33] compared the effect of pH on the selectivity coefficients for cobalt uptake on montmorillonites from different sources. The differing selectivity coefficients were correlated with the varying proportions of 'broken bond' to ion-exchange sites available in the montmorillonite samples used.

Two kinds of metal ion sorption sites on montmorillonite were also proposed by Banin[39] to explain isotherms generated from alkali and alkaline earth cation sorption on monoionic clays.

The desorption of both cobalt and nickel ions by distilled water from montmorillonite and hectorite samples is summarised in table 63.

The quantity of metal ion released showed the following dependence on the anion used in the initial equilibration step; $SO_4^{2-} > ClO_4^- > Cl^-$. The concentration of metal ion retained by the clay after washing exhibited a reverse anion dependence, i.e. $Cl^- > ClO_4^- > SO_4^{2-}$. Monsef-Mirzai[52] also observed a higher release and lower retention of copper from the sulphate salt, as compared with chloride and perchlorate, when contacted with a montmorillonite. However, the relative affinities of Cl^- and ClO_4^- salts for the clay surface were reversed.

In addition to the two classical exchange mechanisms developed for clay minerals,[32,33,36,39] it is postulated that a third exists in which an anion-cation pair are bound to the clay surface through the anion.[a]

Anion sorption on clay minerals has been demonstrated by a number of workers. For example, using H-montmorillonite, Bingham et al[63] were able to absorb five meq of acetate per 100g of clay.

It is proposed that anion sorption occurs on positive sites on the edges of clay particles, which are available due to coordination vacancies of the cations found in octahedral layer sites.

In a similar manner, a mechanism involving cation uptake on 'broken bond' sites on clay particle edges has been suggested by a number of workers. (See preceeding discussion).

[a] Since metal ion sorbed by the anion dependent mechanism is easily removed from the clay it is termed 'labile' - the retained metal ion is termed 'exchanged'.

The higher charge on the sulphate anion infers that it should have a greater affinity for the clay surface than the chloride or perchlorate anions, and hence associate more nickel. A stereochemical factor also may be important in sulphate retention (see fig.32) and was possibly one of the reasons why perchlorate showed a greater affinity for the clay surface than the chloride salt. The perchlorate ion will also have a smaller hydrated ionic radius, so exhibit an enhanced affinity for the clay surface. Bingham et al[63] observed that sulphate was more effective than chloride in releasing acetate from a previously treated montmorillonite indicating a stronger preference for the clay surface.

Nickel sulphate was retained to a lesser extent than nickel chloride, due to the enhanced tendancy of sulphate to form complexes in solution, resulting in a lower Ni^{2+} ion activity.

Utilizing solutions of 10^{-5}M $NiCl_2$ in high background sodium (0.1N) and calcium (0.02N) sulphate and chloride media, Bowman et al[110] observed a higher sorption onto a Na-montmorillonite from the chloride media. Their hypothesis that $NiSO_4^0$ complexes were not sorbed and $NiCl^+$ complexes sorbed only slightly if at all, was derived from plots of Ni^{2+} activity against concentration which eliminated significant differences between corresponding initial isotherms.

These data clearly demonstrated that the total amount of metal removed from solution by a particular clay depends on the counter-ion present. The affinity of the anion for the positive edge of the

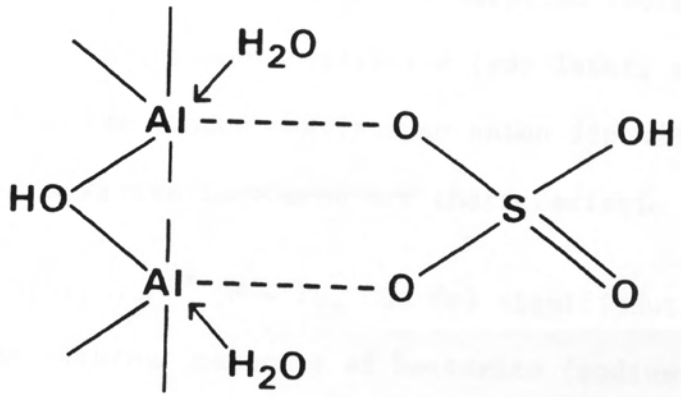

Fig.32 - Illustration of how SO_4^{2-} (or HSO_4^-) may bind to positive edge sites of clay crystals.

crystal appeared to be the major factor affecting uptake on the 'labile' sites, whereas the ability to form complexes in solution was most influential on the 'exchange' mechanism.

Confirmation of this proposal was gained from experiments which showed that more nickel was released from a previously treated $NiCl_2$/montmorillonite, by a $NiSO_4$ solution (of lower concentration) than a $NiCl_2$ solution (table 32). K_d values for both perchlorate and sulphate salts lie further from the sorption isotherm generated for $NiCl_2$ sorption on Na-montmorillonite (see later, section 3.5.2.10, fig.22) than chloride, which confirms an anion dependent sorption effect and that sorption isotherms are characteristic for each anion.

An uptake of $[M(bipy)_3]^{2+}$ (M = Ru, Cu, Fe) significantly greater than the cation exchange capacity of hectorite (sodium form) was observed by Traynor et al.[42] Two sorption mechanisms were suggested: (1) replacement of sodium ions in the native mineral by cation exchange up to its cation exchange capacity, and (2)'intersalation' of excess salt beyond the exchange capacity. The iron and copper complexes (ClO_4^- form) were sorbed to a greater extent than the ruthenium salt (Cl^- form) possibly, it was thought, due to the counter-ion. Further investigation of $[Fe(bipy)_3]^{2+}$ sorption again demonstrated an anion dependent effect, iron uptake decreasing in the order SO_4^{2-}, $Br^- \gg ClO_4^- > Cl^-$. The suggestion that excess complex salt is readily accommodated in the interlayer regions between the coulombically bound monolayers of exchange cations (i.e. 'intersalation') is at variance with the observed 18Å basal spacing, typical of a monolayer of complex, and the mechanism previously proposed in

the present study (i.e. anion-cation sorption onto positive edge sites) seems more likely. It is also interesting to note that Traynor et al[42] were able to remove a significant portion of metal ion from the clay upon washing with water, which agrees with results found in sections 3.5.2.1 to 3.5.2.5.

Sorption of the pesticide chlordimeform (N'-(4-chloro-2-methylphenyl)-N,N-dimethylmethanimidamide hydrochloride) also appears to involve the proposed anion-cation mechanism. Perez-Rodriguez et al[111] stated that sorption occurred essentially as a cation exchange reaction, on Wyoming montmorillonite containing different exchangeable cations (Na^+, K^+, Ca^{2+}, Mg^{2+}). However a significant quantity of chlordimeform in excess of the calculated cation exchange capacity was taken up by the Na-, K- and Ca-clays, and this portion of cation could be removed on washing with water. The authors infer that two sorption sites exist: (1) one in which chlordimeform is adsorbed externally and is weakly bonded so may be removed easily by washing with water, and (2) an interlamellar position in which the chlordimeform is strongly sorbed. However, the observation that the amount of outgoing inorganic cation was smaller (10-20%) than the quantity of adsorbed organic cation, and the d(001) spacing (12.0-12.6Å) characteristic of a monolayer of organic cations in the interlamellar region, indicates that sorption is again more readily accounted for by the three mechanisms proposed in this study.

The reactions of the tris(acetylacetonato)silicon(IV) cation ($[Si(acac)_3]^+$) with Na^+-, Mg^{2+}- and Co^{2+}- exchanged forms of hectorite and montmorillonite were investigated by Manos et al.[112] In acetone

as the solvating medium, $[Si(acac)_3]^+$ binds to the Na^+- and Mg^{2+}-clays with the desorption of only a small fraction (≈5%) of the initial exchange cation, suggesting that the complex binds as the ion pair $[Si(acac)_3]^+.Cl^-$. However, Manos et al[112] stated that in the Co^{2+} system $[Si(acac)_3]^+$ was most likely bound initially as an ion pair as with the Na^+ and Mg^+ systems, but subsequent complex formation of Co^{2+}, Cl^- and acetone in the interlayers led to the formation of a neutral $CoCl_2L_2$ species (L = acetone) which desorbed to solution.

In the absence of any proposal as to the mechanism involved in binding the ion pair to the clay surface, it is assumed that this provides further confirmation of the mechanism proposed in our study.

With water as solvent, solvation forces were assumed, by Manos et al,[112] to be stronger than in acetone, and aqueous $[Si(acac)_3]^+$ was not expected to bind to the clay by an ion pairing mechanism. However, addition of two CEC equivalents of $[Si(acac)_3]^+$ desorbed less than 60% of the native inorganic cation, which may again point to the influence of ion pair sorption and hence a weakly solvated cation as would appear more likely the case on consideration of the size of $[Si(acac)_3]^+$.

Having established an equilibrium time of three days for cobalt and nickel sorption experiments, it was pertinent to consider other variable physical parameters. Such an investigation which involved varying the clay:solution volume ratio (section 3.5.2.7, fig.19) did indicate some influence on sorption.

A similar study involving various clay:solution volume ratios was undertaken (section 3.5.2.8), but on this occasion to assess possible effects on desorption from a nickel treated montmorillonite - again a distinct effect was inferred (fig.20).

The significance of clay particle size also emerged from the sorption of $NiCl_2$ on several hectorite size fractions, the lower size fractions sorbing a greater proportion of metal ion from solution (table 35). This was most likely a consequence of increased contribution of cation sorption sites on external surfaces of clay crystals, as the particle size was reduced[33,113] (see earlier).

These factors pointed to a need for consistency in experimental practice and so constant ratios of clay:solution volume of 10:1 or, more usually, 50:1 were used throughout and individual experiments were performed on a single batch of clay to avoid any possible sample to sample inhomogeneities.

The initial sorption studies were consequently followed by the construction of sorption isotherms on Na-montmorillonite for both cobalt and nickel (figs.21 and 23). Log K_d values are plotted against equilibrium solution concentration in figs.22 and 24.

A characteristically decreasing affinity of metal for the clay with increasing concentration was apparent.

Bansal et al[55] noted that the change in slope of isotherms, was indicative of the saturation of adsorptive sites in the substrate. This loading effect was also observed for nickel sorption on mont-

morillonite by Basu et al[45] and again by Bansal et al[56] and effectively meant that beyond a particular concentration, nickel was no longer almost completely sorbed, but was taken up by an amount determined by the quantity of nickel already on the clay - the higher the concentration of nickel present on the clay, the lower was the quantity of metal extracted from a solution.

A similar loading effect has been reported by Tiller et al[41] and Hodgson[34] for the sorption of cobalt on montmorillonite.

It is interesting to note here that the K_d values from initial sorption experiments involving $NiCl_2$ and $CoCl_2$ (see table 63), fall on the respective sorption isotherm, indicating that anion effects are taken into account by the isotherm.

The desorption distribution coefficients (table 63) also lie on the curves in figs.22 and 24. This is again evidence for the anion sorption mechanism being taken into account.

The sorption isotherms generated can only be used for chloride solutions of the metal concerned since perchlorate and sulphate anions exhibit their influence to a relatively greater extent.

The distribution coefficients (figs.22 and 24) showed a steady increase in value with decreased loading on the clay. When looking at Co(II) sorption, Egozy[32] also observed increasing K_d with decreased cation loading on Na-montmorillonite, but below 10^{-3} millimoles Co(II)/g clay some consistency was observed - the latter is probably due to the very low (10^{-6}-10^{-7}M) equilibrium concentrations of

Co(II) used, as substantiated by the almost complete sorption of Co(II) on hectorite observed by Tiller[57] up to a solution concentration of 10^{-5}M above which the K_d value drastically decreased.

Further analysis of the sorption data was performed using the Langmuir equation which, in its linear form may be written as:

$$\frac{C}{(x/m)} = \frac{1}{k.V_m} + \frac{C}{V_m}$$

where C is the equilibrium cation concentration in solution; x is the amount sorbed per unit weight m of clay; k and V_m are constants, the latter being identifiable with the monolayer capacity of the adsorbent. Data for the characteristic plot of $\frac{C}{(x/m)}$ versus C is calculated in tables 64 and 65 for both nickel and cobalt sorption on Na-montmorillonite, and plotted in figs.33 and 34.

Farrah et al[47] were able to construct linear Langmuir isotherms for Cu^{2+}, Ca^{2+}, Mg^{2+}, Cd^{2+}, Pb^{2+} and Zn^{2+} sorption onto Na-montmorillonite. The adsorption of cobalt, nickel and copper on K- and Ca-montmorillonite also followed a linear Langmuir plot according to Borovec.[114] The slight curvature exhibited in figs. 33 and 34 does not conform to the above behaviour. However, the data may also be interpreted in terms of a linear relationship between log $\frac{C}{(x/m)}$ and log C, but extension of the isotherm to include data points at lower equilibrium solution metal ion concentrations revealed a definite curvature (see later - figs.37 and 38). This curvature is, from comparison with other literature, most likely

Table 64 - Langmuir isotherm data and selectivity coefficients derived for cobalt sorption on Na-montmorillonite.

Initial Co concentration (mmol/L)	Final Co concentration(C) (mmol/L)	$\frac{C}{(x/m)}$	X_{Co}	$\overline{X}_{Co}$	K_s'	$\ln K_s'$
17.0	9.8	28	0.41	0.79	15	2.69
8.48	3.4	13	0.25	0.46	3.6	1.29
5.09	0.62	2.7	0.065	0.38	13	2.57
3.39	0.104	0.63	0.0156	0.255	28	3.32
1.70	0.020	0.24	0.0059	0.116	25	3.21

Table 65 - Langmuir isotherm data and selectivity coefficients derived for nickel sorption on Na-montmorillonite.

Initial Ni concentration (mmol/L)	Final Ni concentration(C) (mmol/L)	$\frac{C}{(x/m)}$	X_{Ni}	$\overline{X}_{Ni}$	K_s'	$\ln K_s'$
17.0	10.7	33	0.45	0.65	3.6	1.28
8.52	2.2	6.9	0.15	0.64	24	3.18
5.11	0.34	1.4	0.0344	0.42	33	3.51
3.41	0.068	0.41	0.0101	0.26	46	3.83
1.70	0.0072	0.086	0.0021	0.116	70	4.24

Fig.33 - Langmuir plot of data from cobalt sorption on Na-montmorillonite.

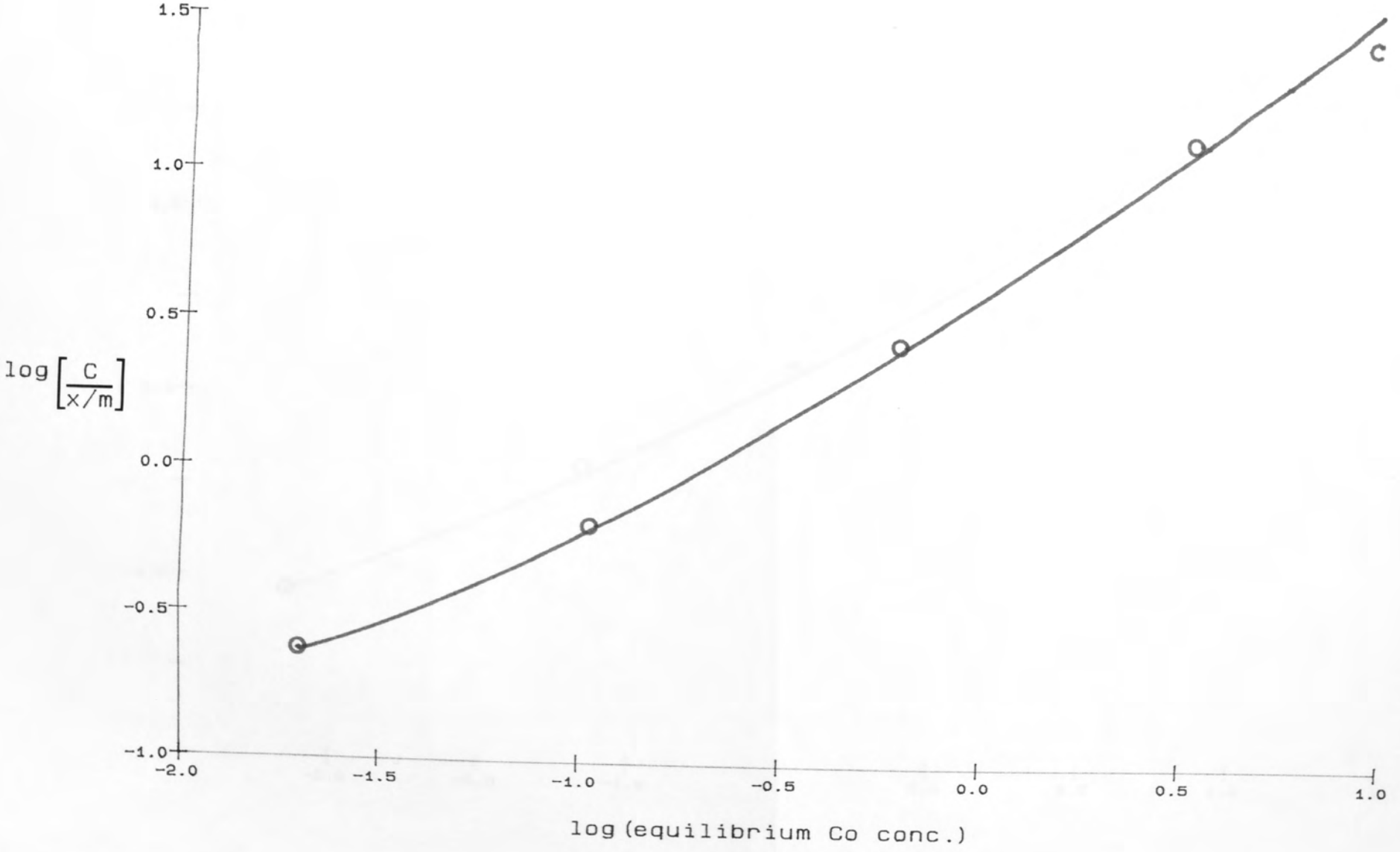

Fig.34 - Langmuir plot for nickel sorption on Na-montmorillonite.

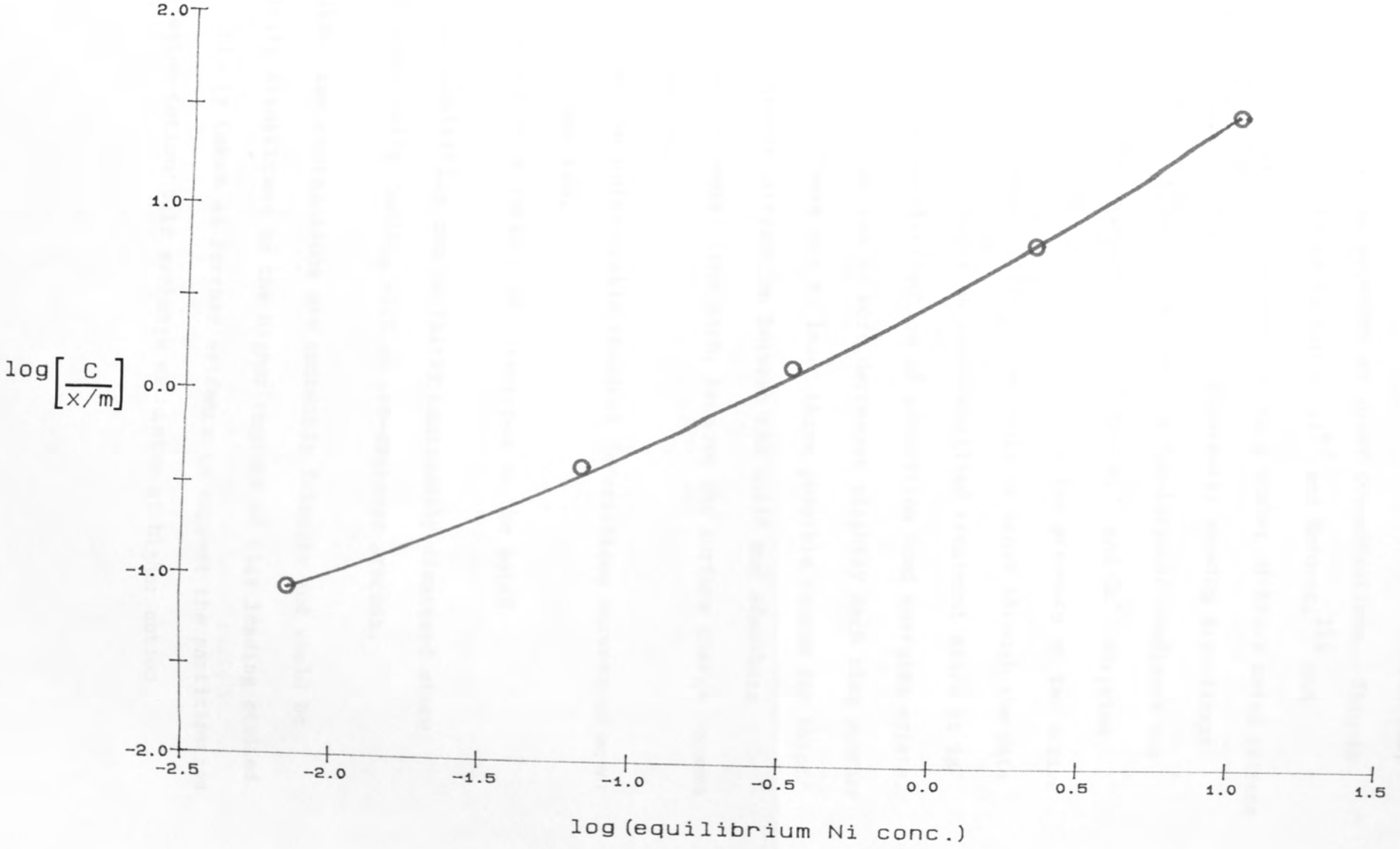

associated with the isotherm at higher metal ion concentrations, with a linear portion apparent at lower concentrations. This is supported by the work of Farrah et al[47] and Borovec,[114] and Benjamin's[115] data on the sorption of a number of heavy metal cations onto α-SiO_2, γ-FeOOH and γ-Al_2O_3 apparently showing significant deviation from a linear behaviour. A non-Langmuir obedience was also reported by Takahashi et al[116] for Ni^{2+} and Cu^{2+} sorption onto Na-montmorillonite. They suggested the presence of two active sites since two intersecting lines could be drawn through the data points. This is probably an oversimplified treatment since it is more likely that a distribution of adsorption bond energies exists. The tendancy for an ion to sorb decreases slightly each time another ion is sorbed. There are at least three possible causes for this:

1. The coulombic attraction between the solid and adsorbate decreases as metal ions sorb, because the surface charge becomes more positive.
2. There may be unfavourable chemical interactions between adjacent adsorbed species.
3. There may be a variety of site-types on the solid.

The first possibility can be fairly confidently dismissed since we are essentially dealing with an ion-exchange process.

The latter two explanations are eminently feasible and would be especially significant in the higher regions of clay loading studied here. This is taken as further evidence to suggest the participation of the anion-cation pair exchange mechanism at higher cation

concentrations, since non-linearity of isotherms was not noted at the lower equilibrium concentrations used by Farrah[47] and Borovec.[114]

Thermodynamic parameters can be estimated from the sorption isotherms constructed for cobalt and nickel using the treatment of Gaines and Thomas.[117]

When:

$$K_s = \frac{\overline{X}_M 2+}{(\overline{X}_{Na})^2} \cdot \frac{(X_{Na})^2}{X_M 2+} = K'_s \cdot \frac{\gamma^2_{Na}}{\gamma_M 2+} \quad ,$$

using the standard reference states for clay minerals,[118] and approximating solution activity coefficients to unity;

$$\ln K = (Z_{Na} - Z_M 2+) + \int_0^1 \ln K'_s \cdot d\overline{X}_M 2+ \quad ,$$

followed by the conventional relationship between Gibbs free energy (G) and the equilibrium constant;

$$\Delta G = -RT \ln K$$

Plots of $\ln K'_s$ versus $\overline{X}_M 2+$ are shown for Na-montmorillonite treated with cobalt and nickel solutions, in figs.35 and 36, and the relevant data displayed in tables 64 and 65.

For Co-Na exchange, K = 5 and for Ni-Na is 12.

K_s = selectivity coefficient, K'_s = experimental selectivity coefficients
$\overline{X}$ = equivalent fraction on solid
X = equivalent fraction in solution
K = Thermodynamic equilibrium constant
γ = activity coefficient

Fig.35 - ln K_s'(Co) versus $\bar{X}_{Co}$ for cobalt sorption on Na-montmorillonite.

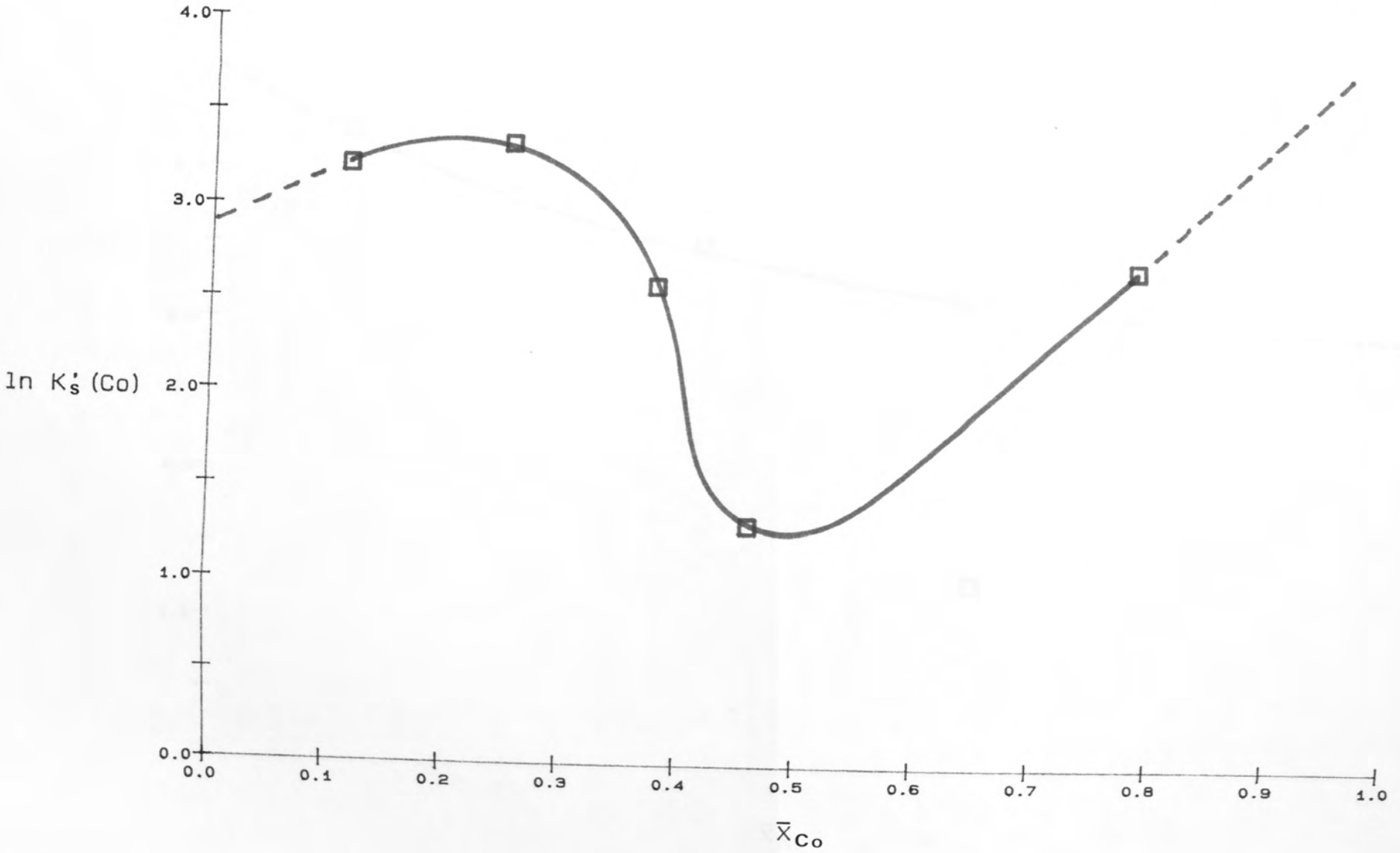

Fig.36 - ln K_s' (Ni) versus $\bar{X}_{Ni}$ for nickel sorption on Na-montmorillonite.

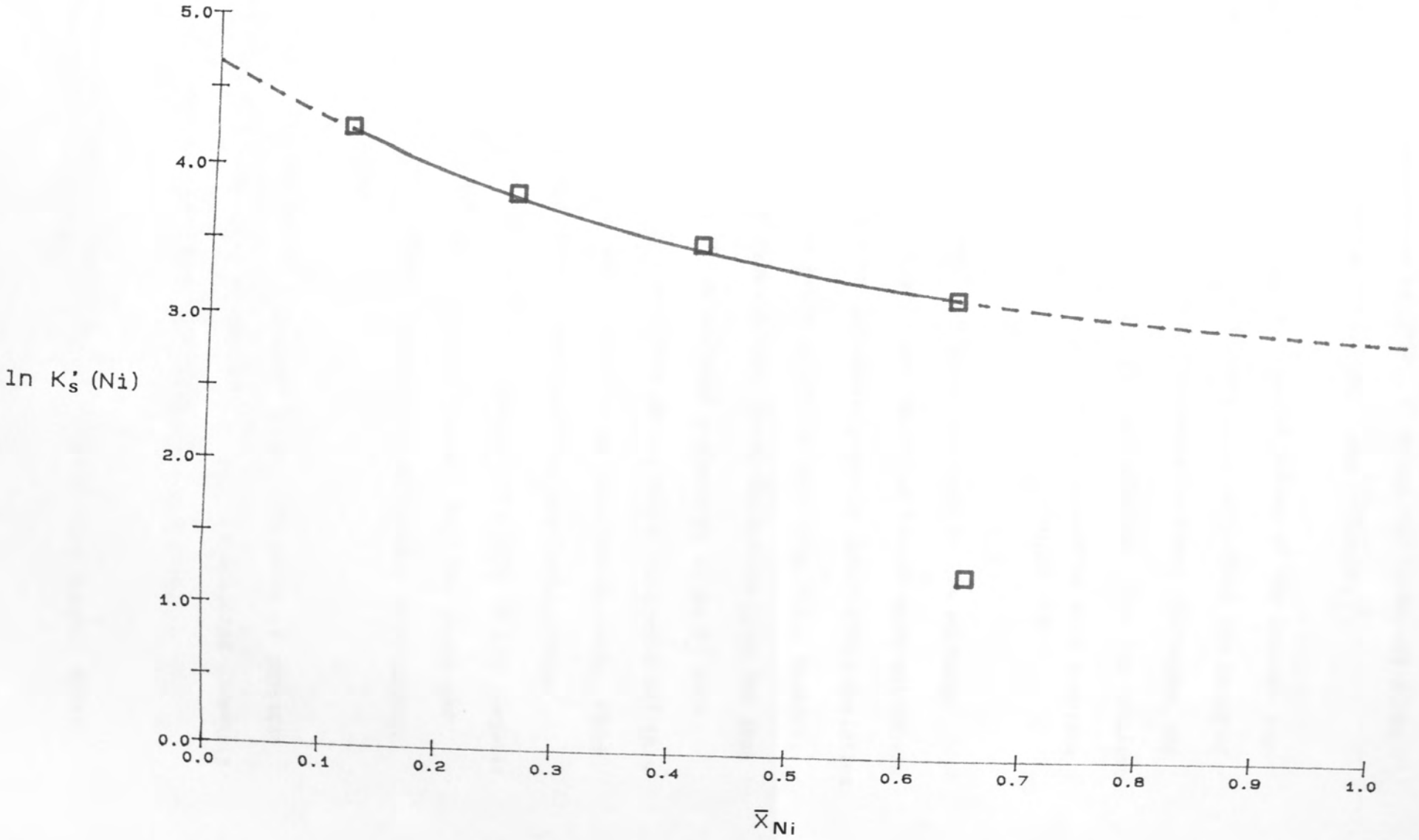

At an ambient temperature of 293K, G values for Co-Na and Ni-Na exchange were estimated at $-500 cal eq^{-1}$ and $-700 cal eq^{-1}$.

The divalent cations exhibited positive values of the natural logarithm of the selectivity coefficient (K'_s) throughout the range of solid loading studied, for both divalent-monovalent exchanges, and this indicated, along with negative free energies, that the divalent species was always preferred. This was in agreement with numerous other published studies on metal ion sorption.[40,60,119]

The selectivity coefficient was not a constant in ion exchange reactions on Na-montmorillonite and hence the law of mass-action was not strictly obeyed. A distinct minimum in the selectivity variation was observed in the Co-Na exchange system only (fig.35). However, it cannot be implicitly assumed that the Ni-Na system (fig.36) does not show this property, since although a decrease in $\ln K'_s$ with increasing X_{Ni} is apparent, one data point, which lies well off this curve, is omitted. This may well be on an alternative curve, which includes a similar minimum in selectivity to the Co-Na system. Unfortunately this anomaly was not apparent in a plot of the Langmuir isotherm (fig.34) generated with the original data and since the analysis of K'_s was performed subsequently, no further experimental data could be obtained.

This distinct minimum may be explained by consideration of physical characteristics of the clay suspension, as will be detailed presently for the Co^{2+} system (i.e. tactoid* formation). Initial

* a tactoid is composed of a number of parallel clay layers, which agglomerate in a suspension.

sorption of cobalt takes place on the external surfaces of the montmorillonite particles. As more cobalt is added (and more sodium is released into solution) it invades into interlamellar sorption sites where, because the Co^{2+} ion is less favourably sorbed there than on the external surfaces,[39] the sodium becomes increasingly more effective in competition, and the selectivity coefficient falls. However, the formation of tactoids[39] occurs to an increasing extent as the cobalt added into the solution increases and at $\overline{X}_{Co} = 0.5$ begins to dominate the above factor, becoming progressively more important as $\overline{X}_{Co}$ increases further, thus resulting in increased selectivity coefficients. Banin[39] observed a similar effect for Ca^{2+} exchange with Na- and K-montmorillonite and McBride's[40] data on Ca^{2+}-Na^{+} exchange suggested that the interlayer regions of tactoids preferred divalent to monovalent ions more than external surfaces. Further selectivity coefficient-$\overline{X}_{M}n+$ plots of zinc sorption and cobalt sorption on Na-montmorillonite performed by Singh et al[120] and Singhal et al[119] also showed these distinct minima in selectivity coefficient. It appears however that the data from Maes et al[60] and McBride[40] on Co^{2+},Zn^{2+},Cu^{2+},Cd^{2+},Ni^{2+} sorption and Ca^{2+} sorption on Na-montmorillonite contradict the above hypothesis, since selectivity coefficients steadily increase with increased loading on the clay. These systems however do include high background concentrations of sodium salts, which will affect the physical properties of, and hence formation of tactoids in, the clay suspensions.

Sorption at low cation concentrations

Data from the microscopic sorption experiments on Na-montmorillonite (tables 38 and 40) are plotted in figs.37 and 38 (tables 66 and 67) along with the previous results on macroscopic sorption. In both cases, the sorption isotherm could be extended to include the first point from the low level experiments, but the remaining data points did deviate significantly.

The distribution coefficients (tables 38 and 40) showed a similar trend, the values derived at 10ppm fitting well with previous data (tables 36 and 37), but smaller K_d values were then found with decreasing initial metal ion concentration.

Some doubt is cast on the validity of the latter three data points from the low level nickel work, since previous studies of metal ion (Sr^{2+} and Ni^{2+}; Sr^{2+},Co^{2+} and Cd^{2+}) sorption on Na-montmorillonite and Co^{2+},Zn^{2+} sorption on Na-hectorite performed by Bowman et al,[110] Egozy[32] and Tiller[57] have shown an increasing K_d is associated with decreasing solution metal ion concentration. (The same doubt cannot be inferred from the low level cobalt study since with γ-spectrometric analysis, it was only possible to indicate the lowest solution concentration detectable and actual values may be considerably lower. Of greater consequence is the observation that the K_d value calculated for the 5ppm cobalt sample lies on the curve generated from data gained at higher concentrations, i.e. K_d still appears to be increasing with decreasing equilibrium cobalt concentration, as expected.)

Table 66 - Langmuir isotherm data derived from Ni sorption on Na-montmorillonite, at low concentration.

Initial Ni concentration (ppb)	Final Ni concentration(C) (ppb)	$\frac{C}{(x/m)}$	$\log \frac{C}{(x/m)}$
10 000	7.4	0.015	-1.83
2 000	6.1	0.061	-1.21
500	14	0.57	-0.25
100	12	2.8	0.44

Table 67 - Langmuir isotherm data derived from Co sorption on Na-montmorillonite, at low concentration.

Initial Co concentration (ppb)	Final Co concentration(C) (ppb)	$\frac{C}{(x/m)}$	$\log \frac{C}{(x/m)}$
10 000	29.9	0.06	-1.22
5 000	<6.4	<0.025	<-1.60
1 000	<3.1	<0.063	<-1.20
100	<1.5	<0.31	<-0.51

Fig.37 - Langmuir sorption isotherm for nickel uptake on Na-montmorillonite extended to include data at low cation concentrations.

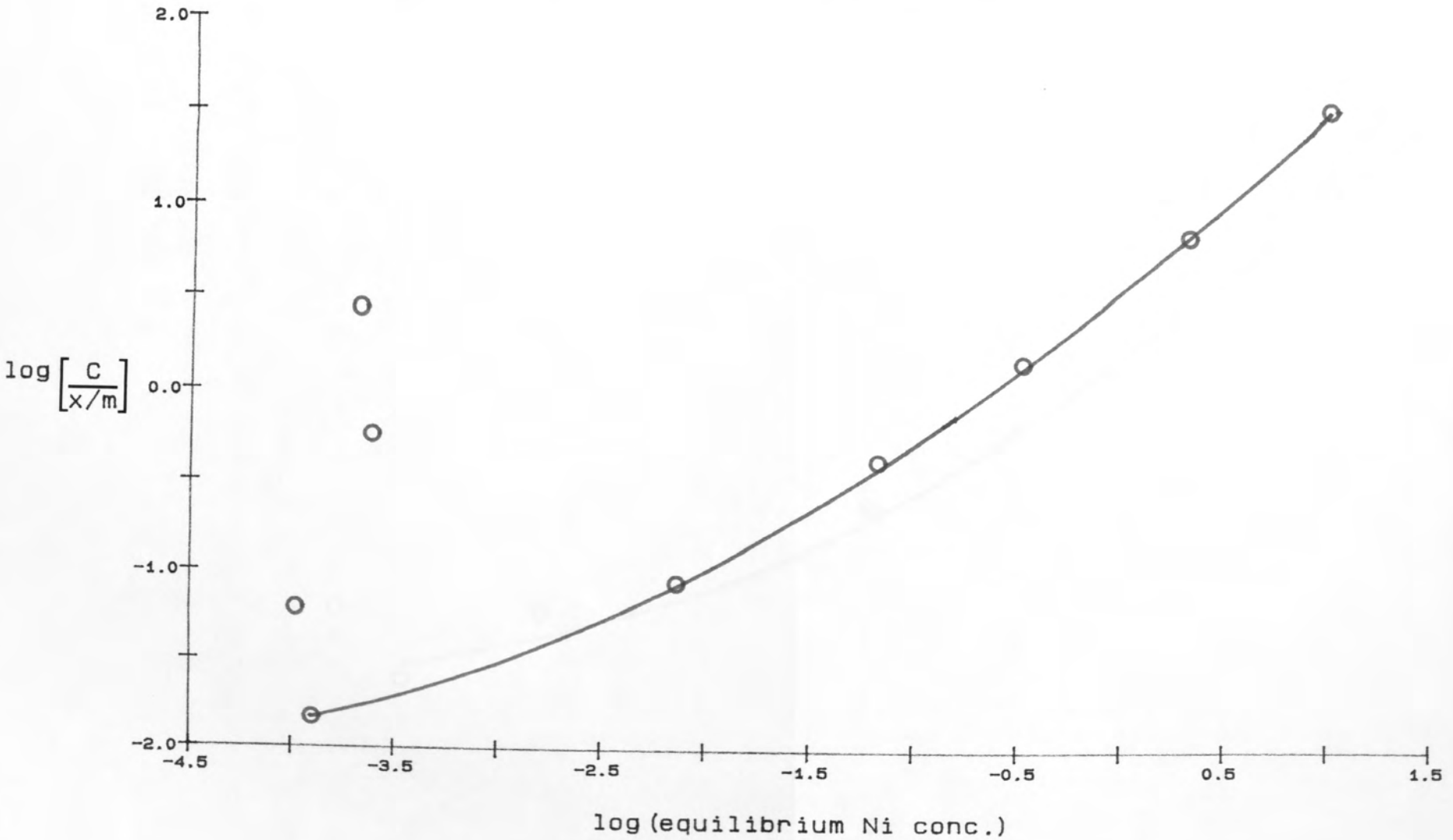

Fig.38 - Langmuir sorption isotherm for cobalt sorption on Na-montmorillonite extended to include data at low cation concentrations.

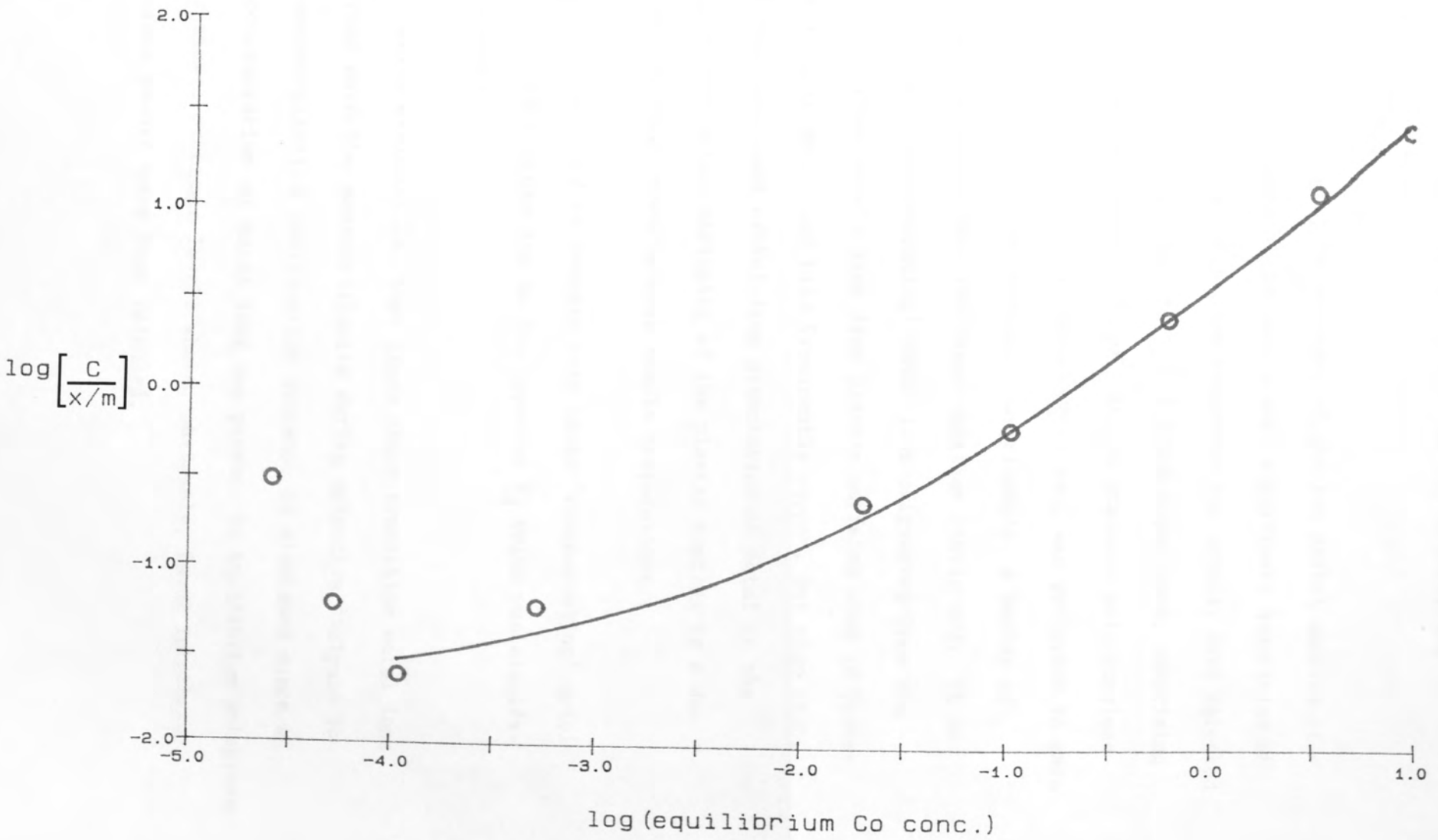

Sorption on container walls was found not to be important (Appendix 2).

During ion chromatographic analysis of the two nickel samples of 500ppb and 100ppb initial concentration, significant quantities of zinc and copper, along with some manganese and cobalt, were detected in the final solutions (table 68). A blank experiment, comprising only de-mineralised water ($12.6cm^3$) in the standard polypropylene centrifuge tube plus plastic coated metal cap, was performed to gain further insight into this problem. Surprisingly, a number of cations were released into the final solution (table 68). It is postulated that 'contaminating' metal ions originated from two sources: (i) Prominently zinc from plastic surfaces used in transferring liquids etc., and (ii) Prominently copper, but also zinc, cobalt, manganese and nickel from dissolution of metal in the centrifuge caps after stripping of the plastic coating by a de-contaminating agent used between sample preparations.

The nickel, thus, had to compete with these 'contaminating' metal ions for sorption sites and so the apparent K_d value was significantly lowered.

An alternative explanation, that these other transition metal ions were sorbed onto the montmorillonite during selective dialysis in the Na-montmorillonite purification process, is dismissed since a larger concentration of metal ions was present in equilibrium solutions at lower nickel exchange levels where, obviously, fewer interlayer counter-ions should have been released.

Table 68 - Cation composition in final solutions from selected low level nickel sorption experiments.

Sample	Final Ni concentration (ppb)	Final solution concentrations (cm)			
		Zn	Cu	Mn	Co
500ppb Ni	14	20	24	0.2	0.2
100ppb Ni	13	16	3.0	-	-
Demineralised water blank	1.2	9	12	0.7	0.2

The dissolution of metallic components is a problem which may be associated with low level sorption experiments, but to a certain extent validates the present study, as radionuclide movement away from a waste disposal vault requires the initial leaching of metallic components stored within such a structure.

The K_d values for nickel and cobalt sorption from 10ppm solutions indicated a higher preference of nickel for the clay surface ($K_d(Ni) = 6.8 \times 10^4, K_d(Co) = 1.7 \times 10^4$), which was in agreement with results at higher concentrations (tables 36 and 37). However the preference was for cobalt at an initial solution concentration of 1000ppm ($K_d(Ni) = 30$, $K_d(Co) = 36$), and so a reversal in roles was apparent at higher concentrations. Cobalt was also sorbed to a greater extent in the initial experiments using 0.1M solutions, providing further confirmation of the above effect. Maes et al[60] reported a distinctly similar behaviour and this phenomenon is able to explain the differing relative positions observed for cobalt and nickel in affinity sequences on clay minerals. Utilizing very low concentrations of cobalt and nickel, Takematsu[46] reported a sorption affinity order of Ni>Co. Cobalt and nickel were sorbed to a similar degree on Na-montmorillonite according to Borovec[114] but his investigation was performed at intermediate concentrations.

However, the data of Hodgson[34] indicated a preference of cobalt rather than nickel for the montmorillonite clay, even though both transition metals were present in very low concentration, apparently contradicting the proposed hypotheses. It must be noted, though, that experiments were performed in the presence of a large con-

centration of added electrolyte (i.e. 0.1N $CaCl_2$), hence sorption was dependent on the total solution molar strength rather than just cobalt or nickel concentration - this effect correlates with the work performed at constant (0.04M) molar strength (see later) in which cobalt was sorbed to a greater extent than nickel even when initially present at a concentration of only 0.4mmolL^{-1}.

Influence of groundwater constituents

Having characterised sorption effects down to a level of 10ppm initial metal ion concentration and observed greater than 99.5% uptake in the microscopic region, it was of relevance to study the influence of external cations which will most likely be present in a typical groundwater environment surrounding any radioactive waste disposal system.

Initial experiments were performed at a constant molar strength of 0.04M and probed the influence of varying ratios of magnesium, calcium, sodium and potassium on nickel and cobalt uptake by Na-montmorillonite.

Almost constant percentages of nickel and cobalt were taken up from combinations with magnesium and calcium throughout the concentration ranges studied (figs.25 and 26), whereas both transition metal ions were sorbed to a greater extent with increasing initial solution concentration when competing with sodium and potassium ions (figs.27 and 28). K_d values showed similar trends (tables 41, 42, 43, 44, 49, 50, 51, 52, fig.29).

It thus appears that at the same total molar strength, the percentage of cobalt (or nickel) sorbed from a solution containing a single competing divalent cation is approximately the same, and this hypothesis could be important in predictions of cation behaviour at low concentrations, such as those envisaged around a waste disposal site.

It is clear from fig.29 that divalent cations compete more successfully than monovalent ions. The consensus of literature data also suggests that monovalent cations exhibit a lower affinity than divalent cations[39,45,109] for the clay surface when sorbed from single metal solutions. Potassium, as expected, is more effective in preventing cobalt (or nickel) sorption than sodium. However, calcium is more effective than magnesium in preventing nickel sorption, but the reverse is true for cobalt sorption.

Of the limited amount of data available in the literature on effects of cation competition on transition metal ion sorption, that of Mukherjee et al[121] and O'Connor et al[122] confirms the behaviour observed in this study.

Experimental data for Co^{2+}, Ni^{2+} and Mn^{2+} sorption on H-montmorillonite in the presence of different concentrations of magnesium, obtained by Mukherjee et al,[121] at a number of constant molar strengths, indicated that Mg^{2+} had a significant effect on suppressing transition metal ion sorption. Further, at a single constant molarity, a consistent percentage of transition metal ion was sorbed. This is good evidence in support of our claim that at the

same molar strength, the percentage of cobalt (or nickel) sorbed from a solution containing a single competing divalent cation is approximately the same.

The uptake of trace concentrations of copper and cobalt on the mineral illite was studied by O'Connor et al[122] as a function of pH, solution composition and solid phase concentration, in an attempt to simulate conditions in fresh and marine water environments. The fraction of copper adsorbed from a solution adjusted to pH5.3 decreased from 60% to 35% with a 100 fold increase in sodium chloride in solution. The fraction of cobalt adsorbed onto illite from an artificial river water was reduced by half, when the solution calcium content was increased from 1.5 to 15ppm. Magnesium was also observed to interfere significantly with cobalt sorption at pH8, an increase in solution concentration of 5ppm to 1000ppm resulting in the fraction of cobalt sorbed being reduced from 0.95 to 0.4, and it was proposed that the detrimental effects observed on transition metal ion sorption were due to direct competition of the additional cation for sorption sites.

The data of O'Connor et al[122] support the proposal that additional cations, typical of groundwaters, may have a considerable influence on transition metal ion uptake by clay minerals.

Thermodynamic treatment of sorption in ternary cation systems is not well developed,[118] but a measure of the relative affinities of the sorbate cations for the clay surface can be derived using the competitive Langmuir equation proposed by Boyd et al:[123]

$$\left[\frac{x}{M}\right]_A = b.\left[\frac{k_A}{k_B}\right] \cdot \left[\frac{C_A}{C_B}\right] \Big/ \left[1+\left[\frac{k_A}{k_B}\right] \cdot \left[\frac{C_A}{C_B}\right]\right]$$

where $\left[\frac{x}{M}\right]_A$ is the amount of species A sorbed, b is capacity for species A; C_A and C_B are the equilibrium solution concentrations; and k_A and k_B are the respective Langmuir constants.

The competitive Langmuir plots for Ni-Mg, Ni-Ca, Ni-K, Co-Mg, Co-Ca, Co-K exchange are shown in fig.39 where A = Ni^{2+} or Co^{2+} (tables 69 to 74). The same type of plot, but with A = Mg^{2+}, Ca^{2+} or K^{+} is shown in fig.40 (tables 69 to 74). Contradictory to Farrah et al's[47] data on competitive adsorption of Pb^{2+}, Cu^{2+}, Zn^{2+}, Cd^{2+}, Mg^{2+} and Ca^{2+} on Na-montmorillonite, no straight line relationship was observed and thus no value for the relative cation affinity parameter $\frac{k_A}{k_B}$ could be derived. It is suggested that Farrah et al's[47] data covered only a small range of competing metal ion ratios and an extension of this range would probably lead to the curvature witnessed in this study.

The factor f (tables 69 to 74) was introduced in an attempt to simplify sorption analysis in bi-cation systems. If, for example magnesium had the same affinity for the clay surface as nickel, then only the nickel isotherm need be determined and the total molar strength of the bi-cation solution used to estimate the value of K_d from the sorption isotherm. Similarly if magnesium had a different, but constant, relative affinity for the clay surface,

Tables 69, 70, 71 - Competitive Langmuir isotherm data derived for cobalt sorption in the presence of competing cations at constant molar strength.

Ratio	Initial Co concentration (mmol/L)	Initial M^{n+} concentration (mmol/L)	Equilibrium Co concentration C_{Co} (mmol/L)	Equilibrium M^{n+} concentration $C_{M^{n+}}$ (mmol/L)	f	$\frac{C_{Co}}{C_{M^{n+}}}$	$\frac{(C_{Co}/C_{M^{n+}})}{(x/m_{Co})}$	$\frac{C_{M^{n+}}}{C_{Co}}$	$\frac{(C_{M^{n+}}/C_{Co})}{(x/m_{M^{n+}})}$
Table 69 Mg:Co									
100:1	0.396	39.6	0.31	30	1.08	0.0106	2.6	93	180
10:1	3.64	36.4	3.0	27	1.07	0.108	3.1	9.3	20
1:1	20.0	20.0	16	15.4	1.05	1.04	5.1	0.96	4.2
1:10	36.4	3.66	29	3.0	0.99	9.9	27	0.101	2.9
Table 70 Ca:Co									
100:1	0.396	39.6	0.28	34	0.94	0.0084	1.5	120	420
10:1	3.64	36.4	2.8	33	0.89	0.084	2.0	12	70
1:1	20.0	20.0	15	17	0.99	0.90	3.9	1.1	7
1:10	36.4	3.66	27	3.1	1.47	8.8	20	0.11	4
Table 71 K:Co									
100:1	0.396	39.6	0.11	35	0.91	0.0031	0.23	300	1400
10:1	3.64	36.4	1.6	28	1.10	0.056	0.54	18	41
1:1	20.0	20.0	15	12	1.48	1.23	3.0	0.81	2.0
1:10	36.4	3.66	29	3.5	0.94	8.3	22	0.12	10

$C_{Co} + C_{M^{n+}}.f = 32.1 mmol L^{-1}$, i.e. C_{Co} at 0.04M $= 32.1 mmol L^{-1}$ $\therefore$ $f = \frac{32.1 - C_{Co}}{C_{M^{n+}}}$

Tables 72, 73, 74 - Competitive Langmuir isotherm data derived for nickel sorption in the presence of competing cations at constant molar strength.

Ratio	Initial Ni concentration (mmol/L)	Initial M^{n+} concentration (mmol/L)	Equilibrium Ni concentration C_{Ni} (mmol/L)	Equilibrium M^{n+} concentration $C_{M^{n+}}$ (mmol/L)	f	$\frac{C_{Ni}}{C_{M^{n+}}}$	$\frac{(C_{Ni}/C_{M^{n+}})}{(x/m_{Ni})}$	$\frac{C_{M^{n+}}}{C_{Ni}}$	$\frac{(C_{M^{n+}}/C_{Ni})}{(x/m_{M^{n+}})}$
Table 72 Mg:Ni									
100:1	0.408	39.6	0.31	31	1.05	0.010	2.1	100	240
10:1	3.44	36.4	2.8	29	1.04	0.096	3.0	10	29
1:1	18.92	20.0	15.5	16.1	1.10	0.96	5.6	1.04	5.4
1:10	34.4	3.66	28	3.0	1.85	9.1	27	0.11	3.6
Table 73 Ca:Ni									
100:1	0.408	39.6	0.35	34	0.98	0.010	3.7	90	320
10:1	3.44	36.4	3.0	32	0.95	0.094	4.4	11	50
1:1	18.92	20.0	16.9	16.7	0.98	1.0	10	0.99	6
1:10	34.4	3.66	30	2.9	1.11	10.4	47	0.096	2.5
Table 74 K:Ni									
100:1	0.408	39.6	0.15	36	0.92	0.0042	0.32	240	1400
10:1	3.44	36.4	1.74	34	0.91	0.051	0.59	20	200
1:1	18.92	20.0	14.8	18.2	1.01	0.82	4.0	1.2	13
1:10	34.4	3.66	29	3.3	1.27	8.7	22	0.12	7.2

$C_{Ni} + C_{M^{n+}}.f = 33.2 mmol L^{-1}$, i.e. C_{Ni} at $0.04M = 33.2 mmol L^{-1}$ $\therefore f = \frac{33.2 - C_{Ni}}{C_{Mn^+}}$

Fig.39 - Competitive Langmuir plots for cobalt/nickel sorption on Na-montmorillonite in the presence of competing cations at constant total molarity (0.04M).

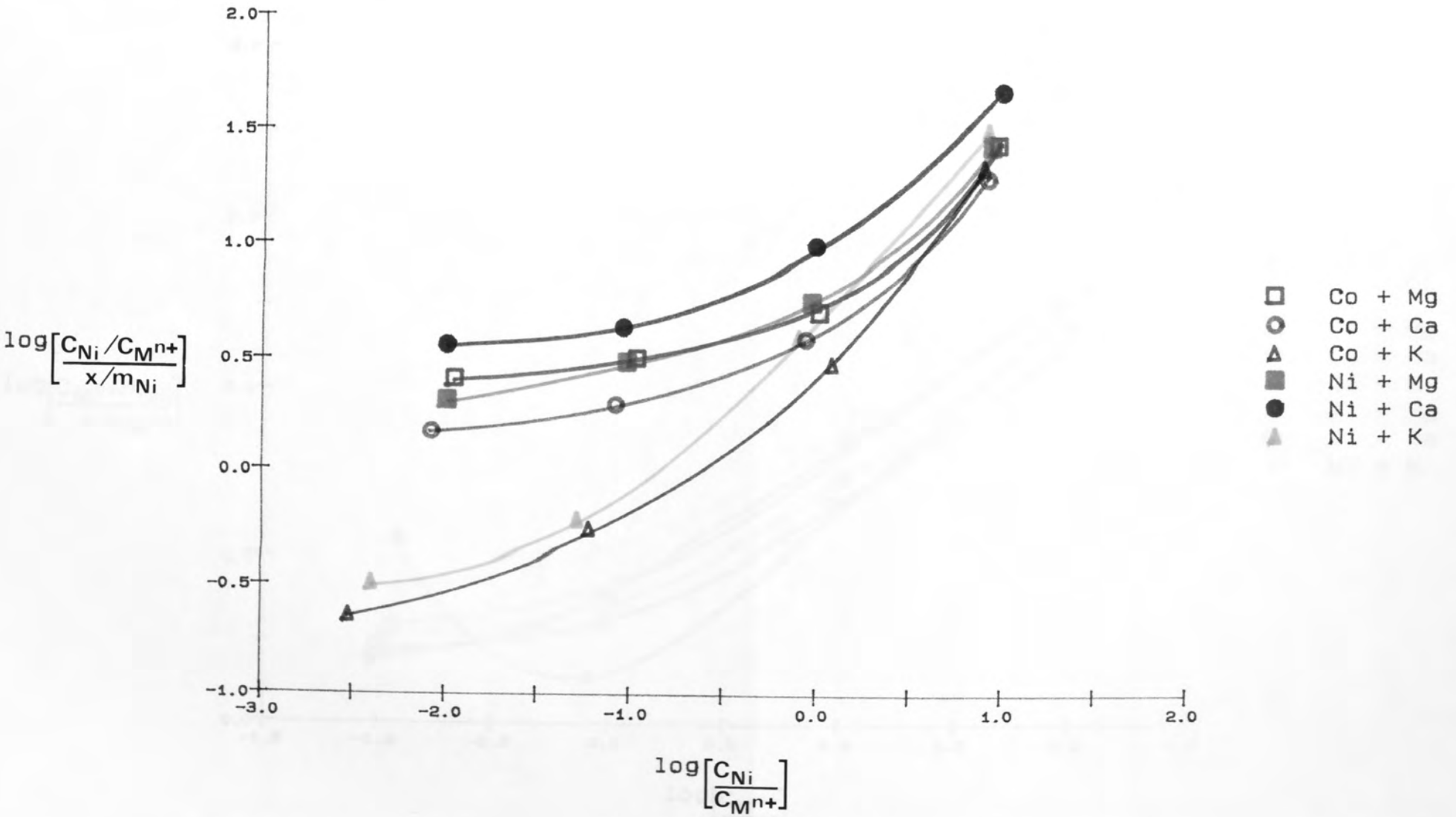

Fig.40 - Competitive Langmuir plots for magnesium/calcium/potassium sorption on Na-montmorillonite in the presence of competing cations at constant total molarity.

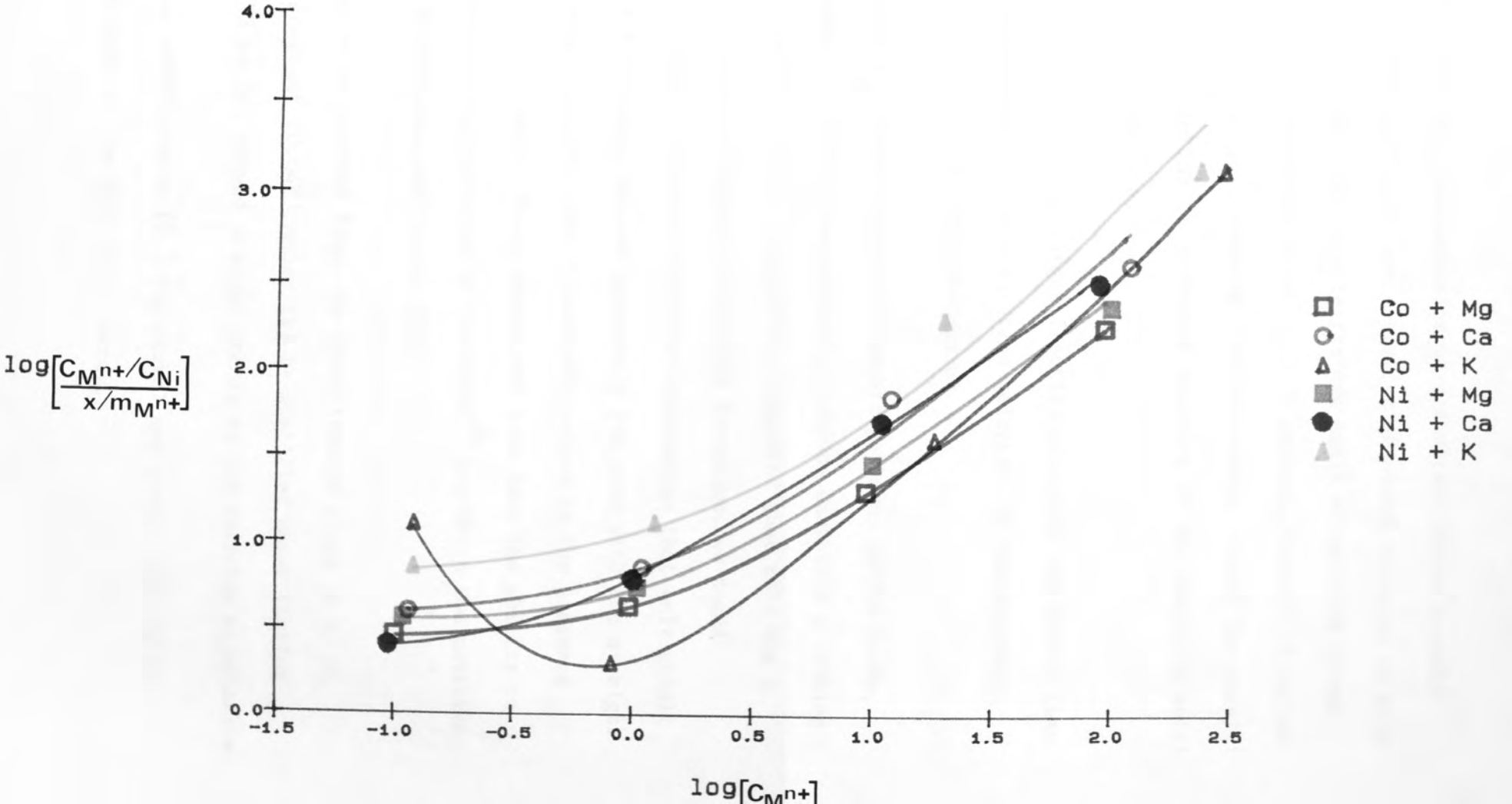

then multiplying its concentration by a constant factor f would bring it to the equivalent concentration of nickel required to give the same effect and hence enable the use again of only the nickel isotherm for the bi-cation solution. In general, however, f varied noticeably, generally increasing with increasing nickel (or cobalt) concentration, pointing to decreased affinity of the competing metal ion for the clay surface.

It should be noted that a larger fraction of cobalt was sorbed than nickel as predicted, at this solution molarity, by the argument developed previously in this discussion.

Although most K_d values followed a smooth pattern, in the Co-Na, Co-K exchange reactions, the competing cations exhibited a seemingly peculiar behaviour. It is tentatively suggested that this was a consequence of the influence of tactoid formation, as noted previously. This is supported by the observation that only cobalt showed this behaviour, as was apparently the case with the straight Co-Na exchange (fig.24), and it was only caused in the presence of monovalent cations. These monovalent ions have the ability to bond to the external surfaces of tactoids,[39] and hence the positive uptake of sodium observed (table 51).

The desorption of cations from the above treated clays (i.e. at initially constant (0.04M) molarity) by distilled water (tables 45 to 48, 53 to 56) showed similar trends to the sorption experiments.

Distribution coefficients (K_d) for nickel and cobalt were approximately the same in the desorption study.

Comparison with the initial sorption data revealed higher K_d values for nickel, cobalt and competing cations when desorbed. Molar strength thus appeared to control K_d values since all the equilibrium solutions from desorption had inherently lower concentrations of metal ions. This is similar to the more fundamental observation of increasing K_d with decreasing solution concentration exhibited by the nickel and cobalt sorption isotherms (figs.22 and 24) on Na-montmorillonite (see also later). A similar pattern of constant K_d, for nickel, cobalt, calcium and magnesium with varying M^{n+}:Ni(Co) ratios to that in initial (0.04M) sorption experiments was followed except for the 100:1 ratio. The K_d(Ni/Co) was anomalously low, which may be a result of the much higher concentration of competing metal ion initially desorbed into solution, which then more effectively competes with the nickel (cobalt) remaining on the clay.

Desorption K_d(Ni/Co) values with calcium and magnesium as competing cations were lower than values with sodium and potassium ions. A similar behaviour was observed in the initial sorption experiments and gives confirmation that divalent metal ions compete more effectively than monovalent for sorption sites on the clay.

A further investigation of the influence of competing cations was performed, again using a number of M^{n+}:Ni(M^{n+}= competing cation) ratios, but with varying total molar concentration and only the initial nickel concentration constant. From the data in tables 57 to 60, nickel sorption appeared to be relatively unaffected when one tenth its concentration of competing cation was present, and

greater than 68% nickel was still sorbed when a ten fold excess of either sodium or potassium was present in solution. However, calcium and magnesium had a considerable effect on nickel uptake by the clay with <18% removed from solution when a ten fold excess of either additional cation was present.

The nickel distribution coefficient was higher in the presence of monovalent than divalent competing cations, increasingly so as the relative concentration of nickel decreased, as expected from the previous investigation at constant molar strength (tables 41, 42, 43, 44).

As the total solution molar strength increased (as the ratio $M^{n+}:Ni^{2+}$ increased), $K_d(Ni)$ values approached those observed in 0.04M constant strength experiments.

$K_d(Ni)$ at a 10:1 molar ratio ($M^{n+}:Ni$) for magnesium and calcium was very close to that found in the constant molar strength solutions. The concentrations of total metal ion sorbed were similar in both cases which indicated the existence of a saturated state, beyond which further metal sorption was not favourable. $K_d(Ni)$ for 1:10 and 1:1 $M^{n+}:Ni^{2+}$ ratios, when compared with their respective values at constant (0.04M) molar strength, however, showed sorption to be dependent on total solution molar strength, since $K_d(Ni)$ values from these variable molarity solutions closest approached those from 0.04M solutions when their total cation concentrations were most similar. Furthermore, it appears that ionic strength, as opposed to molar strength, is the dominant solution variable since $K_d(Ni)$ values for sodium and potassium competing

cations were higher than for the divalent cations in sorption from both solutions of constant and variable molar strength, even though molarities were the same.

It is relevant at this stage to look at the influence of competing cations on K_d(Ni) at the microscopic level (table 61). A straightforward comparison of K_d(Ni) for solutions having 1:1, Na:Ni and Ca:Ni, ratios from all three sets of data further enforces the suggestion of increasing K_d(Ni) with decreasing total solution ionic strength (table 75).

The derogatory effect of calcium in a radioactive waste disposal vault environment was demonstrated very clearly in the low level experiments since a one hundred fold excess over nickel (or cobalt) decreased K_d(Ni/Co) by approximately two orders of magnitude (tables 61 and 62). The influence of sodium on sorption, however, was much less pronounced with a hundred times excess decreasing the sorption coefficient for cobalt and nickel by less than four fold.

In the variable ionic strength experiments a change in pH was observed and enabled calculation of the apparent release of H^+ into solution. The release of H^+ from the clay (tables 57,58,59,60) can only account for $\simeq$1% of the total metal ion sorbed in each case. However, it is apparent that H^+ is released to a relatively greater extent with increasing total metal ion sorbed (fig.41) and with increasing competing cation sorbed (fig.42). Hence, some particular exchange site may be occupied by H^+ - whether it is edge, interlayer or from surface OH groups[36] is uncertain, but it may be stated that this mechanism constitutes only a small proportion of the exchange capacity.

Table 75 - Comparison of nickel distribution coefficient (K_d(Ni)) variation with total solution molarity (at constant 1:1 M^{n+}:Ni).

competing cation	total solution molarity (mmol/L)	K_d(Ni) (cm^3/g)
Na	40	16
Na	3.4	3300
Na	0.068	16000
Ca	40	6
Ca	3.4	410
Ca	0.068	3600

Fig.41 - Variation of apparent H^+ released into solution from a Na-montmorillonite with total metal ion sorbed using solutions of differing ionic strength.

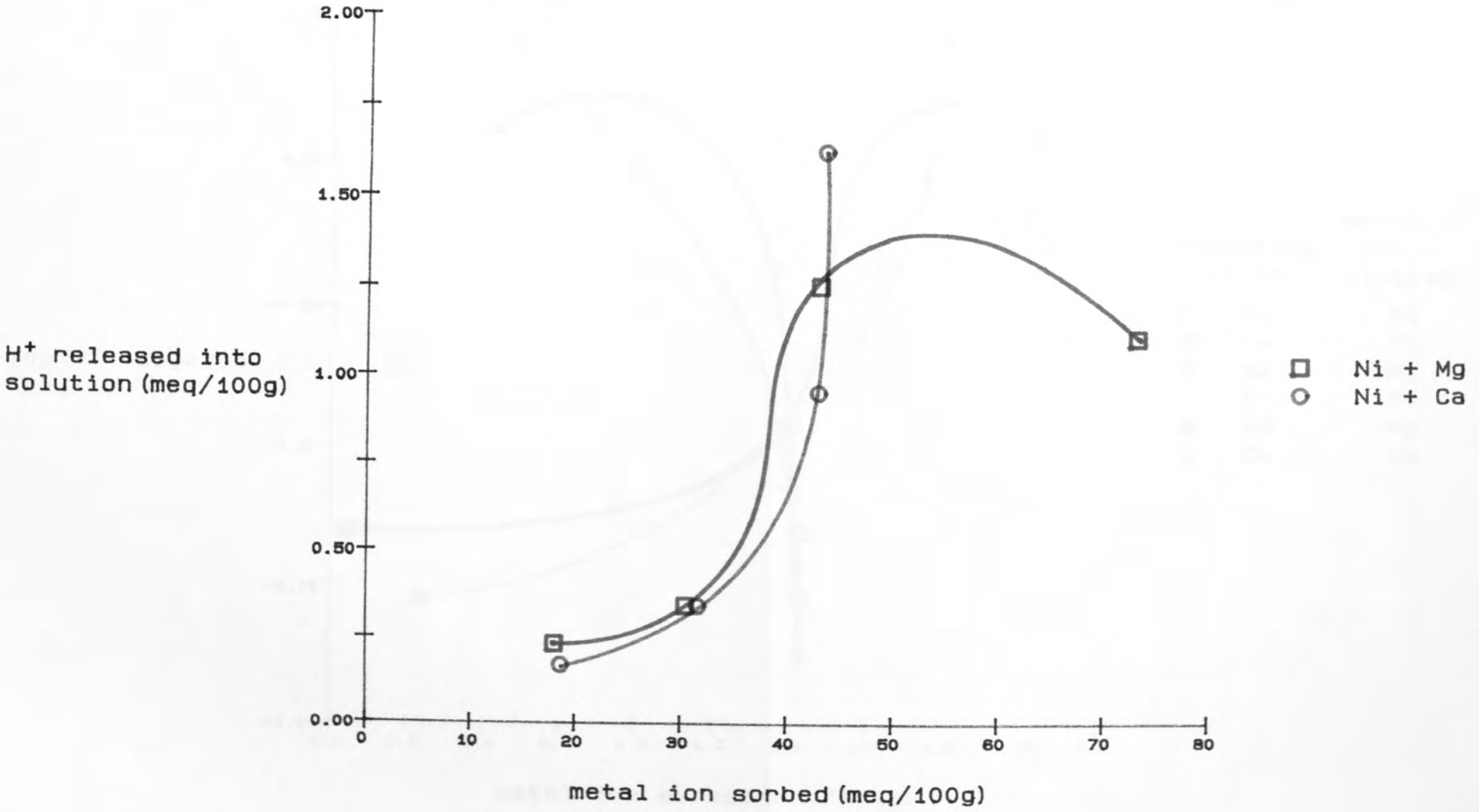

Fig.42 - Variation of apparent H^+ released into solution from a Na-montmorillonite with metal ion (Ni, Mg, Ca) sorbed using solutions of differing ionic strength.

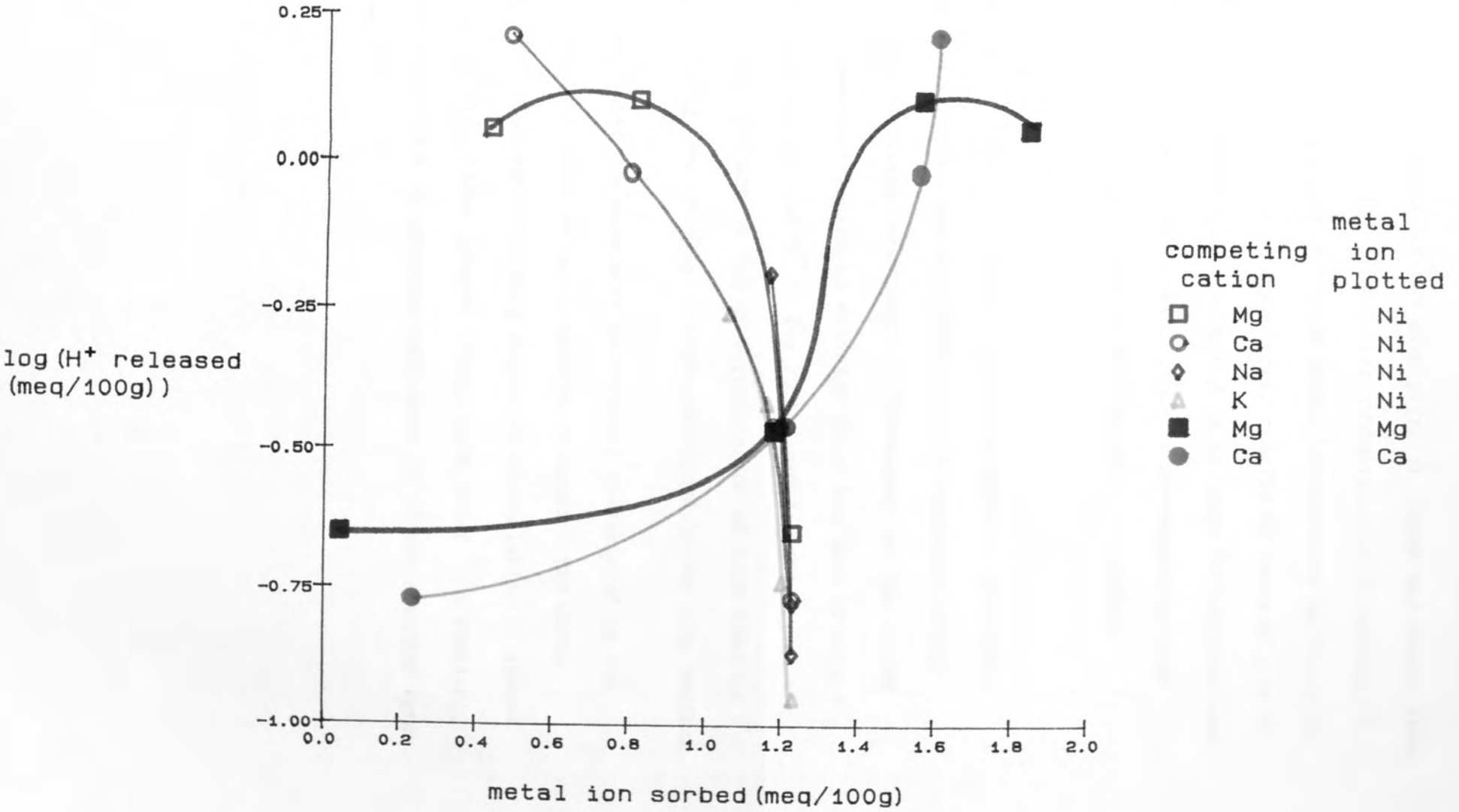

This contradicts a study of the adsorption of copper and cobalt from aqueous solution onto illite and other substrates as a function of pH, solution composition and solid phase concentration performed by O'Connor et al[122] who interpreted their results in terms of a model whereby the trace metals were adsorbed in exchange for surface bound H^+ ions. It must be noted, however, that a non-expanding clay mineral substrate was utilized as well as very low sorbate concentrations.

Additionally, it must be pointed out that a surface catalysed deprotonation reaction may be occuring. A pH decrease during variable ionic strength experiments is obviously not due to the presence of desorbed sodium in solution which has been effectively exchanged with nickel (or M^{n+}), due to the greater acidity of the latter. It may in fact be due to deprotonation of interlamellar water surrounding the exchange cation, catalysed by the clay surface.

Evidence that water is much more extensively dissociated in the interlayer regions than in bulk, appears to support the above argument. NMR studies indicate a degree of dissociation of interlayer water 10^6-10^7 times greater than in bulk water [124]; similarly, from conductance data it appears that about 1% of the adsorbed water is ionized.[125]

CHAPTER 4

THE INFLUENCE OF ORGANIC SPECIES ON SORPTION

4.1 INTRODUCTION

The presence of organic material in groundwaters is well established,[126] but the possible influence of such material on sorption properties of metal ions on clay minerals is not well documented. Three ways in which organic compounds affect transition metal-sorbent interactions are apparent. Organic material may;

(i) influence transport of the transition metal ion, in groundwater solution, by complexation, e.g. precipitation,

(ii) affect the stability of a transition metal treated clay by complexation, e.g. promote desorption,

(iii) be sorbed onto the clay substrate itself.

The direct sorption of ammonia from aqueous solution onto soils was first reported by J. T. Wray in 1852.[19] Recent work has covered the sorption of such complex organic molecules as pesticides and compounds of biological importance, e.g. amino acids and peptides.[27]

The majority of transition metal sorption studies involving organic ligands have been concerned with the uptake of simple complexes onto clay minerals, e.g. tris(1,2-propylenediamine)Co(III) onto Laponite,[53] and their characterisation using a variety of spectroscopic methods.[127,128]

In this study, an initial qualitative investigation involving addition of simple organic ligands to previously prepared Ni(Co)-clay samples, was followed by a quantitative examination which further included likely groundwater organic constituents. Having established the initial effects of addition of organic compounds,

the stability of the transition metal "complexes" on the clay so formed, towards cations in external solutions, was examined.

Selection of hectorite for this work facilitated the characterisation of sorbed transition metal complex ions by their absorption spectra, since it has a very low structural iron content.

4.2 MACROSCOPIC EFFECTS

4.2.1 Influence of organic compounds on atomic absorption analysis of nickel and cobalt

Before any experiments could be performed on the quantitative desorption effects of added organic ligands on Ni- and Co-hectorite clays, an assessment of the possible influence of the organic material on solution flame spectrophotometric analysis was initialised.

4.2.1.1 $250cm^3$ solutions were formulated, comprising 1.0ppm Ni^{2+} (chloride salt) plus three different organic compounds, including ammonia for convenience, respectively, generating the following organic:metal ratios ; ammonia - 1:10, 1:1, 10:1, 40:1, 400:1, 2000:1, 10000:1 ; ethylenediamine - 1:10, 1:1, 10:1, 100:1 ; butanoic acid - 1:10, 1:1, 10:1, 100:1. The solutions were analysed by atomic absorption using the usual technique and results are displayed in table 76 and fig.43.

4.2.1.2 $250cm^3$ solutions were made up comprising 1.52ppm Co^{2+} (chloride salt) plus three different organic compounds, respectively, generating the following organic:metal ratios ; ammonia - 1:10, 1:1, 10:1, 40:1, 100:1, 400:1, 2000:1, 10000:1 ; ethylenediamine - 1:10, 1:1, 10:1,

Table 76 - Influence of organic material on nickel detection by atomic absorption.

Initial Ni concentration (ppm)	organic added	organic:Ni ratio	log organic:Ni ratio	Ni detected (ppm)	% Ni detected
1.00	-	-	-	1.01	101
1.00	NH_3	1:10	-1	0.98	98
1.00	NH_3	1:1	0	0.97	97
1.00	NH_3	10:1	1	0.68	68
1.00	NH_3	40:1	1.6	0.96	96
1.00	NH_3	400:1	2.6	1.04	104
1.00	NH_3	2000:1	3.3	1.04	104
1.00	NH_3	10000:1	4	1.00	100
1.00	-	-	-	0.99	99
1.00	en	1:10	-1	0.99	99
1.00	en	1:1	0	0.99	99
1.00	en	10:1	1	0.75	75
1.00	en	100:1	2	0.98	98
1.00	-	-	-	0.98	98
1.00	BA	1:10	-1	0.97	97
1.00	BA	1:1	0	0.99	99
1.00	BA	10:1	1	0.99	99
1.00	BA	100:1	2	1.00	100

Abbreviations: NH_3 - ammonia
en - ethylenediamine
BA - butanoic acid

Fig.43 - Atomic absorption analysis of nickel in the presence of organic compounds.

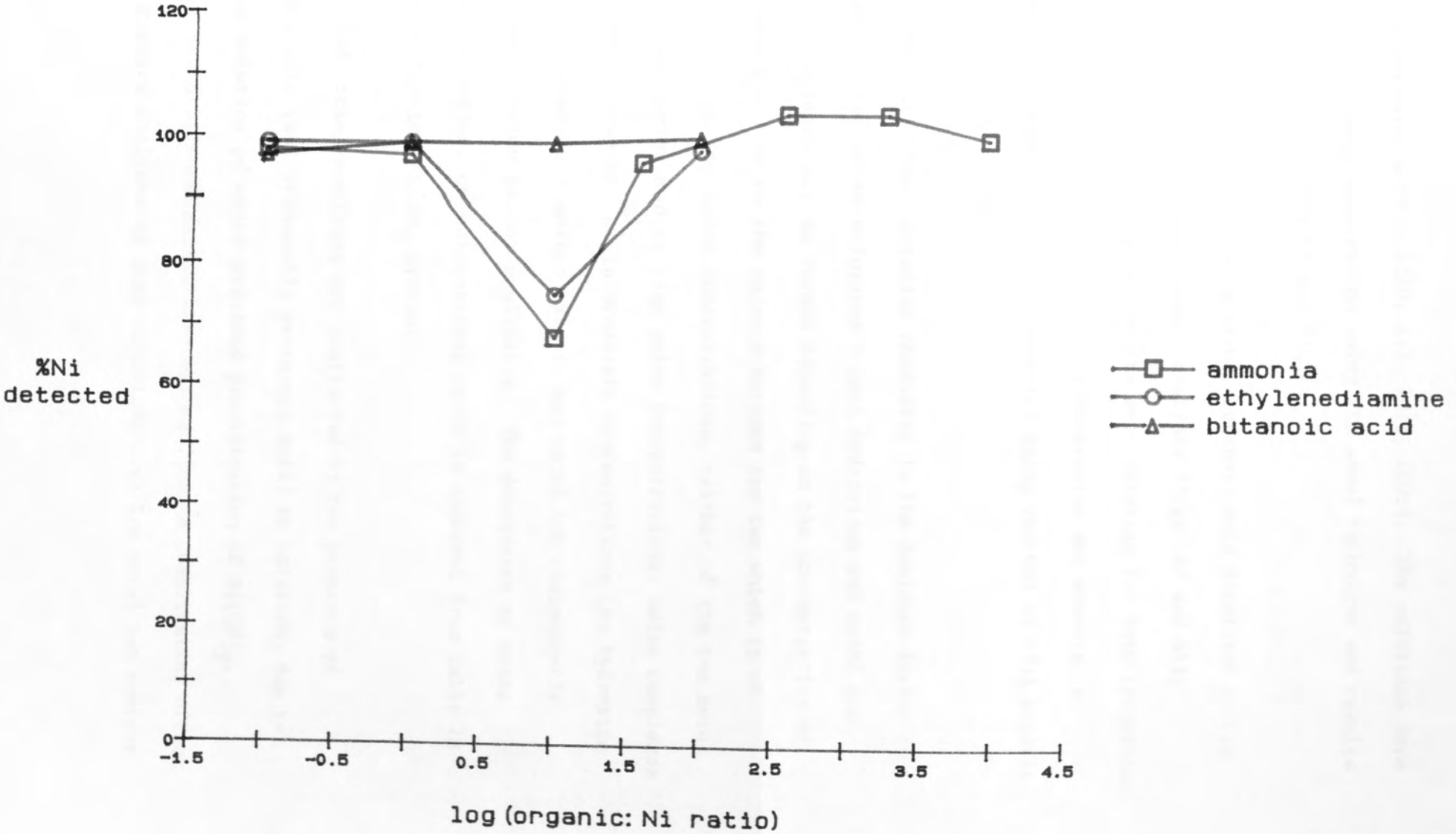

100:1 ; butanoic acid - 1:10, 1:1, 10:1, 100:1. The solutions were analysed by atomic absorption using the usual technique and results are displayed in table 77 and fig.44.

In the concentration range studied, butanoic acid displayed little effect on both nickel and cobalt analysis (figs. 43 and 44). However, anomalous analysis results were obtained for both transition metals when in the presence of ethylenediamine and ammonia, a minimum in actual % metal ion detected being reached at ≈ 5:1 organic: metal ion ratio.

It is postulated that solution chemistry is the dominant factor in analysis of the amine solutions - both hydroxides and metal ion-NH_3(en) complexes may be formed depending on the concentration of amine added and it is the balance between the two which is of importance. At low amine concentrations, neither of the two metal species are formed and at high amine concentrations, amine complexes are formed - however, at intermediate concentrations the hydroxide is precipitated to a marked extent, and metal ion consequently lost from solution is not analysable. The dependence of amine complex formation, on amine:nickel ratio is apparent from table 78 generated for the Ni/NH_3 system.

Cobalt and nickel analyses are unaffected by the presence of butanoic acid (and presumably pentanoic acid) in solution, due to the low solution pH which prevents precipitation of $Ni(OH)_2$. Ammonia and ethylenediamine, however, manifest a complicating effect which renders analyses of some solutions with low metal ion content

Table 77 - Influence of organic material on cobalt detection by atomic absorption.

Initial Co concentration (ppm)	organic added	organic:Co ratio	log organic:Co ratio	Co detected (ppm)	% Co detected
1.52	-	-	-	1.52	100
1.52	NH_3	1:10	-1	1.51	99
1.52	NH_3	1:1	0	1.46	96
1.52	NH_3	10:1	1	1.19	78
1.52	NH_3	40:1	1.6	1.20	79
1.52	NH_3	100:1	2	1.28	84
1.52	NH_3	400:1	2.6	1.40	92
1.52	NH_3	2000:1	3.3	1.43	94
1.52	NH_3	10000:1	4	1.46	96
1.52	-	-	-	1.51	99
1.52	en	1:10	-1	1.49	98
1.52	en	1:1	0	1.34	88
1.52	en	10:1	1	1.47	97
1.52	en	100:1	2	1.41	93
1.52	-	-	-	1.52	100
1.52	BA	1:10	-1	1.49	98
1.52	BA	1:1	0	1.47	97
1.52	BA	10:1	1	1.51	99
1.52	BA	100:1	2	1.51	99

Table 78 - Proportion of amine complexes formed in the Ni/NH_3 system at a number of different NH_3:Ni ratios.

NH_3:Ni ratio \ complex formed *	x = 1 /M	x = 2 /M	x = 3 /M	x = 4 /M	x = 5 /M	x = 6 /M
1:1	1.81×10^{-7}	5.33×10^{-10}	4.81×10^{-13}	1.25×10^{-16}	1.18×10^{-20}	2.12×10^{-25}
10:1	1.77×10^{-6}	5.28×10^{-8}	4.79×10^{-10}	1.25×10^{-12}	1.18×10^{-15}	2.12×10^{-19}
100:1	1.29×10^{-5}	4.86×10^{-6}	4.68×10^{-7}	1.24×10^{-8}	2.07×10^{-11}	3.46×10^{-11}

* complex formed in each case is: $[Ni(H_2O)_{6-x}(NH_3)_x]^{2+}$

Ni concentration in each case is 1.0ppm

Stability constant values, K_x, where $K_x = \dfrac{[Ni(H_2O)_{6-x}(NH_3)_x]^{2+}}{[Ni(H_2O)_{7-x}(NH_3)_{x-1}]^{2+}.[NH_3]}$

are: $K_1 = 631$, $K_2 = 174$, $K_3 = 53.7$, $K_4 = 15.5$, $K_5 = 5.60$, $K_6 = 1.07$

Fig.44 - Atomic absorption analysis of cobalt in the presence of organic compounds.

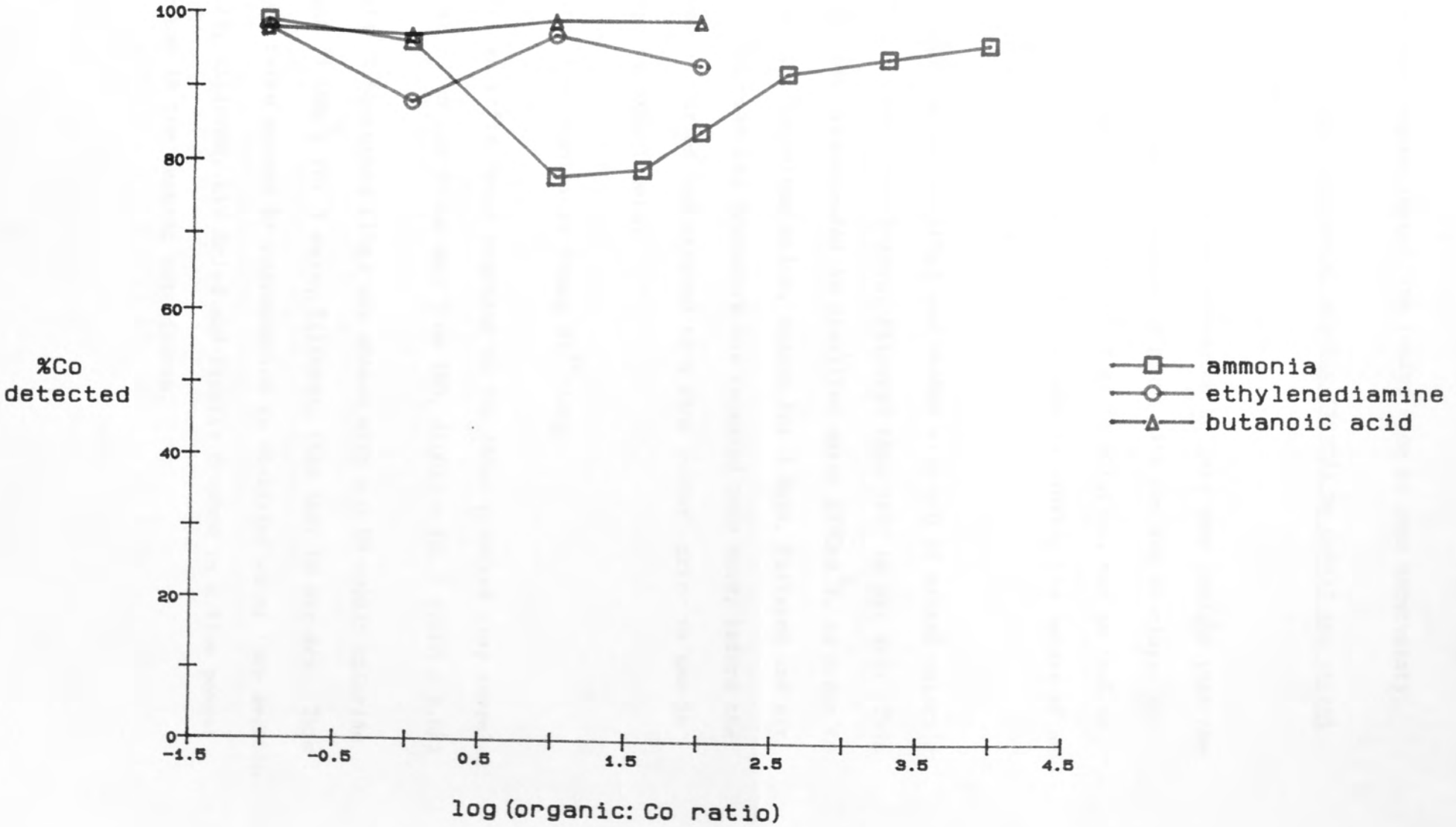

and certain organic:metal ion ratios open to some uncertainty.

4.2.2 Qualitative effect of model organic ligands on cobalt and nickel saturated hectorite

This initial investigation attempted to gain some insight into the interactions of model organic ligands with Co- and Ni-clays, to discover if complexation occurred as in solution, and to look at the application of physical techniques in probing the nature of any clay complexes generated.

4.2.2.1 A sample of hectorite (15g) was shaken with a 0.1M nickel chloride solution ($150cm^3$) for 3 days, filtered then left to air dry. This clay was then resuspended in distilled water ($150cm^3$), in order to wash out any entrained salts, shaken for 3 days, filtered and air dried. This washing procedure was repeated once more, before the clay was air dried and crushed to a fine powder, prior to use in the ensuing experiments.

The final clay contained 46meq Ni^{2+}/100g

The diffuse reflectance spectrum of the final prepared clay revealed peaks at 395nm and 660nm and from XRD, d(001) = 15.1Å (FWHM = 2.6Å)

4.2.2.2 A sample of hectorite (15g) was shaken with a 0.1M cobalt chloride solution ($150cm^3$) for 3 days, filtered, then left to air dry. This clay was twice washed by resuspension in distilled water (see section 4.2.2.1), filtered, air dried and finally crushed to a fine powder before use in the ensuing experiments.

The cobalt treated clay contained 50meq Co^{2+}/100g.

The diffuse reflectance spectrum of the clay revealed peaks at 459nm and 512nm and from XRD, d(001) = 15.3Å (FWHM = 3.0Å).

4.2.2.3 Ni-hectorite clay (2g/0.5mmol Ni^{2+})(see section 4.2.2.1) was added to a 0.03M NH_3 solution ($50cm^3$/1.5mmol-NH_3:Ni ratio of 3:1) and the mixture was stirred for 4 hours. The solid was filtered off, air dried at room temperature and the c-spacing obtained from XRD (table 79) along with the diffuse reflectance spectrum (table 80).

No colour change was observed during the reaction, the suspension retaining its green colour. After filtration and drying, the solid was green and the filtrate colourless.

4.2.2.4 Ni-hectorite samples (2g/0.5mmol) were added to separate solutions ($50cm^3$) of 0.1M NH_3 (5mmol), 0.25M NH_3 (12.5mmol), 0.09M ethylene-diamine (4.5mmol), 0.03M dimethylglyoxime (1.5mmol) (in ethanol) and 0.025M 2,2'-bipyridyl (1.25mmol) and treated as in the previous experiment (section 4.2.2.3).

The appropriate colours, d(001) values and visible absorption maxima of the treated clays are shown in tables 79 and 80.

4.2.2.5 Co-hectorite (3g/0.75mmol) was added to a 0.03M NH_3 solution ($50cm^3$/1.5mmol-NH_3:Co ratio of 2:1) and this mixture stirred for 4 hours, with NH_3-saturated air bubbling through the suspension. The solid was filtered off and air dried at room temperature.

Table 79 - d(001) values obtained from Ni-hectorite treated with model organic ligands.

organic ligand added	organic:Ni ratio	colour of solid product	d(001)/Å	*FWHM/Å
NH_3	3:1	green	14.0	5.7
NH_3	10:1	**green	12.8	3.6
NH_3	25:1	**green	12.8	3.2
en	9:1	violet-pink	14.7	3.6
DMG	6:1	orange	14.3	2.8
bipy	5:1	red-brown	18.2	3.0

* Full Width of peak at Half Maximum peak height.

** The blue colour exhibited by both samples initially was lost on air drying.

Table 80 - Peaks derived from diffuse reflectance spectra of Ni-hectorite treated with model organic ligands.

organic ligand added	organic:Ni ratio	Absorption peaks/nm			
NH_3	3:1	391(m-s)			669(w)
NH_3	10:1	392(m-s)			684(w)
NH_3	25:1	392(m-s)			686(w)
en	9:1	356(s)	456(w)	542(m-w)	
DMG	6:1	369(m-w)	422(m-w)	534(m-w)	
bipy	5:1	367(m-s)	422(w)	536(m-s)	

Peak intensities: s - strong, m - medium, w - weak, v - very

The dispersion initially turned red-brown after 3-4 minutes, the colour darkening after a further 20 minutes, this colour being retained until completion of the experiment. Upon filtration, the filtrate was colourless. The solid, after air drying, was a red-brown colour. Absorption peaks observed in the diffuse reflectance spectrum of the solid are shown in table 82. The basal spacing gained from XRD is shown in table 81. No ESR signal could be obtained from the solid.

4.2.2.6 Portions of Co-hectorite were added to separate solutions ($50cm^3$) of 0.1M NH_3 (5mmol), 0.25M NH_3 (12.5mmol), 0.009M ethylenediamine (0.45mmol) and 0.08M ethylenediamine (4mmol) and treated as in the previous section (4.2.2.5), except that the ethylenediamine/clay suspensions were treated with a bubbling stream of air free from NH_3.

XRD and diffuse reflectance data of the air dry clays are given in tables 81 and 82, along with their respective colours. Additionally, neither of the 10:1 or 25:1 NH_3 treated samples exhibited a distinguishable ESR signal.

4.2.3 <u>The influence of typical organic groundwater constituents on sorption properties of nickel and cobalt hectorite</u>

Having gained some background into the consequences of adding model organic ligands to Co- and Ni-hectorite, further investigations were performed using organic compounds commonly known to be present in natural groundwaters. As well as continuing the physical

Table 81 - d(001) values from Co-hectorite treated with model organic ligands.

wt. Co-hectorite used/g	organic ligand added	organic:Co ratio	colour of solid product	d(001)/Å	FWHM/Å
3.00	NH_3	2:1	red-brown	13.1	3.2
2.00	NH_3	10:1	yellow-brown	12.7	3.2
2.00	NH_3	25:1	red-brown	13.5	3.0
1.75	en	1:1	yellow-brown	14.9	4.0
1.75	en	9:1	light-brown	15.2	3.3

Table 82 - Peaks derived from diffuse reflectance spectra of Co-hectorite treated with model organic ligands.

organic ligand added	organic:Co ratio	Absorption peaks/nm		
NH_3	2:1	385(m-w)	531(w)	
NH_3	10:1	384(m-w)	527(m-w)	
NH_3	25:1	399(m-w)	454(vw)	
en	1:1	348(w)	465(w)518(m)	570(w)
en	9:1	349(s)	466(s)	573(w)

characterisation of species generated on the clay surface, a more quantitative approach was developed.

4.2.3.1 A sample of hectorite (15g) was shaken with 0.1M nickel chloride solution ($150cm^3$) for 3 days, filtered, then redispersed in a 1M solution of nickel chloride ($150cm^3$) and shaken for 3 days before filtration. To remove excess salt, the clay was rinsed with distilled water twice - a portion of this clay (5g) was retained for use in subsequent experiments (i.e. Ni-hectorite/rinse). Following this, the clay (10g) was redispersed in distilled water ($100cm^3$), shaken for 2 hours, then separated by ultracentrifugation. The clay was once again redispersed and the above procedure repeated 4 more times before the clay was filtered and left to air dry (i.e. Ni-hectorite/wash).

Metal ion content of the prepared clays was deduced from atomic absorption analysis of the relevant contacting solutions;

Ni-hectorite/rinse - 64meq Ni^{2+}/100g clay
Ni-hectorite/wash - 56meq Ni^{2+}/100g clay

Diffuse reflectance data from these light green nickel treated clays is summarised in table 83 and d(001) values in table 84.

4.2.3.2 A sample of hectorite (15g) was shaken with 0.1M cobalt chloride ($150cm^3$) for 3 days, filtered, then treated with a 1M cobalt chloride solution ($150cm^3$) and shaken for 3 days before filtration. To remove excess salt, the clay was rinsed with distilled water twice - a portion of this clay (5g) was retained for succeeding experiments

Table 83 - Diffuse reflectance data from Ni- and Co-hectorite, rinse and wash.

clay	Absorption peaks/nm			
Ni-hectorite/rinse	395(m-w)			668(vw)
Ni-hectorite/wash	395(m-w)			669(vw)
Co-hectorite/rinse		458(w)	518(m)	
Co-hectorite/wash		462(w)	518(m)	

peak intensities: m - medium, w - weak, v - very

Table 84 - d(001) values for Ni- and Co-hectorite, rinse and wash.

clay	d(001)/Å	FWHM/Å
Ni-hectorite/rinse	15.0	2.7
Ni-hectorite/wash	15.1	2.5
Co-hectorite/rinse	15.1	3.3
Co-hectorite/wash	15.3	2.7

(i.e.) Co-hectorite/rinse). Following this, the clay (10g) was washed a further 5 times with distilled water, being separated by ultracentrifugation between each wash, and finally filtered and left to air dry (i.e. Co-hectorite/wash).

Analysis of the relevant solutions gave the following cobalt ion content of the clays:

Co-hectorite/rinse - 69meq Co^{2+}/100g clay
Co-hectorite/wash - 64meq Co^{2+}/100g clay

Basal spacing and diffuse reflectance data for the light pink coloured cobalt clays are displayed in tables 83 and 84.

4.2.3.3 Portions (0.2g) of Ni-hectorite/rinse (0.064mmol Ni^{2+}) and Ni-hectorite/wash (0.056mmol Ni^{2+}) were covered separately with solutions (10cm^3) of ammonia (0.08M, 0.80mmol), ethylenediamine (0.08M, 0.80mmol), butanoic acid (0.08M, 0.80mmol), pentanoic acid (0.08M, 0.80mmol) and with distilled water, and stirred for 3 days. The suspensions were subsequently separated by ultracentrifugation, the solid air dried at room temperature and the supernatent solution retained (for Ni-hectorite/rinse, organic:Ni ratio is 12.5:1; for Ni-hectorite/wash, organic:Ni ratio is 14.3:1).

The ammonia and ethylenediamine treated suspensions all showed rapid colour changes, whereas the organic acids and distilled water prompted no apparent colour change. The dry solid in each case was subjected to diffuse reflectance, XRD and infrared investigation (table 85). The visible spectrum of the final solution was observed, along with the pH, and the quantity of nickel released into solution from the clay determined by atomic absorption (table 86).

Table 85 - Physical characteristics of Ni-hectorite clay samples after treatment with solutions of organic 'ligands'.

clay	organic added	colour of solid product	d(001)/Å	FWHM/Å	peaks resolved from diffuse reflectance spectrum/nm
Ni-hectorite/rinse	NH_3	light green	12.5	3.1	394(m-w) 678(vw)
Ni-hectorite/rinse	en	light mauve	14.9	2.5	342(m) 465(m-w) 555(vw)
Ni-hectorite/rinse	BA	v.light green	16.3	3.6	394(w)
Ni-hectorite/rinse	PA	v.light green	15.8	3.2	391(w)
Ni-hectorite/rinse	blank-dw	light green	15.2	3.3	392(m-w) 665(vw)
Ni-hectorite/wash	NH_3	light green	12.8	3.6	395(m-w) 676(v-w)
Ni-hectorite/wash	en	light mauve	14.9	2.2	345(m) 460(m-w) 556(vw)
Ni-hectorite/wash	BA	v.light green	16.2	3.1	394(w)
Ni-hectorite/wash	PA	v.light green	15.6	3.3	395(w)
Ni-hectorite/wash	blank-dw	light green	15.0	2.8	396(m-w) 666(vw)

Abbreviations: NH_3 - ammonia, en - ethylenediamine, BA - butanoic acid, PA - pentanoic acid
dw - distilled water

Table 86 - Physical characteristics of equilibrium solutions remaining from treatment of Ni-hectorite clays with organic 'ligands'.

clay	organic added	Initial solution pH	Final solution pH	Ni released from clay (meq/100g)	% Ni released	peaks resolved from visible spectrum/nm
Ni-hectorite/rinse	NH_3	10.36	10.23	0.048	0.08	ND
Ni-hectorite/rinse	en	10.82	10.78	0.19	0.30	ND
Ni-hectorite/rinse	BA	3.30	4.48	55	85	392(m)
Ni-hectorite/rinse	PA	3.31	4.46	52	82	392(m)
Ni-hectorite/rinse	blank-dw	5.51	6.89	1.16	1.8	ND
Ni-hectorite/wash	NH_3	10.36	10.22	0.049	0.09	ND
Ni-hectorite/wash	en	10.82	10.62	0.21	0.37	ND
Ni-hectorite/wash	BA	3.30	4.37	48	85	392(m)
Ni-hectorite/wash	PA	3.31	4.40	50	89	392(m)
Ni-hectorite/wash	blank-dw	5.51	6.58	0.82	1.4	ND

ND - No peaks detectable

4.2.3.4 Portions (0.2g) of Co-hectorite/rinse (0.069mmol Co^{2+}) and Co-hectorite/wash (0.064mmol Co^{2+}) were covered separately with solutions ($10cm^3$) of ammonia (0.08M, 0.80mmol), ethylenediamine (0.08M, 0.80mmol), butanoic acid (0.08M, 0.80mmol), pentanoic acid (0.08M, 0.80mmol) and with distilled water and stirred for 3 days. Separation of the suspensions by ultracentrifugation was subsequently performed, the solid air dried and the aqueous phase retained for further analysis (for Co-hectorite/rinse, organic:Co ratio is 11.6:1; for Co-hectorite/wash, organic:Co ratio is 12.5:1).

Rapid colour changes of the initial suspension were only observed upon addition of ammonia and ethylenediamine solutions to the clays. The solid product was investigated using diffuse reflectance, XRD and infrared techniques (table 87). Physical characterisation of the supernatent involved determination of the visible spectrum, pH, and cobalt concentration (table 88).

4.2.3.5 Portions (0.2g) of Ni-hectorite/rinse (0.064mmol Ni^{2+}) and Ni-hectorite/wash (0.056mmol Ni^{2+}) were stirred with pure diethyl phthalate (DEP) ($10cm^3$, 50.4mmol) for 3 days, then separated by ultracentrifugation. The solid was dried at room temperature in air and the supernatent retained for further analysis (for Ni-hectorite/rinse, DEP:Ni ratio is 800:1; for Ni-hectorite/wash, DEP:Ni ratio is 900:1).

The solid products from above were coloured light green.

Diffuse reflectance revealed peaks at 284, 395, 664nm and 280, 394, 667nm for the Ni-hectorite/rinse and Ni-hectorite/wash samples, respectively. The treated Ni-hectorite/rinse clay exhibited a d(001) value of 19.5Å (FWHM = 3.6Å), the Ni-hectorite/wash clay a value of 19.4Å (FWHM = 3.4Å). Difficulties encountered with the

Table 87 - Physical characteristics of Co-hectorite clay samples after treatment with solutions of organic 'ligands'.

clay	organic added	colour of solid product	d(001)/Å	FWHM/Å	peaks resolved from diffuse reflectance spectrum/nm			
Co-hectorite/rinse	NH_3	beige	13.1	4.0	381(m-w)	454(vw)	525(w)	593(vw)
Co-hectorite/rinse	en	red-brown	15.4	3.7	342(m)	466(w)	562(vw)	
Co-hectorite/rinse	BA	v.light pink	16.4	4.1			522(w)	
Co-hectorite/rinse	PA	v.light pink	16.2	3.5		470(vw)	522(w)	
Co-hectorite/rinse	blank-dw	light pink	15.0	3.5		465(w)	521(m)	
Co-hectorite/wash	NH_3	beige	13.0	3.6	386(m-w)	456(vw)	528(w)	585(vw)
Co-hectorite/wash	en	red-brown	15.1	3.5	341(m-s)	464(w)	558(vw)	
Co-hectorite/wash	BA	v.light pink	16.4	3.6		454(vw)	524(m-w)	
Co-hectorite/wash	PA	v.light pink	16.0	3.3		462(vw)	519(m)	
Co-hectorite/wash	blank-dw	light pink	15.1	3.0		459(w)	517(m)	

Abbreviations: NH_3 - ammonia, en - ethylenediamine, BA - butanoic acid, PA - pentanoic acid, dw - distilled water

Table 88 - Physical data from equilibrium solutions remaining after treatment of Co-hectorite clays with organic 'ligands'.

clay	organic added	Initial solution pH	Final solution pH	Co released from clay (meq/100g)	% Co released	peaks resolved from visible spectrum/nm
Co-hectorite/rinse	NH_3	10.36	10.27	0.058	0.08	ND
Co-hectorite/rinse	en	10.82	10.71	2.0	2.9	ND
Co-hectorite/rinse	BA	3.30	4.29	50	71	512(m)
Co-hectorite/rinse	PA	3.31	4.32	49	72	512(m)
Co-hectorite/rinse	blank-dw	5.51	7.17	2.0	2.9	ND
Co-hectorite/wash	NH_3	10.36	10.02	0.048	0.08	ND
Co-hectorite/wash	en	10.82	10.71	2.1	3.3	ND
Co-hectorite/wash	BA	3.30	4.17	49	76	512(m)
Co-hectorite/wash	PA	3.31	3.84	49	77	512(m-w)
Co-hectorite/wash	blank-dw	5.51	6.76	1.10	1.7	ND

ND - No peaks detected in spectrum

aspiration of diethyl phthalate into the flame in atomic absorption led to the use of a simple colourimetric method for the determination of nickel. This involved the addition of $5cm^3$ of a 1% DMG solution, in ethanol, to the sample ($5cm^3$) and observation of the resultant colour of the solution. The non-appearance of the characteristic scarlet red $Ni(DMG)_2$ colouration indicates (from simple sensitivity tests on the method) that $<$1meq/100g Ni^{2+} was released from both clays by the diethyl phthalate (and probably considerably less than this).

4.2.3.6 Portions (0.2g) of Ni-hectorite/wash (0.056mmol Ni^{2+}) were added separately to solutions ($10cm^3$) of ammonia (17mM, 1.2mM, 0.12mM giving NH_3:Ni ratios of 3:1, 1:5 and 1:50) and butanoic acid (8.0mM, 0.8mM, 0.08mM giving acid:Ni ratios of 14:1, 1:7, 1:70) and treated as in section 4.2.3.3. Co-hectorite/wash samples (0.2g/0.064mmol Co^{2+}) were treated similarly upon addition to solutions ($10cm^3$) of ethylenediamine (8.0mM, 0.8mM, 0.08mM giving en:Co ratios of 1.25:1, 1:8 and 1:80) and butanoic acid (8.0mM, 0.8mM, 0.08mM giving acid:Co ratios of 1.25:1, 1:8 and 1:80).

Visible absorbance and pH data for the supernatent solutions are shown in tables 89 and 91 along with the concentration of transition metal ion released from the clay. The resultant solids were subjected to diffuse reflectance, XRD and infrared investigation (tables 90 and 92).

4.2.3.7 A sample of hectorite (2.4g) was shaken with a bimetallic solution ($50cm^3$) composed of 0.0073M nickel chloride and 0.0073M cobalt chloride and shaken for 3 days, before ultracentrifugation. The clay was then washed 5 times by redispersion in distilled water

Table 89 - Physical data from equilibrium solutions remaining after treatment of Ni-hectorite clays with organic 'ligand' solutions at various concentrations.

Clay - Ni-hectorite/wash

organic added	organic:Ni ratio	Initial solution pH	Final solution pH	Ni released from clay (meq/100g)	% Ni released	peaks resolved from visible spectrum/nm
NH_3	3:1	9.98	9.44	0.014	0.02	ND
NH_3	1:5	9.20	7.08	0.18	0.32	ND
NH_3	1:50	6.68	6.75	0.43	0.76	ND
BA	1.4:1	3.66	4.68	14	25	394(m)
BA	1:7	4.02	6.56	3.8	6.6	393(vw)
BA	1:70	4.70	6.78	1.36	2.4	ND

Table 90 - Physical characteristics of Ni-hectorite clay samples after treatment with ammonia solutions at various concentrations.

Clay - Ni-hectorite/wash

organic added	organic:Ni ratio	colour of solid product	d(001)/Å	FWHM/Å	peaks resolved from diffuse reflectance spectrum/nm	
NH_3	3:1	light green	13.8	5.6	392(m)	666(vw)
NH_3	1:5	light green	16.0	3.3	393(m)	664(vw)
NH_3	1:50	light green	15.8	3.1	392(m)	

Table 91 - Physical data from equilibrium solutions remaining after treatment of Co-hectorite clays with organic 'ligand' solutions at various concentrations.
Clay - Co-hectorite/wash

organic added	organic:Co ratio	Initial solution pH	Final solution pH	Co released from clay (meq/100g)	% Co released	peaks resolved from visible spectrum/nm	
en	1.25:1	10.47	7.23	0.36	0.56	ND	
en	1:8	9.91	7.15	1.15	1.8	ND	
en	1:80	9.17	7.07	0.93	1.5	ND	
BA	1.25:1	3.51	4.81	18	28	466(w)	513(m)
BA	1:8	3.98	6.38	3.7	5.8	462(vw)	511(w)
BA	1:80	4.52	7.04	1.09	1.7	ND	

Table 92 - Physical characteristics of Co-hectorite clay samples after treatment with organic 'ligand' solutions at various concentrations.
Clay - Co-hectorite/wash

organic added	organic:Co ratio	colour of solid product	d(001)/Å	FWHM/Å	peaks resolved from diffuse reflectance spectrum/nm			
en	1.25:1	dark pink	15.1	4.0	348(m)	468(vw)	513(m-s)	557(vw)
en	1:8	light pink	15.1	3.3	347(vw)		511(m)	
en	1:80	light pink	15.0	3.4		462(w)	516(m)	
BA	1.25:1	v.light pink	15.4	3.1			520(m-w)	
BA	1:8	light pink	15.1	3.0		462(vw)	517(m)	
BA	1:80	light pink	15.0	3.3			519(m)	

($50cm^3$) with subsequent ultracentrifugation, and finally dried in air at room temperature.

The following metal ion content of the clay was derived from analysis of the supernatent solutions:

Ni^{2+} - 23meq/100g clay
Co^{2+} - 24meq/100g clay

The solid was characterised by peaks at 392 and 514nm in the diffuse reflectance spectrum and a d(001) value of 15.0Å (FWHM = 4.2Å). An infrared spectrum was also taken.

4.2.3.8 Portions (0.2g) of the above nickel/cobalt-hectorite (i.e. Ni/Co-hectorite) (0.023mmol Ni^{2+}, 0.024mmol Co^{2+}) were covered separately with solutions ($10cm^3$) of ammonia (0.08M, 0.8mmol) and butanoic acid (0.08M, 0.8mmol) and stirred for 3 days. Separation of the suspensions by ultracentrifugation was subsequently performed, the solid air dried and the aqueous phase retained for further analysis (in each case, organic:Ni ratio was 36:1 and organic:Co ratio was 34:1).

A rapid colour change was apparent only on addition of the ammonia solution. The dry solid was characterised using diffuse reflectance, XRD and infrared techniques (table 93). The visible spectrum and pH of the reaction solution were determined, and atomic absorption analysis gave nickel and cobalt concentrations (table 94).

Table 93 - Physical characteristics of Ni/Co-hectorite clay samples after treatment with organic 'ligand' solutions at various concentrations. Clay - Ni/Co-hectorite

organic added	colour of solid product	d(001)/Å	FWHM/Å	peaks resolved from diffuse reflectance spectrum/nm	
NH_3	off white	14.7	6.0	390(w)	528(w)
BA	white	15.9	3.4	395(w)	526(w)

Table 94 - Physical data from equilibrium solutions remaining after treatment of Ni/Co-hectorite samples with organic 'ligand' solutions. Clay - Ni/Co-hectorite

organic added	Initial solution pH	Final solution pH	Ni released from clay (meq/100g)	Co released from clay (meq/100g)	% Ni released	% Co released	peaks resolved from visible spectrum/nm
NH_3	10.36	10.24	0.022	0.019	0.10	0.08	ND
BA	3.30	3.93	7.2	6.3	32	27	389(vw) 511(vw)

4.2.4 The desorption of tris(ethylenediamine)nickel(II) from exchange sites on hectorite by inorganic cations

As an extension of the work on the influence of organic material in groundwaters on sorption, it was deemed necessary to investigate the stability of transition metal complexes once formed on the clay. A quantitative look at the affinity of sodium and calcium ions for the surface of a $[Ni(en)_3]^{2+}$-saturated hectorite was followed by some observations on the copper treated system.

4.2.4.1 Ni-hectorite/wash (2.2g, 0.62mmol Ni^{2+}) was added to a 0.084M ethylenediamine solution (110cm^3, 9.2mmol) and stirred for 24 hours. The resulting suspension was filtered, then washed with 3 x 25cm^3 of distilled water, and these washings were retained for nickel analysis. The air dry solid was a pale violet colour, had a d(001) value of 14.9Å (FWHM = 2.1Å) and characteristic peaks at 550, 465, 342nm in the diffuse reflectance spectrum.

The final Ni^{2+}content of the clay (i.e $[Ni(en)_3]^{2+}$-hectorite) was 56meq/100g.

4.2.4.2 Portions (0.2g) of $[Ni(en)_3]^{2+}$-hectorite (0.056mmol Ni^{2+}) were added separately to solutions (10cm^3) of sodium chloride (30mM, 6.0mM, 1.2mM giving Na:Ni ratios of 5:1, 1:1 and 1:5) and calcium chloride (30mM, 6.0mM, 1.2mM giving Ca:Ni ratios of 5:1, 1:1 and 1:5), and distilled water, and stirred for 3 days. After ultracentrifugation the supernatent solution was analysed for nickel content and pH (table 95).

Table 95 - Nickel (copper) content and pH values of equilibrium solutions remaining after contacting $[Ni(en)_3]^{2+}$-hectorite with a number of inorganic salt solutions.

Cation added	M^{n+}:Ni ratio	Ni in final solution(mmol/L)	% Ni desorbed	Initial solution pH	Final solution pH
Na	5:1	0.052	0.94	5.76	8.92
Na	1:1	0.0121	0.22	5.69	8.75
Na	1:5	0.0058	0.10	5.65	8.84
Ca	5:1	0.37	6.7	5.72	8.88
Ca	1:1	0.18	3.2	5.65	8.85
Ca	1:5	0.047	0.85	5.57	8.58
dw	-	0.0039	0.07	5.51	8.92
*Cu	1:1	3.7	66	4.95	7.07

*Cu in final solution = 0.72mmol/L

% Cu sorbed = 88

dw - distilled water

4.2.4.3 $[Ni(en)_3]^{2+}$-hectorite (0.2g, 0.056mmol) was added to a 0.006M copper(II) chloride solution (10cm^3, Cu:Ni ratio of 1:1), stirred for 3 days, then ultracentrifuged (40 000rpm for 40 minutes). The mauve-pink air dry solid exhibited peaks at 558, 465, 374nm in the diffuse reflectance spectrum and a d(001) value of 13.0Å (FWHM = 1.5Å). The visible spectrum of the supernatent solution exhibited absorption maxima at 374nm and 558nm. The final solution pH, nickel and copper concentrations are shown in table 95.

4.3 MICROSCOPIC EFFECTS

Since expected concentrations of any radionuclides escaping from a radioactive waste disposal site will be very low, it was essential to get some feel for the effects organic groundwater constituents may have on sorption at these metal ion levels (i.e. microscopic level).

This work involved spiking a hectorite sample with a low concentration of ^{60}Co, subsequent treatment of this clay with various solutions of organic compounds and analysis of the equilibrium solution for cobalt content. The similarity of this experimental design to that used in the macroscopic studies should enable recognition of any patterns in sorption behaviour.

4.3.1 Preparation of ^{60}Co doped hectorite

4.3.1.1 Na-hectorite (2.92g) was added to a 1.87ppm solution of cobalt chloride (^{60}Co labelled) (265.2cm^3, 0.0084mmol Co^{2+}) and shaken for 3 days. The suspension was then filtered and redispersed twice in

distilled water, before ultracentrifugation. The clay was air dried for 3 days, then ground to a fine powder using an agate pestle and mortar, prior to use in subsequent experiments.

Υ-spectrometric analysis of the relevant solutions determined the cobalt content of the clay (i.e. ^{60}Co-hectorite) to be 0.35meq/100g.

4.3.2 Influence of solutions of organic compounds on the stability of ^{60}Co-hectorite

4.3.2.1 Portions (0.204g) of the ^{60}Co-hectorite clay (0.35μmol Co^{2+}) were added separately to solutions (10.2cm^3) of ammonia (0.44mM, 0.11mM, 0.008mM giving NH_3:Co ratios of 12.5:1, 3:1 and 1:5) and butanoic acid (0.44mM, 0.044mM, 0.0044mM; BA:Co ratios of 12.5:1, 1.25:1 and 1:8) and demineralised water, shaken for 8 days, then ultracentrifuged and the final solution analysed for cobalt content by Υ-spectrometry (table 96).

Centrifugation did not appear to separate all the solid material from the sample treated with 0.44mM NH_3. This was, therefore, filtered through a 0.22μ filter, all surfaces being subsequently washed with aqueous cobalt chloride to remove adhered ^{60}Co, and the resultant clear solution, analysed.

4.4 Redox properties of tris(2,2'-bipyridyl)cobalt(III) exchanged hectorite

The generation of transition metal complexes on the surface of hectorite has been demonstrated previously (section 4.2.2), and it

Table 96 - Cobalt released from a ^{60}Co-hectorite by solutions of organic compounds.

organic added	organic:Co ratio	Co in final solution (µmol/L)	% Co released
NH_3	12.5:1	0.28	0.80
*NH_3	12.5:1	0.025	0.07
NH_3	3:1	0.14	0.40
NH_3	1:5	0.82	2.4
BA	12.5:1	7.0	20
BA	1.25:1	3.3	9.4
BA	1:8	0.068	<0.18
dw	-	1.5	4.3

BA - butanoic acid

dw - demineralised water

*After re-analysis(see 4.3.2.1)

was felt that the redox properties of certain exchanged clays may facilitate a number of catalytic processes. Several years ago[129] it was shown that $[Co(bipy)_3]^+$ (bipy = 2,2'-bipyridyl) would catalyse the borohydride reduction of nitrobenzene to aniline. It was thus apparent that it should be possible to use a $[Co(bipy)_3]^{3+}$ exchanged clay to effect catalytic organic redox reactions. It seemed sensible to evaluate the idea by consideration of the nitrobenzene to aniline reduction.

4.4.1 Preparation of $[Co(bipy)_3]^{3+}$-hectorite

A sample of Na-hectorite (12g) was added to a 0.1M cobalt chloride solution ($100cm^3$), shaken for three days, filtered and air dried. The clay thus treated contained 51meq $Co^{2+}/100g$. The cobalt exchanged clay was then treated with 2,2'-bipyridyl (2.0g) in ethanol ($100cm^3$), in air, over 4 hours after which it was filtered, washed with $4 \times 20cm^3$ aliquots of ethanol and air dried.

The resultant yellow coloured clay exhibited a d(001) spacing of 18.8Å, a value consistent with the intercalation of a large complex cation. The diffuse reflectance spectrum showed peaks at 451nm and 317nm (c.f. literature data for $[Co(bipy)_3](ClO_4)_3$:448, 317nm[130]) confirming the air oxidation of Co(II) to Co(III) in the presence of the ligand.

4.4.2 Generation of $[Co(bipy)_3]^+$-hectorite

Two methods were employed.

4.4.2.1 Electrochemical generation

$[Co(bipy)_3]^{3+}$-hectorite was ground to a fine powder and allowed to flocculate from acetonitrile suspension onto the surface of a platinum electrode ($1.87cm^2$) (approx. 11.4mg). The electrode was positioned horizontally in a conical flask together with a bright platinum electrode. An acetonitrile solution, 0.1M in tetrabutylammonium hexafluorophosphate, was introduced as supporting electrolyte. Passage of a current of 4mA for 2 mins. resulted in the appearance of the deep blue $[Co(bipy)_3]^{+}$ on the cathode. The colour faded (≃1 min) when the current was disconnected, but could be maintained for periods of over 1 hr on continued passage of current.

4.4.2.2 Chemical generation

$[Co(bipy)_3]^{3+}$-hectorite (1g, 0.025mmol) was stirred for 1 hr with $NaBH_4$ (0.037g, 1.0mmol) in distilled water ($10cm^3$) and finally filtered under dinitrogen. Diffuse reflectance showed bands at 623nm and 396nm. $[Co(bipy)_3](ClO_4)_3$ reduced either with Na/Hg or $NaBH_4$ gave bands at 610nm and 390nm according to an earlier report.[131]

4.4.3 Reduction of nitrobenzene

Two methods were used in the clay catalysed reduction process. Nitrobenzene was added to the $NaBH_4$ reduced clay (damp) with or without additional $NaBH_4$ solution. In each case aniline was formed (glc), the more effective reduction occuring in the presence of

$NaBH_4$. This technique was therefore adopted in the deduction of optimum conditions for the reduction process, where the effect of varying $NaBH_4$, nitrobenzene and clay concentrations were investigated (table 97).

Table 97 - Reaction parameters used in clay catalysed nitrobenzene reduction systems.

Sample	wt. clay used (g)	$NaBH_4$ added (mmol)	nitrobenzene added (mmol)	Compounds identified from glc	Unidentified glc peaks:retention time (mins)
*1	1g	-	32	$PhNH_2$(vvw), $PhNO_2$(vs)	
*2	-	1.6	-	$PhNH_2$(vvw), $PhNO_2$(vs)	3.6(vvw)
3	1g	1.6	32	$PhNH_2$(vvw), $PhNO_2$(vs)	3.7(vvw)
4	1g	1.0	8	$PhNH_2$(w), $PhNO_2$(vs)	3.8(vvw), 0.95(vvw)
5	1g	1.6	8	$PhNH_2$(m-w), $PhNO_2$(s)	3.8(vvw), 0.95(vvw)
6	1g	4.8	4	$PhNH_2$(s)	0.95(m)
7	1g	40	4	$PhNH_2$(vs)	

Key: s - strong, m - medium, w - weak, v - very, $PhNH_2$ - aniline, $PhNO_2$ - nitrobenzene

*Only in sample 1 was $NaBH_4$ not added immediately after nitrobenzene addition, but approximately 1 day later. Extraction of the supernatent before and after $NaBH_4$ addition, gave samples 1 and 2.

4.5 DISCUSSION

Previous workers have demonstrated the ability to generate transition metal complex exchanged clays simply by addition of the clay to a solution of the transition metal complex.[42,53,67] However, very little work has been performed on the synthesis of these transition metal complex-clays by addition of a solution of the organic ligand to the transition metal treated clay. The latter approach would appear to be of greater interest in the prediction of possible radionuclide migration mechanisms from a radioactive waste disposal site, since any radioactive metal ions released would most likely be sorbed onto the surrounding clay mineral formation before contact with organic material from the local groundwater.

An initial study into the effect of organic groundwater constituents on sorption involved probing the ability of model organic ligands to complex with nickel and cobalt ions on the respective transition metal saturated hectorite (section 4.2.2). Complexation of the metal did occur, although anomalies were also observed.

The Co- and Ni-hectorite clays prepared for reaction with organic ligand solutions (sections 4.2.2.1, 4.2.2.2) exhibited d(001) values typical of a clay saturated with divalent metal ion.[26] Diffuse reflectance spectra of the two clays showed bands at 395 and 660nm, and 459 and 512nm, respectively, characteristic of $[Ni(H_2O)_6]^{2+}$ and $[Co(H_2O)_6]^{2+}$ species.[132] The d^8 Ni^{2+} ion has a $^3A_{2g}$ ground state and application of the Ligand Field Theory indicates the bands at 395 and 660nm to be associated with the transitions $^3A_{2g} \rightarrow {}^3T_{1g}(P)$

and $^3A_{2g} \longrightarrow {}^3T_{1g}(F)$. The latter band is actually one half of a doublet formed due to spin-orbit coupling which mixes the $^3T_{1g}(F)$ and ^1Eg states which are very close in energy at the crystal field splitting given by $6H_2O$ (other band not observed here due to spectral range being<700nm).[132]

Interpretation of the $[Co(H_2O)_6]^{2+}$ spectrum is not so easy due to poor spectral resolution and closeness of the important quartet states $^4A_{2g}$ and $^4T_{1g}(P)$ in the Orgel diagram of the octahedral d^7 ion. It is most likely that the band at 512nm corresponds to the transition $^4T_{1g} \longrightarrow {}^4T_{1g}(P)$ with the shoulder at higher frequency being attributed to spin-orbit coupling effects or to transitions to doublet states.[132] The $^4T_{1g} \longrightarrow {}^4A_{2g}$ transition should give rise to a band at ≃560nm but as it is a two electron process it is very weak and not observed in the spectrum here.[132]

It seemed sensible to take the Full Width at Half Maximum (FWHM) derived from the d(001) values of the two clays as being standard, since their preparation should have generated a homogeneous clay product, and any substantial deviations from these FWHM values should be taken as indicating inhomogeneity in the complex(es) formed between the clay layers.

The addition of 2,2'-bipyridyl to Ni-hectorite revealed diffuse reflectance (table 80) and XRD (table 79) characteristics typical of the tris(2,2'-bipyridyl)nickel(II) complex.[77,133] The complex formed on addition of ethylenediamine (en) solutions to Co-hectorite depended on the en:Co ratio. A 1:1 ratio generated both $[Co(en)_3]^{3+}$

and $[Co(H_2O)_6]^{2+}$ on the clay as evidenced from the diffuse reflectance data (table 82) and the 14.9Å 001 reflection (table 81), the breadth of which was typically larger than that expected for a single homogeneous octahedral complex distributed between the clay layers. A nine-fold excess of the ligand produced only the $[Co(en)_3]^{3+}$ complex, as confirmed by the diffuse reflectance spectrum[134] and smaller FWHM than in the 1:1 treated sample (3.3Å c.f. 4.0Å). It must be noted that there was no evidence for the formation of $[Co(en)_3]^{2+}$ or $[Co(en)_2]^{2+}$ on the clay. Only one Ni-hectorite sample was contacted with ethylenediamine (9:1 ratio), this giving evidence for the presence of $[Ni(en)_2]^{2+}$ as well as $[Ni(en)_3]^{2+}$. Schoonheydt et al[127] also were able to generate $[Ni(en)_2]^{2+}$ on the surface of a montmorillonite clay - the band observed by them at 465nm agrees well with that observed here (table 80). Schoonheydt et al[128] were also able to prepare $[Co(en)_2]^{2+}$ on a hectorite clay, but that complex did not result from any of the treatments used here.

The dimethylglyoxime treated Ni-hectorite exhibited the characteristic visible spectrum of the expected planar bis(dimethylglyoximato) nickel(II) complex (table 80).[135] The d(001) value, however, was larger than the 12.5-13.0Å expected for a square planar complex. It is well documented[132] that crystals of $Ni(DMG)_2$ consist of planar $Ni(DMG)_2$ units stacked above one another, but with each one rotated at 90° to those units above and below. Since this arrangement is discouraged by the small space between clay layers, the $Ni(DMG)_2$ units may have orientated themselves perpendicular (as opposed to parallel) to the clay surface, thus allowing build up of the 'normal'

structure in the a and b directions.

Both Ni- and Co-hectorite exhibited anomalous behaviour when treated with ammonia solutions, but physical investigation enabled a number of conclusions to be drawn. The distinct colour changes observed in the Ni-hectorite/NH_3 systems gave a clear indication as to the processes occuring. Although all three dry clays were green, the 0.10M (10:1 ratio, NH_3:Ni) and 0.25M ammonia treated samples did exhibit a blue colour, characteristic of the $[Ni(NH_3)_6]^{2+}$ species, at some stage in the reaction. It is suggested that the NH_3 initially coordinated to nickel was lost from the clay surface during air drying, leaving a partially dehydrated product. This accounted for the d(001) value of 12.8Å. Although the diffuse reflectance data (table 80) showed similar peak positions to those of $[Ni(H_2O)_6]^{2+}$, this complex was discounted due to the ≈15.0Å d(001) value with which it is usually associated (see earlier). In a study of Ni-montmorillonite involving successive dehydration, bands at 403 and 694nm were attributed by Tarasevich et al[136] to a $[Ni(O_1)_3H_2O]^{2+}$ species (where O_1, is a lattice oxygen atom). Thus, visible absorption bands from the clay remaining after 0.10M and 0.25M NH_3 treatments, indicated a similar crystal field environment to the hexaaquo complex, but the c-spacing confirmed the suggestion of a partially dehydrated clay.

The Ni-hectorite sample treated with a three times excess of ammonia was, however, intermediate between the hydrated and dehydrated systems as evidenced by the 14.0Å c-spacing. The concentration of ammonia added was not enough (in this case) to replace all the

coordination sites around nickel in the parent clay so that when ammonia was lost on drying only a partial dehydration occurred. The large FWHM confirmed the presence of more than one complex between the clay interlayers. In a study of the sorption of non-ionic aliphatic molecules on montmorillonite, Hoffman et al[137] reported difficulty in isolating air dry complexes due to the concomitant evaporation of the organic substance and water. In a similar fashion, ammonia may be lost.

The anomalous effects observed in the Co-hectorite/NH_3 system were not caused by the same phenomenon as in the Ni-hectorite/NH_3 system. In a study of the successive dehydration of a Co-montmorillonite, the bands designated by Tarasevich et al[78] to partially dehydrated clay were at 455 and 554nm for the $[Co(H_2O)_3(O_1)_2]^{2+}$ species and 533, 579 and 635nm for the $[Co(O_1)_3(H_2O)]^{2+}$ species, which do not correspond to any of the bands from the cobalt-clays in table 82. The presence of the most likely 'simple' complex, $[Co(NH_3)_6]^{3+}$ was observed, from diffuse reflectance examination, in the 25:1 NH_3:Co treatment and very weakly in the 10:1 treatment (table 82). However, bands at approximately 390 and 530nm were observed throughout this series of experiments and are attributed to the formation of $[Co(NH_3)_5O_2(NH_3)_5Co]^{4+}$ peroxy species. Bridged polynuclear cobaltammines can be formed when molecular oxygen is passed through cobalt(II)-ammonia solutions, the structure containing a peroxo -O-O- bridge between cobalt atoms.[132] They are characteristically red or brown complexes which would account for the colours observed in this study. The d(001) values (table 81), all below 13.6Å, also

point to a low occupation (if any) of exchange sites by $[Co(NH_3)_6]^{3+}$ or $[Co(NH_3)_6]^{2+}$, and the fact that the Co-O-O-Co structure lies parallel to the clay layers and not perpendicular. In contrast to the 10:1 NH_3:Co treated clay, the slightly larger c-spacing of the 25:1 clay was due to the presence of more $[Co(NH_3)_6]^{3+}$, and that of the 3:1 treated clay, due to the presence of some $[Co(H_2O)_6]^{2+}$. The oxidation of peroxo (O_2^{2-}) to superoxo (O_2^-) cobalt species on the ammonia treated clay surfaces was discounted both from the lack of the characteristic green colour of the latter and from the absence of any ESR signal.

It appeared from this initial investigation that complex formation would occur when the ligand was added to the transition metal ion saturated clay. The complex formed was dependent on the added ligand: metal ion ratio, although some anomalous behaviour was observed in the presence of clay minerals. Diffuse reflectance and XRD proved very useful in the characterisation of species generated on the hectorite.

The preceding work on transition metal-clay/organic ligand interactions gave some qualitative information from which it was deemed useful to undertake further appraisal of the influence of organic compounds on cation sorption onto clay minerals. This inevitably involved a quantitative approach and the introduction of organic compounds commonly found in groundwaters (sections 4.2.3, 4.2.4, 4.3), both modifications enabling a convergence to the aim of the overall study, i.e. identification of parameters which may be important in

migration of radionuclides from a radioactive waste disposal site.

Addition of greater than a ten-fold excess of the organic compounds ammonia, ethylenediamine, butanoic acid and pentanoic acid to both Co- and Ni-hectorites (sections 4.2.3.3, 4.2.3.4) immediately enabled two categories of 'ligand' to be separated: (i) acids, (ii) amine compounds.

Although pH values were able to indicate the removal of both the amine (pH decrease) and the acid compounds (pH increase) from solution, they were essential in the verification of the atomic absorption solution analyses (see section 4.2.1). In all cases the pH of butanoic acid, pentanoic acid and distilled water treated samples was too low for nickel or cobalt hydroxide precipitation. Also, both ethylenediamine and ammonia treated samples exhibited reliable analyses, even though the hydroxide concentration was high enough to cause precipitation, due to the formation of complexes with transition metal ions released into solution (see section 4.2.1).

Greater than 70% metal ion was released from the Co- and Ni-hectorite clays when treated with excess butanoic and pentanoic acids. This may be compared with less than 4% metal ion released by both ammonia and ethylenediamine solutions at the same concentration, indicating a vast difference in mechanism of interaction of the two classes of compound (tables 85 to 88).

The visible spectra of the equilibrium solutions remaining from treatments with the class(i) compounds provided evidence for the presence of the respective hexaaquo transition metal ion, whereas

class(ii) compounds gave no detectable solution spectrum. The transition metal ions were also still present as hexaaquo complexes on the acid treated clays (diffuse reflectance - tables 85 and 87), but concentrations had been considerably reduced.

The evidence collected pointed to the occurrence of a displacement reaction on addition of the organic acids to the Ni- and Co-clays. The acid dissociation constant (K_a) for both butanoic and pentanoic acid is approximately 10^{-5}mol/L and so the process;

$$RCOOH \rightleftharpoons RCOO^- + H^+$$

lies almost completely to the left. However, since the H^+ ion is strongly sorbed by clay minerals,[138] acid dissociation may be encouraged to replace the H^+ exchanged onto the clay from solution. This process may continue until a large proportion of the clay is saturated by H^+ ions, and hence the effectiveness of the organic acids in promoting transition metal desorption from hectorite.

An important feature to note also was the consistently higher proportion of nickel released compared with cobalt (tables 86 and 88). This feature is in agreement with earlier observations in which cobalt had a greater affinity than nickel for the clay surface at high cation loadings (section 3.5.2, fig.16).

Infrared spectra of the acid treated clays confirmed the continued presence of the respective hexaaquo transition metal ion (fig.45) (i.e. very similar spectra to those of the untreated Ni- and Co-hectorite starting materials). However, some undissociated acid

(A)

(B)

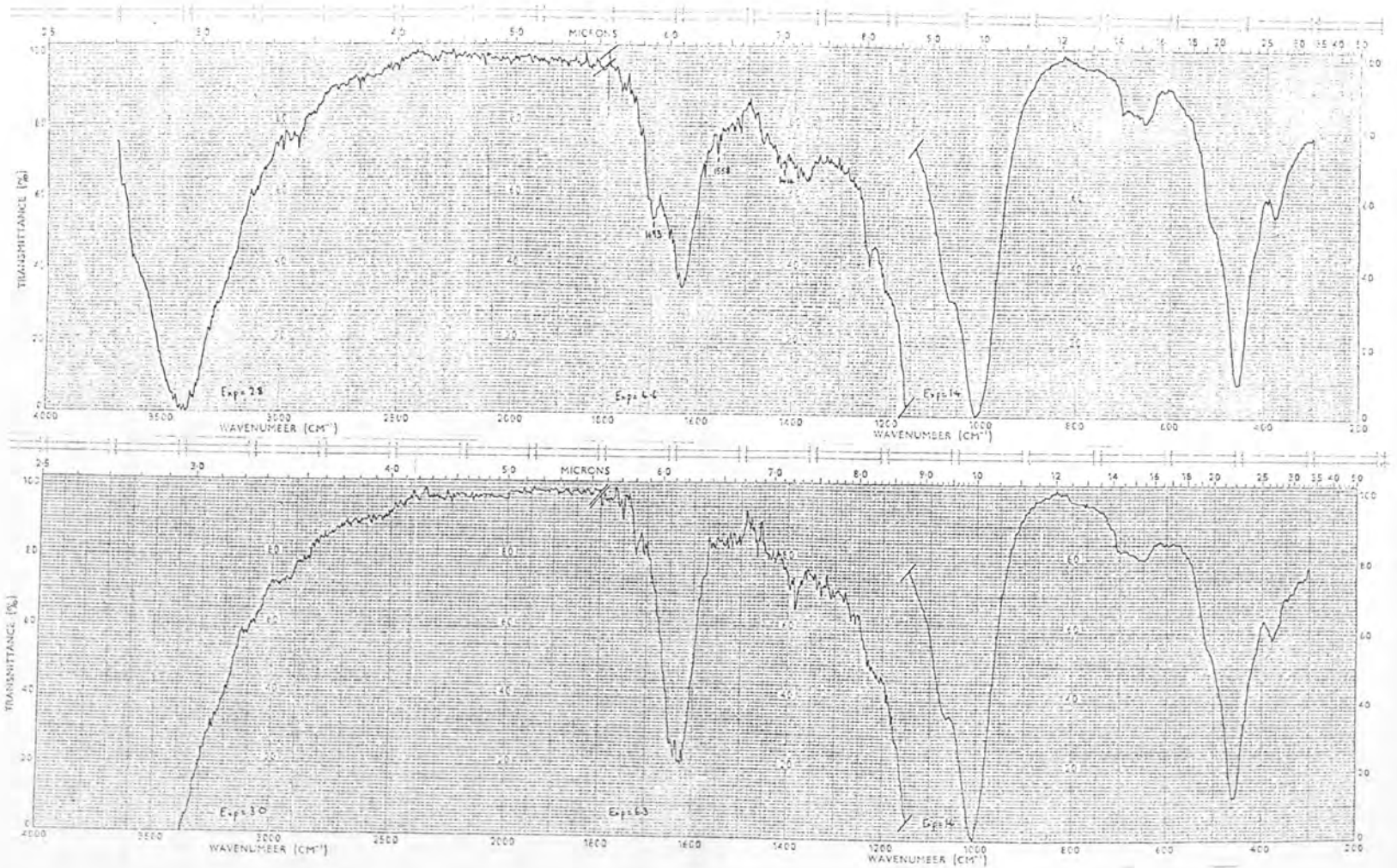

Fig.45 - Infrared spectra of (A) Co-hectorite/pentanoic acid (B) Co-hectorite only.

was also evident on the clay surface. A band at ≈1690cm^{-1} frequently observed in the infrared spectra of the acid treated clays (fig.45) was significantly shifted from that of the hydrogen-bonded dimer[139] (1770cm^{-1}) and that of the monomer (1712cm^{-1}). The acid is apparently undergoing some interaction in the clay interlayer region, the two most likely possibilities being either direct coordination with the interlayer cation, or, coordination to the interlayer cation through a water molecule in the 1st coordination sphere;

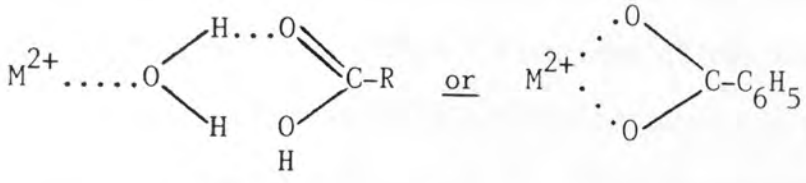

Comparison with data from Yariv and coworker's[140] investigation of the sorption of benzoic acid on montmorillonite samples indicated the latter mechanism. Their infrared data for clay sorbed benzoic acid was also inconsistent with either the dimer or monomer form, but Ca^{2+}-, Mg^{2+}-, Cu^{2+}- and Al^{3+}-montmorillonites all exhibited approximately the same value for the carbonyl stretching frequency, pointing to a similar interaction through a bridging water molecule. However, when these clays were dehydrated, the large shifts to lower frequency were correlated with different interactions, through direct coordination with the interlayer cations. Since only small frequency shifts from the dimer carbonyl stretching frequency were observed in our case, coordination through a water molecule seems the most likely explanation. An increase in c-spacing from 15.1Å to >15.6Å,

of the Ni- and Co-hectorites when treated with organic acids provided further confirmation that intercalation had occurred and it appeared that the plane of the acid molecule was inclined at a high angle to the plane of the clay layers. Yariv et al's[140] infrared data on benzoic acid sorption also indicated orientation of the plane of the molecule to be at a high angle to the montmorillonite layers.

The carboxylate (i.e. benzoate) ion could be generated on the surface of montmorillonite, by Yariv et al,[140] when using lower acid concentrations in sorption experiments. The presence of bands around $1400cm^{-1}$ and $1550cm^{-1}$ from some of the butanoic and pentanoic acid treated clays here (fig.45), indicated the presence of the respective carboxylate anion.[141] This is important in view of the previously proposed 'anion-cation pair' fixation mechanism (section 3.7). The significant sorption of acetate from aqueous solution onto the surface of a H-montmorillonite[63] observed by Bingham et al, corroborates the above proposal.

An interpretation of data from class(ii) ligands inevitably involves comparisons with that from distilled water treated samples (table 98).

Although more cobalt than nickel was lost when the clays were contacted with distilled water, it was evident that a small portion of 'labile' metal ion was still held by the rinsed clays. However, all clays released a similar quantity of metal ion when treated with ammonia (table 98), with all showing a relatively enhanced distribution coefficient for the transition metal ion on the hectorite. Ethylene-diamine also induced an increased affinity of nickel for the surface

Table 98 - Summary of transition metal ion release from hectorite by a number of aqueous solutions.

clay	organic added	Ni/Co released from clay (meq/100g)	% Ni/Co released
Ni-hectorite/rinse	NH_3	0.048	0.08
Ni-hectorite/rinse	en	0.19	0.30
Ni-hectorite/rinse	blank-dw	1.16	1.83
Ni-hectorite/wash	NH_3	0.049	0.09
Ni-hectorite/wash	en	0.21	0.37
Ni-hectorite/wash	blank-dw	0.82	1.45
Co-hectorite/rinse	NH_3	0.058	0.08
Co-hectorite/rinse	en	2.0	2.9
Co-hectorite/rinse	blank-dw	2.0	2.9
Co-hectorite/wash	NH_3	0.048	0.08
Co-hectorite/wash	en	2.1	3.3
Co-hectorite/wash	blank-dw	1.10	1.7

of the clay, but cobalt exhibited a relatively low distribution coefficient, a greater quantity being released by the ethylenediamine solution than by distilled water.

Physical investigation of the treated clays, revealed significant interaction of ligands with the exchanged transition metal ions, as expected (section 4.2.2). Good agreement was observed with the physical characteristics obtained from Ni- and Co-hectorite samples treated with model organic ligands (section 4.2.2).

The diffuse reflectance spectra of the Ni-hectorite/NH_3 treated samples demonstrated parameters similar to those of the hexaaquo Ni(II) species indicating a similar Ni^{2+} environment. However, a large degree of dehydration was apparent from the d(001) spacings and the loss of coordinated ammonia molecules to air on drying again accounted for these observations. No significant differences were observed in the infrared spectra of the treated and untreated clays. In particular infrared investigation revealed no sign of the N——H deformation and stretching modes typical of hexaammine Ni(II),[142] as well as the absence of a peak from NH_4^+.[143]

Diffuse reflectance suggested that the ethylenediamine treated Ni-clays had a small proportion of $[Ni(en)_2]^{2+}$ on their surface, but the significant fraction of Ni^{2+} was present in the $[Ni(en)_3]^{2+}$ form, as confirmed by the d(001) value of 14.9Å.[127] Infrared data further reinforced the above claim. Peaks at 3360, 3286, 2887, 1458, 1334, 1284 and 652cm^{-1} (fig.46) proved comparable with those obtained by Powell et al[144] for $[Ni(en)_3]PtCl_4$, but only two weak peaks at

(A)

(B)

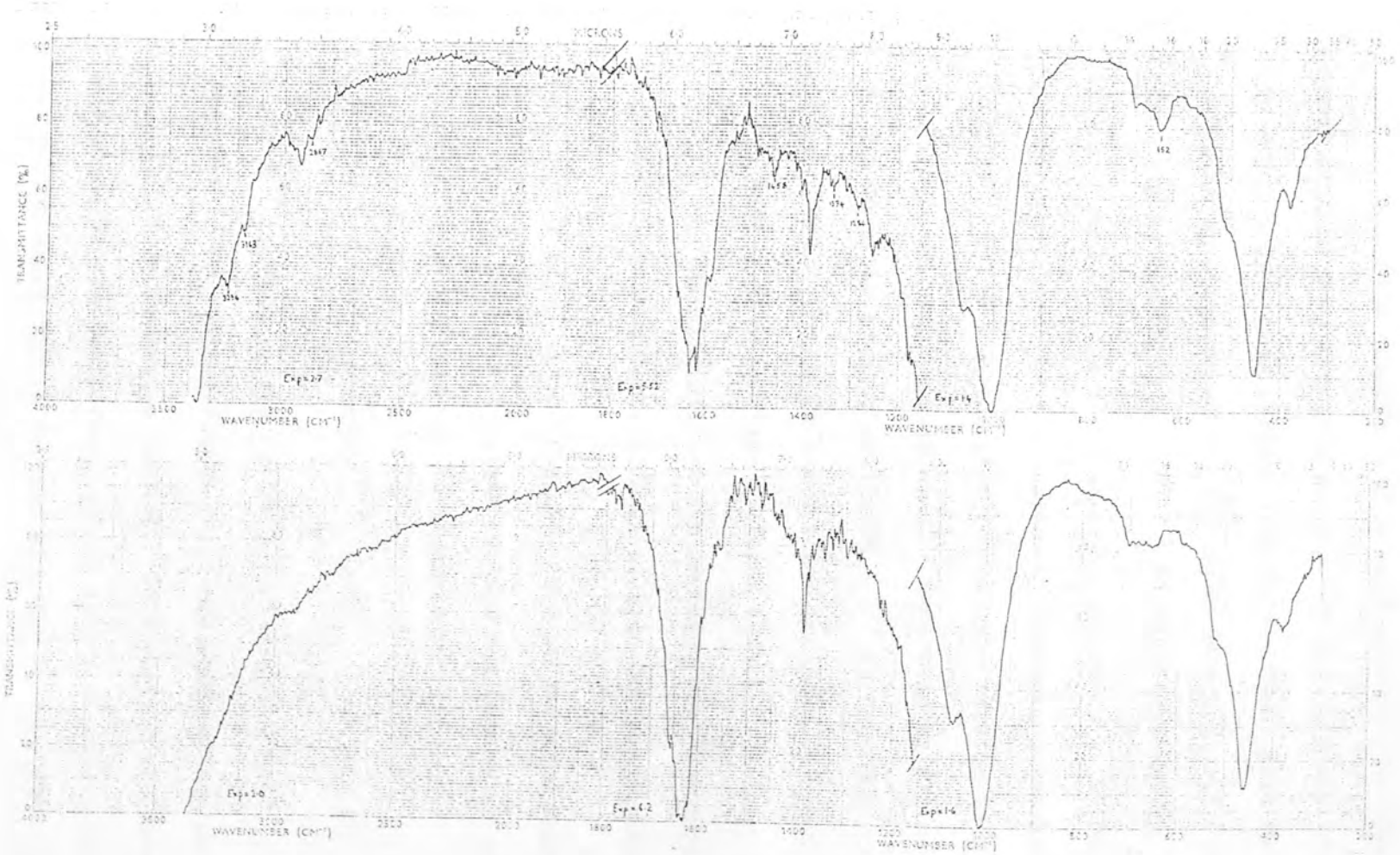

Fig.46 - Infrared spectra of (A) Ni-hectorite/ethylenediamine (B) Ni-hectorite only.

3234 and 750cm^{-1} could be ascribed to $[Ni(en)_2]^{2+}$.[145]

The Co-hectorite samples treated with ammonia also show significant similarities to those generated in the previous section (4.2.2), on model clay/organic ligand reactions. Weak peaks in the diffuse reflectance spectrum at 460 and 590nm were indicative of a small quantity of $[Co(NH_3)_6]^{3+}$. In conjunction with earlier results, peaks around 525 and 385nm were attributed to a $[Co(NH_3)_5O_2(NH_3)_5Co]^{4+}$ peroxy species on the clay surface. However, weak bands at 3324, 3253 and 1350cm^{-1} in the infrared spectra attributed to N——H vibrations of ammonia molecules[142] indicated only a small fraction of the Co atoms present as $[Co(NH_3)_6]^{3+}$ on the clay surface and the assumption that bands in the diffuse reflectance spectra were due to a cobalt-peroxy species, appeared invalid. A large peak at 1400cm^{-1}, though, is characteristic of the ammonium ion[146] - this observation allowed a more confident account of the reaction mechanism.

Mortland et al[147] showed that NH_3 chemisorbed on montmorillonite saturated by mono- or divalent cations was completely converted to NH_4^+. This reaction was interpreted as follows:

$$[M(H_2O)]^{z+} + NH_3 \longrightarrow [M——OH]^{(z-1)+} + NH_4^+$$

where M^{z+} represents the cation adsorbed on the clay, i.e. the reaction of NH_3 with strongly polarized water molecules in the vicinity of exchangeable cations. By a similar mechanism, water molecules in the inner coordination sphere of cobalt may provide the proton which reacts further with NH_3 to form NH_4^+. If two protons were removed from the inner coordination sphere, $Co(OH)_2$

may be precipitated in the clay interlayers and the resulting NH_4^+ ions may occupy the vacated exchange sites;

$$2NH_3 + [Co(H_2O)_6]^{2+} \longrightarrow 2NH_4^+ + Co(OH)_2 + 4H_2O$$

The displacement of $Co(OH)_2$ into the interlayer region and the consequent sorption of NH_4^+ ions was also observed by Fripiat et al[143] in their study on the thermal decomposition of $[Co(NH_3)_6]^{3+}$ on montmorillonite surfaces. They proposed the following mechanism:

$$6[Co(NH_3)_6]^{3+} + 12H_2O \longrightarrow 6Co(OH)_2 + 18NH_4^+ + 16NH_3 + N_2$$

on montmorillonite at greater than 100°C.

It is therefore not surprising that the d(001) spacing approached that of a monovalent cation saturated clay (≃12.5Å). However, the additional 0.6Å and the FWHM (table 87) suggest the presence of another, larger species, presumably $[Co(NH_3)_6]^{3+}$, in the interlayer region. Although this assertion appears to contradict the observation of Mortland et al[147] that NH_3 was completely converted to NH_4^+ ions, only montmorillonite exchanged with group I and group II cations were used in their study. The possibility of coordination of NH_3 to interlayer cobalt would seem much more likely than in their case.

The low solubility of $Co(OH)_2$ in the interlayers may also contribute to the very low % cobalt leached from Co-hectorite when contacted with ammonia solutions.

Addition of ethylenediamine to Co-hectorite appeared to simply

generate the $[Co(en)_3]^{3+}$ species on the solid. Diffuse reflectance absorption peaks at 341, 465 and 560nm (table 87) and d(001) values (table 87) were used to distinguish this complex. Excellent confirmation of this assignment was gained from infrared spectra, which showed bands very similar to those of $Co(en)_3Cl_3$[148] at 3423, 3213, 3102, 1579, 1459, 1340, 1050 and 788cm^{-1}.

It would initially seem, from the above evidence of coordination on both Ni- and Co-hectorite with both class(ii) 'ligands', that the stabilisation effect of class(ii) ligands is due to coordination with the interlayer transition metal ion. The extent to which NH_3 promotes stabilisation, however, is greater than that due to ethylenediamine and this contradicts the stability of the complexes expected from the spectrochemical series. It is suggested that competition of protonated ethylenediamine molecules, enH^+, for exchange sites, accounts for this phenomenon (although $Co(OH)_2$ precipitation also plays an important role in Co-hectorite/NH_3 systems). enH^+ is not expected to be as strongly sorbed as H^+ due to its larger size and only displaces a small portion of metal ion. In a characterisation study of $[Ni(en)_x]^{2+}$ (x = 1,2,3) on montmorillonite surfaces, desorption experiments and infrared data, performed by Schoonheydt et al[127] pointed to the presence of some protonated ethylenediamine molecules. However, their assignment of very weak bands between 1500 and 1550cm^{-1} to N——H deformation vibrations of ——NH_3^+ is somewhat uncertain and a similar assignment cannot be unambiguously stated here for the Ni-hectorite/en samples. However, three bands in the region 1505 to 1555cm^{-1} in

the infrared spectra of the Co-hectorite/en treated clays are consistent with the presence of enH^+. This would explain the larger % metal ion desorbed from the Co-clay compared with the Ni-clay (table 98).

Visible spectra of the equilibrium solutions from ammonia, ethylenediamine and distilled water treated clay samples revealed no detectable absorbances in all cases. This further supported the low percent metal ion desorbed from the clay and consequently observed in atomic absorption analysis.

Equilibrium solution analyses from the control samples, in which distilled water was contacted with the respective Ni- and Co-hectorite, demonstrated higher cation release from the rinsed clay than the washed clay (tables 86 and 88). This led to the assumption that a significant portion of 'labile' (section 3.7) metal ion resided on the rinsed clays. Traynor et al[42] observed removal of $[M(bipy)_3]^{2+}$ (M=Ru,Cu,Fe) complexes from solution, onto Na-hectorite to be in a large excess of the cation exchange capacity of the clay and attributed this to an anion dependent intersalation reaction. Adams et al[149] were also very careful to remove excess salt from prepared monoionic montmorillonite samples before use in sorption experiments, ultilizing several treatments of washing with deionised water followed by centrifugation.

Ethylenediamine solutions released very similar quantities of cation from the rinsed and washed clays indicating that ethylenediamine did not distinguish between the metal ion on different sorption sites.

Solutions of ammonia also desorbed very similar quantities of cation, once again indicating that the 'labile' metal ion must undergo a similar mechanism to the exchange metal ion (section 3.7) on the clay surface resulting in a significant increased affinity of metal ion for the external clay surfaces.

It appears then, that the 'labile' metal ion is also stabilised to a great extent on the clay, as well as the 'exchanged' cation, by addition of solutions of the type (ii) amine ligands.

Similar conclusions could be drawn from data obtained from addition of butanoic and pentanoic acid solutions (tables 86 and 88) to the clays, with the percent cation desorbed assuming close agreement for both rinsed and washed samples. It was not possible to distinguish whether, as expected, the 'labile' metal ion was released more readily than the 'exchanged' portion, by the organic acid treatment.

It is sensible, at this point, to look at the Ni-hectorite samples treated with diethyl phthalate (ortho-substituted) (section 4.2.3.5).

The structure of diethyl phthalate does not enable it to be categorised into either of the two classes of 'ligands' recognized previously in this section. The lack of readily ionisable protons would support its omission from the class (i) 'ligands'. Desorption effects exhibited by diethyl phthalate, though, did point to its inclusion in the class (ii) group. Interaction of diethyl phthalate with the clay occurred by a different mechanism to that demonstrated by the amine compounds. Diffuse reflectance spectra of the final

clay products were still characteristic of the hexaaquo Ni(II) species, although a band at 282nm was assigned to the $\sigma \rightarrow \pi^*$ transition of the conjugated C═C in diethyl phthalate. The diethyl phthalate, used undiluted as here, appeared to be acting as an 'inert' solvent and was unable to interact with the interlayer transition metal ion by any of the previously suggested mechanisms. However, indications from diffuse reflectance investigations, for significant sorption of diethyl phthalate were confirmed by the 19.5Å d(001) value gained from XRD analysis. Since there was no evidence for interaction of the diethyl phthalate with interlayer Ni(II), it must be sorbed on the silicate (lattice) surfaces of the interlayer region. Diethyl phthalate is very insoluble in water (hence its use as a pure liquid here) and would therefore not be expected to be present in the vicinity of the hydrated interlayer cation - but, its attraction to the silicate surfaces indicates some degree of hydrophobicity of this region. This hydrophobicity may account for the lack of hydrogen bonding of (and hence the insignificant interaction between) interlayer water molecules to the clay interlayer surfaces observed by a number of workers using infrared spectroscopy.[27]

Having observed definite interactions between a number of organic molecules and Ni-(Co-)hectorite clays and a significant influence on sorption properties, a more detailed quantitative investigation was performed using a number of solution organic 'ligand' concentrations (section 4.2.3.6). Quantitative analysis of metal ion desorption from the clays is summarised in fig.47 which includes

Fig.47 - %Ni (Co) desorbed from Ni/Co-hectorite by various organic 'ligands' at a number of initial solution concentrations.

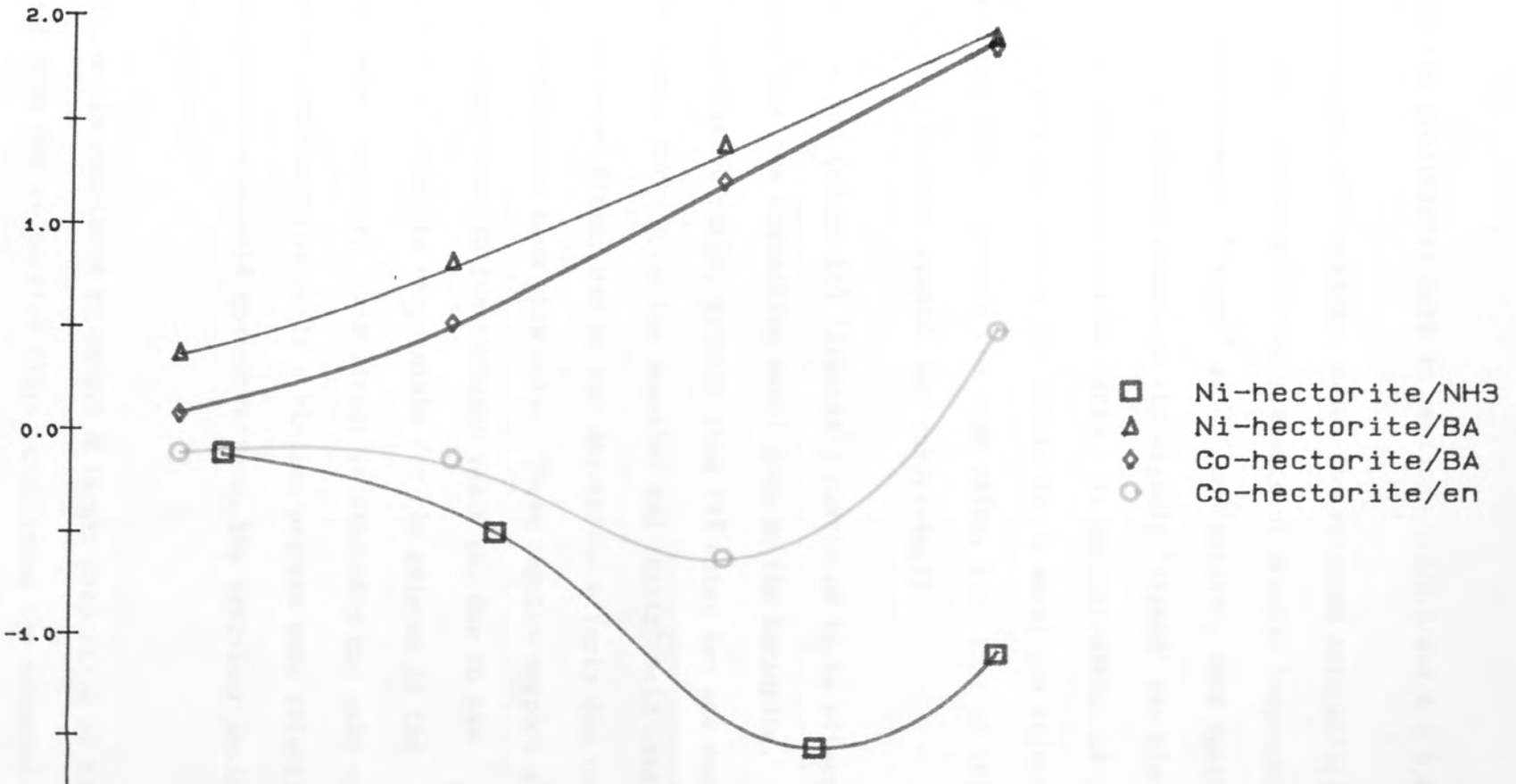

data from the preliminary work in sections 4.2.3.3 and 4.2.3.4.

The concentration of transition metal ion released into solution was very clearly affected by the presence of organic compounds, and the two classes of 'ligand' as defined earlier, were again separable. The effectiveness of the organic 'ligand' was also dependent on the organic:cation ratio. As concentrations of the organic solutions approached low levels the % metal ion released from the clays tended towards the same value, i.e. that of the distilled water control sample, not surprisingly.

The organic acids (class (i) 'ligands') continued to be effective 'desorbants' for the transition metal ions on the hectorite. Even at a 1:1 acid:cation ratio, greater than 15% metal ion was desorbed. The relationship between cation desorbed and initial acid concentration (fig.47) is almost linear and so the desorption effects due to acids are quite predictable from this data. These results support the previous proposal that an ion-exchange reaction, due to the generation of H^+ ions, is responsible for the release of the transition metal cations. This linear relationship may take on considerable importance since if a similar process were effective at the low groundwater acid concentrations, its behaviour would be quite predictable.

The organic acids continued to desorb a larger proportion of nickel than cobalt from the respective clays, confirming the enhanced affinity of cobalt for the hectorite surfaces at high clay saturation.

Characteristics of the acid treated clays demonstrated the same pattern - dependent on organic:cation ratios - as the desorption effects (tables 89 to 92).

Infrared spectroscopy clearly showed the decreasing acid content of the clay, characterised by the slow loss in intensity of a peak around 1690cm^{-1}. Bands at 1550 and 1400cm^{-1} which were attributed to the caboxylate ion when observed previously in the spectra from clay samples treated with a 14:1 butanoic (pentanoic) acid:cation ratio, did not appear, again pointing to a distinct influence of the organic:cation ratio used.

Basal spacings of these clays decreased with decreasing solution acid content and values approached those characteristic of the hexaaquo interlayer transition metal cation. Thus, at low concentrations, the amount of butanoic acid sorbed was not detectable, but in a 1.25:1 ratio, the acid was clearly present. Diffuse reflectance examination of the solids showed spectra typical of the hexaaquo interlayer cation and visible spectra of the equilibrium solutions also indicated the presence of the same species. It would appear, then, that the acid continues to promote the ion-exchange of dissociated H^+ ions for clay bound transition metal ions, even at lower initial solution concentrations.

The ammonia and ethylenediamine treated clays both exhibited troughs in fig.47, which were due to two different effects. Calculations based on the solubility product for $Ni(OH)_2$ (6.3×10^{-16}) and stability constants for nickel/amine complexes (for ammonia,

K_1 = 631), strongly suggested the precipitation of $Ni(OH)_2$, on addition of ammonia to Ni-hectorite in a 3:1 NH_3:Ni ratio, prior to analysis. The other three data points (fig.47), which were reliable, lie almost in a straight line on which the nickel concentration from the 3:1 NH_3:Ni sample should probably lie. The linear relationship would link favourably with the mechanism suggested previously for the 14:1 NH_3:Ni sample, that initially, complex formation is responsible for the enhanced stability of nickel on hectorite, so that increasing the solution ammonia concentration increases the degree of coordination. Again, no sign of ammonia or ammonium ion is present on the final clay product from the infrared spectra. XRD and diffuse reflectance data were characteristic of a sorbed hexaaquo Ni(II) species, except for the clay treated with a three-fold excess of NH_3, whose data agreed closely with that from the sample (3:1, NH_3:Ni) prepared in the preliminary study on model 'ligands' (section 4.2.2), from which it was concluded that a partially dehydrated Ni-hectorite remained. Visible spectrophotometry demonstrated the absence of significant quantities of any nickel species desorbed into solution.

No evidence could be found for enH^+ on the interlamellar surfaces of ethylenediamine treated Co-hectorite clays of en:Ni ratio below 1.5:1, although weak infrared bands at 3425, 3235, 3019 and 1461cm^{-1} in the 1.25:1 treatment were indicative of $[Co(en)_3]^{3+}$.[148]

Diffuse reflectance was able to show more clearly the increasing concentration of $[Co(H_2O)_6]^{2+}$ at the expense of $[Co(en)_3]^{3+}$ on the

clay surface, as ligand:cation ratio decreased (table 92). This effect was confirmed by XRD analysis of the solids, the 1.5:1 en:Co treated clay exhibiting a distinctive increase in FWHM compared with the parent Co-hectorite (table 92). Physical investigation thus provided evidence that although $[Co(en)_3]^{3+}$ was formed on the clay surfaces, at lower solution ethylenediamine concentrations, the sorption of enH^+ was not important - this led to the very low concentrations of cobalt released into solution when the en:Co ratio was less than 1.5:1.

No conclusions can be drawn regarding the mechanism of formation of enH^+ in the 1.25:1 en:Co treated sample. Although samples with a less than 1.5:1 ratio did not generate enH^+ indicating the absence of a clay surface catalysed mechanism, excess en in the 12.5:1 treatment may have been sorbed and consequently protonated on the clay surface, as opposed to formed in solution. The presence of Brönsted acid sites on clay minerals has been reported on a number of occasions.[27,150]

Conformation of the stability conferred on Ni- and Co-clays when treated with ammonia and ethylenediamine may be drawn from literature data on clay-metal complex interactions. That transition metal/ NH_3,en complexes are very strongly sorbed, and therefore retained, is apparent from studies by Das Kanungo et al and Knudson et al on the uptake of hexamminecobalt(III),[151] tris(ethylenediamine) cobalt(III),[152] tris(1,2-propylenediamine)cobalt(III),[53] and tris(1,3-propylenediamine)cobalt(III)[153] on the minerals laponite,

montmorillonite and bentonite.

Sorption isotherms generated, demonstrated an overwhelming preference of the complex cations, of both divalent and trivalent charge, over the interlayer hexaaquo cation for the surface of the clay minerals used. Fripiat et al[143] also noted that $[Co(NH_3)_6]^{3+}$ was sorbed very strongly on montmorillonite, even when the trivalent Ce^{3+} ion was the initial saturating interlayer cation. The results of a study by Peigneur et al,[67] utilizing selectivity measurements, on the stabilities of some transition metal (including nickel) poly-amine complexes on montmorillonite, showed that the overall stability constants of the complexes on the clay exceeded the corresponding values in solution by some three orders of magnitude. Upon generation of a tetraethylenepentamine treated bentonite, these workers were then able to form transition metal complexes on the clay simply by dispersion of the solid in a solution of the respective transition metal ion.

Following studies on mono-ionic Ni- and Co- saturated clays, a mixed Ni/Co-hectorite was prepared to see if added organic molecules would preferentially interact with one or other of the interlayer cations. This investigation is clearly related to the fact that a natural clay mineral will inherently contain a number of interlayer cations and geologic formations surrounding a radioactive waste disposal site may contain a large proportion of transition metal ions in exchange sites.

A mixed Ni/Co-hectorite starting material was prepared by the

addition of equal quantities of Ni^{2+} and Co^{2+} to a sample of hectorite (section 4.2.3.7), but as has been the case throughout the present study, cobalt was sorbed to a marginally greater extent. The addition of ammonia (in a 17:1 $NH_3:M^{n+}$ ratio, where M^{n+} = Co^{2+} + Ni^{2+}) to the clay desorbed very little metal ion into solution (table 94). However, treatment of the clay with butanoic acid removed a considerable proportion of the interlayer metal ion, again demonstrating the distinction between the amine and acid 'ligands' noted earlier.

The concentration of total metal ion (M^{n+}) desorbed by the ammonia solution from Ni/Co-hectorite correlated with the release from mono-ionic Ni- and Co-hectorites. The concentrations of nickel and cobalt released were also comparable, and so similar interaction mechanisms to those proposed previously for the ≃12.5:1 $NH_3:M^{n+}$ samples seemed likely (see earlier). Infrared evidence confirmed this, a band at 1408cm^{-1} being attributable to the NH_4^+ ion formed concurrently with $Co(OH)_2$,[143] and the absence of any additional bands indicating the continued presence of the divalent hexaaquo interlayer species. The d(001) value (table 93), however, was significantly larger than that observed previously for Ni- and Co-clays (tables 85 and 87) when treated with the higher concentrations of ammonia, possibly pointing to a substantial occupancy of the interlayer region by the hexaaquo species. It was clear, though, from the larger FWHM that a combination of complex species was present in the interlayer region, with the partially dehydrated nickel system (d(001) = 12.7Å) and NH_4^+ -exchanged hectorite

(d(001) = 13.0Å), generated in earlier studies, most likely present in appreciable quantities.

The butanoic acid solution desorbed significantly more nickel than cobalt from the Ni/Co-hectorite, which correlated with earlier findings on the mono-ionic clays, but released, overall, considerably less total metal ion (table 94). The lower pH of the equilibrium solution compared with that from the mono-ionic samples clearly indicated a lower uptake of acid onto the clay, and the absence of a band around 1700cm^{-1} in the infrared spectrum confirmed this, although a weak peak at 1550cm^{-1} may be assignable to the butanoate ion. The d(001) value of the solid was characteristically larger than that of the hexaaquo coordinated system and the FWHM was small, but diffuse reflectance spectroscopy revealed only a weakening of absorbance intensities, with no appreciable peak shifts.

The low cation desorption and absence of butanoic acid in detectable quantities on the Ni/Co-hectorite appears anomalous when comparison is made with the respective Ni- and Co-hectorites treated with the acid previously. The absence of butanoic acid uptake may be related to the lower proportion of H^+ ions sorbed onto the clay, since strong hydrogen bonding of the molecular acid to water molecules in the first and second coordination spheres surrounding interlayer H^+ may occur to a lesser extent than in clays of a high H^+ content. Any acid which is taken up by the clay appears to be in a dissociated form, as indicated by the detection of the butanoate ion. The lower desorption of M^{n+} from the Ni/Co-hectorite clay remains unexplained, but is obviously related to the bimetallic nature of the clay surface.

A generally enhanced affinity of transition metal ions for the hectorite surface after treatment of the clay with solutions of class (ii) amine 'ligands' has been demonstrated. Their stability must now be assessed with respect to inorganic cations that may also constitute typical groundwaters. A $[Ni(en)_3]^{2+}$-saturated hectorite was thus contacted with a variety of inorganic salt solutions. In a representative experiment, one sample was contacted with a Cu^{2+} solution, since a number of transition metals would most likely be released at the same time in the event of a radioactive waste container being breached. Concentrations of ppb transition metal ions may likely be present in natural groundwaters[154] anyhow, and analyses of pore water squeezed from samples of Oxford clay[155] exhibited significant (0.54 to 45ppm) amounts of iron, nickel and copper in their constitution.

Diffuse reflectance examination of the $[Ni(en)_3]^{2+}$-hectorite starting material did not show evidence of $[Ni(en)_2]^{2+}$ formation (section 4.2.4.1). A homogeneous exchanged clay was apparent from the small FWHM and the d(001) value was typical of the $[Ni(en)_3]^{2+}$ species. Data from the treatment of the $[Ni(en)_3]^{2+}$-hectorite with various inorganic salt solutions (table 95) is summarised in fig.48.

The observation that very little nickel was released from the $[Ni(en)_3]^{2+}$-hectorite when contacted with distilled water again confirmed that the complexed transition metal ion was considerably more stable on the clay than the hexaaquo species. Although neither cation was very effective, Ca^{2+} was more prominent than Na^{+} in facilitating desorption (fig.48) which corresponds with results in

Fig.48 - %Ni desorbed from Ni/en-hectorite by inorganic cations.

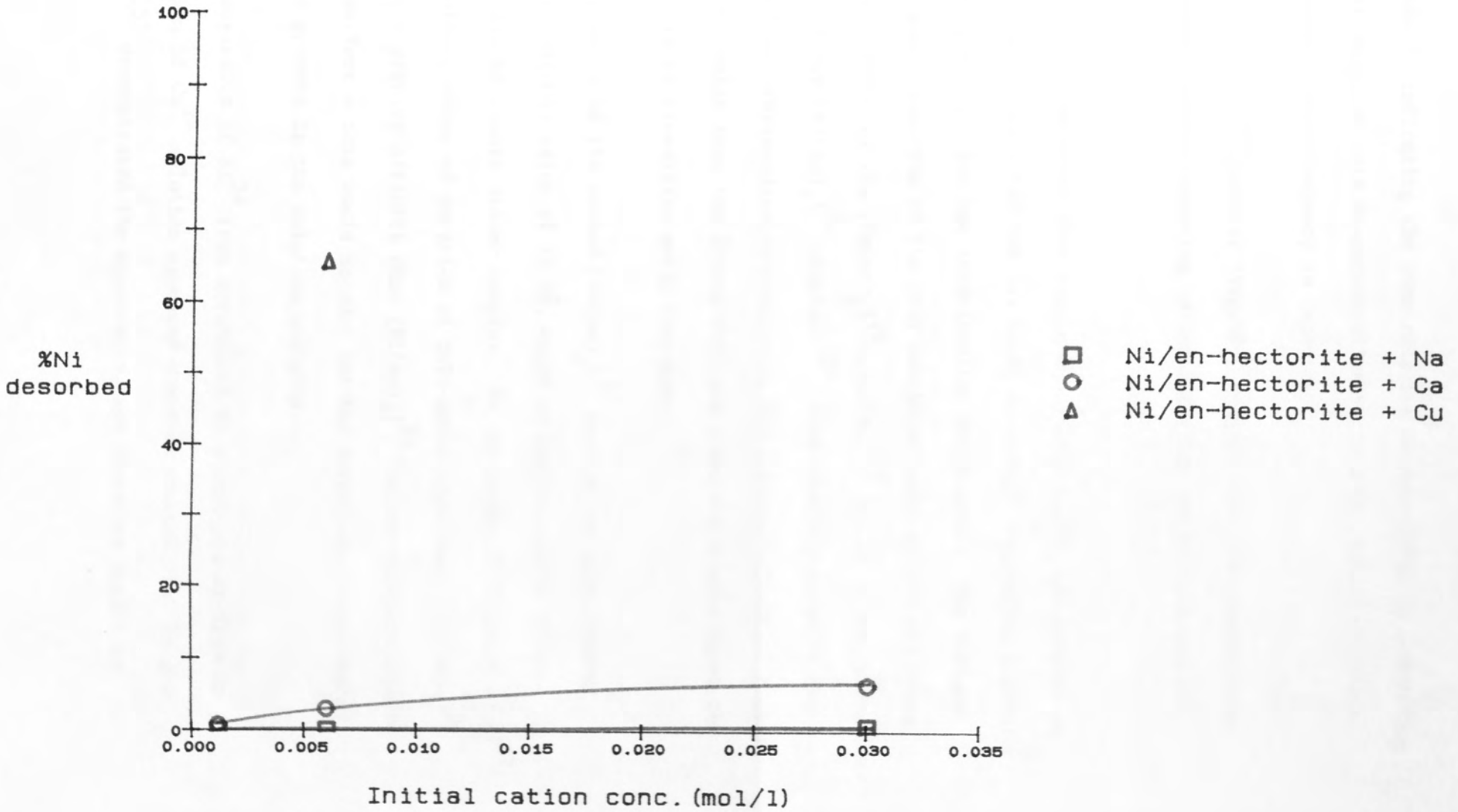

chapter 3, indicating the same relative effectiveness in preventing nickel sorption onto Na-montmorillonite from an aqueous solution, suggesting cation valency is important.

Results for Cu^{2+}, however (fig.48), suggest that the coordination properties of the competing cation dominates the effects due to valency.

It must also be noted that considerably more copper was present on the Ni-hectorite after the 1:1 Cu:Ni treatment, suggesting a greater affinity of Cu^{2+} for the interlamellar environment. The diffuse reflectance spectrum of the clay exhibited peaks at 558 and 374nm characteristic of the $[Cu(en)_2]^{2+}$ complex,[156] and at 465nm, characteristic of the $[Ni(en)_2]^{2+}$ complex.[127] Upon identification of the respective ethylenediamine complexes, the enhanced uptake of copper is predictable from the Irving-Williams order which catalogues the stability of transition metal complexes.

The presence of the sorbed $[Cu(en)_2]^{2+}$ species was also evident from the d(001) value of 13.0Å, which is characteristic of an intercalated square planar complex. In the study of Peigneur et al[67] on thermodynamics of sorption of poly-amine complexes, $[Cu(en)_2]^{2+}$ showed a greater affinity than $[Ni(en)_3]^{2+}$ for the montmorillonite clay surface - this would account for the larger concentration of nickel present in the solution analysis.

The conversion of Ni^{2+} from octahedral to square planar form on addition of Cu^{2+} solution appeared somewhat unusual, but Velghe et al[157] demonstrated the appearance, and therefore stability, of

$[Ni(en)_2]^{2+}$ on a montmorillonite when loaded with small amounts of $[Ni(en)_3]^{2+}$. Cu^{2+} ions sorbed in excess of the desorbed Ni^{2+} ions (table 95) most likely prompted this change in Ni^{2+} coordination, due to its strong requirement for square planar coordination with the ethylenediamine ligand and its enhanced affinity for the ligand itself. Infrared spectroscopy (fig.49) was unable to confirm the presence of any particular metal/ethylenediamine complex species on the clay due to the close proximity of bands from the metal complexes themselves and to interference from strong absorptions of the clay lattice, but bands at 1598, 1582, 1466cm^{-1} plus four between 654 and 702cm^{-1} were ascribed to the presence of one or more Ni^{2+}, Cu^{2+}/en complexes.[142,145]

The visible spectrum of the equilibrium solution (fig.50) exhibited strong absorbances characteristic of $[Cu(en)_2]^{2+}$, but showed no sign of any nickel species. This indicates that the Ni^{2+} released from the clay may be present as the $[Ni(H_2O)_6]^{2+}$ species, whose characteristic absorbance bands are masked by those from the Cu^{2+} species.

Of the limited literature data available on desorption effects on clay minerals, that of Das Kanungo et al[151] demonstrated that hexamminecobalt(III) was desorbed from bentonite more strongly by divalent inorganic cations than monovalent. This work was supported by the desorption behaviour of tris(1,2-propylenediamine)cobalt(III) on laponite and vermiculite, observed by Sarkar et al.[53] Interestingly, in both studies, the meq of complex desorbed showed a linear dependence on the concentration of Na^+ added, but a non-linear dependence

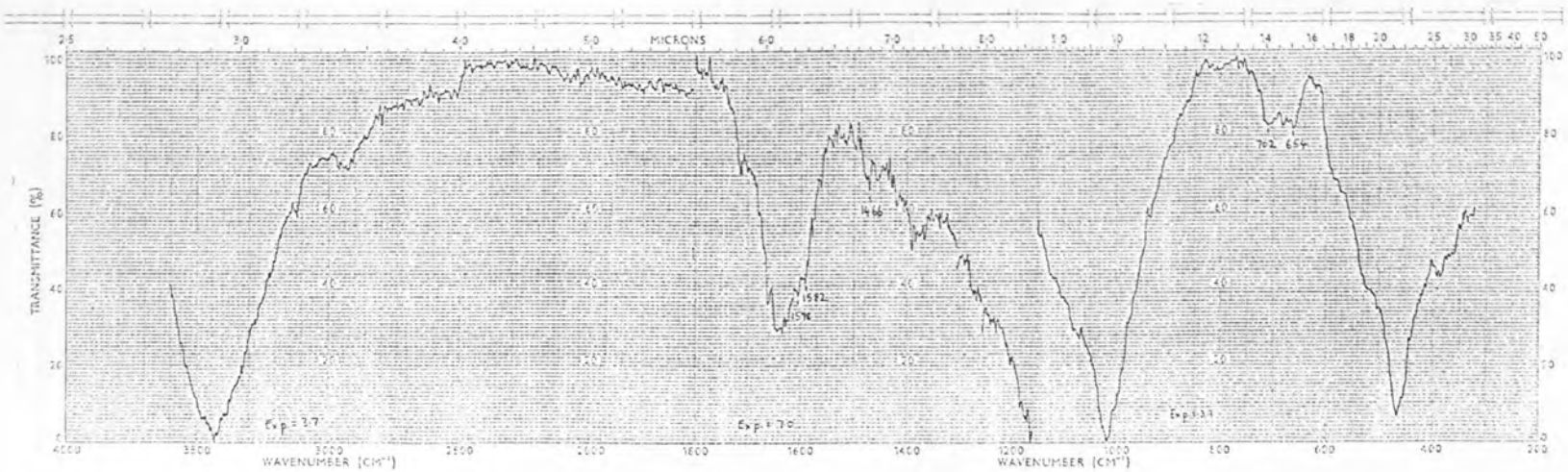

Fig.49 - Infrared spectrum of $[Ni(en)_3]^{2+}$-hectorite + Cu^{2+}.

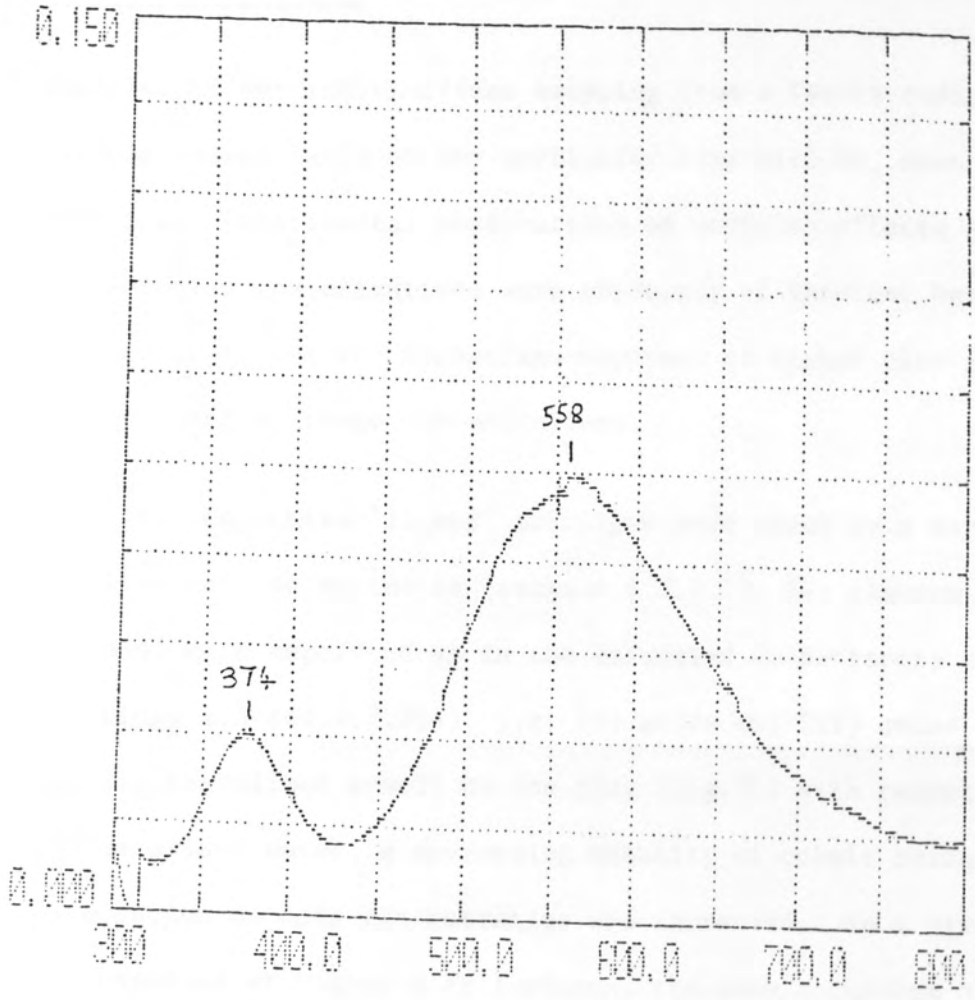

Fig.50 - UV/visible spectrum of equilibrium solution remaining from treatment of $[Ni(en)_3]^{2+}$-hectorite with Cu^{2+}.

on Ca^{2+} added, as observed in the present study (fig.48).

Microscopic Effects

The flux of any radionuclides escaping from a faulty radioactive waste disposal vault at any particular time will be, most certainly, very low. Experimental observations on sorption effects at very low solution concentrations were obviously of interest here, in particular to see if mechanisms apparent at higher clay loadings were evident at these concentrations.

When the respective 'ligand' solutions were added to a partially cobalt-saturated hectorite (section 4.3.2.1), two classes of organic compound were separated as in the saturated Co-hectorite system (sections 4.5 and 4.2.3.4), i.e. (i) acids and (ii) amine compounds. Ammonia stabilised cobalt on the clay (fig.51) with respect to demineralised water, a decreasing quantity of cobalt being released as solution ammonia concentration was increased. As a similar effect was observed at higher clay loadings, the same mechanism of interaction is proposed, i.e. stabilisation due to initial complexation of cobalt in the interlayers. No minimum in the plot of log %Co desorbed versus log [initial ligand concentration] (cf. fig.51 and fig.47) was observed in this case, as the solubility product of $Co(OH)_2$ was never exceeded, dismissing the possible precipitation of Co^{2+} ions from the analysis solutions.

Although the 12.5:1 NH_3:Co sample exhibited peculiar behaviour on initial analysis, the solution actually appeared a straw colour, even after ultracentrifugation, previous experience pointing to the

Fig.51 - Desorption of cobalt from a Co-60/hectorite by organic 'ligand' solutions.

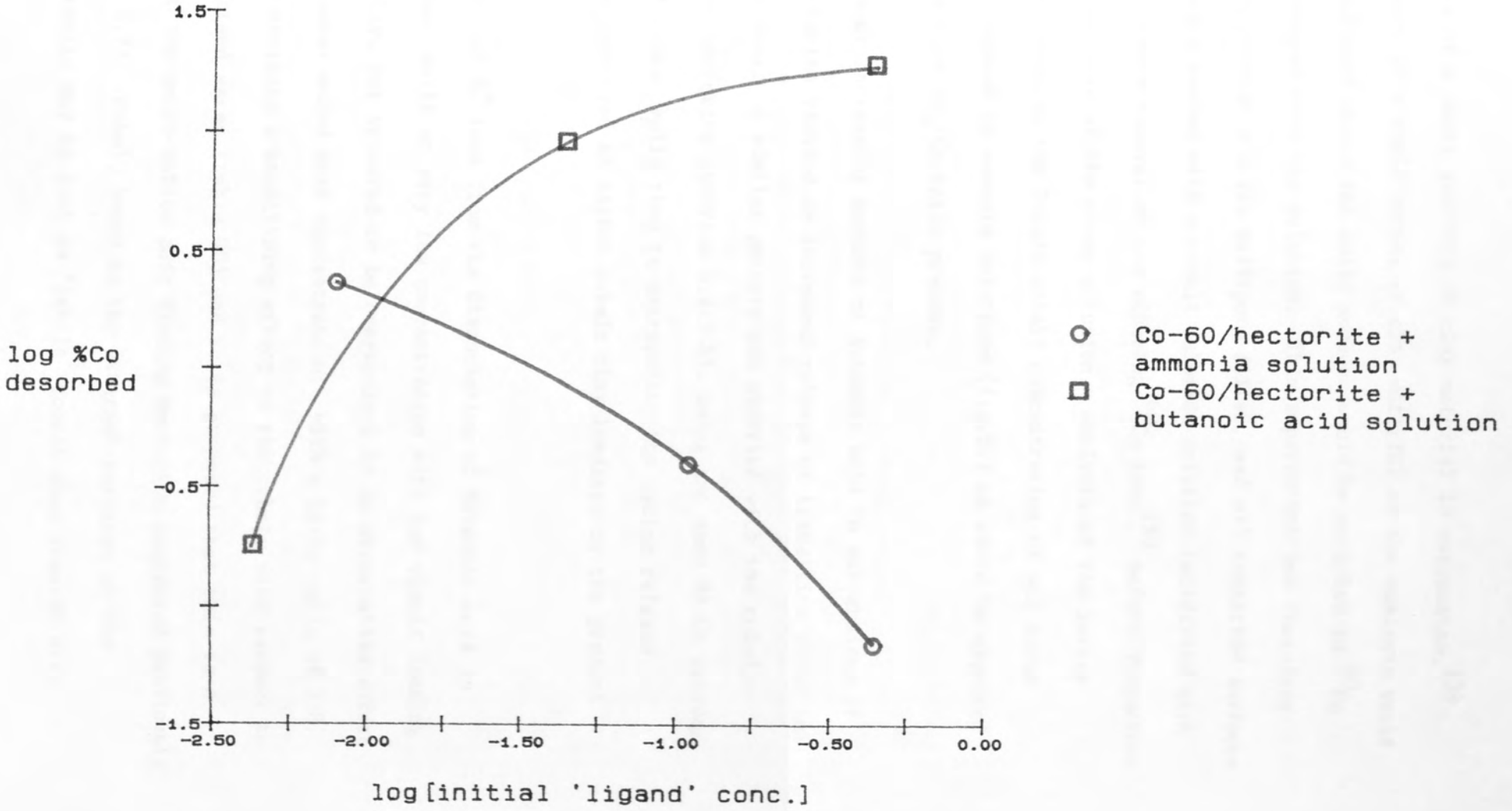

presence of a small quantity of clay material in suspension.[158] The effect of a small amount of clay material on the analysis would be significant since the solid sorbent would be enriched in ^{60}Co ions compared with the solution. This supernatent was therefore filtered through a 0.22μ millipore filter, and all contacted surfaces immediately washed with a cobalt chloride solution (acidified with HCl) to ensure removal of any adhering ^{60}Co ions[159] before γ-spectrometric analysis of the clear solution. Analysis of the latter solution revealed the lowest cobalt concentration of all three samples exposed to ammonia solutions (fig.51) as would be expected from the high NH_3:Co ratio present.

Addition of increasing amounts of butanoic acid to suspensions of ^{60}Co-hectorite yielded an increased release of transition metal ion from the clay. A similar pattern was observed with the cobalt-saturated hectorite (section 4.2.3.6), using the same BA:Co ratios. It would appear valid then to extrapolate the cation release mechanism observed at higher cobalt clay loadings to the present system.

Generation of H^+ ions from the dissociation of butanoic acid is significant still at very low concentration with low cobalt loading on the clay, but appeared to be overwhelmed by an alternative effect at the lowest added acid concentration. With a BA:Co ratio of 1:8, the acid exhibits a stabilising effect on the cobalt with respect to demineralised water (table 96) and it is proposed that this is a result of the anion-cation pair binding mechanism suggested previously (section 3.7). Cobalt bound to the external surfaces of the ^{60}Co-hectorite may be lost as 'labile' cobalt when treated with

demineralised water alone. When butanoic acid is added in a ratio of 1:8, this 'labile' cobalt is again released into solution, but is immediately complexed by butanoate ions (from the dissociation of the acid) and re-adsorbed onto the external surfaces of clay particles by the anion-cation pair mechanism. This process would most likely dominate at low butanoic acid concentrations for two reasons: firstly, the H^+ ion concentration is very low (4.4μM if all the acid were dissociated - comparable to that from demineralised water at pH5.7) and secondly, the concentration of Co^{2+} ions released from the ^{60}Co-hectorite is smallest at the lowest butanoic acid concentrations, hence giving a considerably higher ratio of acid:Co^{2+} ions in solution. The same mechanism may also be operative in samples having 12.5:1 and 1.25:1 BA:Co ratios, leading to reduced %Co desorption compared with the respective samples at high clay loading. This effect may, however, result from the bimetallic (Na,Co) nature of the hectorite exchange sites, which encouraged preferential removal of less strongly held sodium ions by hydrogen ions - this effect was obviously not apparent in the mono-ionic saturated Co-clay system, in which H^+ ions simply exchanged for Co^{2+} on the clay.

Clay supported redox catalysis

Clay minerals have been used in the catalysis of a wide variety of reactions. The conversion of propan-1-ol to di(prop-1-yl)ether using an Al^{3+}-exchanged montmorillonite and the reaction of hex-1-ene with ethanol in the presence of Al^{3+}-montmorillonite to yield 2-ethoxyhexane and 3-ethoxyhexane has been observed by Ballantine et al.[160,161] Also, Monsef-Mirzai et al demonstrated that mont-

morillonite exchanged with a phase transfer catalyst (e.g. $PhCH_2NBu_3^+$) will bring about the phase transfer catalysis of several organic and organometallic reactions.[162] The previously reported reduction of nitrobenzene to aniline using borohydride in the presence of $[Co(bipy)_3]^+$ instigated an investigation into the catalytic redox properties of the complex on a clay support. Redox reactions on clay modified electrodes have also been reported, in particular on montmorillonite exchanged with $[Ru(bipy)_3]^{2+}$.[163]

It was apparent from this information that clay supported redox catalysts could, under some circumstances, offer practical advantages particularly in terms of facilitating work up and ease of storage of a reversible catalyst.

Oxidation of Co^{2+} on hectorite occurred when the clay was treated with 2,2'-bipyridyl in air, as characterised by the absorption spectrum. Flocculation of $[Co(bipy)_3]^{3+}$-hectorite onto a platinum electrode allowed electrochemical reduction to a deep blue colour. The absorption spectrum agreed well with an earlier report, although it was at that time supposed that the blue species was a <u>bis</u> rather than a <u>tris</u> bipyridylcobalt(I) complex.[131]

The clay supported complex could also be reduced chemically <u>via</u> borohydride reduction. The addition of nitrobenzene to the damp reduced clay produced some aniline; however the best catalytic conversion was obtained when nitrobenzene together with borohydride was added to the reaction vessel containing the reduced clay. Some intermediate products were evident in the early reaction systems, but optimum conditions for this process were found on addition of

nitrobenzene (4mmol) together with $NaBH_4$ (40mmol) to the reaction flush used to generate $[Co(bipy)_3]^+$-hectorite (4.4.2.2), the conversion being 100% with no evidence for unreacted intermediates (table 97).

As would be anticipated with large cations, d(001) does not alter (18.7Å) as a function of oxidation state of the cobalt. The resultant pillaring effect in the interlayers is probably important in allowing ingress of the organics to the catalyst.

In summary, both inorganic cations (chapter 3) and organic compounds (chapter 4) have the potential to significantly affect sorption properties of cobalt and nickel ions on clay minerals.

In general, interference mechanisms observed at higher Ni/Co concentrations were also, apparently, effective at low level.

An anion dependent mechanism was identified for cation sorption, and the influence of additional cations was found to depend on (1) $Ni/Co:M^{n+}$ (M^{n+} = competing cation) ratio, (2) nature of M^{n+}, (3) total solution ionic strength.

The organic ligands used could be separated into two classes, according to the way in which cation sorption properties were modified: (i) acids, (ii) amine compounds. Complexes could be formed on the substrate by addition of a ligand solution to the respective clay, but the final product was dependent on the initial ligand:cation ratio.

CHAPTER 5

PHYSICAL INVESTIGATION INTO THE NATURE OF SORBED METAL IONS ON MONTMORILLONITE AND HECTORITE

5.1 INTRODUCTION

Although knowledge of the influence of inorganic cations (chapter 3) and organic material (chapter 4) on nickel and cobalt sorption onto clay materials was required for in situ evaluations of radionuclide migration from a radioactive waste disposal site, it was also of interest to instigate a more fundamental investigation into the nature of the sorbed cation. X-ray photoelectron spectroscopy (XPS), scanning electron microscopy (SEM) and Mössbauer spectroscopy were therefore used to probe the physical characteristics of clay sorbed transition metal ions.

The use of XPS was prompted by the observation of more than one cation sorption site (section 3.7), which, it was hoped, could be discriminated. XPS, a technique having high surface sensitivity, has only recently found application in the investigation of clay sorbed species.[69]

Mössbauer spectroscopy has been used in clay mineralogy mainly as a tool for the study of the valence state and coordination of structural iron. Some recent studies have demonstrated the usefulness of the technique in characterising iron species present on sorbent surfaces.[75]

5.2 X-RAY PHOTOELECTRON SPECTROSCOPY

Montmorillonite and hectorite samples which had been treated with nickel and cobalt salts (chloride or sulphate) were analysed. The elucidation of a suitable calibration procedure led to the derivation

of metal 2p electron binding energies (BE) and the position of complementary satellite photopeaks.

5.2.1 Calibration of the $Si2p_{\frac{1}{2},\frac{3}{2}}$ photopeak of Na-montmorillonite and natural hectorite, by comparison with the $Au4f_{\frac{7}{2}}$ peak from a thin gold surface deposit (and with 'pump oil' C1s peak) yielded the values in table 98.

5.2.2 A Co^{2+}-hectorite was prepared by addition of a 0.1M cobalt chloride solution ($100cm^3$) to a sample of hectorite (10g), stirring the suspension for 3 days, before filtration. After air drying, a portion (6.5g) of the resultant clay (which contained 53meq Co^{2+}/100g hectorite) was resuspended in distilled water ($100cm^3$) and filtered. After air drying, this washing procedure was repeated and the clay again air dried (Co^{2+}-hectorite/2 wash). A further portion (3.5g) of this twice washed clay was then washed a further three times before filtration and air drying (Co^{2+}-hectorite/5 wash).

XPS spectra of Co^{2+}-hectorite, Co^{2+}-hectorite/2 wash, Co^{2+}-hectorite/5 wash were taken using AlKα as incident radiation, both for the untreated specimen and after ten minutes argon ion etching. Spectral data are summarised in table 99.

5.2.3 A Ni^{2+}-hectorite was prepared by stirring a suspension of hectorite (10g) in a 0.1M nickel chloride solution ($100cm^3$), for three days, before filtration and air drying. A portion (6g) of the resultant clay (which contained 49meq Ni^{2+}/100g hectorite) was twice re-suspended in distilled water ($100cm^3$) and filtered, before being left

Table 98 - Corrected silicon 2p binding energy from montmorillonite and hectorite.

Sample	$Si2p_{\frac{1}{2},\frac{3}{2}}$ binding energy/eV
Montmorillonite	103.1 (±0.1)
Hectorite	103.2 (±0.1)

Table 99 - Cobalt $2p_{\frac{3}{2}}$ binding energies for cobalt treated hectorite samples.

Sample	etch time /min	$Co2p_{\frac{3}{2}}$ binding energy /eV
Co^{2+}-hectorite	0	782.5
	10	781.6
Co^{2+}-hectorite/2 wash	0	782.9
	10	782.2
Co^{2+}-hectorite/5 wash	0	782.4
	10	782.1

(BE precision, ±0.3eV)

to air dry (Ni^{2+}-hectorite/2 wash). A portion (3g) of this clay was washed a further three times with distilled water before filtration and air drying (Ni^{2+}-hectorite/5 wash).

XPS analysis of Ni^{2+}-hectorite, Ni^{2+}-hectorite/2 wash, Ni^{2+}-hectorite/5 wash was performed using MgKα incident radiation, on the samples before, and after, a five minute surface etching period. The relevant data are displayed in table 100.

5.2.4 A $NiCl_2$-montmorillonite was prepared by addition of a 0.1M nickel chloride solution ($100cm^3$) to a sample of Na-montmorillonite (10g), stirring for three days, before filtration. After air drying, a portion (6g) of the resultant clay (which contained 54meq Ni^{2+}/100g) was resuspended in distilled water ($100cm^3$) and filtered. After air drying, this washing procedure was repeated and the clay again air dried ($NiCl_2$-montmorillonite/2 wash). A portion (3g) of this clay was then washed a further three times before air drying ($NiCl_2$-montmorillonite/5 wash).

XPS spectra of the three samples were taken using MgKα incident radiation, both prior to and after argon ion etching. The spectral data are summarised in table 101.

5.2.5 A $NiSO_4$- montmorillonite was prepared by stirring a suspension of Na-montmorillonite (10g) with a 0.1M nickel sulphate solution ($100cm^3$), for three days, before filtration. Upon air drying, a portion (6g) of the resultant clay (which contained 58meq Ni^{2+}/100g) was washed twice ($NiSO_4$-montmorillonite/2 wash) and a portion (3g) of that clay treated on a further three occasions with distilled

Table 100 - XPS parameters from hectorite after nickel sorption.

Sample	etch time /min	$Ni2p_{\frac{3}{2}}$ binding energy /eV	*counts($x10^3$)
Ni^{2+}-hectorite	0	857.5	8
	5	857.2	27
Ni^{2+}-hectorite/2 wash	0	857.4	66
	5	857.2	71
Ni^{2+}-hectorite/5 wash	0	857.4	101
	5	857.7	92

*All spectra recorded under the same conditions of start BE, scan width, stepsize, counting period, gun current and voltage.

(BE precision = ±0.3eV)

Table 101 - $Ni2p_{\frac{3}{2}}$ binding energies for nickel chloride sorbed on montmorillonite.

Sample	etch time /min	$Ni2p_{\frac{3}{2}}$ binding energy /eV
$NiCl_2$-montmorillonite	0	856.1
	5	856.0 853.0
	30	856.6 852.8
	40	856.2 852.8
$NiCl_2$-montmorillonite/2 wash	0	856.2
	5	856.0 853.2
	30	856.5 853.5
$NiCl_2$-montmorillonite/5 wash	0	856.6
	5	856.6 852.8
	30	856.4 853.0
	40	852.8

(BE precision = ±0.3eV)

water ($100cm^3$) ($NiSO_4$-montmorillonite/5 wash) before air drying.

XPS analysis of $NiSO_4$-montmorillonite, $NiSO_4$-montmorillonite/2 wash, $NiSO_4$-montmorillonite/5 wash was performed using MgKα incident radiation, on the samples before and after subsequent surface etching. Table 102 contains the relevant XPS data.

5.3 SCANNING ELECTRON MICROSCOPY

SEM was applied to several modified montmorillonite samples to gain supportive analytical data for the conclusions drawn from XPS studies (section 5.2, 5.5) and sorption experiments (chapter 3). Initial investigations were performed on a natural 'Berkbond' montmorillonite (supplied by Steetly Minerals Ltd.) and after chemical treatment of the clay with separate nickel chloride and nickel sulphate solutions. However, the 'Berkbond' montmorillonite was quickly discarded upon recognition of a wide range of impurities, and replaced with the 'Steetly' montmorillonite used throughout the sorption studies (section 2.19). The latter clay was also saturated with Ni^{2+} ions from both nickel sulphate and nickel chloride solutions, prior to analysis under the electron microscope.

5.3.1 A sample of 'Berkbond' montmorillonite (5g) was saturated on exchange sites with Ni^{2+} in the usual manner (see section 5.2.2) using nickel sulphate solution. A portion of the Ni^{2+}-clay was subsequently washed five times with distilled water (see section 5.2.2) and both materials were examined using an SEM/energy dispersive analysis (EDAX) system. The relevant analyses are shown in tables 103 and 104.

Table 102 - $Ni2p_{\frac{3}{2}}$ binding energies for nickel sulphate treated montmorillonite samples.

Sample	etch time /min	$Ni2p_{\frac{3}{2}}$ binding energy /eV
$NiSO_4$-montmorillonite	0	856.3
	2	856.1 853.3
	10	856.1 853.2
$NiSO_4$-montmorillonite/2 wash	0	856.1
	1	856.8
	5	856.5 854.0
	10	856.6 853.1
$NiSO_4$-montmorillonite/5 wash	0	856.3
	1	856.1 853.8
	5	856.4 853.9
	10	853.3

(BE precision = ±0.3eV)

Table 103 - SEM/EDAX analysis of nickel sulphate treated 'Berkbond' montmorillonite, before washing.

Element	% abundance					
	Particle 1	2	3	4	5	6
Mg	1.0	1.7	0.7	1.9	1.6	0.6
Al	7.3	9.7	7.5	14	12	3.8
Si	27	34	29	44	22	13
S	1.7	1.9	0.8	0.2	1.1	0.4
K	2.5	2.4	3.0	1.9	1.1	0.7
Ca	31	28	38	13	54	73
Ti	0.1	0.0	0.2	0.9	0.5	0.0
Fe	17	11	9.6	9.0	4.2	4.5
Ni	13	12	12	15	4.3	4.0
Si/Al	3.7	3.5	3.9	3.1	1.9	3.4
Fe/Al	2.3	1.1	1.3	0.63	0.36	1.2
Fe/Si	0.61	0.32	0.34	0.20	0.19	0.34
Ni/Fe	0.8	1.2	1.2	1.6	1.0	0.9
Ni/Al	1.8	1.3	1.6	1.0	0.37	1.0
Ni/Si	0.49	0.37	0.41	0.33	0.20	0.31

Slash denotes elemental ratio.

Table 104 - SEM/EDAX analysis of nickel sulphate treated 'Berkbond' montmorillonite, after washing.

Element	% abundance					
	Particle 1	2	3	4	5	6
Mg	0.8	0.8	1.4	1.0	2.0	1.7
Al	6.1	8.9	11	13	15	15
Si	21	32	36	44	52	48
S	0.0	0.7	0.0	0.1	0.1	0.8
K	2.4	3.5	2.5	4.4	1.3	2.1
Ca	29	30	26	13	3.4	8.3
Ti	0.7	1.1	1.1	1.7	1.5	0.3
Fe	15	11	12	11	13	11
Ni	25	13	12	13	12	13
Si/Al	3.4	3.6	3.4	3.4	3.5	3.3
Fe/Al	2.5	1.2	1.1	0.82	0.90	0.77
Fe/Si	0.73	0.34	0.32	0.24	0.26	0.23
Ni/Fe	1.6	1.2	1.0	1.2	0.92	1.1
Ni/Al	4.0	1.4	1.1	0.97	0.83	0.87
Ni/Si	1.2	0.4	0.3	0.28	0.24	0.26

5.3.2 A Ni^{2+}-montmorillonite ('Berkbond') was generated utilizing a nickel chloride solution (see section 5.2.2), and subsequently analysed under the SEM. The results are reported in table 105.

5.3.3 Results from an SEM study of natural 'Berkbond' montmorillonite are displayed in table 106.

5.3.4 Two samples of Ni^{2+}-saturated 'Steetly' montmorillonite were prepared in the usual manner (see section 5.2.2), by treatment with nickel chloride and nickel sulphate solutions, respectively. According to the procedure previously employed (see section 5.2.2), portions of the two clays were redispersed on five separate occasions in distilled water. The four Ni^{2+}-modified clays were subsequently analysed along with the untreated clay, using SEM, and the results are displayed in tables 107, 108, 109, 110 and 111.

5.4 MÖSSBAUER SPECTROSCOPIC INVESTIGATION OF IRON IONS EXCHANGED ONTO HECTORITE

^{57}Fe Mössbauer spectroscopy was applied to hectorite samples treated with both Fe^{2+} and Fe^{3+} ions to gain information on the cation environment on the clay surfaces. As well as Fe^{2+} and Fe^{3+} saturated hectorite, a clay sample containing $^{57}Fe^{3+}$ in only a fraction of exchange sites was prepared and examined. All the samples were subsequently heated to 400°C in a nitrogen atmosphere before further Mössbauer investigation.

5.4.1 Preparation of Fe^{3+}-hectorite

An Fe^{3+}-exchanged hectorite was prepared by dispersing a sample of

Table 105 - Analytical data from SEM/EDAX analysis of nickel chloride treated 'Berkbond' montmorillonite.

Element	% abundance					
	Particle 1	2	3	4	5	6
Mg	0.4	0.5	1.2	0.3	0.6	2.7
Al	4.2	13	12	14	1.4	14
Si	14	50	44	51	5.3	49
S	0.1	0.1	0.1	0.3	0.2	1.0
Cl	0.1	0.1	0.3	0.2	0.3	0.4
K	0.6	20	2.8	21	0.3	1.4
Ca	73	7.7	9.9	6.3	88	6.7
Ti	0.4	0.3	1.4	0.3	0.4	0.8
Fe	3.7	3.5	14	3.1	1.7	13
Ni	3.7	5.5	14	4.2	1.8	12
Si/Al	3.2	3.8	3.6	3.7	3.9	3.4
Fe/Al	0.89	0.27	1.2	0.23	1.3	0.90
Fe/Si	0.27	0.07	0.33	0.06	0.32	0.26
Ni/Fe	0.99	1.6	0.99	1.4	1.0	0.94
Ni/Al	0.87	0.42	1.2	0.30	1.3	0.84
Ni/Si	0.27	0.11	0.33	0.08	0.33	0.24

Table 106- SEM/EDAX analysis of natural 'Berkbond' montmorillonite.

Element	% abundance					
	Particle 1	2	3	4	5	6
Mg	1.2	1.3	1.7	1.7	1.6	1.8
Al	12	8.8	10	13	13	13
Si	52	40	46	57	56	50
S	0.2	0.0	0.0	0.1	0.2	0.1
Cl	0.0	0.0	0.3	0.5	0.6	0.8
K	0.1	0.3	0.3	0.6	0.6	0.6
Ca	5.7	4.9	12	1.0	1.3	5.2
Ti	1.7	0.6	1.0	0.7	0.6	0.8
Fe	27	44	28	25	26	28
Ni	0.0	0.2	0.0	0.2	0.5	0.0
Si/Al	4.4	4.5	4.5	4.2	4.1	4.0
Fe/Al	2.3	5.0	2.7	2.0	2.0	2.2
Fe/Si	0.53	1.2	0.6	0.45	0.47	0.55

Table 107 - SEM/EDAX analysis of nickel sulphate treated 'Steetly' montmorillonite, before washing.

Element	% abundance					
	Particle 1	2	3	4	5	6
Mg	1.0	0.6	1.5	1.9	1.1	1.3
Al	12	12	13	14	14	14
Si	49	49	50	52	53	52
S	0.2	0.0	0.5	0.6	0.1	0.0
Cl	0.1	0.2	0.3	0.8	0.4	0.2
K	0.3	0.3	0.4	0.7	0.6	0.2
Ca	0.2	0.3	0.9	0.0	0.3	0.4
Ti	0.7	0.8	0.3	1.1	0.5	0.9
Fe	33	32	30	25	27	28
Ni	3.5	3.7	3.3	3.9	3.2	3.0
Si/Al	4.1	4.0	3.9	3.8	3.9	3.8
Fe/Al	2.8	2.6	2.3	1.9	2.0	2.1
Fe/Si	0.68	0.65	0.60	0.49	0.51	0.55
Ni/Fe	0.11	0.12	0.11	0.15	0.12	0.11
Ni/Al	0.29	0.30	0.26	0.28	0.24	0.22
Ni/Si	0.07	0.07	0.07	0.07	0.06	0.06

Table 108 - SEM/EDAX analytical data from nickel sulphate treated 'Steetly' montmorillonite, after washing.

Element	% abundance					
	Particle 1	2	3	4	5	6
Mg	1.5	1.5	1.8	1.5	1.2	1.5
Al	13	13	13	13	13	14
Si	52	54	51	54	52	50
S	0.4	0.0	0.1	0.1	0.5	0.6
Cl	0.2	0.0	0.2	0.0	0.0	0.3
K	0.6	0.2	0.5	0.4	0.0	0.8
Ca	0.8	1.2	1.0	0.8	0.8	2.0
Ti	0.5	0.7	0.3	0.6	0.6	0.8
Fe	28	26	27	27	28	26
Ni	3.5	3.5	4.0	2.6	4.4	4.5
Si/Al	3.9	4.1	4.0	4.1	3.9	3.7
Fe/Al	2.1	1.9	2.1	2.1	2.1	1.9
Fe/Si	0.53	0.47	0.53	0.51	0.54	0.51
Ni/Fe	0.13	0.13	0.15	0.10	0.16	0.18
Ni/Al	0.27	0.26	0.31	0.20	0.33	0.33
Ni/Si	0.07	0.06	0.08	0.05	0.09	0.09

Table 109 - SEM/EDAX analysis of 'Steetly' montmorillonite after treatment with nickel chloride, before washing.

Element	% abundance					
	Particle 1	2	3	4	5	6
Mg	0.9	1.7	0.1	1.5	1.4	0.9
Al	9.7	14	1.3	13	14	14
Si	50	55	95	55	54	55
S	0.0	0.0	0.0	0.1	0.3	0.1
Cl	0.2	0.3	0.2	0.1	0.4	0.0
K	0.6	1.1	0.0	1.6	1.1	0.8
Ca	0.2	0.6	0.0	0.6	0.6	0.5
Ti	1.2	1.4	0.0	0.6	1.0	0.3
Fe	33	24	3.4	26	26	27
Ni	4.2	1.6	0.1	1.9	1.7	1.6
Si/Al	5.2	3.9	71	4.2	3.8	3.9
Fe/Al	3.4	1.7	2.6	2.0	1.8	1.9
Fe/Si	0.66	0.43	0.04	0.48	0.48	0.49
Ni/Fe	0.13	0.07	0.02	0.07	0.07	0.06
Ni/Al	0.43	0.11	0.04	0.14	0.12	0.11
Ni/Si	0.08	0.03	0.001	0.03	0.03	0.03

Table 110 - SEM/EDAX analytical data from 'Steetly' montmorillonite after nickel chloride treatment and subsequent washing.

Element	% abundance					
	Particle 1	2	3	4	5	6
Mg	1.4	1.3	1.6	0.3	1.8	1.2
Al	14	14	14	16	14	14
Si	54	54	54	62	55	52
S	0.1	0.0	0.1	0.2	0.2	0.0
Cl	0.0	0.3	0.2	0.1	0.1	0.3
K	0.8	1.1	1.2	10.0	1.3	1.1
Ca	0.1	0.1	0.2	0.0	0.1	0.2
Ti	0.7	0.7	0.9	0.4	0.7	3.4
Fe	28	27	27	11	26	27
Ni	0.8	1.7	1.7	0.5	1.3	1.2
Si/Al	3.8	3.8	3.9	3.8	3.9	3.9
Fe/Al	1.9	1.9	1.9	0.66	1.8	2.0
Fe/Si	0.51	0.50	0.49	0.18	0.46	0.52
Ni/Fe	0.03	0.06	0.06	0.05	0.04	0.05
Ni/Al	0.06	0.12	0.12	0.03	0.09	0.09
Ni/Si	0.02	0.03	0.03	0.01	0.02	0.02

Table 111 - SEM/EDAX analysis of natural 'Steetly' montmorillonite.

Element	% abundance					
	Particle 1	2	3	4	5	6
Mg	1.6	1.6	1.9	1.4	1.7	1.6
Al	15	15	17	16	19	17
Si	56	55	54	56	52	52
S	0.0	0.0	0.0	0.1	0.3	0.0
Cl	0.0	0.1	0.0	0.3	0.4	0.2
K	0.1	0.1	0.4	1.8	0.6	0.3
Ca	1.1	0.8	1.2	0.9	1.1	1.3
Ti	0.4	0.1	0.4	0.3	0.9	0.8
Fe	26	28	26	23	24	27
Ni	0.1	0.0	0.0	0.1	0.0	0.2
Si/Al	3.7	3.7	3.3	3.5	2.7	3.1
Fe/Al	1.7	1.9	1.6	1.4	1.2	1.7
Fe/Si	0.45	0.50	0.48	0.40	0.46	0.51

hectorite (1.5g) in a 0.1M $FeCl_3.6H_2O$ solution ($75cm^3$) previously adjusted to pH1.0 using 1M HCl, stirring the suspension for 3 days, before filtering. The clay was then washed with 2 aliquots of 0.005M HCl ($25cm^3$), dried in air at room temperature, then crushed to a fine powder using an agate pestle and mortar, before Mössbauer examination at room temperature (fig.52).

The Fe^{3+}-hectorite was a sandy colour and atomic absorption analysis of the remaining supernatent solution revealed an uptake of 54meq $Fe^{3+}/100g$.

5.4.2 Preparation of Fe^{2+}-hectorite

A sample of hectorite (1.5g) was added to a 0.1M $FeCl_2.7H_2O$ solution ($75cm^3$), previously adjusted to pH1.4 using 1M HCl, in a nitrogen* atmosphere, and stirred for 3 days. The suspension was subsequently filtered (in a glove box under nitrogen), washed twice with 0.005M HCl ($15cm^3$), and dried over saturated sodium acetate trihydrate (relative humidity ≈76%) under N_2.

The yellow Fe^{2+}-hectorite contained 50meq $Fe^{2+}/100g$. The Mössbauer spectrum of the product was acquired at both room temperature and 80K (fig.53).

*Throughout the series of experiments in section 5.4, only deoxygenated nitrogen was used. This encompassed passing cylinder N_2 through two gas wash bottles filled with an aqueous solution containing 160g sodium dithionite, 130g sodium hydroxide and 40g anthraquinone-2-sulphonic acid per litre.

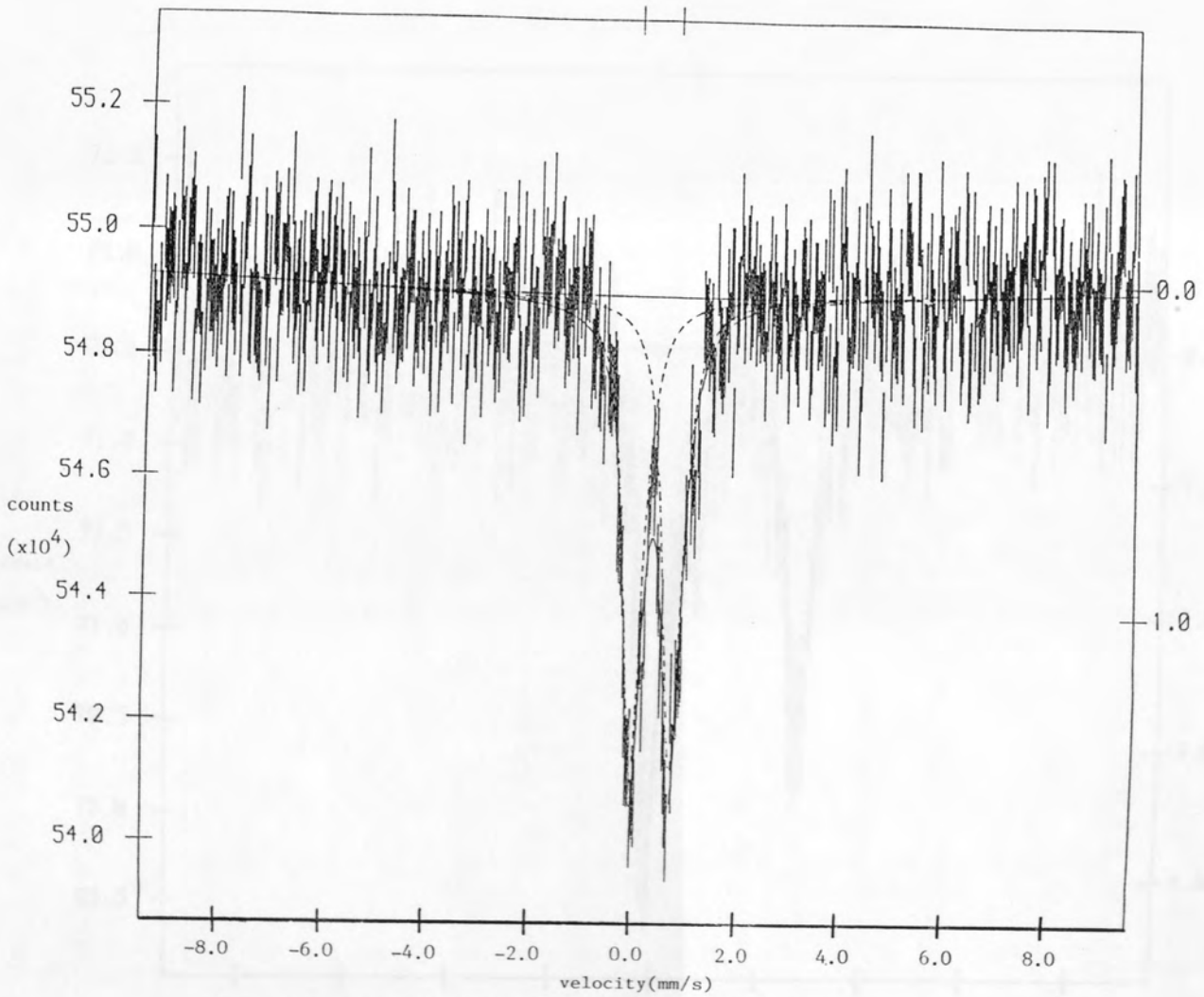

Fig.52 - Room temperature Mössbauer spectrum of Fe^{3+}-hectorite

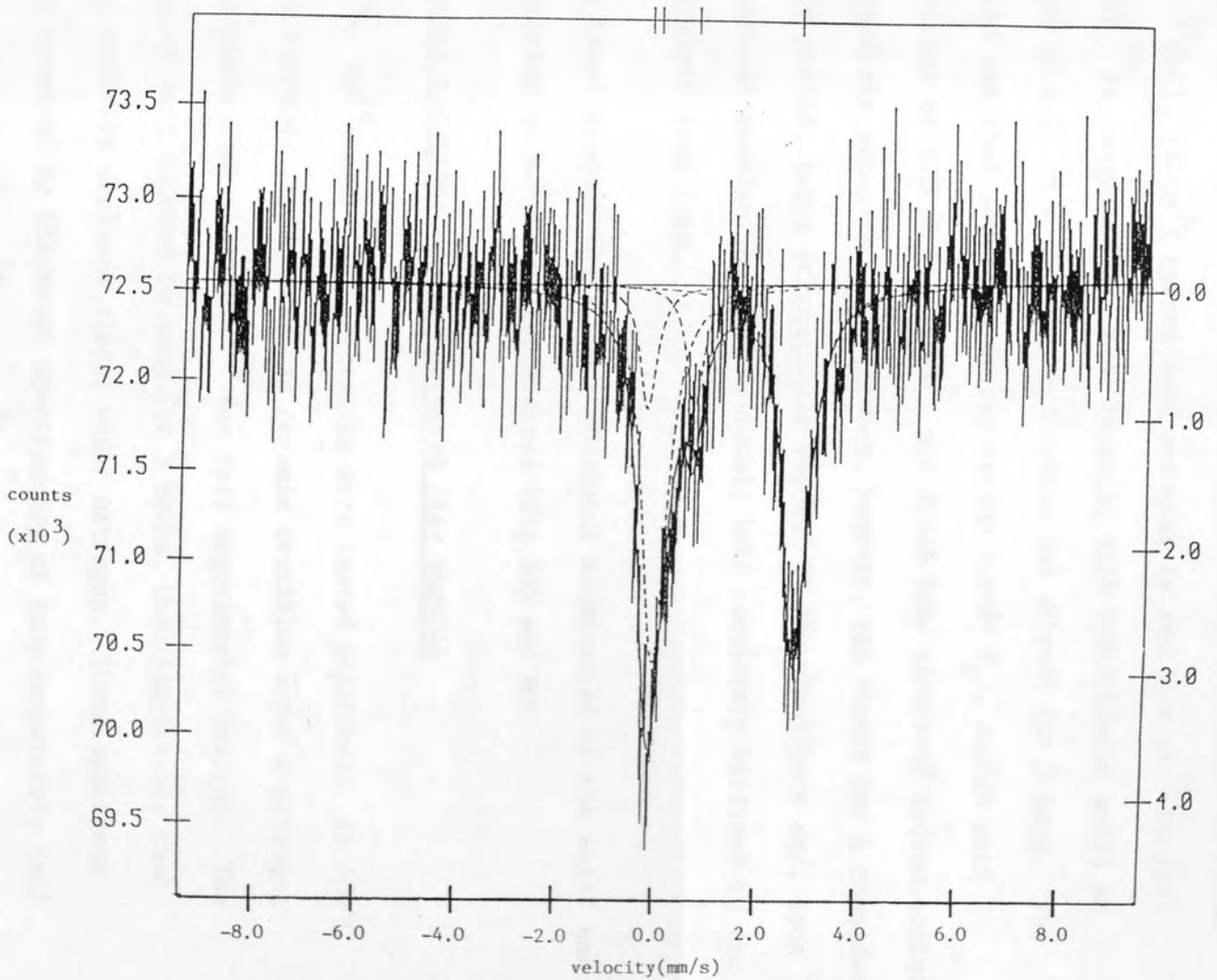

Fig. 53 - Mössbauer spectrum of Fe^{2+}-hectorite taken at 80K

5.4.3 Preparation of $^{57}Fe^{3+}$-hectorite

An $^{57}Fe^{3+}$-hectorite sample was prepared by air oxidation of an $^{57}Fe^{2+}$-hectorite clay.

A portion (4.0g) of hectorite was covered with a 0.0083M solution of $^{57}FeCl_2$ ($40cm^3$) (previously prepared by reaction of ^{57}Fe foil (95% ^{57}Fe, supplied by AERE, Harwell) with hydrochloric acid) at a pH of 1.2, in a nitrogen atmosphere and stirred for 3 days. The solid was then separated by filtration (under N_2), washed with 2 portions of 0.005M HCl ($15cm^3$) and dried over saturated sodium acetate trihydrate solution. The product, however, was stored for a considerable period, being occasionally exposed to the atmosphere and, upon Mössbauer examination, had obviously been completely oxidised to the trivalent iron form.

The final product was white. Mössbauer examination of the solid was performed at both room temperature (fig.54) and 80K.

5.4.4 Thermal treatment of iron doctored clay samples

Fe^{3+}-, Fe^{2+}- and $^{57}Fe^{3+}$-hectorite were heated separately, at 400°C in a furnace, for 4 hours, in ceramic crucibles under a nitrogen atmosphere (see Gillespie[164] for full experimental design). The samples were allowed to cool for 3 hours, then immediately cast into araldite enclosed discs, under nitrogen. These specimens were examined by Mössbauer spectroscopy at room temperature (all 3 clays) and 80K (Fe^{3+}- and Fe^{2+}-hectorite only). The fitted spectra are shown in figs. 55 to 59.

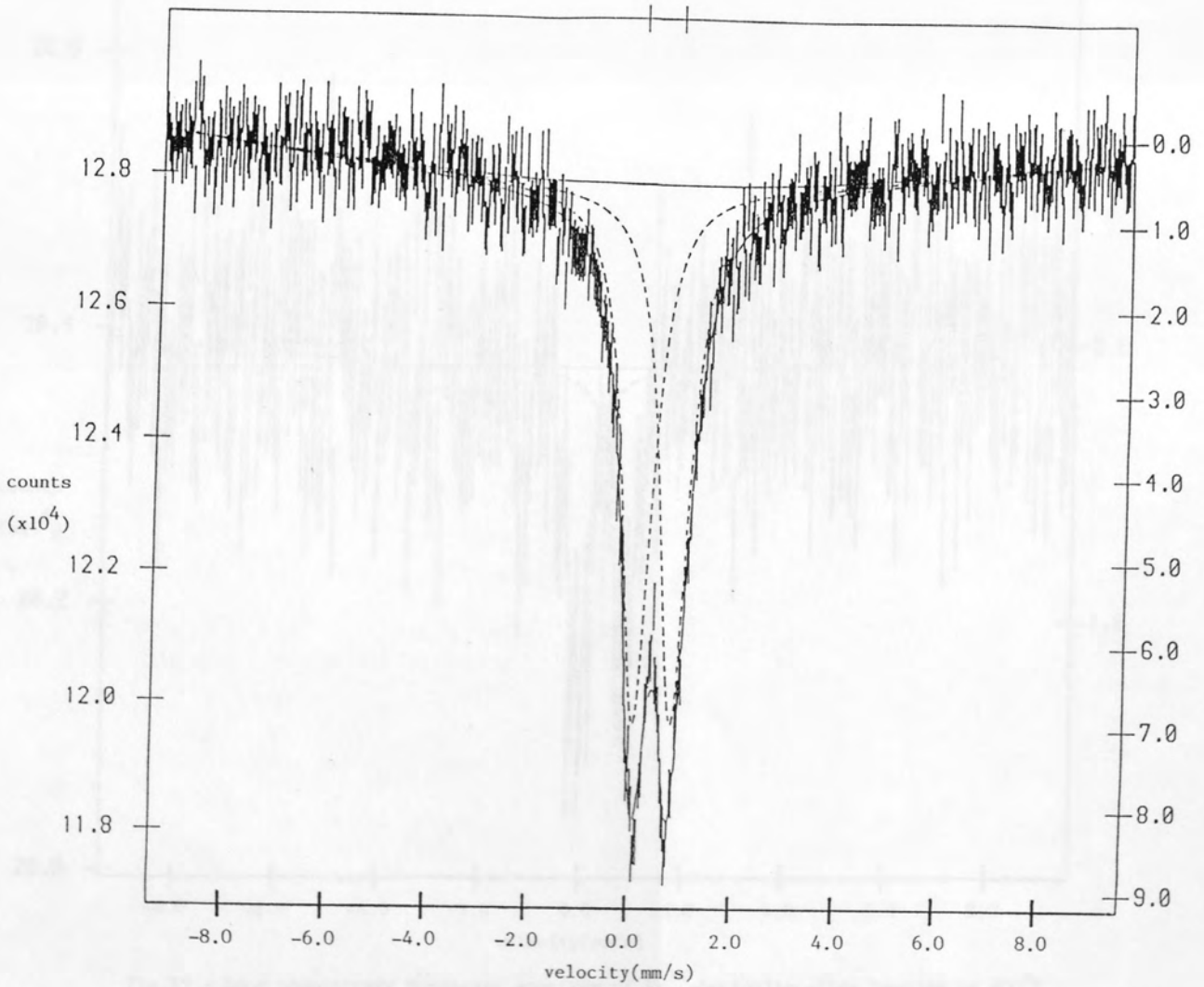

Fig.54 - Room temperature Mössbauer spectrum of $^{57}Fe^{3+}$-hectorite

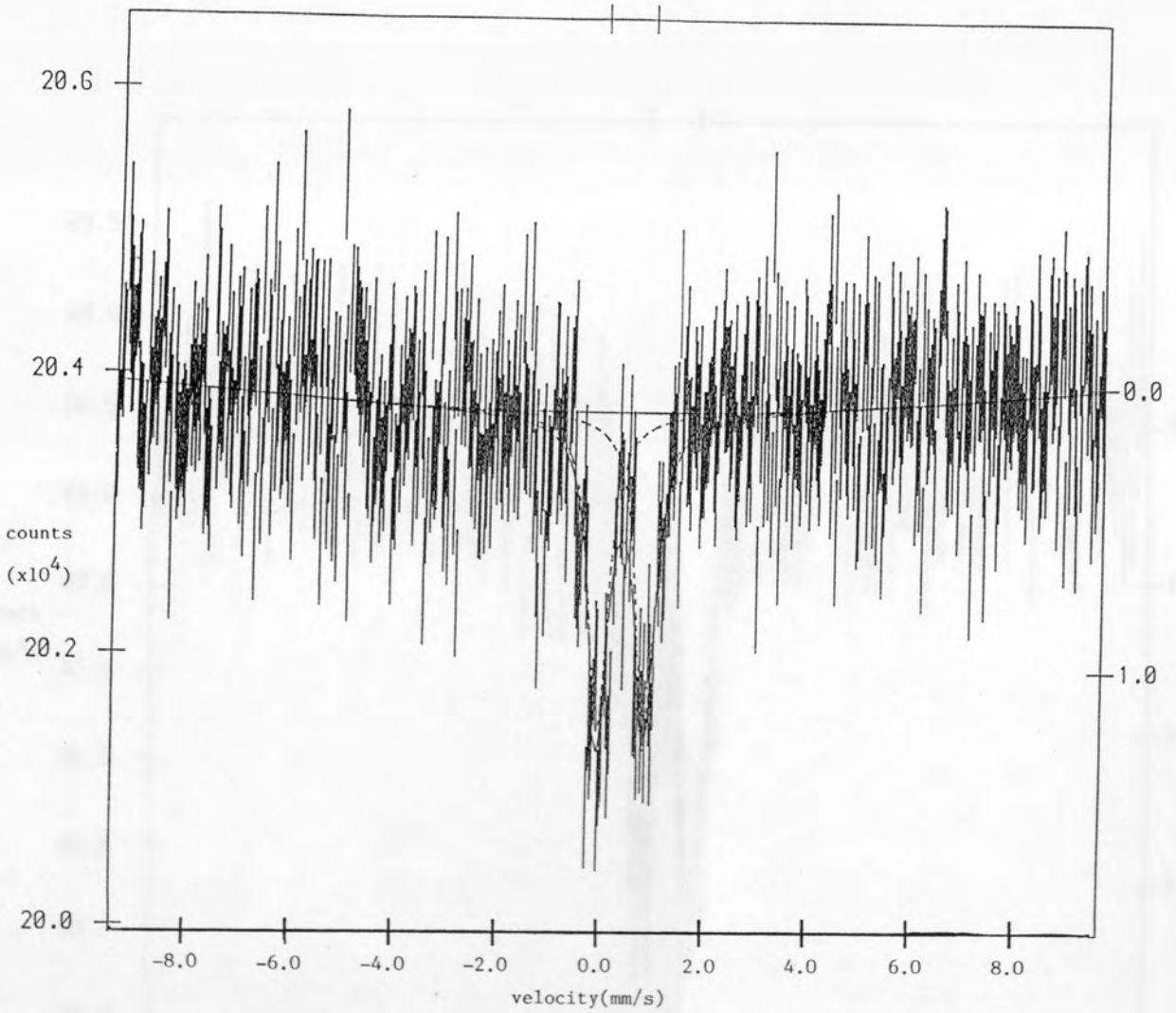

Fig.55 - Room temperature Mössbauer spectrum of Fe^{3+}-hectorite after heating to 400°C

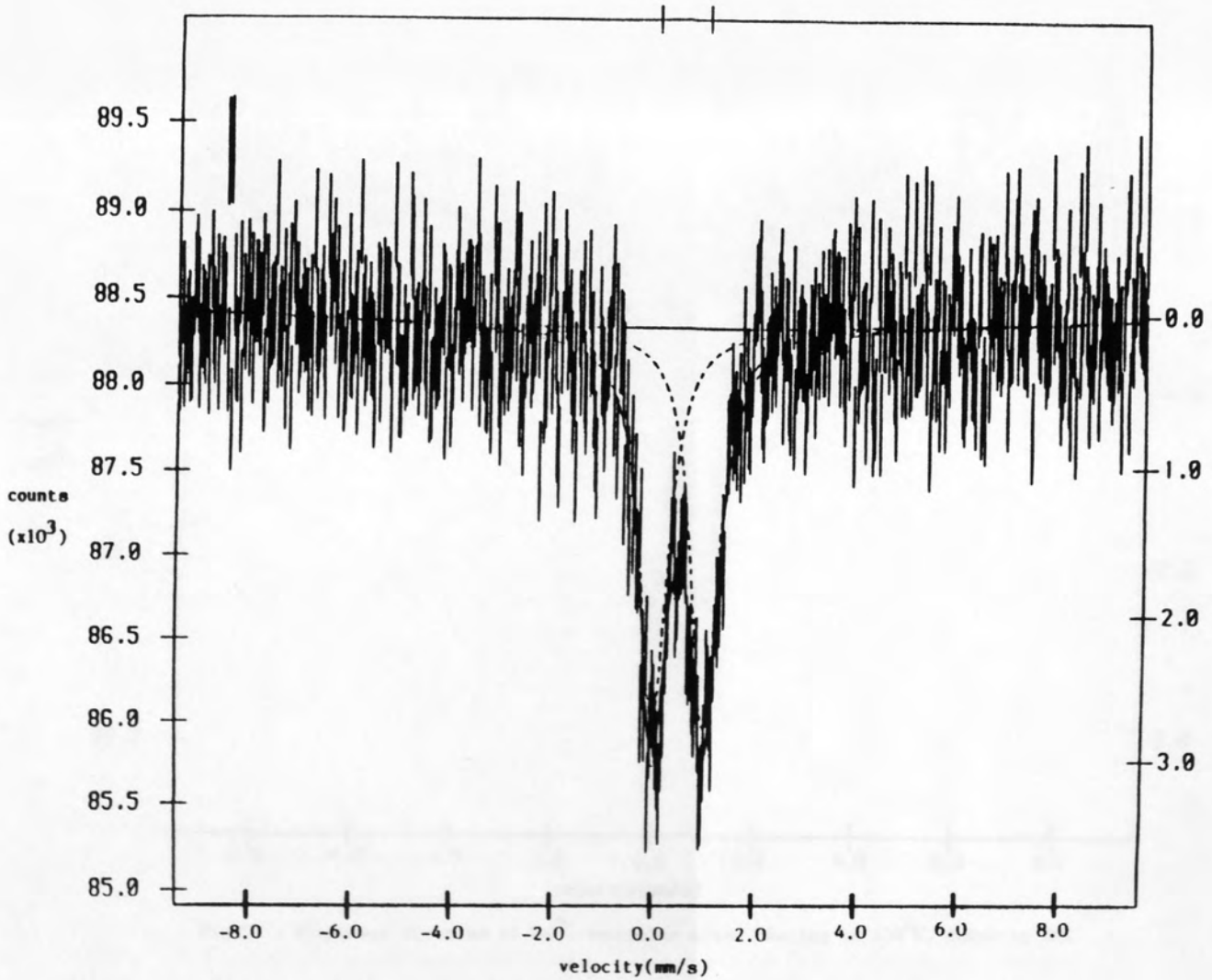

Fig. 56 - Mössbauer spectrum (80K) of Fe^{3+}-hectorite thermally treated at 400°C

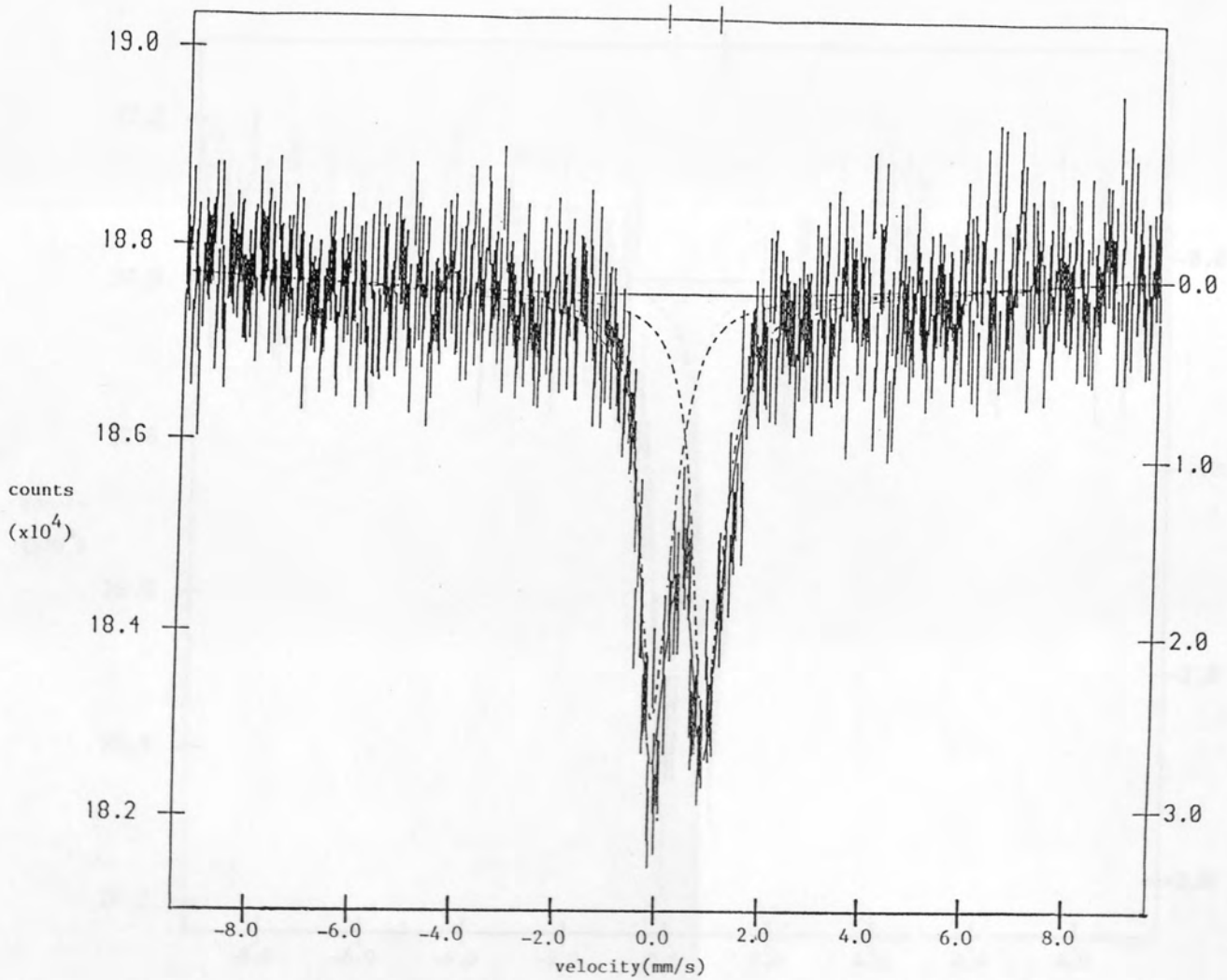

Fig.57 - Mössbauer spectrum of Fe^{2+}-hectorite after heating to 400°C, taken at 80K

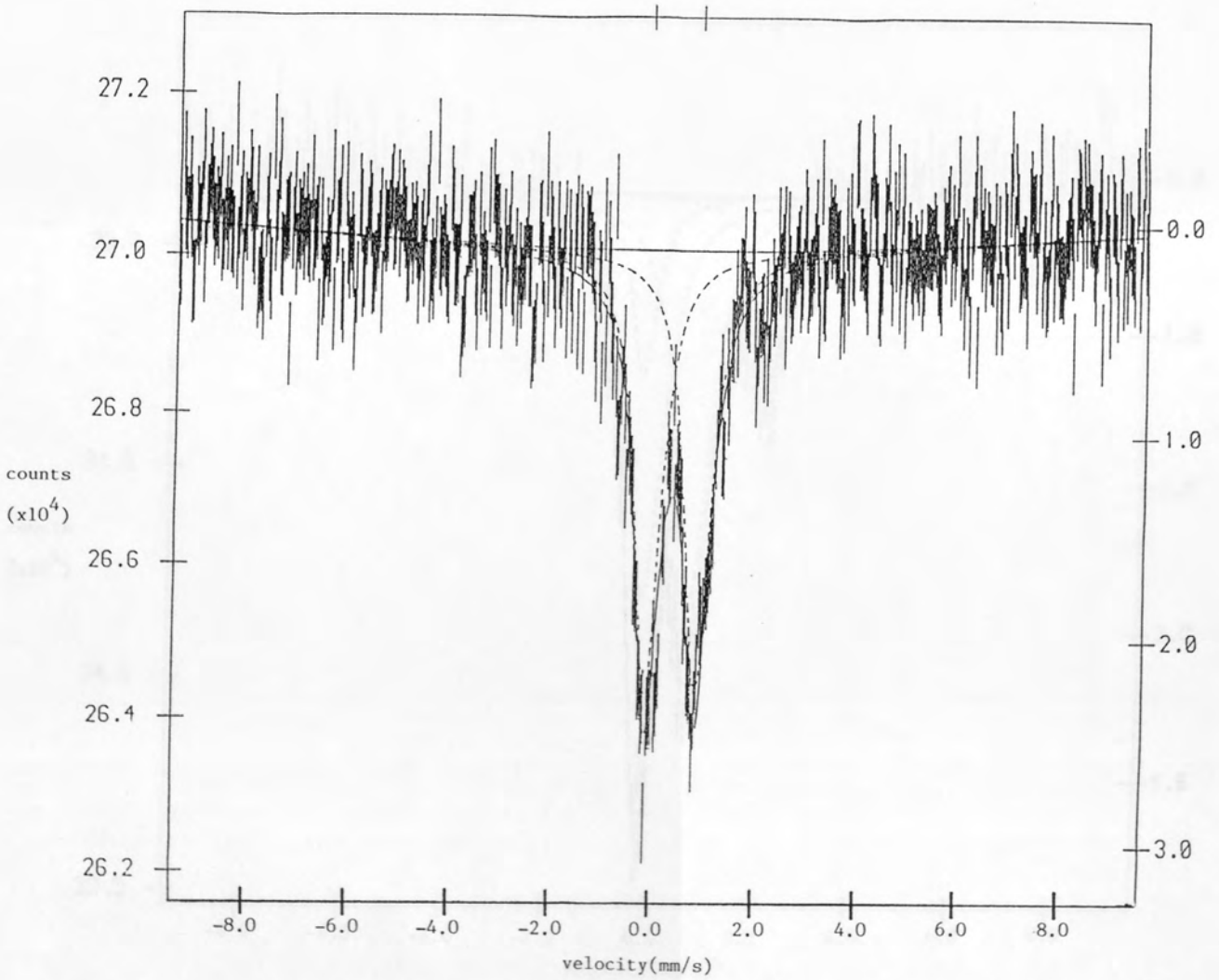

Fig.58 - Room temperature Mössbauer spectrum of Fe^{2+}-hectorite heated to 400°C

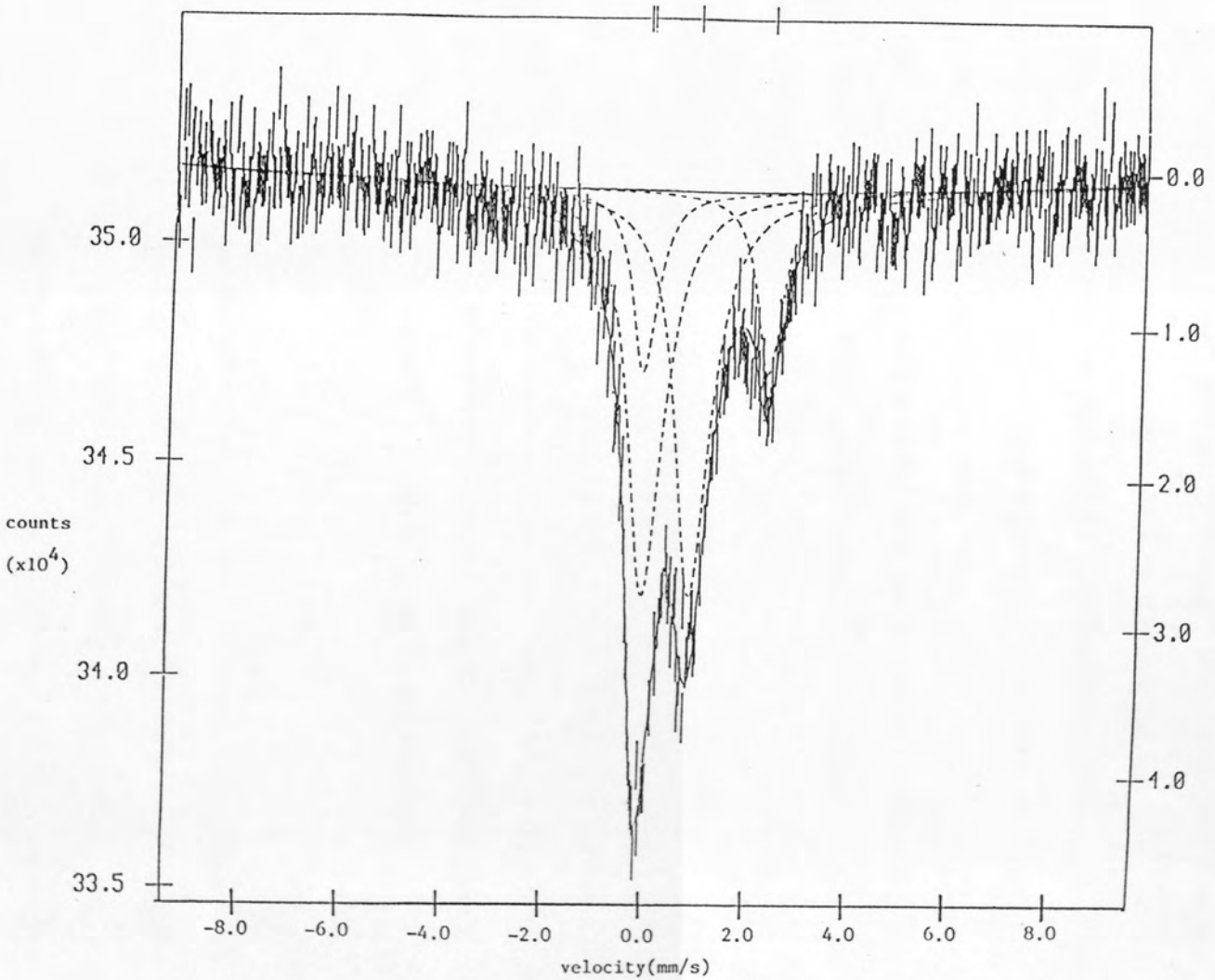

Fig.59 - Room temperature Mössbauer spectrum of $^{57}Fe^{3+}$-hectorite heated to 400°C

After thermal treatment, the clays exhibited the following colours:

Fe^{3+}-hectorite : sand

Fe^{2+}-hectorite : sand

$^{57}Fe^{3+}$-hectorite : grey

5.5 DISCUSSION

Evidence for transition metal sorption on a number of significantly different sites has been obtained in the present study (chapters 3 and 4), and additionally by other workers.[32,36] Previously, X-ray photoelectron spectroscopy, scanning electron microscopy and Mössbauer spectroscopy have been used in mineralogy to study properties of bulk solids, and rarely applied to the characterisation of sorbed species in systems involving clay minerals. Attempts at physical characterisation of transition metal ions sorbed onto montmorillonite and hectorite were therefore made, and initial examination utilized the property of XPS to discriminate chemical environments of atoms from core BE determinations.

X-ray photoelectron spectroscopy

Calibration of the $Si2p_{\frac{1}{2},\frac{3}{2}}$ level (table 98) produced very similar binding energies for the two smectites used here, these values comparing favourably with those obtained for chlorite (102.1eV), illite (102.5eV) and kaolinite (102.7eV) by Koppelman et al.[69]

Co^{2+}-hectorite samples

The X-ray photoelectron spectra of Co-hectorite specimens (section 5.2.2) are shown in figs.60, 61 and 62. Although almost all spectra showed significant $Co2p_{\frac{3}{2}}$ photopeaks, all were quite diffuse and not well defined. This phenomenon was demonstrated in the experimental peak widths, all of which were greater than 3.5eV. However, a significant amount of information on the nature of the sorbed metal

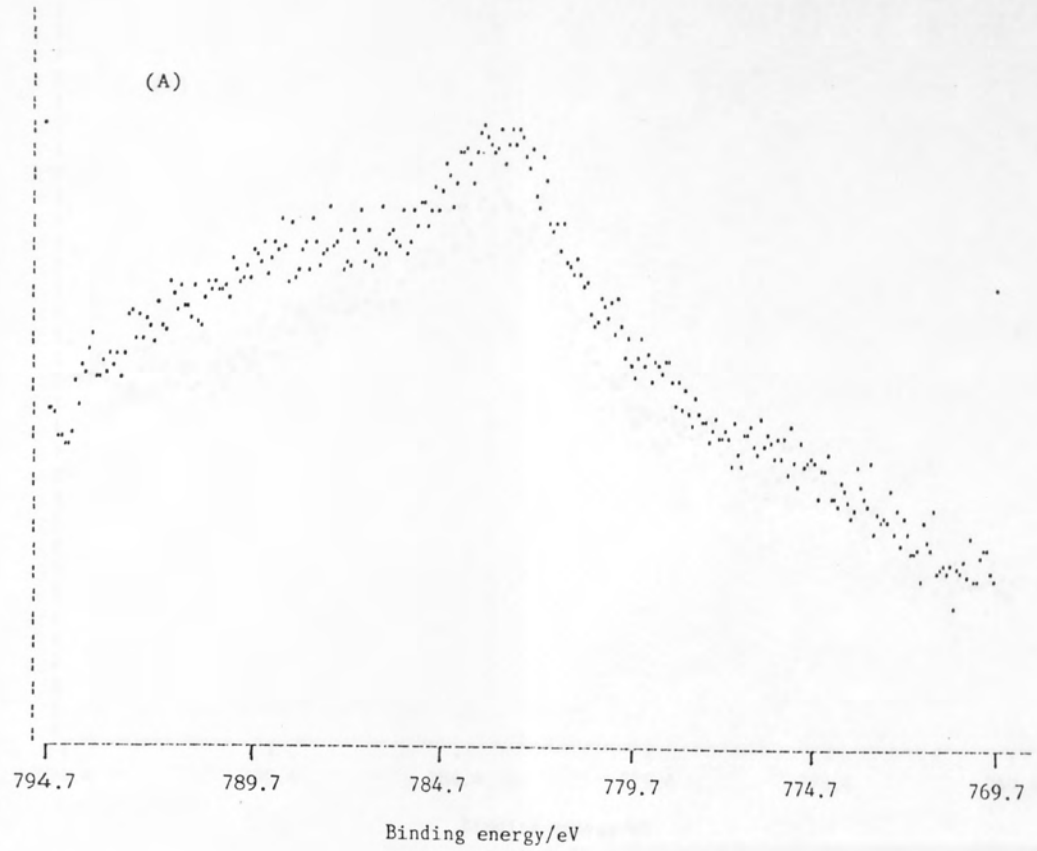

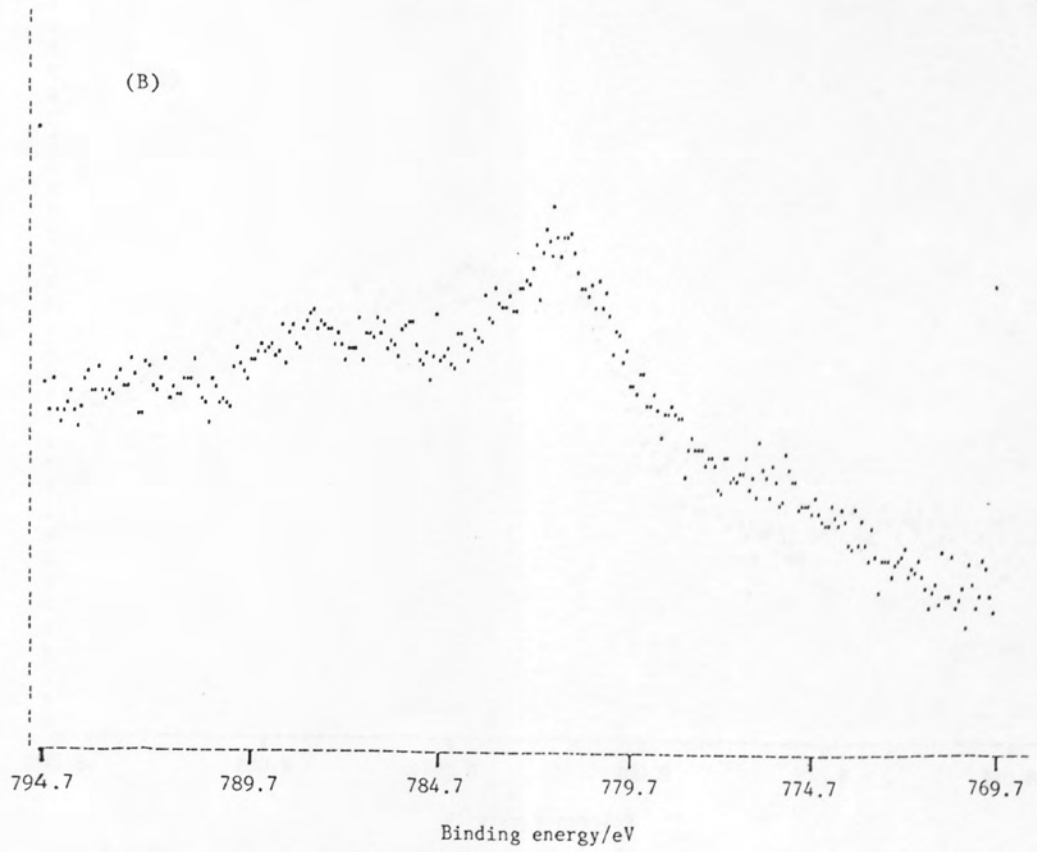

Fig.60 - Co2p binding energy region from XPS spectrum of Co^{2+}-hectorite:
(A) with no ion etching
(B) after 10 mins ion etching

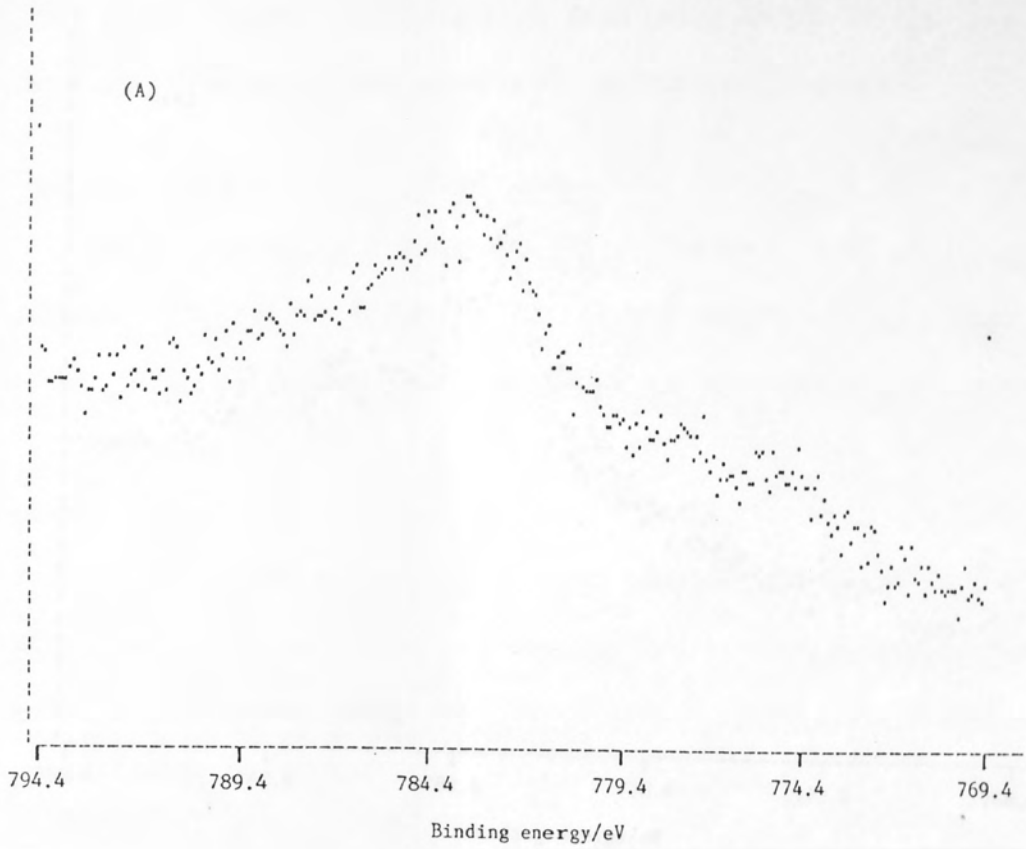

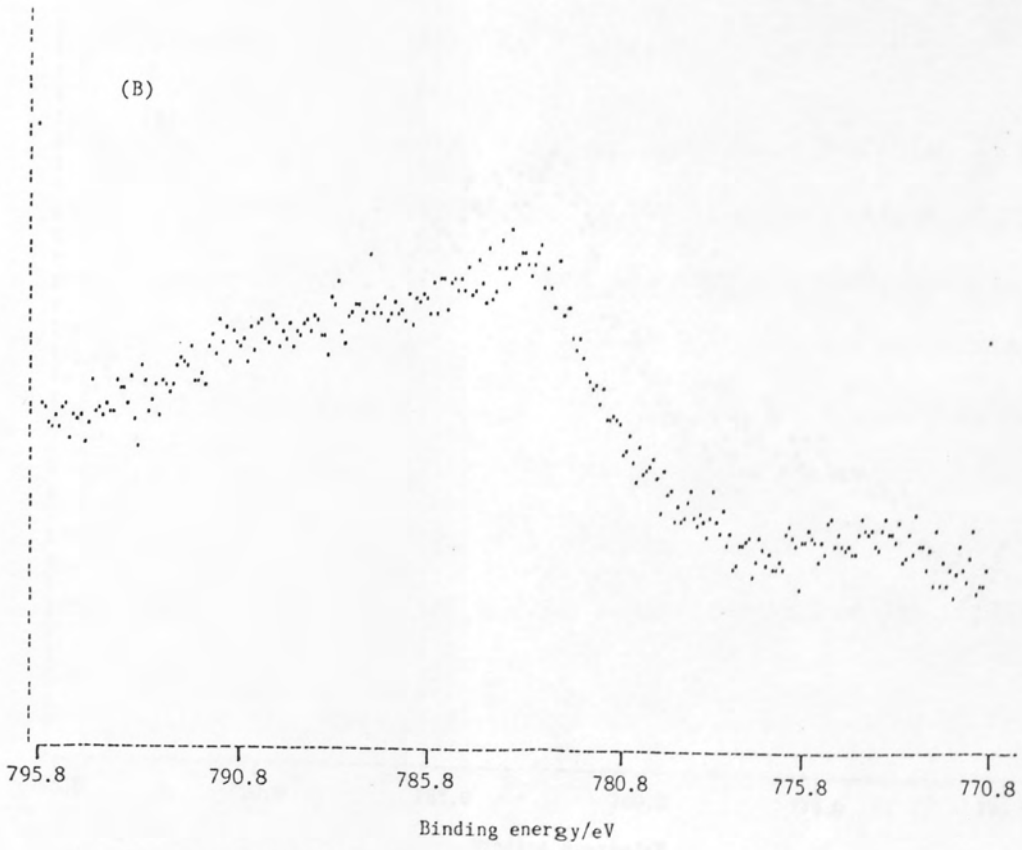

Fig.61 - Co2p region from XPS spectrum of Co^{2+}-hectorite/2 wash:
(A) prior to ion etching
(B) after 10 mins etching

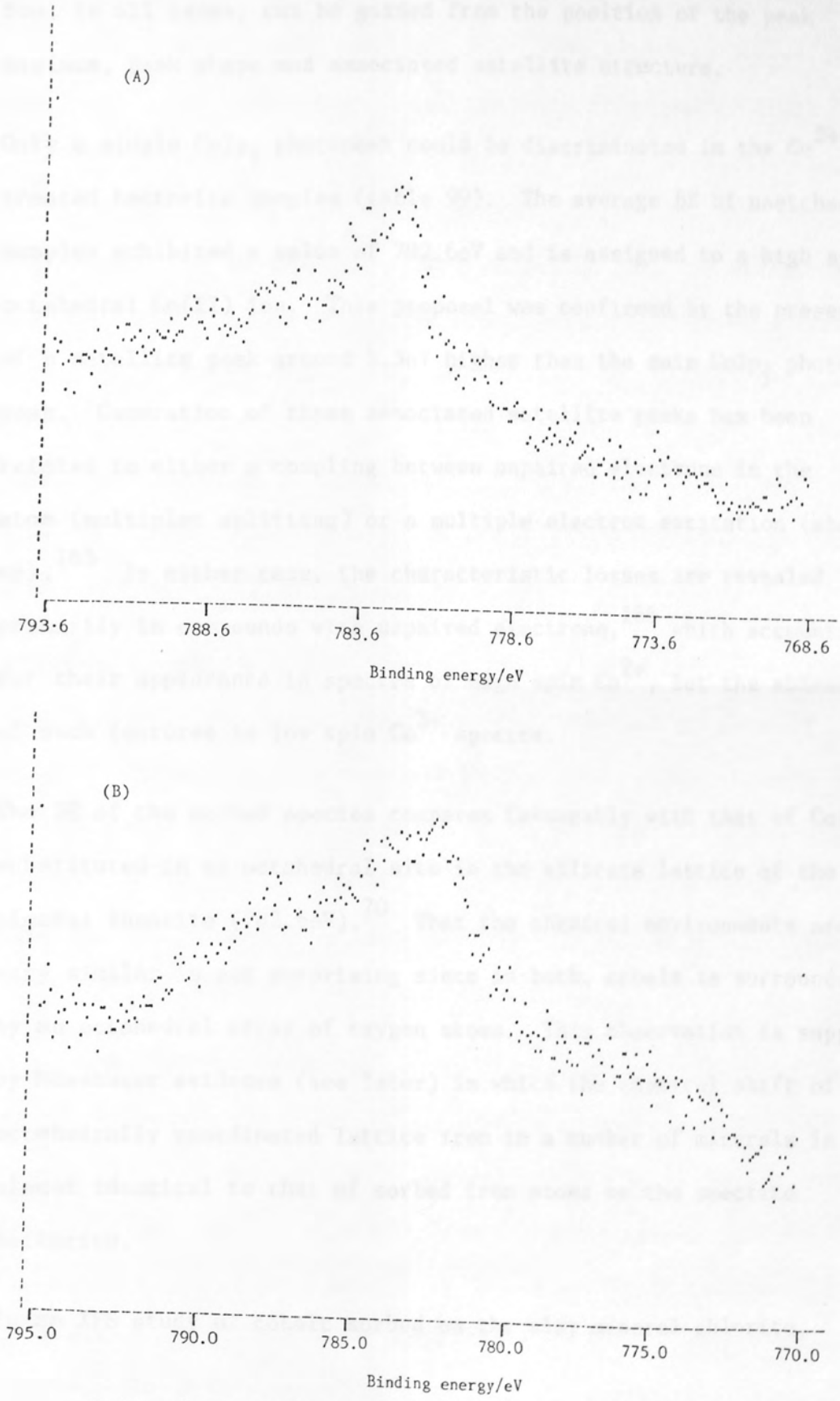

Fig.62 - Co2p region from XPS spectrum of Co^{2+}-hectorite/5 wash
(A) unetched
(B) after 10 mins etching

ion, in all cases, can be gained from the position of the peak maximum, peak shape and associated satellite structure.

Only a single $Co2p_{\frac{3}{2}}$ photopeak could be discriminated in the Co^{2+} treated hectorite samples (table 99). The average BE of unetched samples exhibited a value of 782.6eV and is assigned to a high spin octahedral Co(II) ion. This proposal was confirmed by the presence of a satellite peak around 5.5eV higher than the main $Co2p_{\frac{3}{2}}$ photopeak. Generation of these associated satellite peaks has been related to either a coupling between unpaired electrons in the atom (multiplet splitting) or a multiple electron excitation (shake up).[165] In either case, the characteristic losses are revealed primarily in compounds with unpaired electrons,[166] which accounts for their appearance in spectra of high spin Co^{2+}, but the absence of such features in low spin Co^{3+} spectra.

The BE of the sorbed species compares favourably with that of Co(II) substituted in an octahedral site in the silicate lattice of the mineral lusakite (782.6eV).[70] That the chemical environments are very similar is not surprising since in both, cobalt is surrounded by an octahedral array of oxygen atoms. This observation is supported by Mössbauer evidence (see later) in which the chemical shift of octahedrally coordinated lattice iron in a number of minerals is almost identical to that of sorbed iron atoms on the smectite hectorite.

In an XPS study of cobalt sorbed on the clay mineral chlorite,

Koppelman et al[70] reported a BE of 782.0eV for Co^{2+} sorbed from a solution with initial pH of 6. The concomitant observation of a satellite peak led them to assign the $Co2p_{\frac{3}{2}}$ photopeak to $[Co(H_2O)_6]^{2+}$. However, although this appears to support our proposal, Koppelman et al suggested that the lowering in $Co2p_{\frac{3}{2}}$ BE with respect to that in lusakite may be due to the contribution of negative charge at the sorption site, and compared this effect with a similar BE lowering observed for chromium and iron sorbed onto other clays. The interaction of Co(II) with illite has been studied by XPS,[91] the data again pointing to the sorption of an aqueous Co(II) species at pH6. A similar lowering in BE of the Co(II) with respect to lusakite was observed by Dillard et al.[91]

Previous workers have reported that adsorption of Co(II) on metal oxides yielded surface cobalt hydroxide[71] and that sorption of Co(II) onto various clay minerals at a pH greater than 7, also led to the formation of the hydroxide.[91] No evidence for cobalt hydroxide (BE = 781.0[165]) or Co(III), manifested when Co(II) was adsorbed onto hydrous manganese dioxide in a study by Murray et al,[72] was apparent in the present investigation.

Successive washing of the parent Co^{2+}-hectorite clay appeared to have little effect on the chemical environment of the sorbed species (table 99), but did lower the intensity of the $Co2p_{\frac{3}{2}}$ peak somewhat, inferring the removal of cobalt from surface sorption sites on the clay with a concurrent diminishing of the photopeak intensity. This effect demonstrates the sensitivity of XPS to surface composition. Although incident photons may penetrate the sample to a considerable

depth, the escape depth of photoejected electrons is generally less than 50Å,[167] depending on the energy of the incident radiation, the kinetic energy of the ejected electron, the crystallinity and density of the sample material, but electrons emanating closer to the sample surface have a higher probability of being detected without having undergone inelastic collisions with surrounding atoms.[168]

The application of ion etching to depth profile the Co^{2+}-hectorite samples appeared to be quite uninformative as both BE of the $Co2p_{\frac{3}{2}}$ peak and intensity remained about the same (table 99, figs.60, 61, 62). However, it must be noted that a consistent decrease (0.4eV) in the BE of cobalt on etched samples was apparent and signified an alteration in the nature of the sorbed transition metal ion. This effect, though, was likely a function of the etch beam, since chemical alteration of surface speciation due to this process has previously been reported.[169] The similarity in intensity of the $Co2p_{\frac{3}{2}}$ photopeak before and after etching is suggestive of a quite homogeneous distribution of Co^{2+} in the samples studied.

All Co^{2+} treated hectorite samples exhibited a FWHM of at least 3.5eV. Although this is quite a large photopeak width, Dillard et al[91] were unable to gain any acceptable data from the very broad XPS signal of Co(II) sorbed onto illite at pH5. This is likely a result of the higher cation exchange capacity of hectorite which gives rise to an enhanced uptake of Co(II) and thus a stronger $Co2p_{\frac{3}{2}}$ photopeak. In an attempt to resolve the broad $Co2p_{\frac{3}{2}}$ photopeaks computer fitting of the data was attempted. The results of fitting

a single $Co2p_{\frac{3}{2}}$ peak with associated satellite and of fitting two $Co2p_{\frac{3}{2}}$ peaks with two shake up peaks to the spectrum obtained for unetched Co^{2+}-hectorite are displayed in fig.63. Although the two peak fit did correlate closely with the data, the validity of the technique must be in doubt as such parameters as main photopeak: satellite peak ratio, peak height, FWHM, peak shape (i.e. Gaussian/ Lorenztian mix) and peak tailing are all difficult to estimate. The computing procedure may then simply become a fitting of peaks to the data by alteration of the appropriate parameters, with no physical reality. Peak deconvolution was successfully employed by Seyama et al[23] on spectra from a Mg^{2+} treated montmorillonite. A broad (FWHM 4eV) Mgls signal was deconvoluted to two peaks, one ascribed to exchangeable magnesium and the other to non-exchangeable magnesium. This procedure was feasible as the position of non-exchangeable, lattice magnesium had previously been established from XPS examination of the parent montmorillonite before Mg^{2+} ion saturation. In the present investigation no peak positions could be established before the sorption process and further complication arose from the appearance of satellites in the transition metal ion spectra. It was concluded that peak deconvolution could not be employed as a scientifically sound practice.

Despite the unsuitability of peak deconvolution techniques (the results of which cannot be totally discounted as being a true representation) a number of mechanisms may be responsible for peak broadening. Adams et al[170] noted that charging of insulating samples may artificially broaden photopeaks. This may well affect spectra

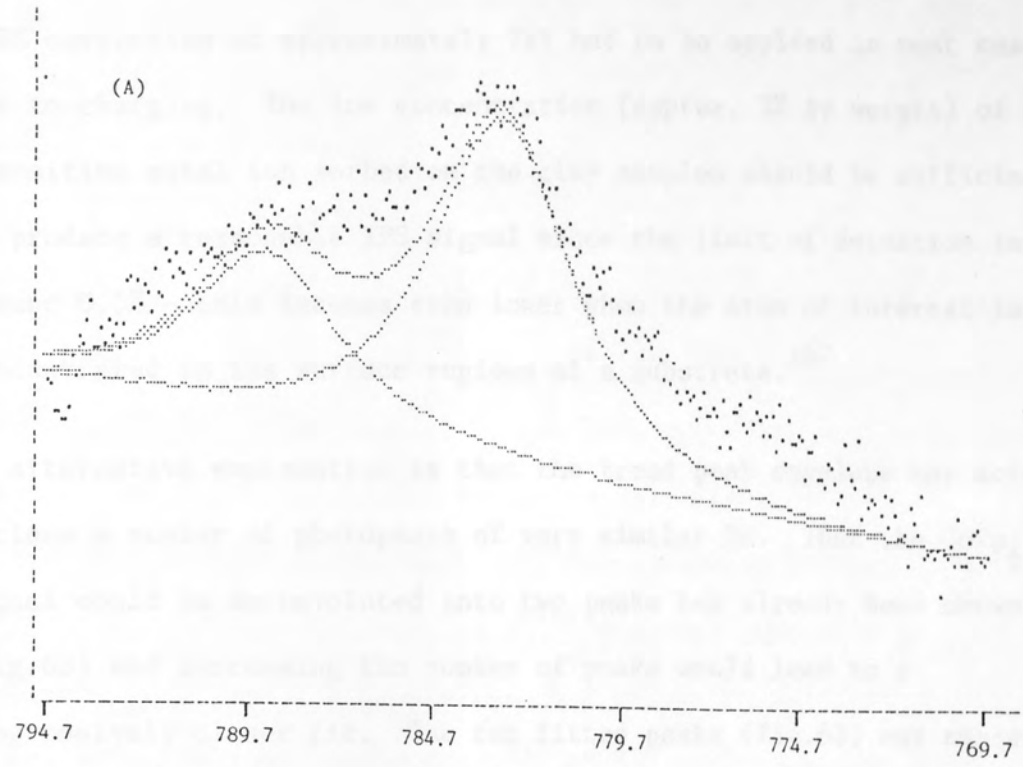

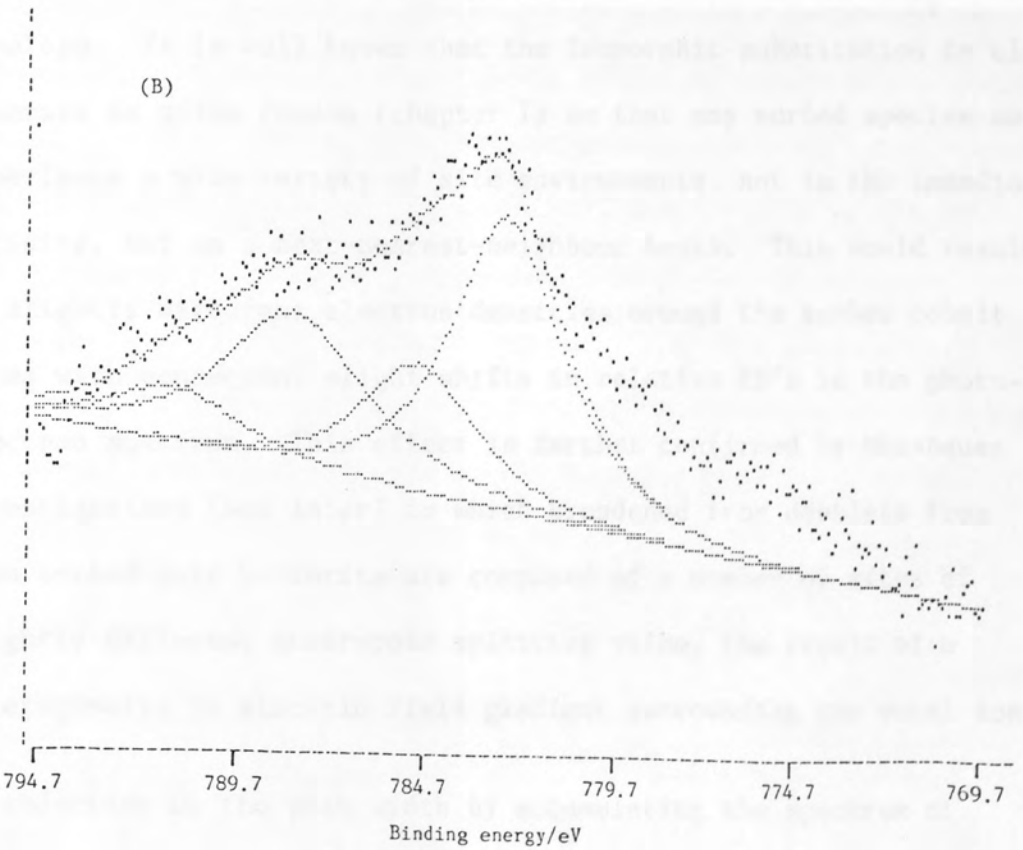

Fig.63 - Co2p photopeak from Co^{2+}-hectorite computer fitted to:
(A) 2 peaks
(B) 4 peaks

from the non-conductive clay samples used in this investigation - a BE correction of approximately 7eV had to be applied in most cases, due to charging. The low concentration (approx. 2% by weight) of transition metal ion sorbed on the clay samples should be sufficient to produce a reasonable XPS signal since the limit of detection is around 0.5% - this becomes even lower when the atom of interest is concentrated in the surface regions of a substrate.[167]

An alternative explanation is that the broad peak envelope may actually enclose a number of photopeaks of very similar BE. That the $Co2p_{\frac{3}{2}}$ signal could be deconvoluted into two peaks has already been shown (fig.63) and increasing the number of peaks would lead to a progressively closer fit. The two fitted peaks (fig.63) may represent the extremes of BE values actually enclosed in the $Co2p_{\frac{3}{2}}$ envelope. It is well known that the isomorphic substitution in clay minerals is quite random (chapter 1) so that any sorbed species may experience a wide variety of site environments, not in the immediate vicinity, but on a next-nearest-neighbour basis. This would result in slightly different electron densities around the sorbed cobalt atoms with consequent slight shifts in relative BE's in the photoelectron spectrum. This effect is further confirmed by Mössbauer investigations (see later) in which broadened iron doublets from iron sorbed onto hectorite are composed of a number of sites of slightly different quadrupole splitting value, the result of a heterogeneity in electric field gradient surrounding the metal ions.

No reduction in the peak width by accumulating the spectrum of

Co^{2+}-hectorite for 16 hours was evident, which lends further support to the above hypothesis.

Ni^{2+}-hectorite samples

The X-ray photoelectron spectra of nickel treated hectorite specimens are shown in figs.64, 65 and 66. BE data from the unetched specimens revealed a $Ni2p_{\frac{3}{2}}$ photopeak at 857.4eV (table 100), with an associated satellite around 6.5eV higher. In an XPS study of a series of nickel compounds by Tolman et al,[171] it was established that divalent nickel ions exhibit a characteristic $Ni2p_{\frac{3}{2}}$ peak in the region 854.9-857.4eV. Also Matienzo et al[172] proposed that BE's in the range 855.0-857.5eV are consistent with octahedrally coordinated Ni(II) as opposed to tetrahedral (853.9-855.4eV) or square planar (852.9-855.3eV) geometry. The BE values therefore indicated the presence of sorption sites comprising Ni(II) in octahedral coordination. The high spin d^8 Ni^{2+} ion is paramagnetic and as a consequence exhibited a satellite peak (figs.64, 65, 66). The BE of the sorbed species compares favourably with the value of 857.5eV measured for the hexaaquo Ni^{2+} ion as the sulphate.[172] The XPS data demonstrated, therefore, that the Ni^{2+} ion is sorbed as an aquated species on the surface of hectorite, perhaps as the hexaaquo ion.

The $Ni2p_{\frac{3}{2}}$ BE was close to that of octahedrally coordinated Ni^{2+} (857.0eV) in the silicate structure lizardite.[51] The chemical environments are therefore quite similar, as was the case with the Co^{2+}-hectorite system (see earlier). Comparison with Koppelman et al's[51] data for Ni(II) sorbed onto the mineral chlorite reveals a distinct 0.8eV lower BE in the latter case. They concluded that

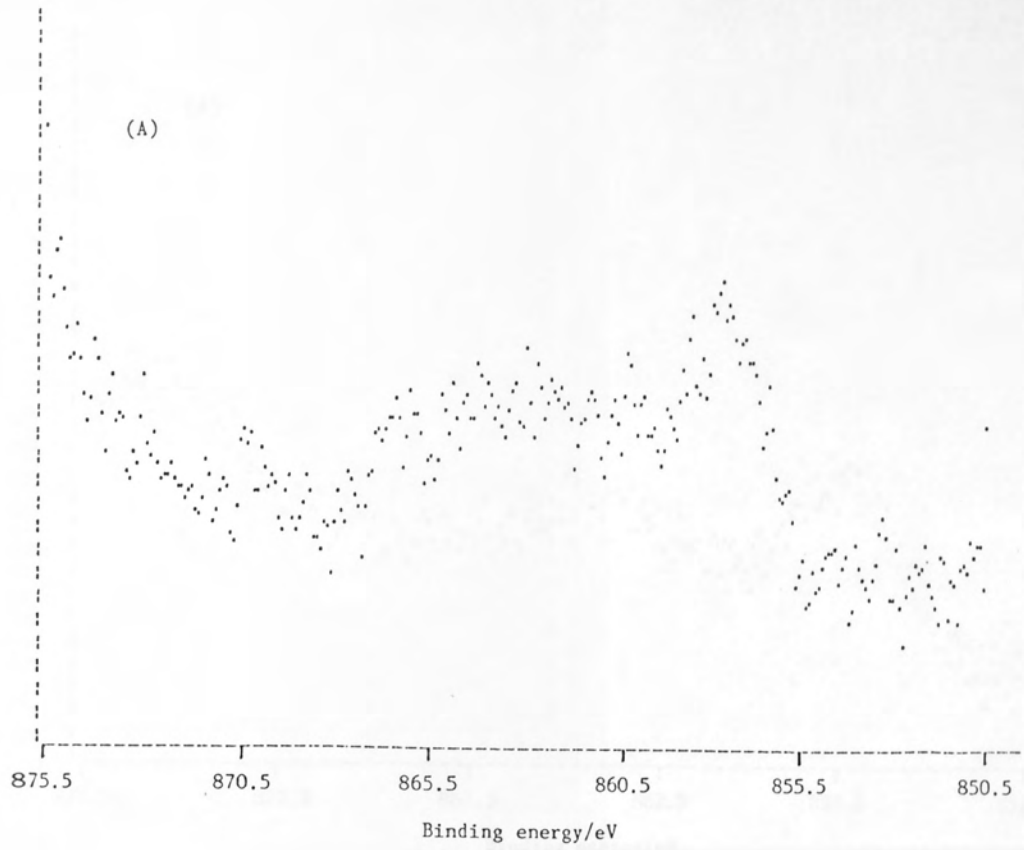

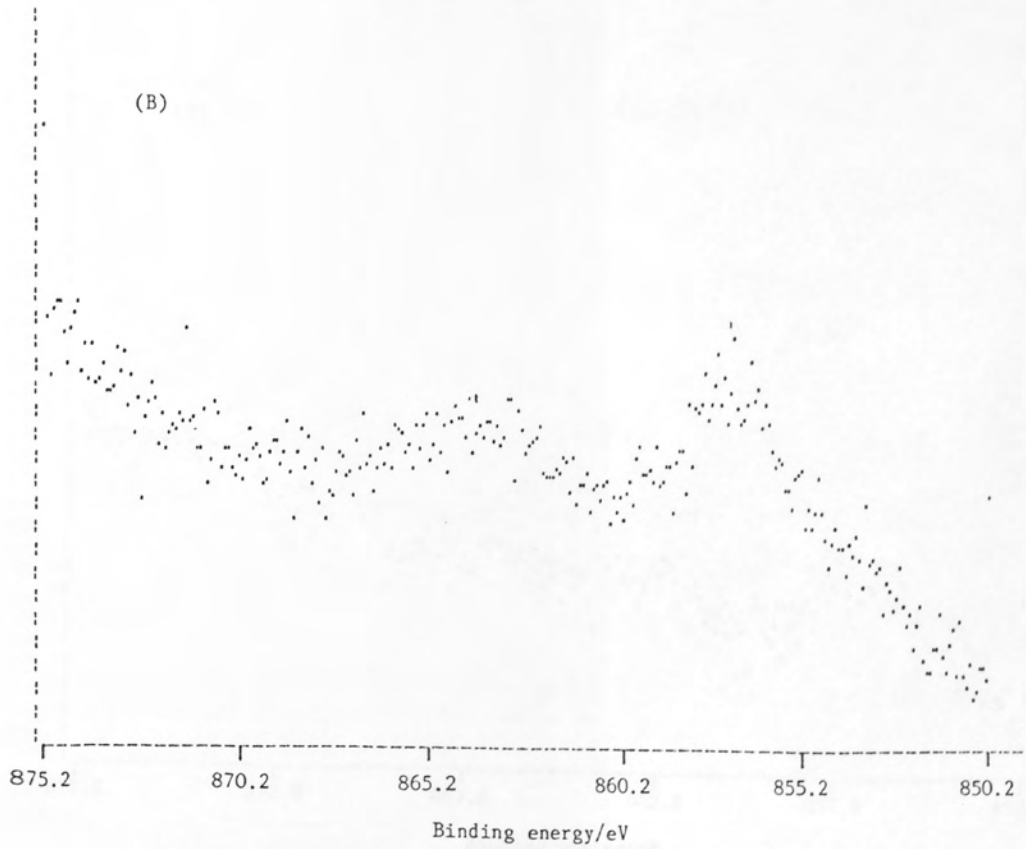

Fig.64 - Ni2p region from XPS spectrum of Ni^{2+}-hectorite: (A) with no ion etching
(B) after 5 mins etching

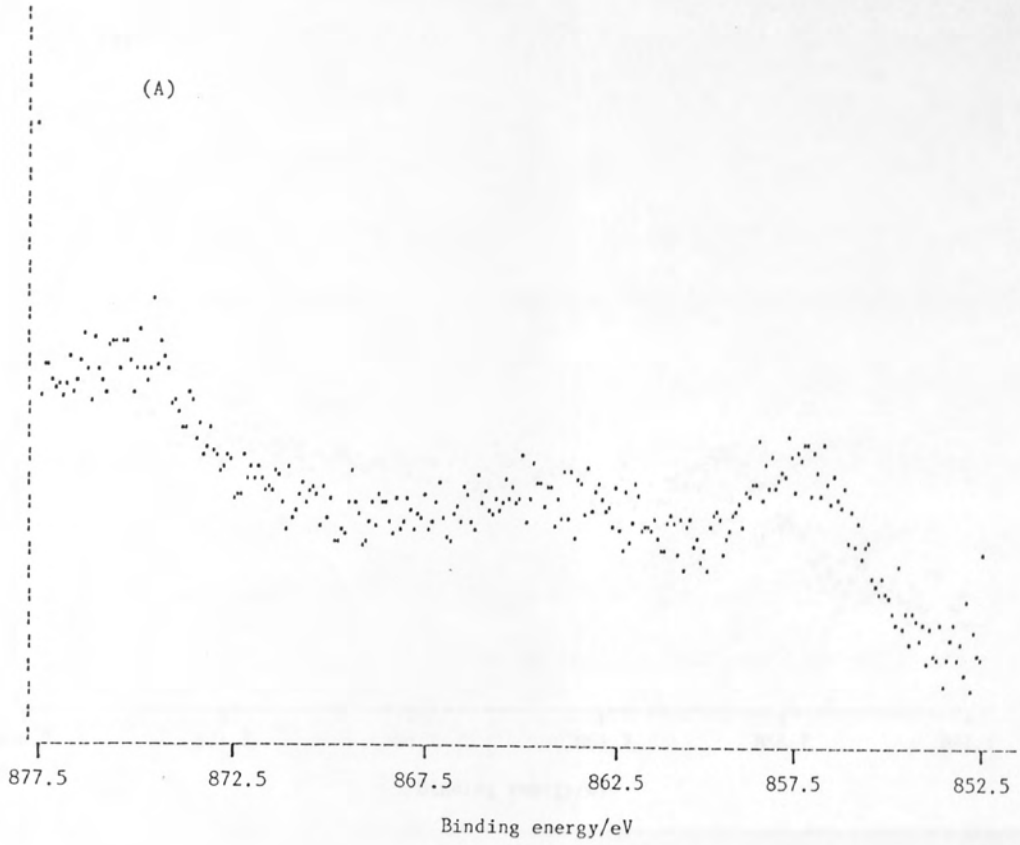

Fig.65 - Ni2p binding energy region from Ni^{2+}-hectorite/2 wash:
(A) unetched
(B) after 5 mins ion etching

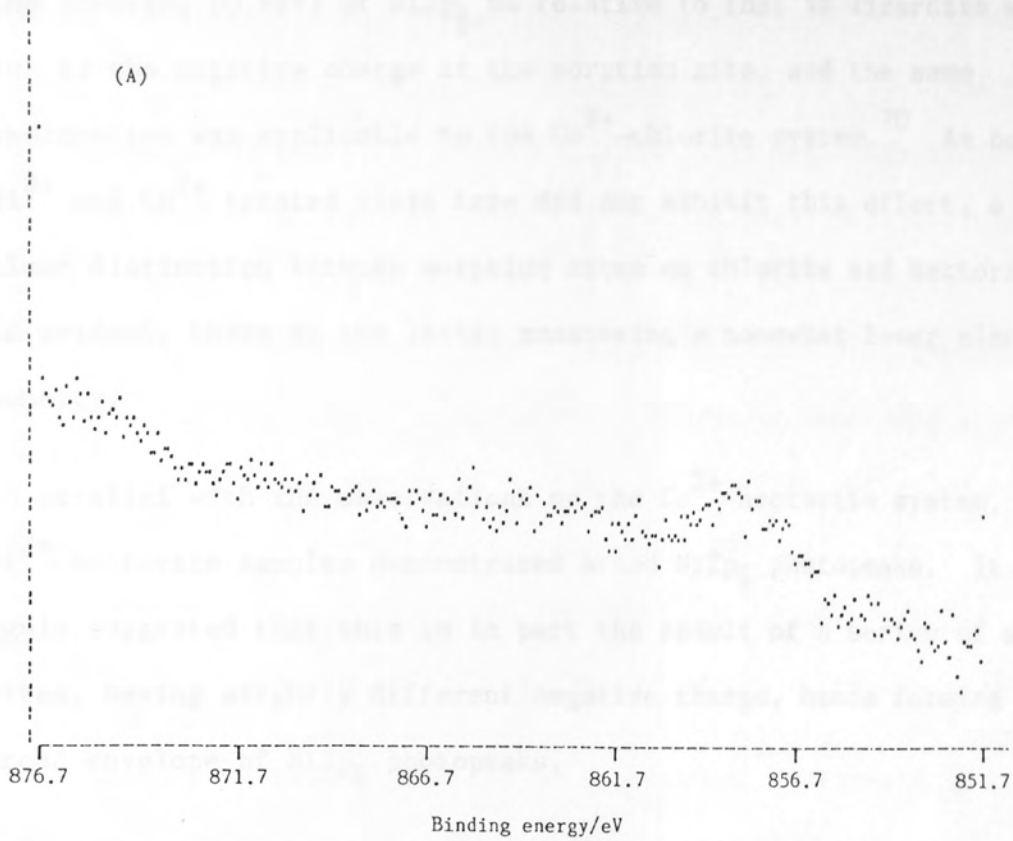

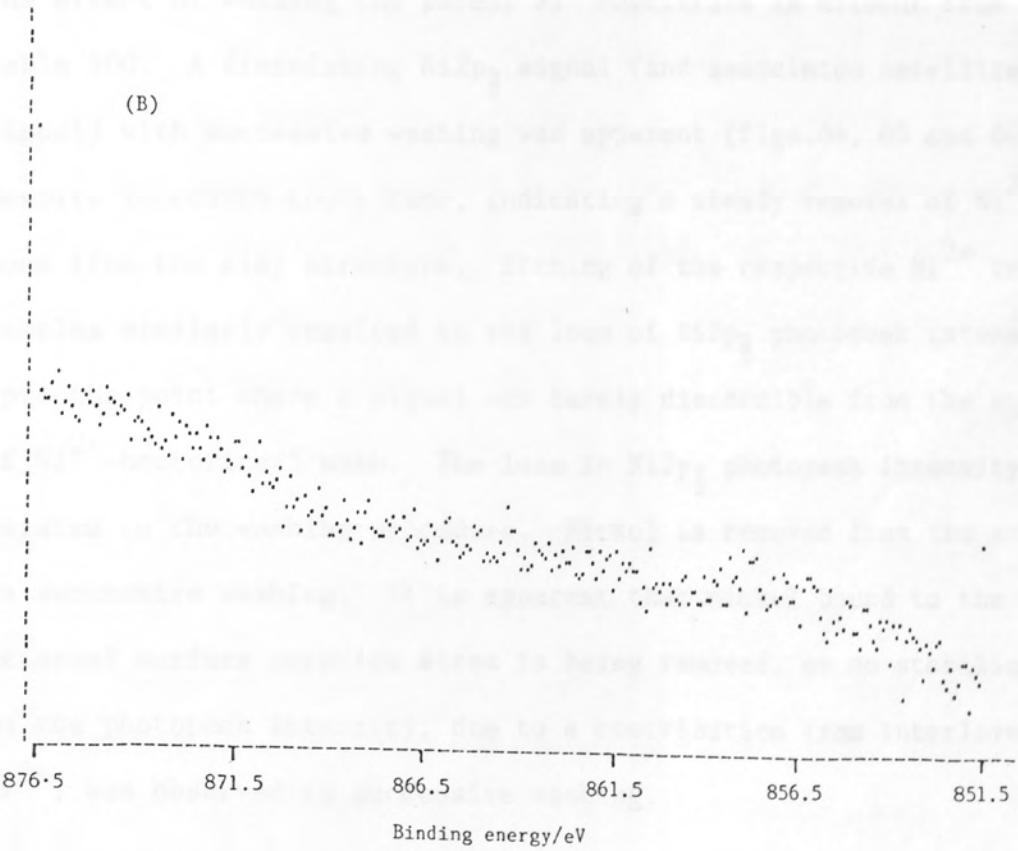

Fig.66 - Ni2p region of XPS spectrum from Ni^{2+}-hectorite/5 wash:
(A) unetched
(B) after 5 mins etching

the lowering (0.4eV) of $Ni2p_{\frac{3}{2}}$ BE relative to that in lizardite was due to the negative charge at the sorption site, and the same explanation was applicable to the Co^{2+}-chlorite system.[70] As both Ni^{2+} and Co^{2+} treated clays here did not exhibit this effect, a clear distinction between sorption sites on chlorite and hectorite is evident, those on the latter possessing a somewhat lower electron density.

In parallel with the observations on the Co^{2+}-hectorite system, all Ni^{2+}-hectorite samples demonstrated broad $Ni2p_{\frac{3}{2}}$ photopeaks. It is again suggested that this is in part the result of a series of sorption sites, having slightly different negative charge, hence forming a broad envelope of $Ni2p_{\frac{3}{2}}$ photopeaks.

The effect of washing the parent Ni^{2+}-hectorite is evident from table 100. A diminishing $Ni2p_{\frac{3}{2}}$ signal (and associated satellite signal) with successive washing was apparent (figs.64, 65 and 66) despite increased count time, indicating a steady removal of Ni^{2+} ions from the clay structure. Etching of the respective Ni^{2+} treated samples similarly resulted in the loss of $Ni2p_{\frac{3}{2}}$ photopeak intensity, upto the point where a signal was barely discernible from the spectrum of Ni^{2+}-hectorite/5 wash. The loss in $Ni2p_{\frac{3}{2}}$ photopeak intensity is related to the washing procedure. Nickel is removed from the sorbent on successive washing. It is apparent that nickel bound to the external surface sorption sites is being removed, as no stabilisation in the photopeak intensity, due to a contribution from interlayer Ni^{2+}, was observed on successive washing.

Further confirmation was gained from the etched samples in which the $Ni2p_{\frac{3}{2}}$ photopeak decreased relative to the parent clays due to the displacement of nickel sorbed externally on the clay particles, but still showed no indication of a photopeak from interlayer Ni^{2+}. The electron escape depth appears critical here, as those electrons ejected from interlayer Ni^{2+} ions (approx. 10Å away from the surface) are unable to contribute appreciably to the $Ni2p_{\frac{3}{2}}$ photopeak intensity. This is likely not a result of a relatively low concentration of interlamellar Ni^{2+} ions, but, as mentioned previously, the small electron escape depth of surface species allows their detection. The surface sensitivity of XPS is clearly demonstrated.

Three sites for cation sorption were postulated in chapter 3, one interlayer and two on external surfaces - one involving cation interaction with broken bonds and one through an anion-cation pair mechanism. The present XPS information provides evidence for the latter two mechanisms, as the loss in $Ni2p_{\frac{3}{2}}$ photopeak intensity on washing is likely related to the loss of 'labile' nickel sorbed by the anion-cation pair mechanism. The residual signal after the sequence of 5 washings may be assigned to nickel on broken bond sites.

Some loss in $Co2p_{\frac{3}{2}}$ photopeak intensity with successive washing (figs.60, 61 and 62) was observed in the Co^{2+} treated hectorite clays, but not as dramatically as with the Ni^{2+} treated system. Co^{2+} appears to be more strongly bound to the hectorite surface than Ni^{2+}. This fundamental contrast in bonding nature may be

related to the difference in BE of the respective transition metal $2p_{\frac{3}{2}}$ peak of the treated clays and that of octahedrally coordinated structural M^{2+} in lizardite or lusakite. The BE of cobalt in Co^{2+}-hectorite is the same as that for the metal in lusakite, whereas that of nickel in Ni^{2+}-hectorite is 0.4eV higher. This represents a relatively lower contribution of the negative charge at the surface sorption sites in the case of the Ni^{2+} ions.

Although two sorption sites have been recognised by the XPS data on hectorite, metal ions bound in the interlayer region could not be discriminated.

Further XPS investigations were performed on the mineral montmorillonite, after exchange with a nickel chloride solution. To gain additional information on the nature of metal-clay bonding, the Ni^{2+}-montmorillonite was treated with a number of washing cycles and probed using ion etching (section 5.2.4).

Nickel chloride-montmorillonite samples

$Ni2p_{\frac{3}{2}}$ BE's for unetched nickel chloride treated montmorillonite* specimens were similar, averaging a value of 856.3eV (table 101). Each sample demonstrated a satellite peak at around 6eV higher than the main photopeak. As surmised from the Ni^{2+}-hectorite study, the XPS parameters are indicative of divalent nickel in octahedral coordination.[171,172] However, the average binding energy of the

*'Steetly' montmorillonite, as opposed to 'Berkbond' montmorillonite was used throughout the XPS studies.

$NiCl_2$-montmorillonite samples is significantly lower, but does conform closely with that of Ni^{2+} sorbed onto chlorite (856.6eV), reported by Koppelman et al.[51] Neither NiO or $Ni(OH)_2$ demonstrate BE's close to that observed here,[165] so are absent on the clay surface, and the $Ni2p_{\frac{3}{2}}$ BE is significantly different from that of structural nickel in lizardite.[51] In accord with Koppelman et al,[51] and data from the transition metal-hectorite clays, the sorption of Ni^{2+} as an aquated species is postulated.

Broad $Ni2p_{\frac{3}{2}}$ photopeaks were again attributed in part to the presence of a number of bonding sites of slightly different electron density.

Successive washing of the parent $NiCl_2$-montmorillonite was effective in reducing the intensity of the $Ni2p_{\frac{3}{2}}$ photopeak, but not to the extent observed with Ni^{2+}-hectorite. This is again attributed to the displacement of Ni^{2+} bound to the external clay surface, but as in the Co^{2+}-hectorite system, stronger bonding is apparent. The fundamental difference in the bonding nature of Ni^{2+} on montmorillonite and hectorite is clearly reflected in the respective BE's which differ by 1.3eV. An enhanced affinity of Ni^{2+} for the surface of montmorillonite is thus evident, the sorption sites possessing marginally greater electron density.

Argon ion etching was responsible for the generation of a second $Ni2p_{\frac{3}{2}}$ peak in some of the $NiCl_2$-montmorillonite samples (table 101). On each occasion this peak was observed at a BE around 4eV lower than the original $Ni2p_{\frac{3}{2}}$ signal, both peaks appearing in a number of spectra. As well as a loss in overall $Ni2p_{\frac{3}{2}}$ photopeak intensity,

a deterioration in satellite intensity was associated with an increased contribution from the lower BE peak, dismissing the possibility that octahedrally or tetrahedrally coordinated Ni(II)[172] was the responsible species. This leaves open the possibility that an alternative, perhaps interlayer, bonding site with Ni^{2+} in square planar coordination, may be responsible for the new signal. As the surface material (and surface Ni^{2+}) was etched away, an increased photopeak contribution from interlayer Ni^{2+} would develop. However, the favoured explanation is that Ni^{2+} is reduced to nickel metal by the ion beam. This is endorsed by the concomitant loss in satellite intensity. That ion etching often affects the nature of analysed transition metal ions is a well documented phenomenon. The photoreduction of Cu^{2+} to Cu^{+} in an XPS study of tetrahydrofuran intercalation on a Cu^{2+}-montmorillonite, was reported by Adams et al.[149] An average BE of 853.1eV was observed for the reduced nickel species in the 30 min etch samples, which closely resembles the value of 852.9eV reported by Kim et al[169] for nickel metal. The absence of a similar low BE peak on etching of Ni^{2+}- and Co^{2+}-hectorite samples dismisses the possibility that interlayer Ni^{2+} is responsible for this phenomenon. It is important to recognize that BE's of Ni^{2+} and Co^{2+} on hectorite decreased with ion etching pointing perhaps to reduction of a small concentration of surface cation or only a partial reduction.

Nickel sulphate-montmorillonite samples

The inability to deconvolute the $Ni2p_{\frac{3}{2}}$ photopeak into contributions from distinct sorption sites, prompted the XPS investigation of a

nickel sulphate treated montmorillonite (table 102).

The average $Ni2p_{\frac{3}{2}}$ binding energy of the three $NiSO_4$-montmorillonite samples before etching was 856.2eV, comparable with that from $NiCl_2$-montmorillonite samples prior to etching. The presence also of an associated satellite led to the conclusion that aquated Ni^{2+} was sorbed onto the montmorillonite surface. Again it would appear that the lowering in BE relative to Ni(II) in lizardite is a consequence of the negative charge at sorption sites. In parallel with the previous investigations, the breadth of $Ni2p_{\frac{3}{2}}$ photopeaks is thought to originate from both sample charging and the existence of a series of bonding sites of slightly different binding energies.

The effect of washing was simply to reduce the intensity of the $Ni2p_{\frac{3}{2}}$ photopeak - no shift in BE was noticeable. As previously stated, this is a result of the loss of surface sorbed Ni^{2+} ions. As with the $NiCl_2$-montmorillonite system a significant $Ni2p_{\frac{3}{2}}$ signal (hence Ni^{2+} concentration) remained after 5 successive washings. This is at variance with Ni^{2+}-hectorite, the difference in the nature of bonding being reflected in the dissimilar $Ni2p_{\frac{3}{2}}$ BE values.

Ion etching of $NiSO_4$-montmorillonite samples revealed a second, lower BE, $Ni2p_{\frac{3}{2}}$ peak as observed in $NiCl_2$-montmorillonite samples (fig.67). However, although all samples after 10 mins etch exhibited a peak around 853eV, with no associated satellite, characteristic of nickel metal, a peak of approximate BE 854eV developed after one or five mins etching of $NiSO_4$-montmorillonite/ 2 wash and /5 wash samples. This may be a result of a two step

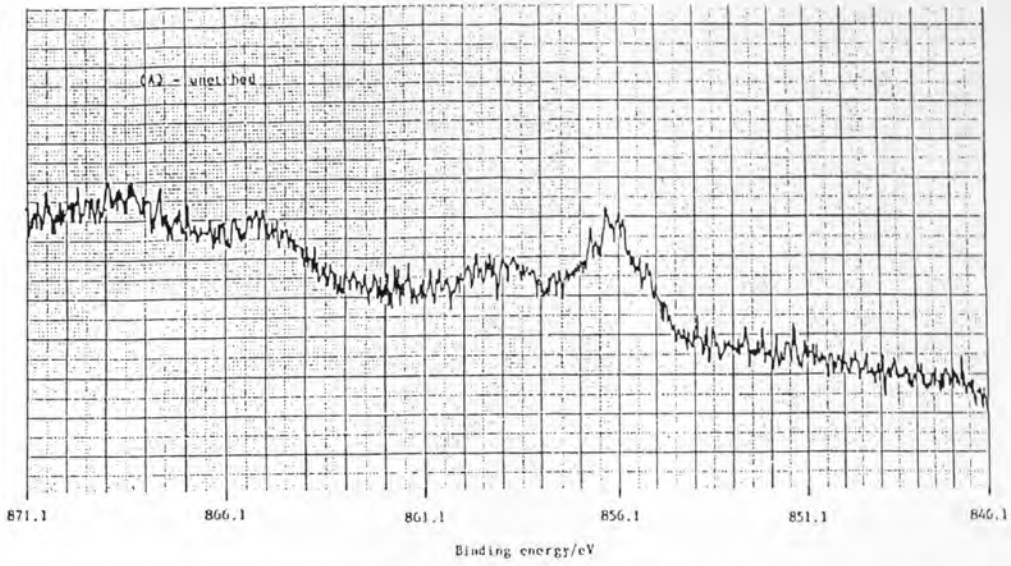

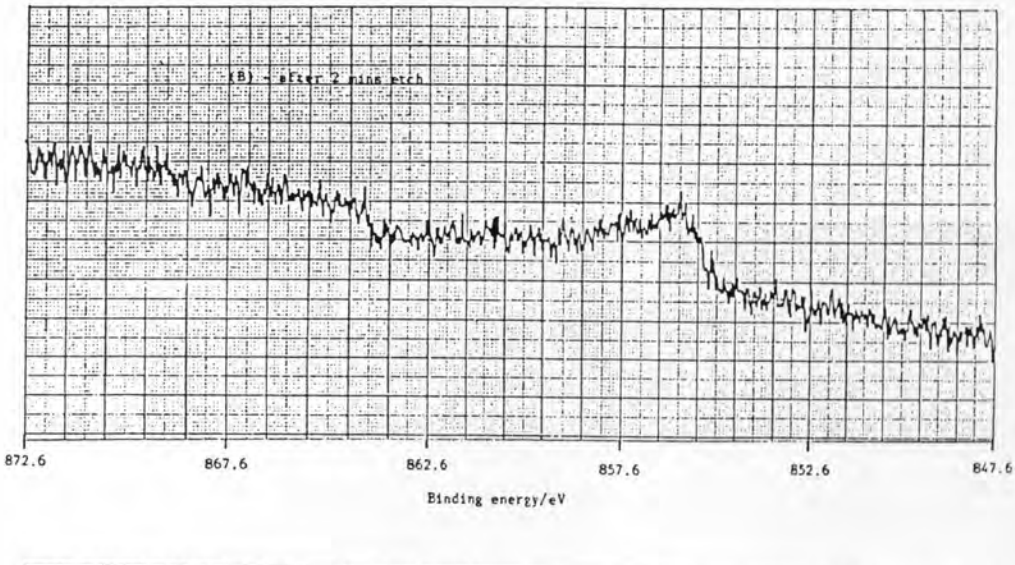

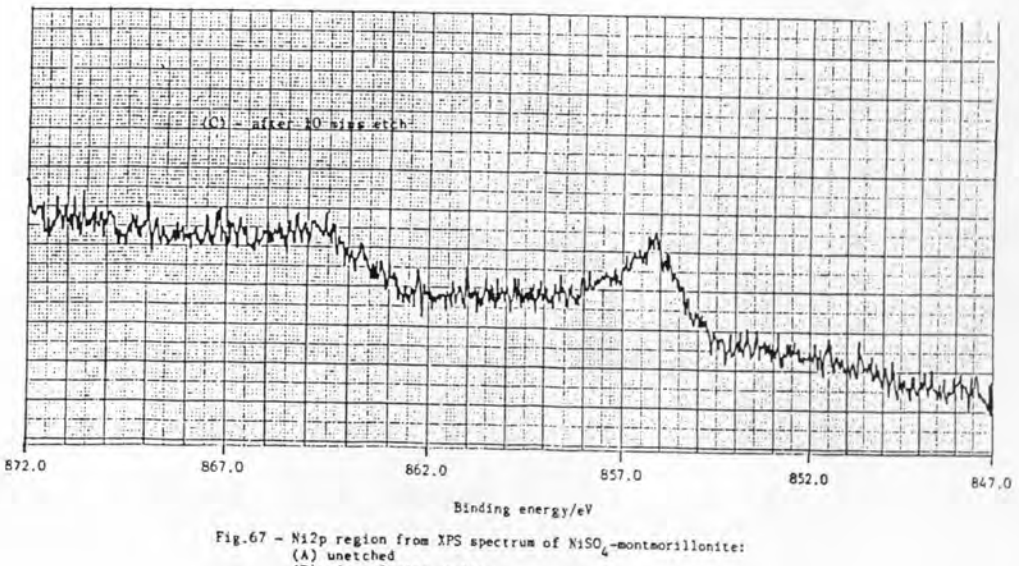

Fig.67 - Ni2p region from XPS spectrum of $NiSO_4$-montmorillonite:
(A) unetched
(B) after 2 mins etching
(C) after 10 mins etching

reduction mechanism in which Ni^{2+} sorbed on the clay surface is decomposed initially to nickel(II) oxide, then reduced to metallic nickel, by ion bombardment. Although the $Ni2p_{\frac{3}{2}}$ BE of NiO reported by Kim et al[169] is 0.5eV higher than that observed here, this is likely a consequence of diffuse photopeaks and uncertainty as to the actual nickel speciation on the clay surface.

Further confirmation of this intermediate stage was not available as the distinctive NiO satellite peak was obscured by the broad photopeak from aqueous Ni^{2+}. The reduction of NiO to nickel metal has previously been reported by Kim et al,[169] whose XPS investigation into ion bombardment of metal-oxygen surfaces using argon and oxygen ion beams demonstrated that reduction of these materials was a common phenomenon. Additionally a variable BE would be difficult to explain in terms of a second metal binding site.

The reason why montmorillonite samples exhibit the reduction mechanism whereas hectorite samples do not is unclear, but it may be related to the higher concentration of surface sorbed cations on montmorillonite.

In order to enhance any contribution to the $Co2p_{\frac{3}{2}}$ photopeak from surface sites with respect to interlayer sites, a sample of Co-hectorite(unwashed) was analysed using an 11^{o} angle between the sample surface and the analyzer entrance, as opposed to the normal 45^{o}. The spectrum obtained demonstrated only a weak broad peak centred on a BE of around 782eV. As well as the characteristic diminution of all peak intensities on decreasing the take off angle,

the presence of surface roughness renders data interpretation difficult, because true photoelectron escape angles are not directly measurable and shading of certain surface regions may occur for both incident photon and electron exit.[167]

The XPS data has enabled characterisation of sorbed species as hexaaquo cations, but differentiated between the nature of sorption sites on montmorillonite and hectorite. The assignment of the identified species to a surface bound site utilized the uniqueness of XPS to probe surface characteristics, and ion etching was effective in modifying cation speciation.

Scanning electron microscopy

Having reached the limit of information to be acquired from X-ray photoelectron spectroscopy, it was hoped that the discrete nature of sorption sites may be confirmed by analytical data from the application of SEM. However, a considerable amount of accessory information was revealed.

It was immediately apparent from the analyses of the 'Berkbond' montmorillonite, both natural and nickel treated (tables 103, 104, 105 and 106), that considerable variations in elemental composition existed throughout the materials. This is attributed to the presence of impurities, which may be recognized in some cases. The presence of calcite is indicated by the high calcium content of a number of particles (e.g. see table 103) (later confirmed by XRD examination of the natural clay), and a variable potassium concentration probably arises from feldspar or illite impurities. A consistent

Si:Al ratio is characteristic of the smectite phase, but no discrete relationship between iron and silicon or aluminium concentrations was observed. In fact, as the silicon (or aluminium) content diminished, the level of iron tended to increase, indicating the presence of a discrete iron containing phase. It was also apparent that the concentration of sorbed nickel was more closely related to the proportion of constituent iron than of silicon or aluminium, suggesting a favourable association with the iron phase. It is not possible to discriminate whether theiron phase is a discrete particulate material or a coating on clay mineral surfaces, but the high affinity for nickel ions is clearly responsible for the enhanced nickel concentrations observed compared with that of the bulk material (approx. 2% by total weight).

The influence of iron oxyhydroxide coatings on transition metal ion sorption by clay minerals has previously been reported,[80,81] and could be of significance here.

It may also be concluded that calcite has a low affinity for Ni^{2+} ions, as particle analyses exhibiting high calcium concentrations were relatively low in nickel.

'Berkbond' montmorillonite patently contained a considerable proportion of impurities so was eliminated from involvement in any further experimental work.

Analyses from 'Steetly' montmorillonite samples (tables 107, 108, 109, 110 and 111) are comparatively much more consistent, confirming the relatively pure nature of this material discerned from previous

studies utilizing infrared, X-ray diffraction and DTA techniques (chapter 3). Although surface roughness should affect the analytical data,[173] the precision of the technique was evidently quite good, but it must be recognized that a constant elemental constitution from particle to particle cannot be guaranteed so an appreciable distribution in clay composition would be expected.

Brissaud et al[174] were also able to attain good agreement between a number of analyses of pottery samples using an SEM/Energy dispersive analysis system, although, as in this study, elemental concentrations below 2 percent could be determined only with some degree of inaccuracy. However, from Lee et al's[175] study of phyllosilicates in rocks transitional from mudstone to slate from LeHigh Gap, Pa., it was concluded that analytical electron microscopy could only determine an average composition and was unable to distinguish between separate intergrowing packets of minerals. The application of analytical electron microscopy, to a mixed smectite-illite material enabled a chemical distinction between the two minerals to be made, but showed that the smectite itself was of variable composition.[176] The variation in elemental composition of the montmorillonite particles, therefore, came as no surprise, but significant precision was evident to enable a number of conclusions to be drawn.

The Si:Al ratio of the 'Steetly' montmorillonite samples was consistently comparable with the value of 3.78 calculated from XRF analysis, but iron concentration was slightly high. A separate iron phase, which is concentrated on external clay surfaces, may

be present as in the 'Berkbond' montmorillonite, however, a considerably lower proportion of the iron phase is admixed with the 'Steetly' clay, as sorbed nickel concentration was much lower and followed the constituent silicon and aluminium contents quite closely.

A larger overall concentration of nickel was observed in the nickel sulphate treated montmorillonite than in the nickel chloride exchanged material. Although an enhanced affinity of the nickel-sulphate ion-pair to the anion-cation pair sorption site, suggested previously (chapter 3), is expected for unwashed samples, the washed materials exhibited a similar phenomenon. This may be related to the retention of a considerable proportion of nickel sorbed on anion-cation pair sites, but, from previous experience, after five washings this seems unlikely. If the anion-cation pair constitutes only 20 percent of the Ni^{2+} initially sorbed (chapter 3), its removal may not significantly affect the nickel concentration determined by SEM due to low analytical precision and particle to particle inhomogeneity.

In agreement with previous characterisation studies of 'Steetly' montmorillonite (chapter 3), both silica and a potassium containing impurity (feldspar?) could be discriminated. The ability of SEM to distinguish these associated mineral impurities is affiliated with analysis on a microscopic scale, in contrast to the macroscopic analysis produced by XRF.

In conclusion, the application of SEM to clay mineral analysis,

although dependent on sample surface roughness, enables an estimation of microscopic clay homogeneity and provides evidence for the sorption of cations. The extent of clay mineral inhomogeneity may be reflected in sorption properties, as any accessory minerals will have appreciably different exchange capacities. The incorporation of impurities may also lead to the introduction of additional sorption sites resulting in a slight broadening of peaks characteristic of sorbed metal ions in XPS and Mössbauer spectroscopy.

The microscopic inhomogeneity disclosed by SEM highlights a universal problem associated with any clay mineral system. The very nature of formation of smectite minerals, usually by in situ alteration of basaltic materials,[21] inevitably results in inherent contamination of the clay by unreacted primary minerals and/or diagenetic material formed upon modification of the smectite. This is clearly demonstrated by the alteration of a mixed illite/smectite from less than 20 percent to about 80 percent illite layers in Oligocene-Miocene sediment, observed by Hower et al,[177] as the stratigraphic interval from which core samples were taken increased from 2000 to 3700m. It was also proposed that the in situ alteration reaction involved potassium feldspar as a primary reactant and produced silica as a byproduct.

It is important to acknowledge, when considering the storage of radioactive waste products, that the process of clay mineral diagenesis may appreciably alter the composition of the host geologic formation, after perhaps 10 000 years, thus modifying inherent mechanical and physical properties.

Mössbauer spectroscopy

Mössbauer spectroscopy was used to investigate the physical characteristics of sorbed Fe^{2+} and Fe^{3+} ions on the surface of hectorite. Both Fe^{2+}- and Fe^{3+}- saturated hectorites were studied along with a partially $^{57}Fe^{3+}$ exchanged sample, the enhanced γ-ray absorption of ^{57}Fe nuclei counteracting the loss in intensity due to the smaller substrate iron concentration.

It was hoped that Mössbauer spectroscopy would enable any differences between the clay having Fe^{3+} in only a fraction of exchange sites and the saturated sample, to be distinguished, in particular the nature of exchange sites occupied. Partial occupation of exchange sites is likely in clay contained radioactive waste disposal sites due to very low radionuclide content of groundwaters, so that any peculiarities at low exchange levels must be assessed.

Although heat may be generated by some categories of radioactive waste (significantly by high and intermediate level material), it was of particular interest to observe the redox properties of the iron species on the clay mineral surface when heated under nitrogen.

After only a very long accumulation time was a distinguishable Mössbauer absorption obtained from hectorite itself. This is not surprising as XRF analysis revealed the presence of only 0.10% Fe_2O_3 in the clay. Although some trivalent iron was present, comparison of the accumulation time with those from the respective modified samples indicated this would not be discernible from the

stronger absorbtions of exchanged iron.

Table 112 summarises data from the Mössbauer spectra obtained. The Fe^{3+} treated hectorite contained only Fe^{3+} in exchange sites. δ and Δ are characteristic of an octahedrally coordinated high spin Fe^{3+} ion and are in close agreement with other literature data concerned with the uptake of Fe^{3+} on a number of smectite samples (table 113).

Table 113 - Mössbauer parameters of Fe^{3+} sorbed onto montmorillonite and hectorite

Sorbent	δ(mm/s)	Δ(mm/s)	reference
montmorillonite	0.25	0.70	Helsen et al[178]
montmorillonite	0.37	0.63	Helsen et al[179]
hectorite	0.37	0.60	Helsen et al[179]
montmorillonite	0.49	0.55	Berry et al[180]

The $^{57}Fe^{3+}$-hectorite demonstrated only one quadrupole split absorbance in its Mössbauer spectrum (fig.54), having very similar parameters to that of the Fe^{3+}-hectorite (table 112). No evidence for any Fe^{2+} was obtained, even at 80K, implying the complete conversion of $^{57}Fe^{2+}$ to $^{57}Fe^{3+}$ by air oxidation prior to analysis.

From the similarity of δ and Δ, it appears that the exchange sites occupied by Fe^{3+} at low exchange levels are almost identical to those occupied at Fe^{3+} saturation levels. It is apparent then that all clay exchange sites have very similar chemical

Table 112 - Mössbauer parameters recorded from iron-exchanged hectorite.

(Standard deviation from computer fits shown in brackets.)

Sample	Temperature of Mössbauer measurement/K	δ(mm/s)	Δ(mm/s)	Γ	χ^2
Fe^{3+}-hectorite	298	0.33 (0.01)	0.76 (0.01)	0.44 (0.02)	520
Fe^{3+}-hectorite	298	0.32 (0.02)	0.91 (0.02)	0.45 (0.04)	553
heated to 400°C	80	0.44 (0.02)	0.98 (0.02)	0.63 (0.03)	466
Fe^{2+}-hectorite	298	0.05 (0.04)	0.78 (0.04)	0.35 (0.08)	500
	80	0.14 (0.05) (18%)	0.93 (0.05)	0.41 (0.09)	489
		1.25 (0.02) (82%)	2.80 (0.02)	0.59 (0.04)	
Fe^{2+}-hectorite	298	0.31 (0.01)	0.99 (0.01)	0.61 (0.02)	514
heated to 400°C	80	0.38 (0.01)	1.01 (0.01)	0.70 (0.03)	558
$^{57}Fe^{3+}$-hectorite	298	0.33 (0.01)	0.74 (0.01)	0.69 (0.01)	542
$^{57}Fe^{3+}$-hectorite	298	0.31 (0.03) (76%)	0.93 (0.03)	0.82 (0.03)	532
heated to 400°C		1.00 (0.04) (24%)	2.47 (0.04)	0.59 (0.05)	

Note - Relative percentages of iron in different oxidation states estimated assuming the recoil free fractions to be the same.

environments, since if a particular set of exchange positions were occupied at low sorbed iron concentrations and additional but distinct sites occupied at saturation concentrations, then the chemical shift and quadrupole splitting parameters would alter to reflect that difference.

However, this interpretation must be qualified in view of the larger linewidth from the $^{57}Fe^{3+}$-hectorite sample, which is indicative of a number of iron exchange sites of similar chemical shift but slightly different quadrupole splitting. This variation in quadrupole splitting is due to inhomogeneity of the electric field gradient, and therefore the molecular environment, around the iron atoms. Line broadening may also result from using a thick sample absorber, but this effect can be eliminated if the absorbers contain less than $10mg/cm^2$ of iron[92] as was used in all clay samples examined in this study. It is, therefore, proposed that the greater inhomogeneity of the iron sites in $^{57}Fe^{3+}$-hectorite is due to the lower concentration of iron ions sorbed onto the hectorite leaving only a partially exchanged hectorite interlayer. This is in contrast to the Fe^{3+}-hectorite which, due to the almost complete saturation of exchange sites by Fe^{3+}, has a considerably more homogeneous interlayer region. It has already been indicated by Johnston et al,[181] in a Mössbauer study of untreated, Ca^{2+}- and K^{+}-saturated nontronites, that interlayer cations influence the electric field gradient experienced by structural iron atoms substituted in octahedral and tetrahedral lattice sites, and there is no reason why similar, or the reverse, effects should not occur. As a consequence of the

mixed cation occupation of interlayers in $^{57}Fe^{3+}$-hectorite, the $^{57}Fe^{3+}$ ions experience much more varied environments than in the Fe^{3+}-hectorite which has only Fe^{3+} ions in the surrounding interlayer region, and this phenomenon gives rise to the observed line broadening.

It is important to note at this stage further consequences which are apparent from the conclusions of Johnston et al.[181] As well as experiencing the effects of other interlayer cations, the quadrupole splitting of exchanged iron is dependent on the nature of substitution in octahedral and tetrahedral sites in the smectite structure. Since in any smectite this substitution is varied and quite random, the interlayer cations will obviously experience a variety of electric field gradients, therefore, exhibit a range of quadrupole splittings, leading to a broadening of the respective absorbance peaks. Thus, Mössbauer absorbances by smectite clays will almost certainly be broadened - this is observed in all the spectra obtained in this study.

It was considered by earlier workers[75,182] that broadened ferric resonances from natural smectite samples were actually composed of two Fe^{3+} doublets with approximately the same isomer shift, but with quadrupole splitting parameters differing by a factor of two. As the point-charge model[183] showed that the quadrupole splitting of Fe^{3+} in octahedral coordination of the type FeX_4Y_2 with the Y ligands in a <u>trans</u> position is twice that when the ligands are <u>cis</u>, the outer doublet was assigned to Fe^{3+} in the octahedral layer of the

clay structure, which consists of $FeO_4(OH)_2$ groupings, with a *trans* arrangement of the OH groups. Similarly, the inner doublet was assigned to the unit with a *cis* arrangement of OH groups. Also, this *cis* doublet is usually about twice as intense as the *trans* doublet which corresponds to the actual ratio of these two sites in the smectite structure, suggesting that iron substitutes to approximately an equal extent in each site.

This interpretation was, however, subsequently contradicted by the findings of Cardile et al.[184] Although Mössbauer spectra of several montmorillonites were fitted again to two Fe^{3+} doublets, their interpretation was very different, implying that the Fe^{3+} was found largely in *trans* octahedral sites. The two doublet computer fits were thought to represent the mean extremes of a continuum of slightly different Fe^{3+} resonances arising from the variable nature of the surrounding environment, which itself was a consequence of the low iron content of the clays. This proposal was in accordance with previous electron diffraction evidence obtained by Tsipursky et al[185] who showed that 75-100% of the *trans* octahedral sites are occupied in Wyoming and other montmorillonites in which the charge is localised in the octahedral layer.

The findings of this study support the latter (and presently favoured) explanation, since peak broadening due to the inhomogeneous nature of the iron environment, in both structural and interlayer regions, is apparent.

The Fe^{2+} treated hectorite sample exhibited a doublet in its room temperature Mössbauer spectrum (table 112), which is assigned to high spin Fe^{3+} in a tetrahedral site, from the characteristic chemical shift value of 0.05mm/s. No Fe^{2+} component could be fitted in this case, but one was clearly identified when the sample temperature was lowered to 80K (fig.53).

It is apparent that an appreciable proportion of Fe^{2+} was oxidised to the ferric state during the preparative stages of the Fe^{2+}-hectorite, even though comprehensive precautions were taken to avoid introduction of air into the system. Other workers have experienced similar difficulties in synthesising Fe^{2+}-doctored clays free from Fe^{3+}. Mössbauer spectra recorded by Berry et al[180] from $FeCl_2.4H_2O$ treated Wyoming montmorillonite and silica (under nitrogen) revealed characteristic Fe^{3+} resonances. Helsen et al[179] were also unable to prepare Fe(II)-exchanged montmorillonite or hectorite without the occurence of partial oxidation, but noted that once exchanged, the Fe(II) content remained very stable even to prolonged air exposure. Although Fe^{2+}-hectorite prepared in this study appeared to behave similarly, the $^{57}Fe^{2+}$-hectorite very readily oxidised to the ferric form with complete loss of any ferrous species. It does appear anomalous, however, that the Fe^{3+} should occupy, apparently, a tetrahedrally coordinated site, since in Fe^{3+}-hectorite (fig.52) and $^{57}Fe^{3+}$-hectorite (fig.54) only octahedral Fe^{3+} coordination is evident.

The interaction of Fe^{3+} in the Fe^{2+}-hectorite clay with the clay

surface is evidently greater than that in the other iron treated clays, as withdrawl of Fe^{3+} ions into ditrigonal holes occurs resulting in tetrahedral coordination, the fourth coordination site being occupied by a water molecule. This effect would appear to be a function of the high cation loading on the clay (cf $^{57}Fe^{3+}$-hectorite) and the low proportion of Fe^{3+} present (cf Fe^{3+}-hectorite).

Since the nature of the site occupied by tetrahedral Fe^{3+} is very likely less influenced by interlayer cations than octahedrally coordinated interlayer Fe^{3+} ions, it is not surprising, following the argument developed previously, that it exhibits a significantly smaller linewidth (table 112), further supporting the proposed interaction.

Dimeric species such as $[(H_2O)_5FeOFe(H_2O)_5]^{5+}$ could, however, be responsible for the Fe^{3+} resonance, even though the Fe^{3+} ions are in octahedral coordination. This hypothesis is discredited by a survey of literature data[186] in which a variety of Fe^{3+} compounds surrounded by an octahedron of oxygen atoms and compounds containing the Fe—O—Fe bridge (e.g. Fe(1,10-phenanthroline)Cl) exhibit values of the chemical shift parameter quite distinct from $\delta = 0.05$mm/s (table 112).

Oxidised Fe^{3+} in clay samples of Helsen et al[179] and Berry et al[180] was present solely in octahedral coordination.

The absence of an Fe^{2+} signal in the room temperature spectrum suggests that it is the simple hydrated Fe^{2+} ion that is associated

with exchange sites. As a consequence, the Fe^{2+} ions would be separated from the clay surface by water molecules which exchange rapidly at room temperature, which results in a low recoil free fraction and low γ-ray absorbtion. At 80K, interlayer Fe^{2+} ions are trapped in a frozen water matrix, which consequently increases the recoil free fraction resulting in an observable Fe^{2+} Mössbauer absorption. Using both organic and inorganic ion-exchange materials Delgass et al[187] concluded that the exchanged ferrous iron is normally trapped in a frozen water matrix. Their evidence consisted of characteristic Fe^{2+} resonances observed when samples were either evacuated at room temperature or analysed at liquid nitrogen temperature. A more comprehensive study was performed by Banin et al[76] who recorded the Mössbauer spectrum of a mixed Fe^{2+}/Fe^{3+}-montmorillonite as a function of temperature. The intensity of the Fe^{2+} signal underwent an abrupt transition at 210K, but was undetectable above 250K. This change took place in the same temperature range as the exothermic peak observed in a study by Anderson et al[188] and was assigned to the freezing of molecular water layers on the clay surface. Helsen et al[179] and Berry et al,[180] in their investigations of Fe^{2+} doped minerals also acknowledged the appearance of Fe^{2+} resonances only in low temperature Mössbauer spectra.

The similarity of Mössbauer parameters gained for Fe^{2+} sorbed onto an organic resin and a zeolite by Delgass et al[187] ($\delta \simeq 1.5$mm/s, $\Delta \simeq 3.1$mm/s) to those reported for an ice matrix by Dezsi et al[189] supported their supposition that the Fe^{2+} ions were trapped in a frozen water matrix. Subsequent investigations on the nature of Fe^{2+}

sorbed onto montmorillonite[178,76] hectorite[179] and silica,[180] however, revealed significantly different Mössbauer parameters (table 114).

Table 114 - Mössbauer parameters of Fe^{2+} exchanged onto various sorbents.

Sorbent	δ(mm/s)	Δ (mm/s)	reference
montmorillonite	1.04	3.12	Banin et al[76]
montmorillonite	1.29	3.52	Helsen et al[178]
montmorillonite	1.38	3.36	Helsen et al[179]
hectorite	1.38	3.37	"
montmorillonite	1.40	3.36	Berry et al[180]
silica	1.25	2.59	"

A range of chemical shifts and quadrupole splitting values are observed throughout table 114. The differences in Fe^{2+} environment are most likely related to the particular type of sorbent used and its state of hydration. The significant deviation of δ and Δ observed in this study, from the values observed for Fe^{2+} in a frozen water matrix suggests that the sorbed Fe^{2+} cannot be fully surrounded by a symmetrical arrangement of water molecules. Hence, as the sample temperature is lowered, the vibrational amplitudes of interlayer water molecules decrease, resulting in an increased influence of the negatively charged clay surface on interlayer Fe^{2+} ions. The Fe^{2+} ions consequently experience an unsymmetrical crystal environment giving rise to an appreciable electric field gradient. A significant

lowering of δ and Δ from that of Fe^{2+} in a water matrix is the result.

Further confirmation of this effect is gained from structural considerations of the hectorite sample. Cation exchange capacity determinations for Hector hectorite, carried out under the auspices of the Clay Minerals Society and the OECD,[102] afforded a value of 43.9meq/100g compared with 58meq/100g for the hectorite sample used in the present study. The dissimilarity may arise from the greater degree of isomorphic substitution in the latter clay. The charge imbalance resulting from substitution is neutralized by interlayer cations which will, therefore, in the Hector hectorite, be less strongly attracted to the interlayer surfaces. As a result, the electric field gradient experienced by interlayer Fe^{2+} ions will be weaker and hence give rise to a larger quadrupole splitting than for the hectorite utilized in the present study.

The attraction of interlayer cations to the clay surface explains why a Mössbauer spectrum is obtained for samples containing Fe^{3+} at room temperature. It may be reasoned that Fe^{3+} should be present as the hexaaquo species in the interlamellar region, as well as Fe^{2+}. However, the higher charge of Fe^{3+} encourages a strong interaction with the silicate structure, as has been proposed for Fe(III) on montmorillonite[179] and Cu(II) in partially dehydrated clays.[73]

An alternative explanation proposed by Banin et al,[76] that sorbed Fe^{3+} ions tend to hydrolyze and polymerise on the clay surface forming insoluble hydroxyferric aggregates, is not favoured (although not

totally discounted) as no such compounds are evident from the Mössbauer spectra (e.g. fig.52). Helsen et al[179] observed identical spectra from preparations of Fe(III)-montmorillonites at pH1.4 and 1.8, and since the proportion of any hydroxy species would be expected to be strongly pH dependent, they also discounted Diamant et al's explanation.

The absence of magnetic hyperfine splitting in the ^{57}Fe Mössbauer spectra recorded at 80K suggested that any α-FeOOH or β-FeOOH formed on the iron treated clays was either below the level of detectability or that it was of such small particle size that it exhibited superparamagnetism. The preparative procedures used in this study, which were based on those of Helsen et al,[179] were therefore successful in avoiding formation of hydroxyiron compounds.

Thermally treated iron-hectorite samples

Thermal treatment modified the Mössbauer characteristics of all three iron doctored clays and colour changes were also induced (table 112). Although the oxidation state of iron in Fe^{3+}-hectorite was unaffected, some Fe^{2+} appeared in the $^{57}Fe^{3+}$-hectorite and conversion of ferrous to ferric iron was evident for the Fe^{2+}-hectorite.

The chemical shift and quadrupole splitting values from iron in Fe^{3+}-hectorite heated to 400°C were characteristic of an octahedrally coordinated, high spin Fe^{3+} species (fig.55). The Fe^{3+} environment is chemically very similar, but slightly more distorted than in the untreated material. As no (or at most, very little) interlayer water is present at 400°C,[73] the distance between tetrahedral sheets

in that region will be very small. Octahedral geometry of an Fe^{3+} ion in this environment could very likely occur through coordination to three oxygen atoms of ditrigonal oxygen structures in each of the two tetrahedral sheets. This would give rise to a very similar chemical environment to that experienced by Fe^{3+} in the untreated parent clay, but a larger crystal field distortion due to the slight misalignment of the ditrigonal holes with respect to each other. The chemical similarity of Fe^{3+} environments in both the untreated and dehydrated Fe^{3+}-hectorites is also reflected in the lack of any colour change after thermal treatment.

McBride's[73] electron spin resonance study of the dehydration reactions of exchangeable Cu^{2+} on hectorite showed that when a Cu^{2+}-hectorite was heated to 110°C, all $[Cu(H_2O)_6]^{2+}$ species were eliminated and the planar $[Cu(H_2O)_4]^{2+}$ ion predominated in the interlamellar region. At a temperature of 170°C, ligand water was removed forcing Cu^{2+} to coordinate with silicate oxygens, as proposed above. At higher temperatures, a loss in intensity of the ESR signal was indicative of a lowering of symmetry of the dehydrated, surface-coordinated Cu^{2+} ion. This increased asymmetry, which became more apparent upon heating the clay to higher temperatures, was also observed for the Fe^{3+}-hectorite here, where the electric field gradient increased when the sample was heated to 400°C.

The steady loss of interlayer water with increased temperature and its effect on coordination of interlayer cobalt on montmorillonite was monitored using diffuse reflectance spectrophotometry by Tarasevich et al.[78] Thermal dehydration of the air dry Co-mont-

morillonite, which was initially saturated with the hexaaquo Co^{2+} ion, at 70°C led to the formation of a five coordinate cobalt complex in the interlamellar region. Tarasevich et al[78] suggested that already water had been lost from the coordination sphere of the cobalt ion, it being surrounded by three water molecules and two surface oxygens on the upper and lower aluminosilicate sheets of the clay structure. Dehydration at 150-200°C left Co^{2+} in a tetrahedral environment, which comprised three oxygen atoms from a ditrigonal hole in one tetrahedral sheet, the fourth coordination position being occupied by a water molecule. This water molecule is buried in the ditrigonal hole of the adjacent tetrahedral sheet. Increasing the sample temperature to 250-300°C removed any remaining water molecules. Tarasevich et al[78] suggested that at this temperature, the Co^{2+} ions penetrate deeper into the ditrigonal holes, and are apparently again situated in a tetrahedral environment of three surface oxygen atoms and an oxygen atom of a structural hydroxyl group. However, this was just a suggestion and could not be confirmed due to the poor nature of the spectra obtained. Since a similar cation environment would be expected at 400°C to that at 300°C (since no further water can be removed from the interlayer region) our observation that octahedral coordination exists in this temperature range appears to contradict Tarasevich et al's suggestion.

No further resonances were observed when the sample was cooled to 80K (fig.56). The clay was therefore, free from aquated iron species at room temperature (see earlier).

Mössbauer examination of Fe^{2+}-hectorite heated to 400°C (fig.58) revealed the presence of a high spin, trivalent iron species in an octahedral environment. No additional peaks were exhibited at 80K (fig.57) indicating the absence of any aqueous type iron species at room temperature.

The chemical environment of the Fe^{3+} appears to be almost identical to that of the same ion in thermally treated Fe^{3+}-hectorite (and $^{57}Fe^{3+}$-hectorite), but the larger quadrupole splitting value is indicative of a significantly more distorted surrounding electric field. A 'memory' effect seems to be operative here, since Fe^{3+} in the saturated ferric and ferrous clays after heat treatment does not occupy identical sites. Further, the larger linewidth characteristic of the ferric species in dehydrated Fe^{2+}-hectorite is again indicative of non-identical site occupation in the two heat treated samples. The ferric ion is likely in a very similar environment in thermally treated Fe^{2+}-hectorite to that in the Fe^{3+}-hectorite, but with an enhanced misalignment of adjacent tetrahedral sheets, giving rise to a larger electric field gradient. This distortion appears responsible for the larger linewidth, since it has previously been shown, in this report (see earlier) and by previous workers,[181] that next-nearest-neighbour atoms and neighbouring atoms even further away are responsible for the line broadening, not the immediate octahedral environment of oxygen atoms, which is identical in the two clays anyway, and the former atoms presumeably, therefore, exhibit stronger (or lesser) effects on the electric field environment of iron ions.

The room temperature spectrum of $^{57}Fe^{3+}$-hectorite, after heating to 400°C, was fitted to two quadrupole split resonances (fig.59). The chemical shift and quadrupole splitting parameters (table 112) were characteristic of a high spin, octahedrally coordinated Fe^{3+} ion (δ = 0.31) and a high spin, octahedrally coordinated Fe^{2+} ion (δ =1.00).

The Fe^{3+} species appears, from the Mössbauer parameters, to occupy a very similar site to that in Fe^{3+}-hectorite heated to 400°C. However, the linewidth of the former is considerably larger (almost double). It is postulated that a similar effect is evident in samples heated to 400°C as observed with the untreated parent clays. Thus, the environment around an Fe^{3+} ion in dehydrated Fe^{3+}-hectorite is quite homogeneous due to saturation of exchange sites in the parent clay with ferric ions, but that of Fe^{3+} ions in dehydrated $^{57}Fe^{3+}$-hectorite is distinctly less uniform as a result of the low concentration of exchange sites occupied by $^{57}Fe^{3+}$ ions in the parent clay.

The Fe^{2+} species demonstrates significantly different chemical shift and quadrupole splitting parameters to those of the ferrous ion in untreated Fe^{2+}-hectorite (table 112). As the Fe^{2+} resonance is observed at room temperature, a significant recoil free fraction is evident without the requirement of sample cooling to 80K, confirming that the iron occupys a rigid position and is definitely not in an aqueous type environment. The increased distortion of the surrounding electric field (i.e. decrease inΔ), on (effective) dehydration, of Fe^{2+} correlates with that evident in the Fe^{3+}-hectorite system upon thermal treatment (see earlier). The Fe^{2+} most likely occupys an

octahedron of oxygen atoms, similar to that proposed for Fe^{3+} in heated Fe^{3+}-hectorite, comprising three oxygen atoms from ditrigonal units in each of the two adjacent tetrahedral sheets. The significantly broadened linewidth (table 112) may again be attributed to the multi-cation nature of the original exchange sites in the parent $^{57}Fe^{3+}$-hectorite, which generates a multitude of Fe^{2+} environments centred on $\delta = 1.00$, $\Delta = 2.47$.

The mechanism of formation of Fe^{2+} on thermal treatment of $^{57}Fe^{3+}$-hectorite is unclear. Although the heat treated Fe^{3+}-hectorite initially appears to undergo an alternative mechanism, ferric iron only being detected, this is likely not the case as any relatively weak Fe^{2+} resonances will not be distinguishable from the high background signal. Comparison of the Mössbauer spectra of thermally treated Fe^{3+}-hectorite (fig.55) and $^{57}Fe^{3+}$-hectorite (fig.59) clearly demonstrates this point. Similarly, Fe^{2+} species in the Mössbauer spectrum of heat treated Fe^{2+}-hectorite may also not be discernible.

Even with this assumption, the mechanism of both Fe^{3+} reduction and Fe^{2+} oxidation is not straightforward.

The possibility of mineral alteration, (i.e. incorporation of Fe^{2+}/Fe^{3+} ions into the crystal lattice) on heating is dismissed (in all three thermally treated clays) since dehydroxylation, which is the first stage in thermal decomposition of smectite clays, does not begin until a temperature of 600°C in hectorite, according to earlier differential thermal analysis work (section 3.2.3).

An alternative explanation concerning the initial generation of iron oxyhydroxides on the clay surface due to the increased tendancy for the hydrolysis reaction to occur as interlayer water is lost,[73] which subsequently may decompose to the respective iron oxides is dismissed as no evidence for α-, β- or γ-FeOOH, FeO, Fe_2O_3, Fe_3O_4 was found,[183] i.e. absence of hyperfine splitting and Δ significantly different from $\simeq 0.55 mms^{-1}$ (this is true for all three thermally treated clays).

Air oxidation of Fe^{2+} to Fe^{3+} during further handling of the parent clay before thermal treatment would appear a likely explanation of the oxidation reaction, since the instability of Fe^{2+} on the parent Fe^{2+}-hectorite had already been recognised. Although this mechanism cannot be fully discounted, its influence would appear quite minor when quadrupole splittings of the Fe^{3+} ion in dehydrated Fe^{2+}-hectorite and $^{57}Fe^{3+}$-hectorite are compared. If it is recalled that the $^{57}Fe^{3+}$-hectorite was generated by air oxidation of $^{57}Fe^{2+}$-hectorite, so, when thermally treated, it should produce an identical Fe^{3+} environment to dehydrated, oxidised Fe^{2+}-hectorite. This is not the case, Δ taking a value 0.06mm/s greater for the latter clay.

The possibility of redox reactions on the clay itself, between interlayer Fe^{2+}/Fe^{3+} and transition metal ions substituting in structural octahedral sheet positions is also discounted as the concentration of the latter is too low. Although XRF analysis of hectorite (table 10) does reveal small concentrations of iron and titanium, even the complete reduction/oxidation of these cations would not account for the concomitant oxidation/reduction of all the interlayer Fe^{2+}/Fe^{3+}.

Although E^{o} for the Fe^{2+}/Fe^{3+} couple in aqueous media at room temperature implies reduction of Fe^{3+} should not be spontaneous in an aqueous environment, it may be that at high temperature within the "clay" environment such a process could be more facile.

The reductant has not been identified, any suggestions being only speculative.

Although appreciable data has been reported on the thermal treatment of clay minerals themselves,[183] few studies have given detailed consideration to the influence of interlayer species, particularly below 700°C. In an ^{57}Fe Mössbauer study, Helsen et al[179] noted that irreversible changes in the form of sorbed iron (II and III) on montmorillonite and hectorite resulted from heating and drying of samples, but specified no particular effects.

In an early study, Delgass[190] was able to increase the intensity of the Mössbauer resonance from Fe^{2+} sorbed onto a zeolite by evacuation at room temperature. He also noted that rehydration regenerated the spectrum of the untreated, hydrated, parent clay in each case, but more strikingly, rehydration of a sample heated under vacuum at 400°C for 14h similarly produced the parent clay.

Compendium

It was immediately apparent that a large number of variables existed and that only a selected few could be investigated.

In the study of nickel and cobalt sorption on montmorillonite a period of 3 days was required for equilibrium to be attained. Decreasing solution metal ion concentration gave rise to increasing distribution coefficient values and this effect continued into the 'low level' region. Sorption was proposed to occur by three mechanisms, two sites being of the classical ion exchange type and the third dependent on the co-anion present due, it was envisaged, to 'anion-cation' pair sorption. In order to model disposal site conditions more closely a number of inorganic cations were added to Ni^{2+}/Co^{2+} solutions and in all cases a decreased sorption was observed. The interference effect followed the order $Mg^{2+} \triangleq Ca^{2+} \gg K^{+} > Na^{+}$ from which it was concluded that bivalent cations more strongly interfere with transition metal ion sorption than monovalent and that the extent of sorption depends on the ionic strength of the medium. It was significant that the % Ni^{2+}/Co^{2+} sorbed from bimetallic solutions with Mg^{2+} or Ca^{2+} was quite consistent, at a constant molarity, over a range of concentration ratios. If such an effect were evident at lower solution molar strength prediction of K_d values should be possible, eliminating the need for site specific experiments. Experiments performed at 'low level' confirmed the strong competing effect of calcium for sorption sites and the ineffectiveness of sodium.

Although experimentation utilizing high solution concentrations appears to be irrelevant to the low release rates of radionuclides

expected from a disposal site, if the local groundwater flow is very low, cation concentrations will build up with their continuing influx from the disposal vault. Additionally, the extrapolation of effects from high to low level and the ease of experimentation at higher cation concentrations, make this a viable proposition.

A major problem in sorption experiments concerned the accuracy of the analytical procedures, as they were strongly affected by entrained clay particles, particularly in the low level region.

It is now known that organic constituents are present in a large number of groundwaters. The possible interaction of organic material with radionuclides in a disposal vault environment was initially studied by the addition of a number of model compounds to transition metal saturated clays. Interactions were observed in all cases, as confirmed by visible spectra and c-spacing values, 'straightforward' complexation occurring in most cases. However, anomalous behaviour was observed, as in the partially dehydrated products remaining after air drying of ammonia treated nickel-clays. Although this resulted from concomitant evaporation of ammonia and water, such a process would be unlikely in a consolidated geologic formation.

Organic compounds typically found in groundwaters were used in subsequent work in which their quantitative effect on transition metal desorption was observed. Two classes of organic compounds were separable from this work; (i) acids, which facilitated desorption of clay bound metal ions due to enhanced dissociation of the acid, and (ii) amine compounds, which enhanced the affinity of transition

metal ions for the interlayer region due to complexation. It was also apparent that the quantity of cation released increased/decreased with increasing organic concentration, the class (i) compounds exhibiting an almost linear relationship. Such a relationship should enable prediction of the extent of cation desorption from a minimum of basic information.

Two classes of organic compounds could similarly be discriminated in experiments using only a fraction of clay exchange sites occupied by transition metal ions. The extrapolation of mechanisms observed at higher concentrations to lower concentrations likely to be evident in a disposal site environment was again supported here, although the bication nature of sorption sites was likely responsible for some apparent discrepancies.

The evidence gained so far requires the necessary consideration of organic compounds in prediction of radionuclide migration in groundwater systems and although a wide variety of compounds may be present, it may be plausible to consider only functional groups in an appraisal of their effect on sorption.

Physical investigation of Co^{2+}/Ni^{2+}-saturated clays by XPS further supported the proposal that two sites existed on the external surfaces of clay particles. The adsorbed transition metal ion existed as the hexaaquo species, but was in a significantly different environment on montmorillonite to hectorite.

Iron(II) and iron(III) sorbed onto hectorite were shown by Mössbauer spectroscopy to exist as the hexaaquo species, although the trivalent

cation was more strongly bound to the interlamellar surfaces. A range of sorption sites were proposed to account for the large quadrupole splitting values observed, but sites occupied at high and low exchange levels could not be distinguished. Thermal treatment of the clays resulted in redox processes in the interlayer region although the respective oxidising/reducing agents could not be distinguished.

The inherent micro-inhomogeneity of clay samples was highlighted by SEM and must be considered in any sorption analyses. This effect is also related to clay mineral diagenesis which may occur over the lifetime of a radioactive waste disposal vault.

The study of sorption effects may be extended from that developed here with future investigations concentrating on multi-cation solutions in an attempt to enable prediction of K_d values from theoretical cation concentrations. Although the presence of organic material was highlighted in this study as being important, other potential influential factors such as clay:solution ratio and interaction of the concrete barrier with surrounding groundwater must be considered in any attempt to comprehensively assess radionuclide migration from a radioactive waste disposal site.

Appendix 1

Instrumental settings for atomic absorption analysis

Element	wavelength /nm	slit width /nm	standards/ppm lower	standards/ppm upper	flame[a]	sensitivity /ppm	error
Aluminium	309.3	0.7	2.0	20.0	N-Ac	1	nd
Calcium	422.7	0.7	0.20	5.00	A-Ac	0.08	±3%
Cobalt	240.7	0.2	0.40	2.00	A-Ac	0.15	±4%
Copper	324.8	0.7	0.20	4.00	A-Ac	0.09	±2.5%
Iron	248.3	0.2	0.20	4.00	A-Ac	0.12	±3%
Potassium	766.5	2.0	0.10	1.00	A-Ac	0.04	±4%
Magnesium	285.2	0.7	0.020	0.500	A-Ac	0.007	±2%
Sodium	589.0	0.7	0.10	1.00	A-Ac	0.015	±3%
Nickel	232.0	0.2	0.40	1.60	A-Ac	0.15	±3%
Silicon	251.6	0.2	4.0	20.0	N-Ac	1.8	nd

[a] N-Ac = Nitrous oxide-acetylene
A-Ac = Air-acetylene
nd = not determined

Appendix 2

Sorption on centrifuge tube walls

Experimental - Two centrifuge tubes containing cobalt solutions ($12.6cm^3$; 1000ppb, 100ppb Co) were sealed and shaken for 3 days. After ultracentrifugation, the liquid was poured off and the tubes analysed for entrained cobalt.

Results -

Initial solution concentration/ppb	% cobalt sorbed
1000	1.2
100	2.9

REFERENCES

1 Gabor, D.; Colombo, U.: "Beyond the age of waste." Pergamon, New York, 1978.

2 Bird, G.W.; Fyfe, W.S.: Chem. Geol., 1982,36,1: "The nuclear waste disposal problem - an overview from a geological and geochemical perspective."

3 1st Report from the Environment committee, session 1985-86: "Radioactive Waste", Vol.2: HC 191-II, 253 I-XVII.

4 Flowers, R.H.: Nucl. Energy, 1985,24,2,105.: "The packaging of intermediate and low level radioactive wastes."

5 Ginniff, M.E.: BNES Conf. ('Radioactive waste management'), London, 1984: "Implementation of UK policy and strategy on radioactive waste disposal."

6 Roy, R.: Sci. Basis for Nucl. Waste Management, Symp., 1980, Vol.1, pg.1: "Science underlying radioactive waste management: Status and needs."

7 Heimerl, W.: Sci. Basis for Nucl. Waste Management, Symp., 1980, Vol.1, pg.21: "Techniques for high level waste solidification in Europe."

8 Rusin, J.M.; Browning, M.F.; McCarthey, G.J.: Sci. Basis for Nucl. Waste Management, Symp., 1980, Vol.1, pg.169.: "Development of multi-barrier nuclear waste forms."

9 Jardine, L.J.; Steindler, M.J.: Sci. Basis for Nucl. Waste Management, Symp., 1980, Vol.1, pg.181.: "Metal encapsulation of ceramic nuclear waste."

10 Crandall, J.L.: Sci. Basis for Nucl. Waste Management, Symp., 1980, Vol.2, pg.39.: "Development of solid radionuclide waste forms in the United States."

11 'Plaintalk', NIREX magazine: March, 1986, pg.4.

12 Warnecke, E.; Hollman, A.; Stier-Friedland, G.: Mat. Res. Soc. Symp., Proc., 1984,26,41.: "Migration of radionuclides: Experiments within the site investigation program at Gorleben."

13 Hughes, A.E.; Marples, J.A.C.; Stoneham, A.M.: AERE, Harwell: Report AERE-R 10190. "The significance of leach rates in determining the release of radioactivity from vitrified nuclear waste."

14 Dayal, R.; Wilke, R.J.: 7th Int. Clay Conf., 1981.: Dev. in Sed., 35,771.: "Role of clay minerals as backfill in radioactive waste disposal."

15 Lee, S.Y.; Tank, R.W.: Applied Clay Sci., 1985, 1,145.: "Role of clays in the disposal of nuclear waste: a review."

16 Erickson, K.L.: "Radioactive Waste in geologic storage", A.C.S. Symp. Series, 100 (Ed.Fried,S.) pg.267: "Radioactive sorption studies on Abyssal Red clays."

17 'Plaintalk', NIREX magazine: May, 1986, pg.4.

18 Silva, R.J.; Benson, L.V.; Apps, J.A.: "Radioactive waste in geologic storage", A.C.S. Symp. Series, 100 (Ed.Fried,S.), pg.215.: "Studies of actinide sorption on selected geologic materials."

19 Grimshaw, R.W.: "The chemistry and physics of clays and other ceramic materials", 4th Edition, Benn, 1971.

20 Brindley, G.W.; Robinson, K.: Min. Mag., 1946,27,242: "The structure of kaolinite."

21 Grim, R.E.: "Clay mineralogy", McGraw-Hill, New York, 1953.

22 Nagelschmidt, G.: Min Mag., 1938,25,140: "On the atomic arrangement and variability of the members of the montmorillonite group."

23 Seyama, H.; Soma, M.: J. Chem. Soc., Faraday Trans. I, 1984, 80,237.: "XPS study of montmorillonite containing exchangeable divalent cations."

24 Ericsson, T.; Wappling, R.; Punakini, K.: Geol. Foeren. Stockholm Foerh., 1977,99,3,229.: "Mössbauer spectroscopy applied to clay and related minerals."

25 Brindley, G.W.; De Souza, J.V.: Min. Mag., 1975,40,141.: "Nickel-containing montmorillonites and chlorites from Brazil, with remarks on schuchardite."

26 Alietti, A.; Brigatti, M.F.; Poppi, L.; Del Pennino, U.; Mazzega, E.; Valeri, S.: J. Coll. Int. Sci., 1981,84,2,301.: "Interlayer water and swelling properties of monoionic montmorillonites."

27 Theng, B.K.G.: "The chemistry of clay-organic reactions", Adam Hilger, London, 1974.

28 McEwan, D.M.C.: J. Soc. Chem. Ind., 1946,65,298.: "The identification and estimation of the montmorillonite group of minerals, with special reference to soil clays."

29 Bonne, A.A.; Heremans, R.H.: 7th Int. Clay Conf., 1981: Dev. in Sed., 35,799.: "Investigation of the Boom clay, a candidate rock for final disposal of high level solid waste."

30 Grimshaw, R.W.; Harland, C.E.: "Ion exchange: Introduction to theory and practice", The Chemical Society, Monographs for Teachers, No.29, 1975,73.

31 Van Olphen, H.: "An introduction to clay colloid chemistry", Interscience, London, 1963.

32 Egozy, Y.: Clays Clay Miner., 1980,28,4,311.: "Adsorption of cadmium and cobalt on montmorillonite as a function of solution composition."

33 Peigneur, P.; Maes, A.; Cremers, A.: Clays Clay Miner., 1975,23,71.: "Heterogeneity of charge distribution in montmorillonite as inferred from Co adsorption."

34 Hodgson, J.F.: Soil Sci. Soc. Am.,Proc.,1960,24,3,165.: "Cobalt reactions with montmorillonite."

35 Hodgson, J.F.; Tiller, K.G.: 9th Natl. Conf. on Clays Clay Miner., 1962,404.: "The location of bound Co on 2:1 layer silicates."

36 Maes, A.; Cremers, A.: Soil Sci., 1975,119,3,198.: "Cation-exchange hysteresis in montmorillonite: A pH dependent effect."

37 De Mumbrum, L.E.; Jackson, M.L.: Soil Sci. Soc. Am., Proc., 1956,20, 334: "Infrared absorption evidence on exchange reaction mechanism of copper and zinc with layer silicate clays and peat."

38 Swartzen-Allen, S.L.; Matijevic, E.: Chem. Rev., 1974,74,385. "Surface and colloid chemistry of clays."

39 Banin, A.: Israel J. Chem., 1968,6,27.: "Ion exchange isotherms of montmorillonite and structural factors affecting them."

40 McBride, M.B.: Clays Clay Miner., 1980,28,4,255.: "Interpretation of the variability of selectivity coefficients for exchange of ions of unequal charge on smectites."

41 Tiller, K.G.; Hodgson, J.F.: 9th Natl. Conf. Clays Clay Miner., 1962, 9,393.: "The specific sorption of cobalt and zinc by layer silicates."

42 Traynor, M.F.; Mortland, M.M.; Pinnavaia, T.J.: Clays Clay Miner., 1978,26,5,318.: "Ion-exchange and intersalation reactions of hectorite with tris-bipyridyl metal complexes."

43 Basu, A.N.; Mukherjee, S.K.: J. Ind. Chem. Soc., 1966,43,4,245.: "Interaction of montmorillonite clay and trace element cations."

44 Carter, M.: Ph.D. Thesis, The University of Aston in Birmingham, 1975.

45 Basu, A.N.; Mukherjee, S.K.: J. Ind. Soc. Soil Sci., 1965,13,4,251: "Interaction between montmorillonite clay and trace element cations. II.Exchange behaviour of Co, Ni and Cr in clays."

46 Takematsu, N: J. Ocean. Soc. Japan, 1979,35,36.: "Sorption of transition metals on Mn and Fe oxides and silicate minerals."

47 Farrah, H.; Hatton, D.; Pickering, W.F.: Chem. Geol., 1980,28,55.: "The affinity of metal ions for clay surfaces."

48 Farrah, H.; Pickering, W.F.: Water, Air, Soil, Pollut., 1977,8,189.: "Influence of clay-solute interactions on aqueous heavy metal ion levels."

49 Menzel, R.G.; Jackson, M.L.: Soil Sci. Soc. Am., Proc., 1950,15,122.: "Mechanism of sorption of hydroxy cupric ion by clay."

50 Skytte Jensen, B.: " The geochemistry of radionuclides with long half-lives. Their expected migration behaviour.": 1980, RISØ-R-430.

51 Koppelman, M.H.; Dillard, J.G.: Clays Clay Miner., 1977,25,457.: "A study of the adsorption of Cu(II) and Ni(II) by clay minerals."

52 Monsef-Mirzai, P.: Ph.D. Thesis, The University of Aston in Birmingham, 1980.: "The geochemistry of waste disposal."

53 Sarkar, G.N.; Das Kanungo, J.L.: Intern. J. Trop. Agri., 1983,1,4, 299.: "The effect of adsorbent charge density on the exchange behaviour of $[Co(pn)_3]^{3+}$ on Laponite and vermiculite by monovalent and bivalent inorganic ions."

54 Garcia-Miragaya, J.; Page, A.L.: Soil Sci. Soc. Am, J., 1977,41,718.: "Influence of the exchangeable cation on the sorption of trace amounts of cadmium by montmorillonite."

55 Bansal, O.P.; Singh, H.; Goyal, R.N.: J. Ind. Chem. Soc., 1980,57, 1050.: "Reactions of nickel(II) with acid and base saturated montmorillonites."

56 Bansal, O.P.; Goyal, R.N.; Singh, H.: J. Ind. Chem. Soc., 1981,58, 759.: "Studies of the thermodynamics of adsorption in clays: Ni adsorption on Na-, Ca-, Mg- montmorillonites."

57 Tiller, K.G.: Clay Miner., 1968,7,409.: "Stability of hectorite in weakly acidic solutions.III. Adsorption of heavy metal cations and hectorite solubility."

58 Whittig, L.D.; Page, A.L.: Soil Sci. Soc. Am., Proc., 1961,25,278.: "Fe adsorption by montmorillonite systems: I.Preliminary studies."

59 Farrah, H.; Pickering, W.F.: Chem. Geol., 1979,25,317.: "pH effects in the adsorption of heavy metal ions by clays."

60 Maes, A.; Peigneur, P.; Cremers, A.: Proc. Int. Clay Conf., 1975,319.: "Thermodynamics of transition metal ion exchange in montmorillonite."

61 Sylva, R.N.; Brown, P.L.: J. Chem. Soc., Dalton Trans., 1980,1577.: "The hydrolysis of metal ions. Part 3. Lead(II)."

62 Farrah, H.; Pickering, W.F.: Aust. J. Chem., 1976,29,1177.: "The sorption of copper species by clays. II.Illite and montmorillonite."

63 Bingham, F.T.; Sims, J.R.; Page, A.L.: Soil Sci. Soc. Am., Proc., 1965,29,670: "Retention of acetate by montmorillonite."

64 Monsef-Mirzai, P.; McWhinnie, W.R.: Inorg. Chim. Acta., 1983,73,41.: "Transition metal ion (Cu^{2+}, Mn^{2+}, VO^{2+})- montmorillonite interactions."

65 Gee, G.W.; Campbell, A.C.: "Monitoring and physical characterisation of unsaturated zone transport - laboratory analysis", 1980, PNL-3304.

66 Swanson, J.L.: "Effect of organic complexants on the mobility of low-level waste radionuclides in soils: Status report", 1981, PNL-3927.

67 Peigneur, P.; Maes, A.; Cremers, A.: 6th Int. Clay Conf. Proc., 1978: Dev. in Sed., 27,207.: "Ion-exchange of the poly-amine complexes of some transition metal ions in montmorillonite."

68 Sposito, G.; Holtzclaw, K.M.; Charlet, L.; Jouary, C.; Page, A.L.: Soil Sci. Soc. Am., J., 1983,47,51.: "Na-Ca, Na-Mg exchange on Wyoming bentonite in perchlorate and chloride background ionic media."

69 Koppelman, M.H.; Dillard, J.G.: "An ESCA study of sorbed metal ions on clay minerals." In: T.M. Church (Editor), Marine Chemistry in the Coastal Environment, ACS Symp. Ser.,18,186.

70 Koppelman, M.H.; Dillard, J.G.: J. Coll. Int. Sci., 1978,66,2,345.: "An XPS study of Co adsorbed on the clay mineral chlorite."

71 Tewari, P.H.; Lee, W.J.: J. Coll. Int. Sci., 1975,52,77.: "Adsorption of Co(II) at the oxide-water interface."

72 Murray, J.W.; Dillard, J.G.: Geochim. et Cosmochim. Acta, 1979, 43,5,781.: "The oxidation of Co(II) adsorbed on MnO_2."

73 McBride,M.B.: Clays Clay Miner., 1982,30,3,200.: "Hydrolysis and dehydration reactions of exchangeable Cu^{2+} on hectorite."

74 Monsef-Mirzai, P.; McWhinnie, W.R.: Inorg. Chim. Acta, 1982,58,143.: "Spectroscopic studies of metal ions sorbed onto kaolinite."

75 Goodman, B.A.; Dev. in Sed., No.34,1981,113.: "Mössbauer spectroscopy" (In: 'Advanced techniques for clay minerals analysis').

76 Banin, A.; Diamant, A.; Pasternak, M.: Clays Clay Miner., 1982,30, 1,63.: "Characterisation of adsorbed iron in montmorillonite by Mössbauer spectroscopy."

77 Schoonheydt, R.A.: Dev. in Sed., No.34,1981,163.: "Ultraviolet and visible light spectroscopy." (In:'Advanced techniques for clay minerals analysis.')

78 Tarasevich, Yu.I.; Sivalov, E.G.: Teor. Eksp. Khim.,1975,11,410.: "The electronic spectra of aquo cations of divalent cobalt sorbed by montmorillonite."

79 Paul, A.: "Chemistry of glasses," 1982, Chapman and Hall, London.

80 Jenne, E.A.: "Controls on Mn, Fe, Co, Ni, Cu and Zn concentrations in soils and water: the significant role of hydrous Mn and Fe oxides." In: Trace Inorganics in Water. Advances in chemistry, Series 73, Amer. Chem. Soc.,1968.

81 Means, J.L.; Crerar, D.A.; Borcsik, M.P.; Duguid, J.O.: Geochim. et Cosmochim. Acta, 1978,42,1763.: "Adsorption of Co and selected actinides by Mn and Fe oxides in soils and sediments."

82 Leenheer, J.A.: Env. Sci. Tech., 1976,10,5,445. "Investigation of the reactivity and fate of certain organic components of an industrial waste after deep-well injection."

83 Soroka, I.: "Portland cement paste and concrete", MacMillan Press, London, 1979, pg.149.

84 Muurinen, A.; Rantanan, J.; Ovaskainen, R.; Heionen, O.J.: Mat. Res. Soc. Symp., Proc., 1983,15,777.: "Diffusion measurements in concrete and compacted bentonite."

85 Atkinson, A.; Nickerson, A.K.: "The diffusion of ions through water saturated cement." AERE Report, 1983, AERE-R10952.

86 .Woollam, P.B.: "The potential for reducing the radiological consequences of reactor decommissioning through selection of construction materials for activated components", 1984. CEGB report, TPRD/B/0514/R84, DECOM 84/2.

87 Felstead, L.D.; Woollam, P.B.: " An assessment of all known isotopes, to determine which might be important in the decommissioning of thermal nuclear reactors", 1984. CEGB report, TPRD/B/0386/N84, DECOM 84/1.

88 Francis, A.J.; Dobbs, S.; Nine, B.J.: Appl. Environ. Microbiol., 1980,40,1,108.: "Microbiol activity of trench leachates from shallow-land, low-level radioactive waste disposal sites."

89 "Analytical methods for atomic absorption spectrophotometry", Perkin-Elmer Handbook, 1982.

90 McFeely, F.R.; Kowalezyk, S.P.; Ley, L.; Pollak, R.A.; Shirley, D.A.: Phys. Rev., 1973,B7,5228.: "High resolution X-ray-Photoemission Spectra of PbS, PbSe and PbTe valence bands."

91 Dillard, J.G.; Koppelman, M.H.; Crowther, D.L.; Schenck, C.V.; Murray, J.W.; Balistieri, L.: Adsorpt. aqueous solutions (Proc., symp., Houston), 1980,227.: "X-ray photoelectron spectroscopic studies on the chemical nature of metal ion adsorbed on clays and minerals."

92 Bancroft, G.M.: "Mössbauer spectroscopy: An Introduction for inorganic chemists and geochemists." McGraw-Hill, London, 1973.

93 Wakamatzu, S.H.: Japan Analyst, 1957,6,426: "Determination of cobalt by the acridine method."

94 Vogel, A.I.: "A textbook of quantitative inorganic analysis", 3rd edition, Longmans, London, 1980.

95 Odom, I.E.: Phil. Trans. R. Soc. Lond., A, 1984,311,391.: "Smectite clay minerals: properties and uses."

96 Peech, M.: Soils Soil Sci., 1945,59,25.: "Determination of exchangeable cations and exchange capacity of soils - rapid micro-methods utilizing centrifuge and spectrophotometer."

97 Posner, A.M.; Quirk, J.P.: Proc. R. Soc. Lond., Ser. A., 1964,278,35.: "Adsorption of water from concentrated electrolyte solutions by montmorillonite and illite."

98 Slavin, W.: "Atomic absorption spectroscopy", pg.125, Interscience, New York, 1968.

99 "Dionex ion chromatography training course manual, Section VII", Dionex Corporation, 1983.

100 Matthess, G.: "The properties of groundwater", Wiley, New York, 1982.

101 "Block 5: Surface processes - weathering to diagenesis", The Open University Press, 1981.

102 Van Olphen; Fripiat, J.J. (ed.): "Data handbook for clay materials and other non-metallic minerals", Pergamon, Oxford, 1979.

103 Kerr, P.K.: A.P.I. Research Project 49, Rept. 7, 1951.

104 Ross, C.S.; Hendricks, S.B.: U.S. Geol. Survey Profess. Paper, 205-B, 1945,23.: "Minerals of the montmorillonite group: their origin and relation to soils and clays."

105 Sudo, T.; Shimoda, S.: "Clays and clay minerals of Japan", Developments in Sedimentology,No.26, 241: Elsevier, New York, 1978.

106 Mackenzie, R.C. (Editor): "The differential thermal investigation of clays", The Central Press, Aberdeen, 1957.

107 Gadsden, J.A.: "Infrared spectra of minerals and related inorganic compounds", Butterworths, London, 1975.

108 Farzenah, F.; Pinnavaia, T.J.: Inorg. Chem., 1983,22,2216: "Metal complex catalysts interlayered in smectite clay. Hydroformylation of 1-hexene with rhodium catalysts ion-exchanged into hectorite."

109 Basu, A.N.; Seal, B.K.; Mukherjee, S.K.: J. Ind. Chem. Soc., 1962,39, 2,71.: "Selectivity coefficients of trace elements on a montmorillonite clay and a humic acid system."

110 Bowman, R.S.; O'Connor, G.A.: Soil Sci. Soc. Am. J., 1982,46,933: "Control of nickel and strontium sorption by free metal ion activity."

111 Perez-Rodriguez, J.L.; Hermosin, M.C.: Dev. Sedimentol., 1979,27 (Int. Clay Conf., Proc., 6th, 1978),227.: "Adsorption of chlordimeform by montmorillonite."

112 Manos, Jr., C.G.; Mortland, M.M.: Clays Clay Miner., 1984,32,2,93.: "Tris(acetylacetonato)silicon(IV) binding to montmorillonite and hydrolysis to interlayer silicic acid."

113 Jonas, E.C.: Science, 1963,140,3562,75: "Ion-exchange at edge and interlayer in montmorillonite differing in size."

114 Borovec, Z.: Casopis pro mineralogii a geologii,1983,28,2,113: "Co, Ni and Cu adsorption on clay minerals and its relation to cation exchange capacity."

115 Benjamin, M.M.: "Effects of competing metals and complexing ligands on trace metal adsorption at the oxide/solution interface." Ph.D. Thesis, Stanford University, 1979.

116 Takahashi, Y.; Imai, H.: Soil Sci. Plant Nutr., 1983,29,2,111.: "Adsorption of heavy metal cations in montmorillonite."

117 Gaines, G.L.; Thomas, H.C.: J. Chem. Phys. 1953,21,714.: "Adsorption studies on clay minerals. II. A formulation of the thermodynamics of exchange adsorption."

118 Townsend, R.P.: Phil. Trans. R. Soc. Lond., A, 1984,311,301.: "Thermodynamics of ion-exchange in clays."

119 Singhal, J.P.; Singh, R.P.: J. Soil Sci., 1973,24,2,271.: "Thermodynamics of cobalt(II)-sodium exchange on montmorillonite clay."

120 Singh, R.P.; Saxena, S.K.: Colloids and Surfaces, 1986,17,123.: "Sodium-zinc exchange equilibria on montmorillonite."

121 Mukherjee, D.C.; Basu, A.N.; Adhikari , A.M.: J. Ind. Soc. Soil Sci., 1973,21,1,27.: "Exchange reaction of Mn^{2+}, Co^{2+} and Ni^{2+} with Mg^{2+} as a complementary ion on a montmorillonite clay."

122 O'Connor, T.P.; Kester, D.R.: Geochim. et Cosmochim. Acta, 1975,39, 1531.: "Adsorption of copper and cobalt from fresh and marine systems."

123 Boyd, G.E.; Schubert, J.; Adamson, A.W.: J. Am. Chem. Soc., 1947, 69,2818.: "The exchange adsorption of ions from aqueous solutions by organic zeolites. I. Ion exchange equilibria."

124 Woessner, D.E.; Snowden, B.S.: J. Coll. Int. Sci., 1969,30,1,54.: "Study of the orientation of adsorbed water molecules on montmorillonite clay, by pulsed nuclear magnetic resonance."

125 Fripiat, J.J.; Jelli, A.; Poncelet, G.; Andre, J.: J. Phys. Chem., 1965, 69,7,2185.: "Thermodynamic properties of adsorbed water molecules and electrical conduction in montmorillonite and silicas."

126 Keith, L.H. (editor): "Identification and analysis of organic pollutants in water", Ann Arbor Science Publishers Inc., Michigen, 1976.

127 Schoonheydt, R.A.; Velghe, F.; Utterhoeven, J.B.: Inorg. Chem., 1979, 18,7,1842.: "Characterization of $[Ni(en)_x]^{2+}$ (x = 1,2,3; en = ethylenediamine) on the surface of montmorillonites."

128 Schoonheydt, R.A.; Pelgrims, J.: J. Chem. Soc., Faraday Trans., 1983,79,2,1169: "Preparation, spectroscopy and reaction with oxygen of $[Co(en)_2]^{2+}$ on the surface of hectorite."

129 Vlček, A.A.; Rusina, A.: Proc. Chem. Soc., 1961,161: "Reduction of aromatic nitro compounds by sodium borohydride catalysed by transition-metal complexes."

130 Martin, B.; Waind, G.M.: J. Chem. Soc., 1958,4248: "2,2-Bipyridine complexes of cobalt, rhodium, and iridium. I. Trivalent rhodium and iridium complexes."

131 Császár, J.: Naturwissenschaften, 1959,46,488.: "Extinction curve of the $[Co(I)(Dyp)_2]ClO_4$ complex."

132 Nicholls, D.: "Complexes and first row transition elements", MacMillan Press Ltd., London, 1983.

133 Palmer, R.A.; Piper, T.S.: Inorg. Chem., 1966,5,864.: "2,2'-bipyridine complexes. I. polarized crystal spectra of tris(2,2'-bipyridine-copper(II),-nickel(II),-cobalt(II),-iron(II) and -ruthenium(II)."

134 Roberts, G.L.; Field, F.H.: J. Am. Chem. Soc., 1950,72,4232: "The absorption spectra of certain nickel(II) and cobalt(II) complex ions."

135 IUPAC (Commission on spectrochemical and other optical procedures for analysis): "Spectrophotometric data for colorimetric analysis", pg.397, Butterworths, London, 1963.

136 Tarasevich, Yu.I.; Sivalov, E.G.: Ukr. Khim. Zh., 1975,41,354.: "Electronic spectra of aquo-cations of bivalent nickel adsorbed on montmorillonite."

137 Hoffman, R.W.; Brindley, G.W.: Geochim. Cosmochim. Acta, 1960,20,15.: "Adsorption of non-aliphatic molecules from aqueous solutions on montmorillonite. Clay-organic studies - II."

138 Banerjee, D.K.; Bray, R.H.; Melsted, S.W.: Soil Sci., 1953,75,421.: "Some aspects of the chemistry of cobalt in soils."

139 Herman, R.C.: J. Chem. Phys., 1940,8,252: "Vibration spectra and molecular structure. IX. Further studies of the vapors of the fatty acid series."

140 Yariv, S.; Russell, J.D.; Farmer, V.C.: Israel J. Chem., 1966,4,201.: "Infrared study of the adsorption of benzoic acid and nitrobenzene in montmorillonite."

141 Williams, D.H.; Fleming, I.: "Spectroscopic methods in organic chemistry", 3rd edition, McGraw-Hill, London, 1980.

142 Jang, S.D.; Garwood, G.A.; Rourke, J.E.; Condrate Sr. R.A.: Surf. Interfaces glass ceramics, 1974,7,23.: "The infrared spectra of several N-containing compounds absorbed on montmorillonite."

143 Fripiat, J.J.; Helsen, J.: Clays Clay Miner., 1966,14,163.: "Kinetics of decomposition of coablt coordination complexes on montmorillonite surfaces."

144 Powell, D.B.; Sheppard, N.: Spectrochim. Acta, 1961,17,68.: "The assignment of infra-red absorption bands to fundamental vibrations in some metal-ethylenediamine complexes."

145 Berg, R.W.; Rasmussen, K.: Spectrochim. Acta, 1974,30A,1881.: "Infrared and far infrared spectra of bis(ethylenediamine)nickel(II)-tri- and tetra-iodomercurate(II)."

146 Miller, F.A.; Wilkins, C.H.: Anal. Chem., 1952,24,8,1253: "Infrared spectroscopy and characteristic frequencies of inorganic ions."

147 Mortland, M.M.; Fripiat,J.J.; Chaussidon, J.; Utterhoeven, J.: J. Phys Chem., 1963,67,248.: "Interaction between ammonia and the expanding lattices of montmorillonite and vermiculite."

148 Hill, D.G.; Rosenberg, A.F.: J. Chem. Phys., 1956,24,6,1219.: "Infrared absorption spectra of complex cobalt compounds."

149 Adams, J.M.; Thomas, J.M.; Walters, M.J.: J. Chem. Soc., Dalton, 1976,112.: "Surface and intercalate chemistry of the layered silicates. Part VI. Tetrahydrofuran intercalates of a series of cation-exchanged montmorillonites."

150 Mortland, M.M.: Advan. Agron., 1970,22,75.: "Clay-organic complexes and interactions."

151 Das Kanungo, J.L.; Chakravarti, S.K.; Mukherjee, S.K.: J. Ind. Chem. Soc., 1968,45,8,685.: "Studies on the sorption and desorption of $Co(NH_3)_6Cl_3$ on Bentonite."

152 Knudson, Jr., M.I.; McAtee, Jr., J.L.: Clays Clay Miner., 1973,21,19.: "The effect of cation exchange of tris(ethylenediamine)cobalt(III) for sodium on nitrogen sorption by montmorillonite."

153 Das Kanungo, J.L.; Sarkar, G.N.: J. Ind. Chem. Soc., 1984,61,216.: "A comparison of the exchange behaviour of tris-trimethylene diamine Co(III) onto montmorillonite and laponite and its release by tetraalkylammonium, alkanediammonium and long chain surface active ions."

154 Hem, J.D. "Study and interpretation of the chemical characteristics of natural water", 2nd Edition, 1985, Reston, New Jersey.

155 Jeffries, N. (Harwell): Personal Communication (based on work performed by BGS).

156 Peigneur, P.; Lunsford, J.H.; De Wilde, W.; Schoonheydt, R.A.: J. Phys. Chem., 1977,81,1179.: "Spectroscopic characterisation of copper(II) ethylenediamine complexes on solid surfaces. I. Synthetic Faujasites types X and Y.

157 Velghe, F.; Schoonheydt, R.A.; Utterhoeven, J.B.: Proc. Eur. Clay Conf., 3rd, 187.: "Spectroscopic characterisation and thermal stability of tris(ethylenediamine) Ni(II) on the surface of a Camp Berteau montmorillonite."

158 Hooper, A.J. (CEGB, Berkeley): Personal Communication.

159 Subramanian, K.S.; Chakrabarti, C.L.; Sueiras, J.E.; Maines, I.S.: Anal. Chem., 1978,50,3,444.: "Preservation of some trace metals in samples of natural waters."

160 Ballantine, J.A.; Davies, M.E.; Purnell, H.J.; Rayanakorn, M.; Thomas, J.M.; Williams, K.T.: J. Chem. Soc., Chem. Comm., 1981,427.: "Chemical conversion using sheet silicates: Novel intermolecular dehydrations of alcohols to ethers and polymers."

161 Ballantine, J.A.; Davies, M.E.; Patel, I.; Purnell, H.J.; Rayanakorn, M.; Williams, K.J.; Thomas, J.M.: J. Mol. Cata., 1984, 26,1,37: "Organic reactions catalysed by sheet silicates: ether formation by the intermolecular dehydration of alcohols and by addition of alcohols to alkenes."

162 Monsef-Mirzai, P.; McWhinnie, W.R.: Inorg. Chim. Acta, 1981,52,211.: "Clay supported catalysts: an extension of phase transfer catalysis."

163 Ghosh, P.K.; Bard, A.: J. Am. Chem. Soc., 1983,105,5691.: "Clay modified electrodes."

164 Gillespie, P.A.: Thermochimica Acta, 1981,51,129.: "A study of the interactions of iron metal, haematite and calcium carbonate between 700 and 1100°C in a nitrogen atmosphere using Mössbauer spectroscopy."

165 McIntyre, N.S.; Cook, M.G.: Anal. Chem., 1975,47,13,2208.: "X-ray photoelectron studies on some oxides and hydroxides of cobalt, nickel and copper."

166 Nefedov, V.I.; Baranovskii, I.B.; Molodkin, A.K.; Omuralieva, U.O.: Russ. J. Inorg. Chem., 1973,18,5,684.: "X-ray electron study of cobalt compounds."

167 Koppelman, M.H.: NATO Adv. Study Inst. Ser., Ser. C, 1980,63,205.: "Application of X-ray photoelectron spectroscopy to the study of mineral surface chemistry."

168 Defosse, C.; Rouxhet, P.G.: NATO Adv. Study Inst. Ser., Ser. C., 1980,63,205.: "Advanced chemical methods for soil and clay minerals research. Introduction to X-ray photoelectron spectroscopy."

169 Kim, K.S.; Baitinger, W.E.; Amy, J.W.; Winograd, N.: J. Electron Spectrosc., 1974,5,351.: "ESCA studies of metal-oxygen surfaces using argon and oxygen ion-bombardment."

170 Adams, J.M.; Thomas, J.M.; Walters, M.J.: J. Chem. Soc., Dalton, 1975,1459.: "The surface and intercalate chemistry of the layered silicates. Part IV. Crystallographic, electron-spectroscopic, and kinetic studies of the sodium montmorillonite-pyridine system."

171 Tolman, C.A.; Riggs, W.M.; Linn, W.J.; King, C.M.; Wendt, R.C.: Inorg. Chem., 1973,12,12,2770.: "Electron spectroscopy for chemical analysis of nickel compounds."

172 Matienzo, L.J.; Yin, L.I.; Grim, S.O.; Swartz, Jr., W.E.: Inorg. Chem., 1973,12,12,2762.: "X-ray photoelectron spectroscopy of nickel compounds."

173 Bertin, E.P.: "Introduction to X-ray spectrometric analysis", Plenum Press, New York, 1978, pg.294.

174 Brissaud, I.; Houdayer, A.; Jehanno, C.; Sabir, A.: J. Radioanal. Nucl. Chem., 1985,89,2,473.: "Pottery analysis using PIXE, neutron activation, scanning electron microscopy and X-ray fluorescence techniques."

175 Lee, J.H.; Peacor, D.R.; Lewis, D.D.; Wintsch, R.P.: Contrib. Mineral Petrol., 1984,88,372.: "Chlorite-illite/muscovite interlayered and interstratified crystals: A TEM/STEM study."

176 Ahn, J.H.; Peacor, D.R.: Clays Clay Miner., 1986,34,2,165.: Transmission and analytical electron microscopy of the smectite-to-illite transition.

177 Hower, J.; Eslinger, E.V.; Hower, M.E.; Perry, E.A.: Geol. Soc. Am. Bull., 1976,87,725.: "Mechanism of burial metamorphism of argillaceous sediment: 1. Mineralogical and chemical evidence."

178 Helsen, J.; Lafaut, J.P.; Schmidt, K.: Reunion Hispano-Belga Miner. Arcilla, An., 1970,173.: "Application of Mössbauer spectroscopy to iron(II) and iron(III) montmorillonite."

179 Helsen, J.; Goodman, B.A.: Clay Miner., 1983,18,117.: "Characterization of iron(II)- and iron(III)-exchanged montmorillonite and hectorite using the Mössbauer effect."

180 Berry, F.J.; Haynes, M.H.; Jones, S.L.: Inorg. Chim. Acta, 1986,122, 19: "Investigations of intercalation in inorganic solids with layered structures: Iron-57 Mössbauer spectroscopy studies of size fractionated and iron-exchanged montmorillonite clays.

181 Johnston, J.H.; Cardile, C.M.: Clays Clay Miner., 1985,33,1,21.: "Iron sites in nontronite and the effect of interlayer cations from Mössbauer spectra."

182 Rozenson, I.; Heller-Kallai, L.: Clays Clay Miner., 1977,25,94.: "Mössbauer spectra of dioctahedral smectites."

183 Goodman, B.A.: NATO Adv. Study Inst. Ser., Ser. C., 1980,63,1.: "Advanced chemical methods for soil and clay mineral research. Mössbauer spectroscopy."

184 Cardile, C.M.; Johnston, J.H.: Clays Clay Miner., 1986,34,3,307.: "^{57}Fe Mössbauer spectroscopy of montmorillonites: A new interpretation."

185 Tsipursky, S.I.; Drits, V.A.; Clay Miner., 1984,19,177.: "The distribution of octahedral cations in the 2:1 layers of dioctahedral smectites studied by oblique-texture electron diffraction.

186 Greenwood, N.N.; Gibb, T.C.: "Mössbauer spectroscopy", pg.161, Chapman and Hall Ltd., London, 1971.

187 Delgass, W.N.; Garten, R.L.; Boudart, M.: J. Chem. Phys., 1969,50,11, 4603.: "Mössbauer effect of exchangeable ferrous ions in Y zeolite and Dowex 50 resin."

188 Anderson, D.M.; Tice, A.R.: Soil Sci. Soc. Am. Proc., 1971,35,47.: "Low-temperature phases of interfacial water in clay systems."

189 Dezsi, I.; Keszthelyi, L.; Pocs, L.: Phys. Letters, 1965,14,14.: "Mössbauer effect in some iron salts in ice."

190 Delgass, W.N.: "Applications of Mössbauer spectroscopy to catalysis and adsorption", Ph.D, Stanford University, 1969.